

ALIPHATIC SEGMENTED POLY(ESTER AMIDE)S BASED ON SYMMETRICAL BISAMIDE-DIOLS

PROEFSCHRIFT

ter verkrijging van
de graad van doctor aan de Universiteit Twente,
op gezag van de rector magnificus,
prof. dr. W.H.M. Zijm,
volgens besluit van het College voor Promoties
in het openbaar te verdedigen
op vrijdag 28 januari 2005 om 16.45 uur

door

Priscilla Amber Majella Lips

geboren op 19 september 1974
te Didam

Dit proefschrift is goedgekeurd door:

Promotor: prof. dr. J. Feijen

Assistent-promotor: dr. P.J. Dijkstra

To know, is to know that you know nothing.

That is the meaning of true knowledge.

Confucius (551-478 BC)

Committee

Chairman:	prof. dr. ing. G. Weickert	University of Twente
Promotor:	prof. dr. J. Feijen	University of Twente
Assistant promotor:	dr. P.J. Dijkstra	University of Twente
Expert:	dr. R. Broos	Dow Benelux
Members:	prof. dr. ing. M. Wessling	University of Twente
	prof. dr. J.F.J. Engbersen	University of Twente
	prof. dr. C.E. Koning	University of Eindhoven
	prof. dr. E. Chiellini	University of Pisa

The research described in this thesis was financially supported by the European Commission, project: QLK5-1999-01298.

This publication was sponsored by the Dutch Society for Biomaterials (NVB).

Aliphatic segmented poly(ester amide)s based on symmetrical bisamide-diols.

Ph.D Thesis - With references; summary in English and Dutch

University of Twente, Enschede, The Netherlands

ISBN 90-365-2129-7

Copyright © 2005 by P.A.M. Lips.

All rights reserved.

Printed by PrintPartners Ipskamp, Enschede, The Netherlands, 2005.

Cover:

Design by Ype van der Zijpp

Painting by Carola Lips

Voorwoord

Vierenhalf jaar geleden heb ik besloten om mijn baan bij Philips in te ruilen voor een promotieplaats in het verre oosten. Het was een moeilijke keuze maar ik moet toegeven dat ik er geen moment spijt van gehad heb. En dat had zeer zeker te maken met de mensen die hieronder genoemd worden.

Als eerste wil ik het woord tot mijn promotor Jan Feijen richten. Bedankt dat u mij de kans en het vertrouwen heeft gegeven om als Hbo'er aan dit promotieonderzoek te beginnen. Ik dacht altijd dat ik zeer kritisch was maar u heeft me geleerd nog veel kritischer te zijn.

Dan mijn assistent-promotor Piet Dijkstra. Piet bedankt dat je me de vrijheid gaf om zelf dingen uit te zoeken en dus ook zelf fouten te maken. Ik heb daar ontzettend veel van geleerd. Dat mijn proefschrift een samenhangend goed doorlopend verhaal is geworden heb ik mede aan jou te danken.

I would also like to thank all the partners from the Biofoam project for all the nice meetings and discussions: (Dow) Rudy Koopmans, René Broos, Michael de Graaf (British Vita) Ken Hillier, Naz Ghigi, Simon Dixon (A&F) Maarten van der Zee, Elinor Scott, Robert van Tuil (University of Stuttgart) Thilo Kupfer, Marc-Andree Wolf, Cecilia Makishi (CEMEF) Thierry Coupez and Julien Bruchon. I'll miss the half yearly trips and the fantastic dinners.

Ik wil ook graag de analytische afdeling van Dow bedanken voor de vele metingen. In het bijzonder wil ik noemen Mark van Heeringen die enorm veel infrarood metingen heeft verricht. Het is een ontzettend mooi stukje werk geworden wat terug te vinden is een groot deel van mijn proefschrift. Het heeft heel wat voeten in de aarde gehad maar ook de 3D-grafieken zien er prima uit, nogmaals bedankt. Verder wil ik René Broos ook nog apart noemen. René, we hebben zoveel gediscussieerd over poly(ester amide)s en ik denk dat we er nog steeds niet helemaal uit zijn. En dat is maar goed ook want je krijgt als commissielid nog volop de gelegenheid om verder te vragen.

I would like to express my gratitude to Federica Chiellini from the University of Pisa for the cell culturing experiments and the helpful discussions.

I also want to thank Lorenzo Moroni from Isotis for performing the 3D deposition experiments described in appendix A.

Andres Laib en Markus Burkhart from Scanco Medical (Switzerland) are thanked for the micro-CT measurements.

Hylke Sijbesma en Siebrand Metz, bedankt voor al jullie hulp bij het opzetten van de schuim- en sorptie experimenten. Prof. Matthias Wessling, bedankt voor alle nuttige discussies hierover.

Dan wil ik ook Herman Koster (WAXD) en Mark Smithers (SEM) van de universiteit Twente bedanken voor al hun metingen.

In mijn laatste jaar zijn er in samenwerking met de groep van Marja van Luyn van de Universiteit Groningen in vivo experimenten uitgevoerd. Linda (Brouwer), ik wil jou bedanken voor al je hulp bij de in- en explantaties en al je geduld bij het nogmaals aangeven welke cel nu welke is. Marja bedankt voor onze discussies op het ziekenhuis en over de telefoon.

A special thanks to Liangbin Li from the FOM-Institute of Atomic and Molecular Physics for the SAXS and WAXD measurements. Although you were very busy with your new job you took the time to read and discuss chapter 6 with me.

Ik wil Prof. Hugo Bergmans van de universiteit Leuven bedanken voor het kritisch doorlezen van hoofdstuk 6.

Dan kom ik nu bij ons eigen lab. Marc Ankoné, je bent vanaf dag 1 bij mijn project betrokken geweest. Ik waardeer al je pogingen om de monomeren zuiver te krijgen, ik weet dat het niet gemakkelijk was. Eén troost, ondanks de lage opbrengst vormen ze toch de basis van mijn boekje.

Tijdens mijn promotie was ik gezegend met een paar goede studenten. Mark ten Breteler, je werk staat niet in mijn boekje maar ik ga er een artikel van maken. Ik herinner me onze discussies en jouw theorieën en ik was onder de indruk. Ingrid Velthoen, jij bent wat beter bedeed in mijn proefschrift, jouw werk staat gedeeltelijk in hoofdstuk 7, 8 en de appendix. Bedankt voor jullie inzet, ik heb veel van jullie (begeleiden) geleerd.

I'm very glad with the collaboration between our group and the group of prof. Chiellini from the university of Pisa, otherwise I would never have met Francesca Signori. Fra, it was great to have you with us for ten months (scientifically and socially) and I'm really glad we still keep in touch.

Wilco Zuiderduin, Ype van der Zijpp en Ingrid Velthoen wil ik bedanken voor het doorlezen (van gedeeltes) van mijn proefschrift. Wilco, ook bedankt voor alle nuttige discussies over visco-elasticiteit door de jaren heen en Ype bedankt voor je oneindige begrip (NOT) bij het uitleggen van de werking van cellen aan een leek.

John, Zlata, Clemens, Hetty, Karin, Geneviève, Gerda en Cindy, ik wil jullie bedanken voor de onmisbare technische en administratieve ondersteuning. Karin, bedankt voor de morele ondersteuning, die ik toch maar al te vaak nodig had.

Dan ben ik nu aangekomen bij mijn kamergenoten. Luuk en Mark (MOR) het was kort, ik geloof 4 maanden maar gelukkig worden er nu met regelmaat baby's geproduceerd dus zien we elkaar toch nog eens. Fenghua, you were already there when I came and you made me feel "at home". It was an honour to be your paronymf. Laura you came soon after me and we shared good as well as tough times together these 4 years. Qing-pu, I

think you had a hard time at first with all those chatting ladies in your office but later on you were the one that kept us under control. Qing-pu left for England, Christine came and it became an all ladies room also known as the “Chicken room”. Christine, we hebben trouw (bijna) elke week hardgelopen zodat we zonder schroom weer vlaai en koekjes naar binnen konden werken. Ingrid, mijn ex-studentje jij was de laatste die in ons kantoor kwam. Ik hoop niet dat ik je al te gek heb gemaakt met late vragen over je afstudeeropdracht. “Chicks”, ik zal jullie gezelligheid en verhalen missen!

Ik wil iedereen van PBM, STEP, RBT en MTP bedanken voor de ontzettend gezellige tijd en dan denk ik terug aan zeilweekendjes, wadlopen, sinterklaasvieringen, triatlons, labetentjes, cocktail-/glühwein-/oliebollenparty's, koffiepauzes en zo nog even door. A special thanks to Marianne, Audrey, Menno, Fenghua, Zhiyuan, Laura, Francesca S, Martijn vd S, Wilco Z, Debby, Mark t B, Christine, Ingrid, Francesca de R en Boon Hua. Sport is de beste uitlaatklep als je het druk hebt en dat heeft me ontzettend geholpen deze 4½ jaar. En dan heb ik het over de maandelijkse vakgroepvolleybalwedstrijden met Josien, Annemieke, Joost, Ype, Edwin, Debby, Richard, Ingrid, Martijn F, Christine en Zheng. Maar ook de partijtjes single en dubbel met mijn tennismaatjes Menno, Zhiyuan, Laura, Joost en Ype zorgden voor de nodige ontspanning.

Dan ben ik nu toe aan mijn paranimfen: Ellen, we kennen elkaar al vanaf de kleuterschool en we hebben een hele hoop dingen samen meegemaakt. Ik hoop dat we nog heel lang vrienden blijven. Laura, you were a great roommate and friend for the last 4 years. I really enjoyed our visits to Italy where I got to know a bit more about real Italian life. Girls, I'm happy to have you both on stage with me.

Mijn familie en vrienden wil ik bedanken voor de interesse die zij hebben getoond in mijn onderzoek maar bovenal voor het zorgen voor de juiste afleiding. Gelukkig hebben we onze meidenavonden (regelmatig ontbijt of lunch), etentjes en HLO-stapavonden de afgelopen 4½ jaar in stand kunnen houden.

Pap, mam en Carola, jullie hebben mij het vertrouwen gegeven dat ik alles kan en jullie hebben mij altijd gestimuleerd om nieuwe dingen te ondernemen. Soms had ik net dat extra zetje van jullie nodig.

Ik ben nog nooit zoveel in Friesland geweest als in de laatste 3½ jaar. En Ype, je hebt gelijk (*dat valt zwaar*), het is zeker een plek om lekker tot rust te komen en weer helemaal op te laden. Zonder jouw nuchterheid en soms simpele kijk op dingen was ik niet zover gekomen en wij vullen elkaar inderdaad aan. Ik teken voor nog een heleboel jaren samen.

Priscilla

Contents

Chapter 1	
General introduction	1
Chapter 2	
Degradable aliphatic poly(ester amide)s	9
Chapter 3	
Crystallization behaviour of symmetrical bisamide-diols	41
Chapter 4	
Synthesis and characterization of poly(ester amide)s containing crystallizable amide segments	83
Chapter 5	
Incorporation of different crystallizable amide blocks in segmented poly(ester amide)s	121
Chapter 6	
Crystallization behaviour of aliphatic segmented poly(ester amide)s	147
Chapter 7	
Biocompatibility and degradation of aliphatic segmented poly(ester amide)s: <i>in vitro</i> and <i>in vivo</i> evaluation	185
Chapter 8	
Gas foaming of segmented poly(ester amide) films	213
Appendix I	
Preparation of open-cell porous structures of segmented poly(ester amide)s	233
Summary	251
Samenvatting	257
Curriculum Vitae	263

Chapter 1

Introduction

Biofoam project

In the last 50 years the consumption of fossil fuels has increased tremendously and the prognoses are that it will increase even more in the coming decade. This leads to a rapid exhaustion of the world's fossil energy resources and without the necessary precautions a deficiency in fossil fuels is inevitable. Many of the currently used plastics are made from petrochemicals, e.g. gas and oil. Despite the benefits of these plastics like low price, low weight and good performance, recycling of these materials in general is only possible into low value products. In addition, the increasing public awareness on environmental pollution like plastic litter has resulted in a growing commercial interest in the development of biodegradable materials for consumer products. This led to a regained interest in the use of biopolymers, which offers a solution to both of the above-mentioned issues in the long-term. An ideal biopolymer is obtained from renewable biological resources, i.e. non-fossil organic resources such as plants and animals, and is biodegradable at the end of its life. Biopolymers, like proteins and polysaccharides, can be isolated from natural resources and applied for specific applications. However, in many cases the physical and mechanical properties of biopolymers available are not sufficient. A way to overcome this problem is the synthesis of tailor made polymers from monomers or low molecular weight materials derived from renewable resources like corn, molasses and seed oils. These polymers are referred to as bio-source based polymers.

It is concluded that biodegradable bio-source based polymers would cover all demands regarding a better balance between economical and ecological interests. However, the size of the potential value of the market, the polymer performance requirements, and the cost-performance of the polymer as compared to existing petrochemical-based polymers are essential for a commercial success. Therefore, studies that cover all these polymer

aspects are needed. The Biofoam project implements such an innovative method ¹. The development of biopolymers for foam applications is directed via a Life Cycle Management Analysis (LCMA) towards sustainability. LCMA integrates life cycle studies on the environmental, economic and employment (social) impact of new product developments. This means that environmentally sustainable products are developed, which are economically viable and socially acceptable.

Aim

The Biofoam project aims at developing closed- and open-cell foams from bio-source based polymers ¹. The strategic intent of the project is to develop foams without the use of isocyanates that have comparable or better properties than the classic polyurethane foams. To achieve this goal new polymers and/or alternative synthesis routes need to be explored. The envisaged applications of such foams are in higher added value markets in order to compensate for the potentially higher renewable feedstock cost. Such novel polymers should be developed at a cost of less than 1 Euro per kg to compete with polyurethane, polystyrene and polyvinyl alcohol that currently dominate the foam market.

Foam market

Foams are versatile products that fulfill a wide variety of functions such as shock and noise absorption and weight reduction ². Plastic foams, generally consist of a minimum of two phases, a solid polymer matrix and a gaseous phase derived from a physical blowing agent. Foams may be flexible or rigid, depending on whether their glass transition temperature is below or above room temperature. The cell geometry may be open- (interconnected cells) or closed. Closed-cell foams are most suitable for thermal insulation and buoyancy and are generally rigid, while open-cell foams are best for packaging, furniture, transport, bedding, textile and biomedical applications and are generally flexible. Plastic foams can be produced in a great variety of densities ranging from about 1.6 kg.m⁻³ to over 960 kg.m⁻³. Since the mechanical properties are generally proportional to the foam densities, polymer foams are produced in a great variety of densities, depending on their application ^{3, 4}. Thus, rigid foams in load-bearing applications require a high density while low densities are usually used for thermal

insulation. Low-density flexible foams (30 kg.m^{-3}) are usually applied in furniture and automotive seating, while somewhat higher density foams are used for carpet backing and energy absorbing applications.

If bio-source based polymer foams having equal characteristic properties as polyurethane foams can be synthesized a large market would be available for exploitation ¹. High value markets are envisaged such as the medical, filtration and automotive as well as the sport shoe market. But also areas in which rigid, closed cell foams for packaging and noise abatement are applied come to mind.

Because of the versatility of polyurethane chemistry, this class of polymers is not only produced for the foam market but also as thermoplastic elastomers to be used for example in the hygiene market area. However, this specific market including diapers, adult incontinence and feminine hygiene is currently under long-term threat and identifies polyurethane impurities as a problem. Bio-source based polymers might also bring a solution for this market area.

Partners

Biofoam is a project funded by the European Commission (QLK5-1999-01298) in which the partnership comprises a complementary effort of two large companies, three universities and one research institute. Within the Agrotechnology & Food Innovations Institute (A&F) the economic aspects for the bio-source based renewable feedstock will be identified and explored. The University of Stuttgart assists in this effort using a LCMA approach to objectively decide which of the potential options will meet the integrated objectives. An overall software framework will be developed to perform detailed comparisons of selected options like environmental and social implications. At A&F the chemical aspects and technology for the synthesis of potential monomers for the ultimate production of novel polymers is also explored. In the early stages of the project and based on previous work, particular attention has been given to identify renewable feedstock and to define efficient routes to obtain the monomers 1,2-ethanediol, 1,4-butanediol, 1,2-diaminoethane, 1,4-diaminobutane, adipic acid, suberic acid, δ -valerolactone and ϵ -caprolactone, which are building blocks for segmented poly(ester amide)s. In the mean time at the University of Twente segmented poly(ester

amide)s, using petrochemical based monomers, are synthesized and studied for their physical, thermal and mechanical properties. The lab-scale synthetic procedures will form the basis for exploring the scaling-up from gram to kilogram samples. By transferring the knowledge of laboratory scale synthesis of the polymer to Dow Benelux N.V., synthesis of larger quantities of the selected segmented copolymers will be investigated. Finally at British Vita and Dow Benelux N.V. possible foam applications that are economically viable are defined. The activities of British Vita also include foam fabrication, property evaluation and introduction into the market. In parallel to the synthetic activities a program is started at Ecole des Mines de Paris, which focuses on the development of a computational model for dynamic simulation of the foaming process in 3D geometries. In relation to the biopolymer rheological aspects and processing boundary conditions for existing foaming equipment such a model may be valuable in predicting foam morphologies. Dow researchers assist by determining the rheological properties of the biopolymer and defining realistic processing windows. Besides the polymer properties and foaming technology, the biofoam recyclability in terms of material recovery, bio-source recovery, energy recovery and biodegradability will be performed by A&F and the University of Stuttgart.

Poly(ester amide)s

A well-known class of synthetic biodegradable polymers are the aliphatic polyesters. However, most of these polyesters are low melting and often have insufficient mechanical properties. Earlier studies have shown the excellent physico-chemical properties of segmented poly(ester amide)s and have provided insight into their biodegradation⁵⁻⁸. The unique performance properties of these polymers are based on the presence of chain segments that are symmetrical and have the ability to organize by H-bonding.

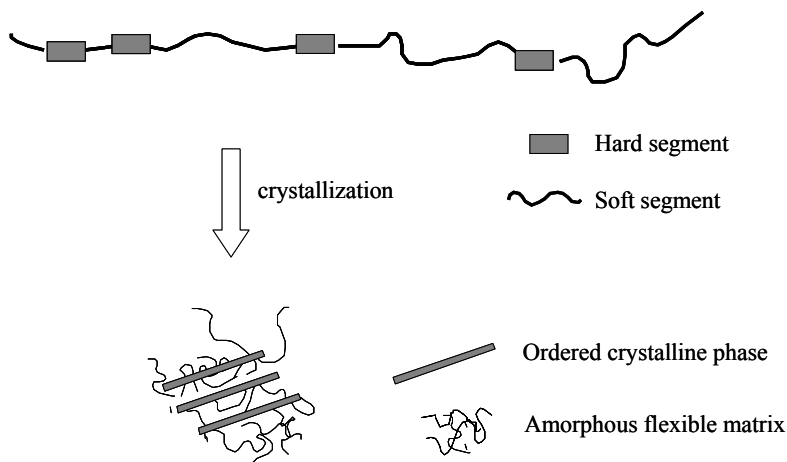


Figure 1.1: Schematic picture of segmented poly(ester amide)s and their crystallization behaviour.

Segmented poly(ester-amide)s belong to the family of thermoplastic elastomers and have a micro-phase separated structure with an amide-rich hard phase and an ester-rich flexible soft phase (fig. 1.1) ⁴. The amide-rich phase usually contains crystalline lamellae and acts as a thermo-reversible physical crosslinker or reinforcing filler for the amorphous phase. The properties depend on the type of hard and soft segment, their ratio and on the degree of phase separation between hard and soft segments. Although, the structure-property relations of these segmented block copolymers are complex, the many structural degrees of freedom allow for a tailored composition that meets specific requirements. This capability is particularly attractive when considering foam applications that need to meet a wide variety of performance requirements.

Objectives

This study is performed within the framework of the Biofoam project. The main objectives are to define an efficient synthetic pathway for economical bio-source based chemicals to produce aliphatic segmented poly(ester amide)s. Previous work has shown that these polymers have physico-chemical properties that may fulfill the physical and mechanical requisites to be applied in foams. Similar segmented poly(ester amide)s need to be synthesized on a larger scale and fully characterized in terms of thermal, physical and mechanical properties. To investigate the structure-property relations of these

polymers, features like phase separation, crystallization behaviour and morphology are of utmost importance.

The second topic of this thesis is related to the exploration of poly(ester amide)s as potential biomaterials. Based on previous studies, these aliphatic segmented poly(ester amide)s comprising water-soluble bisamide units, are expected to degrade and/or resorb in the body. To study their applicability in the biomedical field these polymers should be evaluated with respect to their mechanical properties in the hydrated state, cytotoxicity, cell adhesion and growth, *in vitro* and *in vivo* degradation and tissue response.

The aim of the Biofoam project is to develop foams without the use of isocyanates that can compete with the classic flexible polyurethane foams. Therefore the last part of our research is directed towards developing techniques to prepare open- or closed-cell flexible foams. In this respect, poly(ester amide) foams will be prepared using the physical blowing agent carbon dioxide (CO₂) and the influence of porosity and pore size of the foams on their properties will be investigated.

Outline of this thesis

A literature review on degradable aliphatic poly(ester amide)s is presented in **chapter 2**. The synthesis and properties of alternating, segmented (block) and random copoly(ester amide)s are discussed thoroughly. Finally the degradation of these polymers is assessed. **Chapter 3** deals with the synthesis and characterization of preformed monomers (bisamide-diols), essential building blocks to be incorporated in the aliphatic polyester matrix of poly(butylene adipate). The crystalline structure of these bisamide-diols is also reported. High molecular weight segmented poly(ester amide)s were prepared by melt polycondensation of the preformed bisamide-diols, 1,4-butanediol and dimethyl adipate. The effect of the polymer composition on the thermal, physical and mechanical properties of these poly(ester amide)s is discussed in **chapter 4**. The effect of structural variation of the bisamide-diol on the above-mentioned properties is described in **chapter 5**. Emphasis is given on the crystalline structure of both types of polymers. The phase behaviour of these polymers, based on DSC, FT-IR, AFM and XRD studies, is discussed in more detail in **chapter 6**. Special attention is given to the influence of polymer

composition and type of hard block on the crystallization behaviour of segmented poly(ester amide)s. In **chapter 7**, poly(ester amide)s are evaluated with respect to their mechanical properties in the hydrated state, cytotoxicity, cell adhesion and growth, *in vitro* and *in vivo* degradation and tissue response to study their applicability in the biomedical field. **Appendix A** is linked to chapter 7 and presents two different preparation techniques to obtain porous structures (open-cell foams) which can be used as scaffold materials for tissue engineering applications. **Chapter 8** describes the methodology to prepare closed-cell poly(ester amide) foams using the physical blowing agent CO₂. The porosity and pore size of the foams are determined as a function of foaming temperature and CO₂ saturation pressure. The relation between the thermal and mechanical properties of poly(ester amide)s and their foam morphology is discussed.

References

1. R. Koopmans, **1999**, Dow Benelux N.V., *Report QLRT-1999-01298*.
2. D. Klempner, K.C. Frisch, **1991**, *Handbook of polymeric foams and foam technology*, Hanser, New York.
3. L.J. Gibson, M.F. Ashby, **1988**, *Cellular Solids, Structure and Properties*, Pergamon Press, Oxford.
4. G. Holden, N.R. Legge, R. Quirk, H.E. Schroeder, **1996**, *Thermoplastic elastomers*, Hanser, New York.
5. H.R. Stapert, *PhD thesis*, **1998**, University of Twente, The Netherlands: p. 153.
6. H.R. Stapert, P.J. Dijkstra, J. Feijen, *Macromol. Symp*, **1998**, 130, 91.
7. H.R. Stapert, A.M. Bouwens, P.J. Dijkstra, J. Feijen, *Macromol. Chem Phys.*, **1999**, 200, (8), 1921.
8. H.R. Stapert, M. van der Zee, P.J. Dijkstra, J. Feijen, *Abstracts of Papers of the American Chemical Society*, **1997**, 213, 253.

Chapter 2

Degradable aliphatic poly(ester amide)s*

P.A.M. Lips, P.J. Dijkstra, J. Feijen

Institute for Biomedical Technology (BMTI) and Department of Polymer Chemistry and Biomaterials, Faculty of Science and Technology, University of Twente, P.O. Box 217, 7500 AE Enschede, The Netherlands.

Introduction

Depending on the desired application degradable polymers have to meet many demands. It has been recognized that especially the combination of adequate polymer properties, thermal processing, low price and controlled biodegradability are difficult to fulfil and are an ongoing challenge for polymer scientists. Strategies that may be followed include (chemical) modification of polymers and the synthesis of (newly) designed polymers. Aliphatic polyesters are biodegradable but often lack good mechanical and physical properties whereas aliphatic polyamides do have good mechanical properties but are not biodegradable. The combination of the favourable properties of both classes of polymers has been the fundament for the development of poly(ester amide)s. Structural features like hydrogen bonding in poly(ester amide)s influence the material properties and degradability. In this respect, two different strategies have been followed; placing the amide groups randomly in the polymer chain or incorporate well-defined bisamide containing blocks or segments. In this chapter these materials will be reviewed for their structural characteristics, physical and mechanical properties and biodegradability.

* Published in Biodegradable Polymers, R.Smith Eds, Cambridge, 2004.

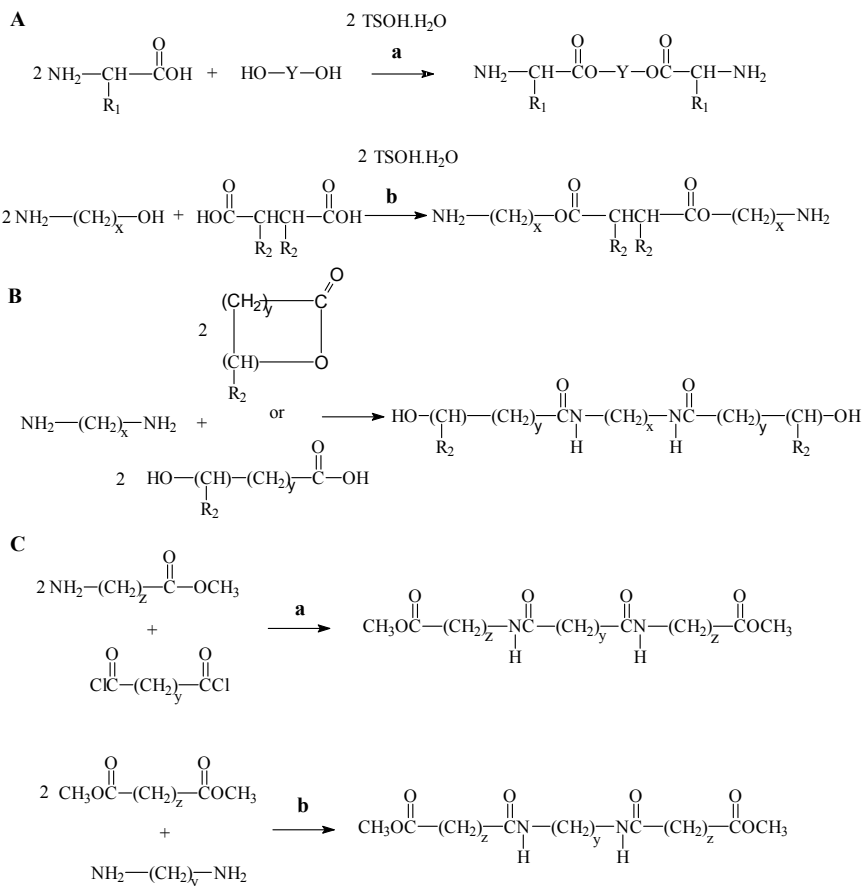
Aliphatic poly(ester amide)s

Poly(ester amide)s are conveniently synthesized by polycondensation techniques as applied in the synthesis of polyesters and polyamides. One can choose either to use methods where preformed monomers are condensed, use ring-opening polymerization or combine both methods. The preformed monomers may contain either ester or amide functional groups and all the possible combinations lead to architectural variations of poly(ester amide)s. The placement of amide and ester groups along the polymer chain can thus be regulated and alternating, segmented (block) and random polymers have been prepared depending on the starting compounds and procedures applied. The structures of preformed symmetrical monomers are depicted in scheme 2.1 and the polymerizations are summarized in schemes 2.2-2.10. The monomers used are described as bisester-diamines, bisamide-diols, bisamide-diesters or oligoesters. From a synthetic point of view alternating and (block) copoly(ester amide)s are mostly prepared from preformed monomers like bisester-diamines, bisamide-diols and bisamide-diesters. The latter never contain activated acid end-groups because intramolecular cyclization reactions are very common for these type of compounds. In the following section the preparation of preformed monomers and the synthesis and properties of successively alternating, segmented (block) and random poly(ester amide)s will be reviewed. Finally the degradation of the polymers will be discussed.

Monomers

Bisester-diamines have been prepared by reacting an amino acid with an aliphatic diol (scheme 2.1A-a) or reversely an amino alcohol with succinic acid or tartaric acid (scheme 2.1A-b) ^{1, 2} in refluxing toluene in the presence of p-toluenesulfonic acid monohydrate. A variety of amino acids and aliphatic diols, PEG or cyclic diols like dianhydrosorbitol or dianhydromannitol have been used ³⁻¹⁸. Bisamide-diols (scheme 2.1B) are generally prepared by reacting a linear aliphatic diamine ($x = 2-16$) with γ -butyrolactone, δ -valerolactone or ϵ -caprolactone or with an hydroxy acid in the melt or in solution ¹⁹⁻²⁸. A side reaction that occurs is the ring-opening of a lactone by the generated hydroxyl end-groups resulting in oligomerization ^{20, 22, 24, 29}. This side reaction can partly be suppressed by performing the reaction in isopropanol at 5 °C ^{23, 24} and is not observed in the reaction of diamines with glycolic acid, glycolide, lactic acid or

lactide (analogous as given in scheme 2.1B) ^{20, 26}. Bisamide-diester have been prepared from a glycine ester or ϵ -aminocaproic ester and a diacid chloride ($y = 2-10$) by a Schotten Bauman reaction in the presence of triethyl amine (scheme 2.1C-a) ^{5, 18, 30, 31}. A bisamide-diester with inverted amide groups has been prepared from 1,4-diaminobutane and dimethyl adipate in the melt in the presence of titanium butoxide (scheme 2.1C-b) ^{32, 33}.



Scheme 2.1: Bisester-diamine (A), bisamide-diol (B) and bisamide-diester (C) monomers used in the synthesis of poly(ester-amide)s with A-a: $\text{R}_1 = \text{H}, \text{CH}_3$ (L, D, LD), $\text{CH}_2\text{C}_6\text{H}_5$, $\text{CH}(\text{CH}_3)_2$, $\text{CH}_2\text{CH}(\text{CH}_3)_2$, $\text{CH}(\text{CH}_3)\text{CH}_2\text{CH}_3$, $(\text{CH}_2)_3\text{CH}_3$, $(\text{CH}_2)_2\text{SCH}_3$; $\text{Y} = (\text{CH}_2)_{2-12}$, $((\text{CH}_2)_2\text{O})_n(\text{CH}_2)_2$, dianhydrosorbitol or dianhydromannitol, $\text{TSOH.H}_2\text{O} = p$ -toluenesulfonic acid monohydrate, A-b: $\text{R}_2 = \text{H}, \text{OCH}_3$; $x = 2-6$, B: $x = 2-16$; $y = 0-4$; $\text{R}_2 = \text{H}$ or CH_3 , C-a: $y = 2-10$; $z = 11$ and C-b: $y = 4$; $z = 4$.

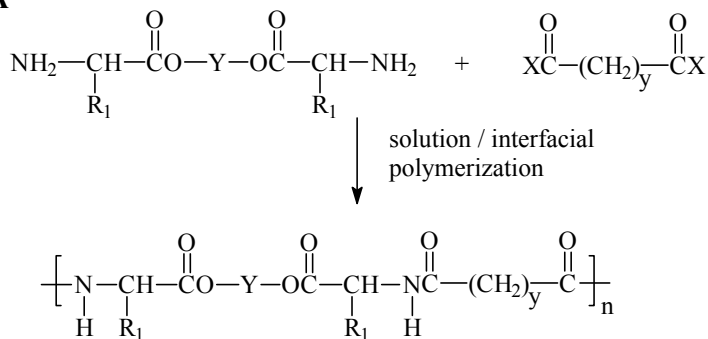
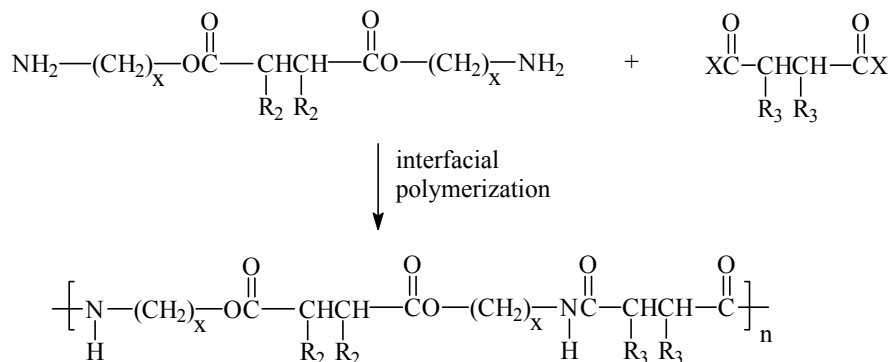
Alternating poly(ester amide)s

In general diester-diamines (scheme 2.1A) are reacted with p-nitrophenyl activated esters in solution in the presence of triethyl amine^{12, 15-17, 34, 35} or with di-acid chlorides or pentachlorophenyl activated esters by interfacial polymerisation in the presence of Na_2CO_3 ^{1, 2, 4-11, 31, 36-38} to give alternating poly(ester amide)s.

Alternating poly(ester amide)s based on glycine or alanine, dianhydrosorbitol as the diol and activated dicarboxylic acid esters with methylene chain lengths of 4-10 (scheme 2.2A) are examples of the large variations in the microstructural architecture¹⁵⁻¹⁷. Most of these poly(ester amide)s are amorphous, except those prepared from sebacic acid and glycine or glycerylglycine units, which are semicrystalline¹⁷.

Especially alanine and glycine based alternating poly(ester amide)s have been prepared and their properties studied in recent years^{5-10, 36}. Alternating poly(ester amide)s prepared from 1,12-dodecanediol and β -alanine or glycine and sebacic acid chloride (scheme 2.2A) have been studied with TEM and X-ray diffraction. The polymers derived from β -alanine crystallize like the α - and β -forms of nylons with intermolecular hydrogen bonds along a single direction that runs parallel to the α crystallographic axis (4.80Å). Similar poly(ester amide)s based on 1,6-hexanediol and glycine and varying di-acid chlorides ($y=2-8$) showed strong hydrogen bonds (scheme 2.2A). The lamellar crystals have a fairly constant thickness, which approximately corresponds to two chemical repeat units. Molecules are folded within the lamellae along the H-bonded sheets⁶⁻⁹. Instead of using an α -amino acid, 4-amino butyric acid has also been applied in monomer synthesis (analogous as given in scheme 2.1A-a). Such poly(ester amide)s based on 4-amino butyric acid have been compared with glycine based polymers (scheme 2.2A). FT-IR spectra revealed that amide-amide H-bonds and ester-amide H-bonds are present in both polymers, whereas the poly(ester amide)s derived from 4-amino butyric acid also contain non H-bonded ester and amide groups¹⁴.

Alternating stereoregular poly(ester amide)s based on 6-aminohexanol and di-O-methyl-L-tartaric acid (scheme 2.2B) are optically active and are semi-crystalline^{1, 2}.

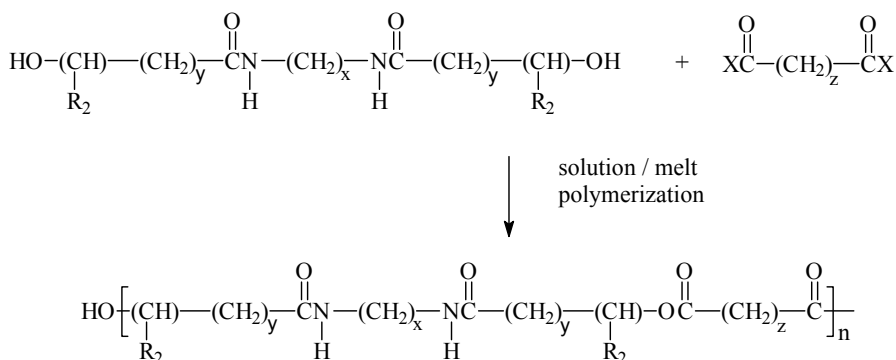
A

B


Scheme 2.2: Alternating poly(ester amide) synthesis from monomers comprising amino acid (A) or tartaric acid (B) moieties. A: $R_1 = \text{H}, \text{CH}_3$ (L, D, LD), $\text{CH}_2\text{C}_6\text{H}_5$, $\text{CH}(\text{CH}_3)_2$, $\text{CH}_2\text{CH}(\text{CH}_3)_2$, $\text{CH}(\text{CH}_3)\text{CH}_2\text{CH}_3$, $(\text{CH}_2)_3\text{CH}_3$, $(\text{CH}_2)_2\text{SCH}_3$; $\text{Y} = (\text{CH}_2)_{2-12}$, $((\text{CH}_2)_2\text{O})_n(\text{CH}_2)_2$, dianhydrosorbitol or dianhydromannitol; $y = 2-10$; $X = \text{Cl}$ or $p\text{-C}_6\text{H}_4\text{NO}_2$, B: $x = 2-6$; $R_2 = \text{H}, \text{OCH}_3$; $R_3 = \text{H}, \text{OCH}_3$; $X = \text{pentachlorophenyl}$.

To prepare alternating poly(ester amide)s (scheme 2.3) derived from bisamide-diols, these monomers were reacted with di-esters or di-acid chlorides using solution polymerization^{3, 21, 26-28} or melt polymerization^{19-21, 27, 28}. Melt-polymerized polymers had a lower melting temperature than solution-polymerized polymers possibly due to side reactions. The use of an asymmetric amide-diol, prepared from ϵ -caprolactone and

ethanolamine, instead of a symmetrical bisamide-diol, based on ϵ -caprolactone and 1,2-ethanediamine, resulted in polymers with a lower melting temperature ²¹.

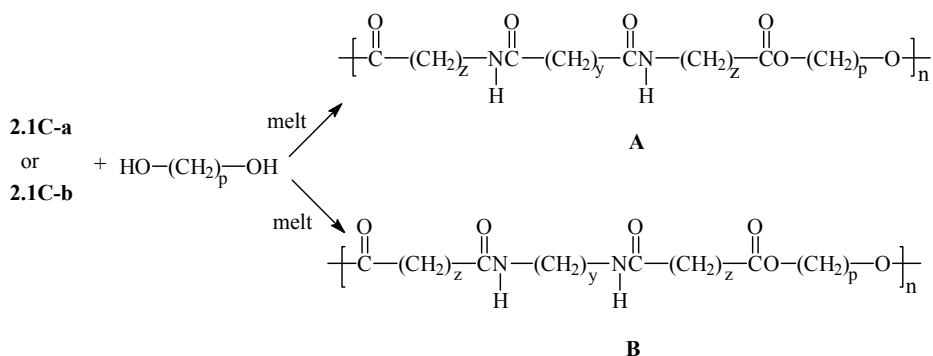
Barrows *et al.* were the first to study aliphatic poly(ester amide)s as potential materials for bioabsorbable sutures ^{26, 29}. Alternating poly(ester amide)s were prepared by solution polymerization from symmetrical bisamide-diols and diacid chlorides (scheme 2.3) and investigated for their fibre forming properties and *in vivo* resorption. Different bisamide-diols were prepared from glycolic acid and diaminoalkanes containing two to twelve methylene groups (scheme 2.1B). The properties of the materials could be optimized by the use of water-soluble bisamide-diols to minimize polymer resorption time. The highest melting temperature in combination with a high fibre strength retention after implantation of the polymer was achieved by using succinyl chloride as the comonomer. Alternating poly(ester amide)s, prepared by melt polymerization starting from bisamide-diols and dimethyl adipate (scheme 2.3), were obtained only as low molecular weight material, most likely due to the difficulty to retain a 1:1 stoichiometry during the condensation reaction ^{19, 20}. The problems encountered when starting from bisamide-diols can be circumvented by using bisamide-diester as in the synthesis of polyesters (scheme 2.4) ^{5, 11, 18, 30, 31, 33, 39}.



Scheme 2.3: Poly(ester amide)s synthesized from bisamide-diols and di-esters or di-acid chlorides with $x = 2-16$; $y = 0-4$, $R_2 = \text{H}$ or CH_3 ; $z = 2-14$; $X = \text{OH}$, OCH_3 , or Cl .

Alternating semi-crystalline poly(ester amide)s can thus be conveniently synthesized from diamide-diester and diols (scheme 2.4A). Within each series, for each polymer

one single melting temperature was found which regularly decreases with increasing number of methylene groups in the diol ³⁰. The material properties are highly dependent on the regularity of the units in the polymer chain. This is illustrated by the higher crystallinity of the alternating polymers as depicted in scheme 2.4A compared to the random poly(ester amide)s as depicted in scheme 2.9B, which have the same monomeric units in the polymer chain ¹⁸. The well known odd-even effect for aliphatic polyamides and poly(ester amide)s becomes visible in the higher melting temperature of adipic- compared to glutaric acid based poly(ester amide)s ³⁹.



Scheme 2.4: Synthesis of poly(ester amide)s by polycondensation of bisamide-diester and diols with A: y = 2-10; z = 1,5; p = 2-12 and B: y = 4; z = 4; p = 4.

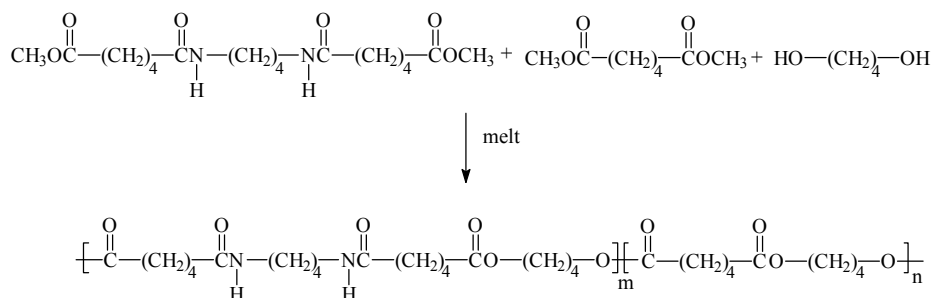
Segmented (block) copoly(ester amide)s

Block or segmented copolymers have been prepared by replacing one of the components in a polyesterification by an amide containing monomer. Thus bisamide-diols and bisamide-diester are the key elements ^{19, 20, 25, 33, 40, 41}.

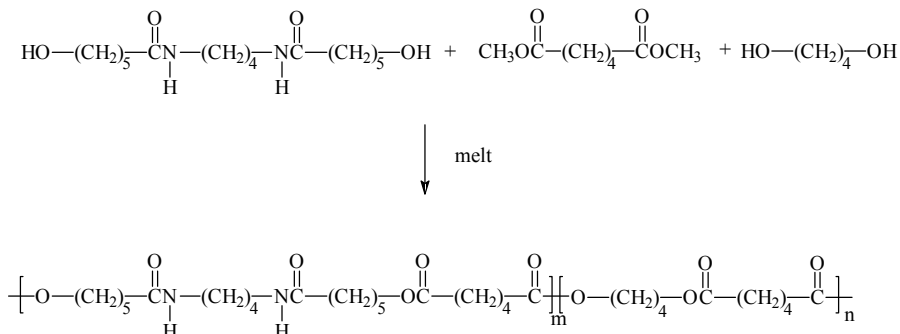
High molecular weight segmented poly(ester amide)s prepared by condensation of bisamide-diester, 1,4-butanediol and dimethyl adipate are easily prepared by melt polymerization (scheme 2.5A) ³³. The uniform amide blocks are randomly distributed in the polymer chain and no cyclization reactions or ester-amide interchange occurs during the polycondensation reaction. Segmented poly(ester amide)s can also be prepared starting from bisamide-diols, 1,4-butanediol and dimethyl adipate (scheme 2.5B) ^{19, 20}. Melt polymerization affords polymers with molecular weights between 20.000 and 50.000. The molecular weight of these polymers decreases with increasing amide

content. As no or little ester-amide interchange occurs between segments of the polymer chain, the symmetrical and uniform structure of the amide segments is retained in the polymer. These polymers show two melt transitions and one glass transition temperature. The low melt transition, which is independent of the amide content, is in between 50 and 70 °C and is attributed to a meta-stable crystalline phase with respect to the higher melting crystalline phase. By increasing the amide content from 10 to 100 mol% the high melt transition and the glass transition temperature increased from 80 to 140 °C and from -58 to -10 °C, respectively. The increase in glass transition temperature indicates the presence of a homogenous amorphous phase.

A



B

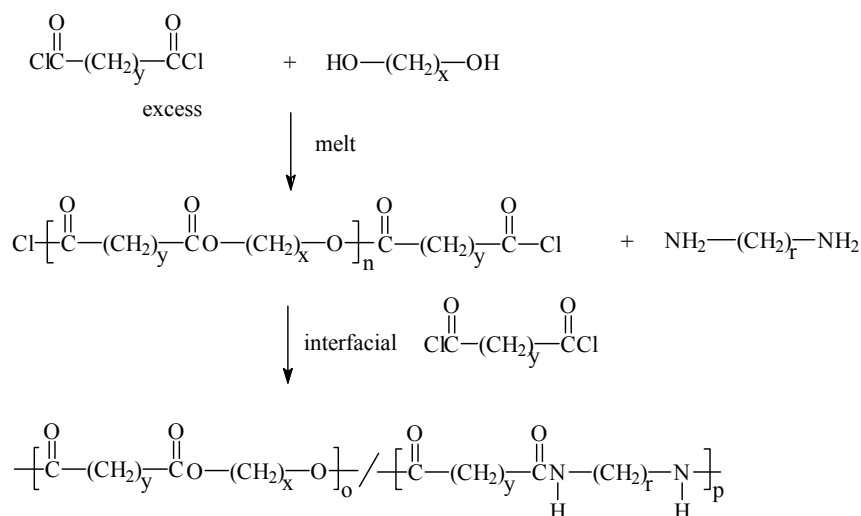


Scheme 2.5: Pathways to segmented poly(ester amide)s by melt polymerization of preformed bisamide-diester or bisamide-diols.

Bera *et al.* prepared segmented poly(ester amide)s from preformed bisamide-diols and hydroxyl end-capped oligoesters^{24, 25}. The bisamide-diol prepared from 1,6-hexanediamine and γ -butyrolactone, was first reacted with adipic acid to form a hard

alternating poly(ester amide) oligomer (scheme 2.3). The oligoester was prepared from 1,2-ethanediol and adipic acid. A series of high molecular weight polymers was obtained by reacting various ratios of hard and soft oligomers in the presence of a catalyst (Sb_2O_3). All polymers have two glass transition temperatures (-40 to -50 °C and 40 to 50 °C) and one melting temperature at ~ 200 °C, indicating the presence of two separate amorphous domains and a crystalline phase. By increasing the hard oligomer content from 20 to 83 mol% the modulus increased from 70 to 600 MPa and the yield stress increased from 1 to 15 MPa. It was shown with temperature dependent IR that amide-amide and ester-amide H-bonds were formed in all polymers^{40, 41}. The ester-amide H-bonds are stable up to 210 °C whereas the amide-amide H-bonds disappear at 170 °C. The largest amount of ester-amide H-bonds is present in the oligo(ester amide), in which the content of ester groups is considerably lower than in the segmented poly(ester amide).

Another way to prepare segmented poly(ester amide)s is to react acid chloride end-capped oligoesters with a diacid chloride and a diamine by interfacial polymerisation (scheme 2.6)^{31, 38, 42}. These polymers have two crystalline phases, with characteristic melting temperatures of the corresponding linear polyesters (75 - 77 °C) and polyamides (242 - 248 °C). Repetitive heat treatments cause randomization of the poly(ester amide).



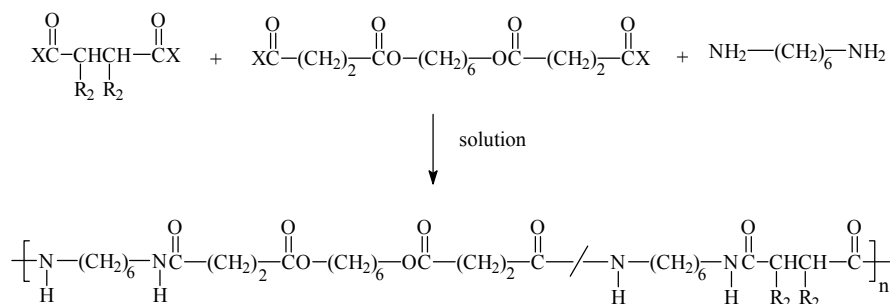
Scheme 2.6: Segmented and random poly(ester amide)s by interfacial polycondensation with $y = 2$ - 4 ; $x = 2$ - 10 ; $r = 2$ - 6 .

Random poly(ester amide)s

A wide range of random copolymers has been prepared starting from monomers 2.1A, 2.1C and oligo-esters with different molecular weights, by condensing them with aliphatic di-amine and di-acid derivatives ^{13, 31, 43-51}. When a mixture of a bisester-diamine and 1,12-dodecanediamine is reacted with sebacoyl chloride, random poly(ester amide)s are obtained ¹³. IR-spectra indicate that amide groups from both bisester-diamine and 1,12-dodecanediamine containing units form H-bonds in the poly(ester amide). The melting temperature of these polymers increases with decreasing bisamide-diester content as the amide/ester ratio increases.

In the development of new biodegradable polymers, poly(lactic acid) oligomers have been used to prepare random poly(ester amide)s. The hydroxyl end-capped poly(lactic acid) oligomer is reacted with an excess of sebacoyl chloride to form an oligomer with acid chloride end-groups which is then reacted with a diamine ^{43, 44}. Random poly(ester amide)s with polyester contents of 23-53 wt% were prepared starting from poly(lactic acid) oligomers with molecular weights of 600, 1000 and 1500. The high melting temperatures are attributed to the melting of the polyamide segments, which was confirmed by WAXS measurements. Castaldo *et al.* synthesized slightly different polymers with high melting temperatures by using a bisamide-diamine instead of an aliphatic diamine ³⁸. Poly(ester amide)s based on 1,6-hexanediamine, adipoyl chloride and an oligoester (scheme 2.6) reveal one melting endotherm in the range of melting temperatures of corresponding linear aliphatic polyamides ³¹. Poly(ester amide)s with higher ester content have an additional melting endotherm which coincides with the melting temperature of the corresponding linear aliphatic polyesters. The glass transition temperature decreases drastically with an increase in ester content, which suggests the presence of a homogeneous amorphous phase. Similar poly(ester amide)s with high amide contents of 60 and 75 wt% show only one melting temperature, which is attributed to a polyamide rich phase, whereas poly(ester amide)s with lower amide content show two melting temperatures, assigned to both polyester and polyamide rich phases ⁴⁹. Moreover, the stress at break increased from 15 to 30 kPa and the strain at break increased from 89 to 343% with increasing amide content (34-54 mol%). It is interesting to note that these poly(ester amide)s possess a distinct characteristic polyamide melt transition while the melt transitions of random poly(ester amide)s

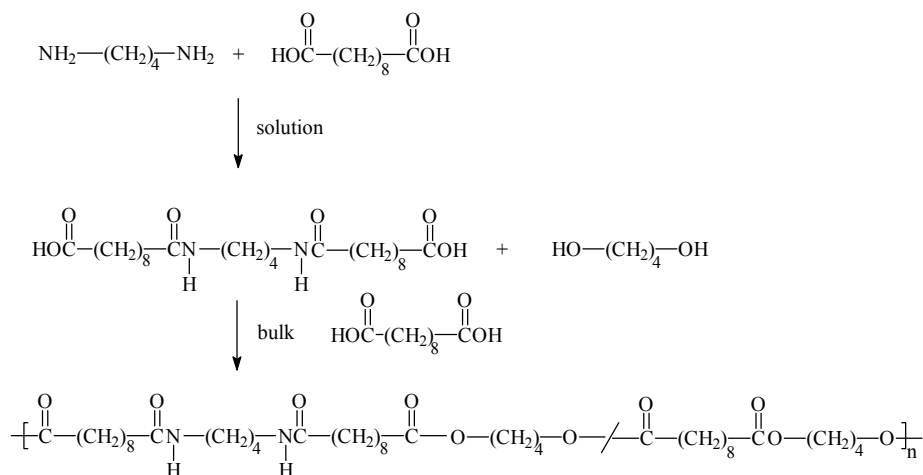
prepared by ring-opening (scheme 2.9A) and alternating poly(ester amide)s (scheme 2.3) are in between those of the corresponding polyamide and polyester. Incorporation of tartaric acid moieties in the polymer backbone (scheme 2.7) affords polymers with high melting and glass transition temperatures. By increasing the ester content from 0 to 20 mol% the melting and glass transition temperature decreased from 232 to 204 °C and from 116 to 59 °C, respectively ⁴⁶. Likewise the modulus decreased from 1600 to 500 MPa and the tensile strength decreased from 53 to 31 MPa. Polymer films, exposed to 100% relative humidity for 72 h, showed a moisture sorption of 8 to 15% with the sorption decreasing with increasing ester content. Perez *et al.* synthesized similar polymers (scheme 2.7) with 0, 3 and 10 mol% of succinate ester groups ⁴⁵. The melting temperature decreased from 230 to 214 °C and the glass transition temperature decreased from 106 to 90 °C by increasing the ester content from 0 to 30 mol%. Correspondingly, the modulus decreased from 1800 to 1250 MPa, the yield stress decreased from 63 to 54 MPa while the strain at break increased from 130 to 200%. The plasticizing effect of water is clearly manifested in the decrease of both yield stress (~30%) and elastic modulus (~40%) and in the increase of strain at break after exposure to 100% relative humidity.



Scheme 2.7: Interfacial polymerization of bisester-diesters, diamines and activated diacids affording random poly(ester amide)s with $R_2 = \text{H}$, OCH_3 and $\text{X} = \text{pentachlorophenyl}$.

Random poly(ester amide)s, prepared from a diamide-diacid, 1,4-butanediol and sebacic acid (scheme 2.8), with amide contents ranging from 10 to 30 mol% revealed two melting endotherms. The higher melting endotherm is a result of the introduction of

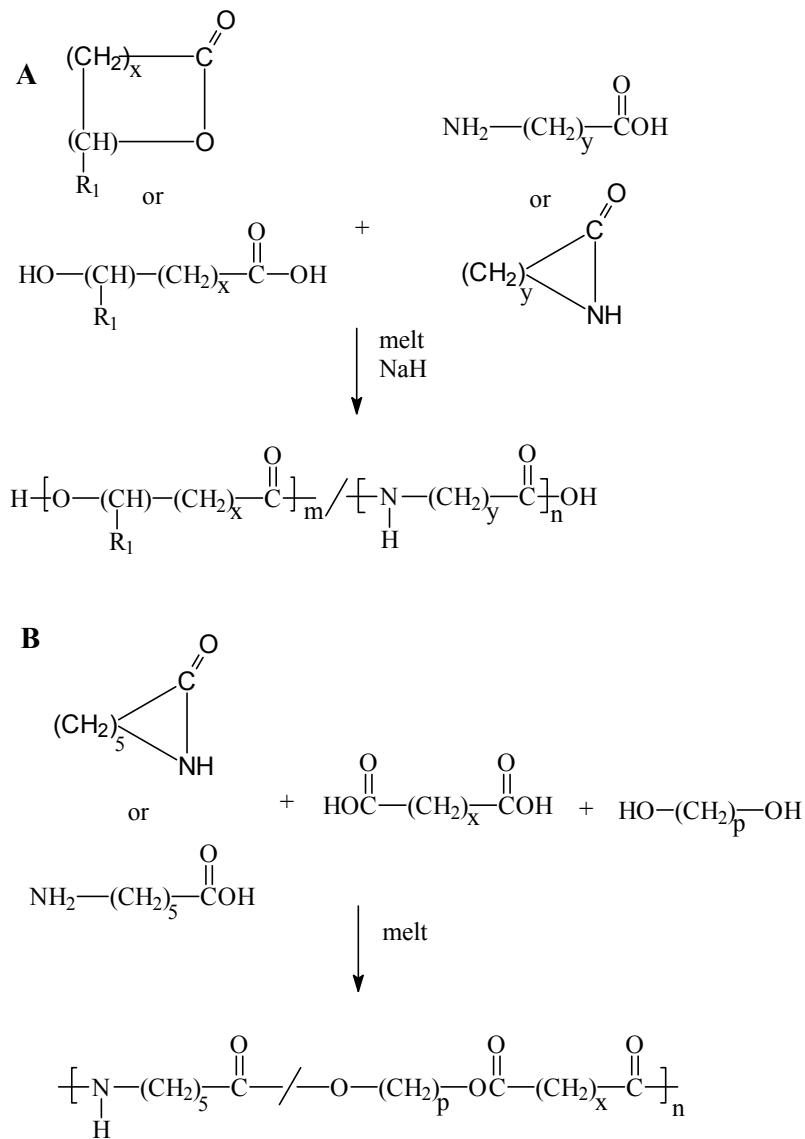
amide segments. The glass transitions shift to higher temperatures as the amide content increases, indicating a homogeneous amorphous phase. IR-spectra showed the presence of H-bonds between amide and ester units as well as between amide units. However, by increasing the amide content (> 10 mol%), H-bonds are mainly observed between amide groups ⁴⁷.



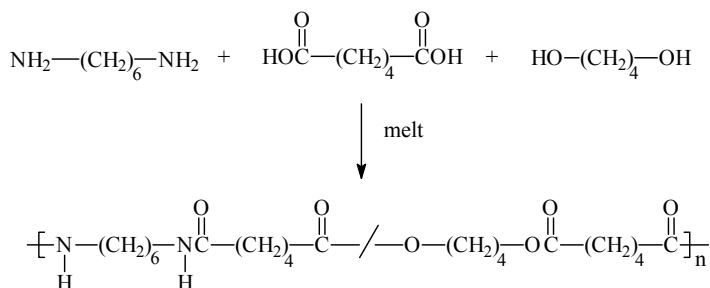
Scheme 2.8: Random poly(ester amide)s prepared from bisamide-diacids, di-acids and diols.

Random poly(ester amide)s based on 11-amino undecanoic acid and ϵ -caprolactone or lactic acid with amide contents of 40-75 mol% were prepared by solution polymerisation (scheme 2.9A) ^{50, 51}. The polymer based on ϵ -caprolactone showed a diffraction pattern similar to the α -form of nylon 11 ⁵¹. With increasing amide content the diffraction peaks become more pronounced. The lactic acid based poly(ester amide)s with an amide content of 40 to 60 mol% showed a diffraction pattern very similar to the γ -form of nylon 11, while increasing the amide content to 75 mol% caused a change in the diffraction pattern resembling the α -form of nylon 11 ⁵⁰. With increasing ester content a decrease in crystallinity was observed which is most likely due to the insertion of ϵ -caprolactoyl or lactyl units into the nylon 11 lattices. Such poly(ester amide)s with an amide segment content of 60 mol% have 3 melt transitions and it is suggested that a

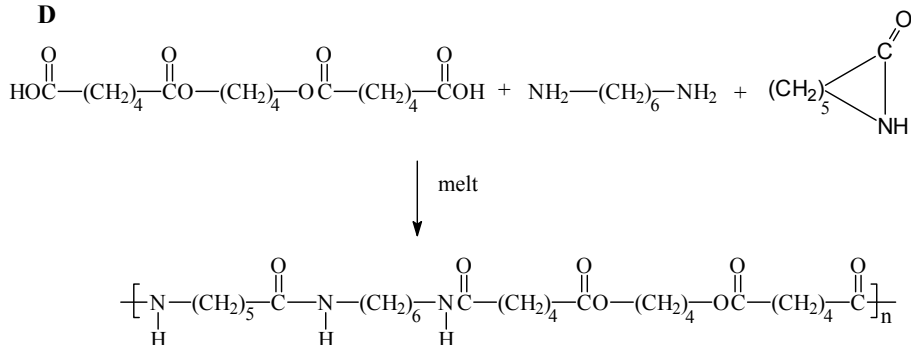
typical micro-phase separated structure is present, including an ester rich phase, a middle phase composed of ester and amide segments and an amide rich phase.



C



D

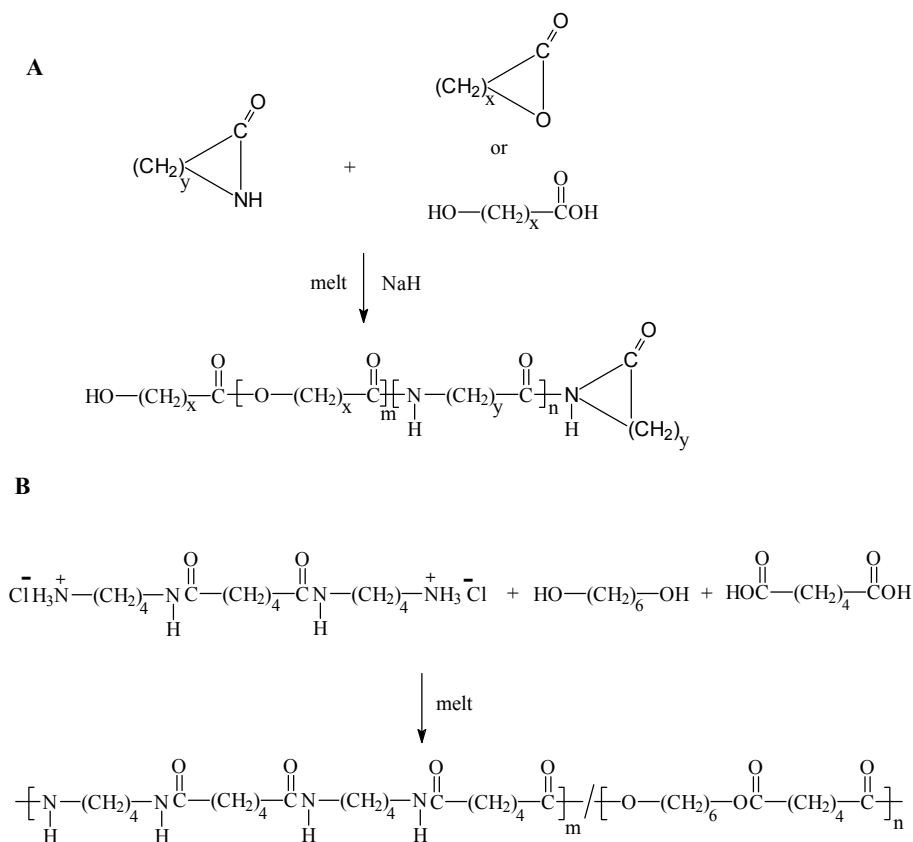


Scheme 2.9: Combined ring-opening and/or polycondensation of monomers to give poly(ester amide)s with A: $x = 0$ or 4; $R_1 = \text{H}$ or CH_3 ; $y = 5$ -10 and B: $x = 2$ -4; $p = 4, 6$.

As ring-opening polymerization of lactones and lactams is an attractive alternative route to prepare random poly(ester amide)s, several groups have focused on a possible commercialization of this class of polymers. Random poly(ester amide)s based on ϵ -caprolactone and ϵ -caprolactam, with an amide content varying from 25 to 90 mol%, are conveniently prepared by anionic ring opening polymerization (scheme 2.9A) ⁴⁹. The poly(ester amide)s have a single melting temperature with an eutectic minimum at an amide content of 45 mol%. The stress at break increased from 13 to 61 kPa while the strain at break decreased from 609 to 320% with increasing amide content (25-90 mol%).

In recent years many random poly(ester amide)s have been prepared according to this methodology (scheme 2.9B-D) ^{39, 52-55}. One example given here are poly(ester amide)s based on ϵ -caprolactam, adipic acid and 1,4-butanediol (scheme 2.9B) with amide

contents of 50 to 70 mol% ³⁹. As the amide content increased to 70 mol% the melting and glass transition temperature increased from 120 to 160 °C and from -20 to 1 °C, respectively. Correspondingly, the modulus, tensile strength and strain at break increased from 128 to 285 MPa, 11 to 29 MPa and 24 to 432%, respectively. IR studies revealed the presence of ester-amide H-bonds as well as amide-amide H-bonds. BAK 1095, a commercial semi-crystalline transparent poly(ester-amide) based on ϵ -caprolactam, adipic acid and 1,4-butanediol (scheme 2.9B) with an amide content of 60 mol% is easily processed and is suitable for a wide range of applications ⁵²⁻⁵⁴. The melting temperature is 125 °C, the modulus is 180 MPa and the strain at break is 400%.



Scheme 2.10: Random (partially block) poly(ester amide)s by ring-opening copolymerization of lactams and lactones or from diols, diacids and bisamide-diamine salts with A: x = 5,11; y = 5,11.

Diblock poly(ester amide)s were prepared from ω -lauractam and ϵ -caprolactone by an anionic ring opening reaction in the presence of sodium hydride (scheme 2.10A) ⁵⁶. However, the polymers show at least a partly random structure, which is attributed to the occurrence of base-catalysed ester-amide interchange reactions and scission of ester bonds by free lactamate anions present. Polymers with an amide content ranging from 30 to 90 mol% crystallize into a γ -form as observed in nylon 12. At low amide content (20 mol%) the poly(caprolactone) is crystallizing. IR-spectra of these polymers indicate the co-existence of ester-amide and amide-amide H-bonds.

Goodman also prepared diblock poly(ester amide)s based on ϵ -caprolactam and ϵ -caprolactone (scheme 2.10A) in the presence of the sodium salt of ϵ -caprolactam ⁵⁷⁻⁵⁹. Polymers with amide contents ranging from 10 to 90 mol% are crystalline over the entire range of compositions. By decreasing the amide content from 90 to 20 mol% the melting temperature decreased from 220 to 50 °C with the latter being an eutectic minimum. Simultaneously, the glass transition temperature decreased from 55 to -60 °C, which indicates the miscibility of the ester and amide sequences in the amorphous state ⁵⁷. Polymers with an amide content of 10 to 40 mol% give separate co-existing crystalline polyamide and polyester phases. Poly(ester amide)s with more than 50 mol% of amide content showed crystals similar to nylon 6. By increasing the amide content from 20 to 90 mol%, the initial modulus and stress at break increased from 215 to 470 MPa and from 34 to 45 MPa, respectively ⁵⁸. However, minima were detected at 25-40 mol% of amide content with a modulus of 90 MPa and a stress at break of 13 MPa. The strain at break was highest (1200%) at 25-40 mol% of amide content. Similar polymers based on 12-hydroxydodecanoic acid and ϵ -caprolactam (scheme 2.10A) with varying amide/ester ratios have been prepared with up to 20 mol% of amide units, the polymers are highly crystalline and are essentially modified polyesters with isolated amide units H-bonded to the ester groups ⁶⁰. Polymers with 20 to 60 mol% show a random dispersion of micro-blocks without clear indications of phase separation. Above 60 mol% of amide units, the polymers contain a discrete crystalline amide phase. This is in contrast to the poly(ester amide)s based on ω -lauractam and ϵ -caprolactone ⁵⁶, which displayed an amide crystalline phase for polymers with an amide content of 20 mol% and higher. Random poly(ester amide)s based on 1,6-hexanediol, adipic acid and bisamide-diamine salt

(scheme 2.10B) were prepared. By increasing the amide content from 5.5 to 28.5 wt% the melting and glass transition temperatures increased from 143 to 225 °C and from -41 to 0 °C, respectively. With increasing 1,6-hexanediol content, these copolymers show a progressive reduction in melting temperature as compared to nylon 6,6 with no indication of an eutectic minimum as was seen for the polymers based on ϵ -caprolactam and ϵ -caprolactone (scheme 2.10A). Only the poly(ester amide) with 5.5 wt% of amide content showed dual melting and crystallization peaks, suggesting the co-existence of separate polyamide and polyester crystalline phases. The amorphous phase is homogeneous as was indicated by the increasing glass transition temperature. The shear modulus at 21 °C increased from 79 to 340 MPa with increasing amide content (5.5 to 28.5 wt%)^{61, 62}.

Degradation

The increasing interest in poly(ester amide)s as biodegradable materials for environmental and biomedical applications also prompted researchers to study the (bio)compatibility of the polymers, the biodegradation process and changes in physical and mechanical properties of the polymer during degradation and cellular interactions.

In general, the hydrolysis of ester linkages in polymers in buffer solution (pH 7.4) at room temperature takes place at a low rate^{2, 10, 13, 18, 36, 43, 45-47, 49, 51, 63}. At elevated temperatures^{1, 10, 18, 36, 39} and at low or high pH values^{10, 18}, the degradation rate increases and bulk degradation with even the occurrence of surface to center segregation has been observed. Since the hydrolysis of polymers occurs almost entirely in the amorphous region the crystallinity of the poly(ester amide)s is important. If dissolution of oligomers takes place the crystallinity of the residual polymer may increase and this will lead to changes in the fraction of ester-amide H-bonds.

To enhance the rate of polymer degradation, enzymes are added to the buffer solution. Enzymes probably involved in the degradation of poly(ester amide)s are proteolytic enzymes (proteases), esterases but also lipases^{64, 65}. Proteases, like papain and proteinase K, hydrolyse peptide (amide) bonds and sometimes ester bonds. Lipases (from *Rhizopus Arrhizus*, *Rhizopus Delemar* or *Candida Cylindracea*) are members of the esterase family, which are involved in hydrolysis of esters. Lipases catalyse the hydrolysis of triglycerides into diglycerides, monoglycerides, glycerol and fatty acids.

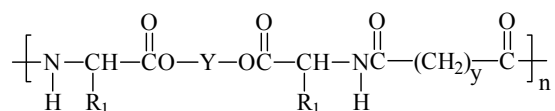
However, some lipases are also capable of hydrolysing polyesters to oligomeric or monomeric products.

Alternating poly(ester amide)s

The hydrolytic and enzymatic degradation of alternating, amino acid containing poly(ester amide)s (scheme 2.11), has been systematically investigated by Rodriguez-Galan and Puiggali^{5, 6, 8-11, 18, 36, 39, 66}. Comparative studies between polymers with a different architecture remain scarce but are becoming available and examples will be discussed. Polymer films, exposed to buffers at different pH values, degrade extremely slowly and the degradation rate increases with decreasing crystallinity and increasing temperature as expected^{10, 18, 36}. All these poly(ester amide)s degrade faster in the presence of enzymes. Proteinase K, lipase, papain and α -chymotrypsin were typical enzymes applied in these studies.

Paredes *et al.* extensively studied the enzymatic degradation of glycine and L-alanine based poly(ester amide)s. All polymers showed a high susceptibility to degradation in the presence of papain^{5, 6, 9-11, 36, 66}. When the α -amino acid was substituted for 4-aminobutyric acid the degradation rate decreased which is ascribed to the presence of H-bonds between ester and amide bonds¹⁴. Appreciable differences in the degradation rates were observed between stereoregular and racemic polymers and it was found that papain hydrolyses the amide functional group when the naturally occurring L-amino-acid is incorporated⁶⁶.

Nagata investigated the enzymatic degradation of poly(ester amide)s based on 1,6-hexanediol, sebacoyl chloride and mixtures of L- and D-alanine (scheme 2.11)⁴. Papain and proteinase K preferentially degrade poly(ester amide)s comprising L-alanine instead of D- alanine moieties. However, degradation mainly takes place by ester cleavage.



Scheme 2.11: Alternating poly(ester amide) synthesis from monomers comprising amino acid moieties with $R_1 = \text{H}, \text{CH}_3$ (L, D, LD), $\text{CH}_2\text{C}_6\text{H}_5$, $\text{CH}(\text{CH}_3)_2$, $\text{CH}_2\text{CH}(\text{CH}_3)_2$, $\text{CH}(\text{CH}_3)\text{CH}_2\text{CH}_3$, $(\text{CH}_2)_3\text{CH}_3$, $(\text{CH}_2)_2\text{SCH}_3$; $\text{Y} = (\text{CH}_2)_{2-12}$, $((\text{CH}_2)_2\text{O})_n(\text{CH}_2)_2$, dianhydrosorbitol or dianhydromannitol; $y = 2-10$.

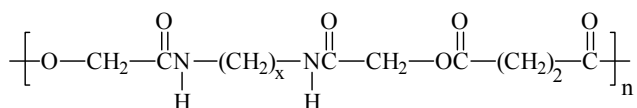
In other studies, a wide range of alternating poly(ester amide)s based on amino-acids (scheme 2.11) were subjected to buffer solutions (pH 7.4) at 37 °C containing α -chymotrypsin^{12, 15}. From these studies it was concluded that an increase in the hydrophobic chain length of the diol or diacid moieties increases the rate of degradation of these polymers. The poly(ester amide)s based on L-phenylalanine showed the highest tendency toward α -chymotrypsin catalysed hydrolysis, while the hydrolysis of the poly(ester amide) containing both the L and D isomers occurred at a lower rate. Similar alternating poly(ester amide)s based on amino-acids and dianhydrosorbitols (scheme 2.11) were subjected to buffer solutions (pH 7.4) at 37 °C containing α -chymotrypsin or lipases. Also in this study the L-phenylalanine based polymer revealed the highest tendency toward α -chymotrypsin catalysed hydrolysis. Lipase was found to be as effective as α -chymotrypsin in the hydrolytic degradation of the polymers.

Alternating poly(ester amide)s based on glycine or alanine, dianhydrosorbitol as the diol and activated dicarboxylic acid esters with methylene chain lengths of 4-10 (scheme 2.11) were exposed for 24 h to a buffer solution (pH 7.0) at 37 °C containing papain or the lipase of a Porcine Pancreas¹⁷. Poly(ester amide)s containing dicarboxylic acid components with a methylene chain length of 4 degraded more readily in the presence of the lipase than the corresponding polyesters. Most of the poly(ester amide)s degraded more rapidly in the presence of papain compared to the corresponding polyesters. The poly(ester amide)s with an odd numbered methylene chain length were less readily degraded by papain. These polymers were also subjected to an environmental degradation study. Polymer films were either buried in soil in a dessicator at 27 °C (relative humidity of 70-80%) or exposed to an activated sludge at 25 °C for 4 d after

which the biological oxygen demand (BOD) was measured. In general, the poly(ester amide)s degraded more slowly than the corresponding polyesters having the same aliphatic dicarboxylic acid unit, both in composted soil and in activated sludge.

A considerable effort has been made to obtain biodegradable polymers with appropriate properties for biomedical applications such as bioabsorbable sutures, bone fixation and implants. Only a few studies of poly(ester amide)s with respect to cytotoxicity, biocompatibility and cell material interaction are available up to now. Paredes *et al.* studied the biocompatibility and cytotoxicity of alternating poly(ester amide)s prepared from L-alanine, 1,12-dodecanediol and sebacic acid chloride (scheme 2.11) ¹⁰. Mouse fibroblast adhered and proliferated on the poly(ester amide)s films. Polymer extracts were also evaluated and no cytotoxic responses were detected after a 24 and 48 h incubation period, but the cytotoxic response increased after 72 h of incubation. After 50 days of exposure to a PBS buffer at 37 °C, the polymer was partially degraded and the oligomers formed might have caused the toxic response. The proliferation of human dermal fibroblast on 4-aminobutyric acid or glycine based poly(ester amide)s films (scheme 2.11) after 7 d of culturing at 37 °C was also studied ¹⁴. The cells proliferated faster on polymer films derived from 4-aminobutyric acid than on poly(ester amide)s derived from glycine. The higher hydrophilicity (lower contact angle) of the 4-aminobutyric acid derived polymer films seems to favour the growth of human dermal fibroblasts.

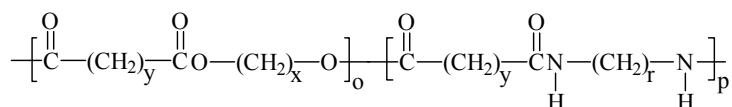
In studies towards new biomedical materials with fibre forming properties Barrows investigated the *in vivo* resorption of poly(ester amide)s based on glycolic acid, a diaminoalkane containing two to twelve methylene groups and succinyl chloride (scheme 2.12) ²⁹. The principal mechanism of *in vivo* degradation appears to be hydrolysis of the ester bonds. This produces the bisamide-diol monomer as a major metabolite, which is non-toxic as determined by LD₅₀ test in rats. In separate experiments the 1,6-diaminohexane based bisamide-diol monomer and the corresponding polymer showed no evidence of acute cytotoxicity.



Scheme 2.12: Poly(ester amide)s synthesized from a diaminoalkane ($x = 2-11$), glycolic acid and succinyl chloride.

Segmented poly(ester amide)s

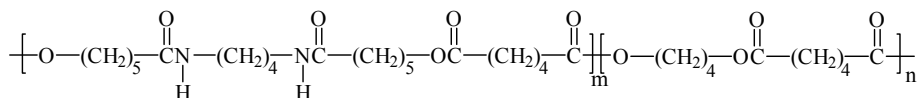
Segmented poly(ester amide)s (scheme 2.13) with varying amide/ester ratios were subjected for 24 h to buffer solutions (pH 7.0) at 37 °C containing lipases from *Rhizopus Arrhizus*, *Rhizopus Delemar* or *Candida Cylindracea*, or the proteases trypsin or α -chymotrypsin⁴². The polymers were hydrolyzed by lipases whereas the proteases did not degrade the polymers. Both hydrophilicity and rigidity of the poly(ester amide)s are the main factors controlling the rate of degradation. Poly(ester amide)s with a short methylene chain length in the ester component showed a low biodegradability. The rate of degradation of the polymers, exposed to an activated sludge, increased with decreasing amide content, which is in agreement with the enzymatic degradation results.



Scheme 2.13: Segmented poly(ester amide)s with $y = 2-4$; $x = 2-10$; $r = 2-6$.

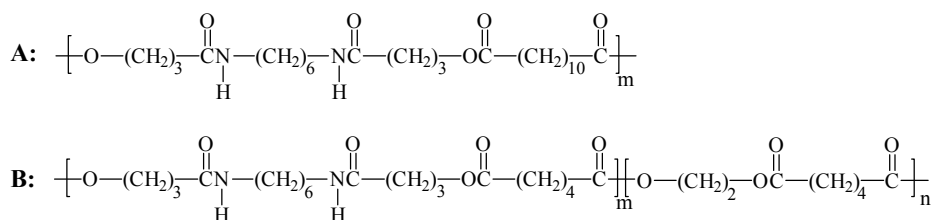
Segmented poly(ester amide)s based on 1,4-diaminobutane, ϵ -caprolactone, 1,4-butanediol and dimethyl adipate (scheme 2.14) were rapidly and completely degraded in a modified Sturm test⁶⁷. This test provides data on the mineralization of degradation products, i.e. their conversion to CO₂. The degradation rate decreased with increasing amide content. Soil burial tests of polymer films revealed that polymers with less than 30 mol% of amide units were completely disintegrated in ~35 days. Analysis of the degraded samples showed that polymer degradation takes place on the surface as well as in the bulk of the material and in amorphous as well as in crystalline regions. Degradation studies using lipases from *Aspergillus Niger* and *Rhizopus Arrhizus* showed that segmented poly(ester amide)s with 10 to 30 mol% of hard segment (m) were fully

degradable. Within 8 days the residual weight of poly(ester amide) dense films (thickness = ~ 0.5 mm) with 10 and 20 mol% of hard segment was less than 5% while polymers with 30 mol% of hard segment had a residual weight of 60 to 85%. This illustrates that degradation mainly proceeds through cleavage of ester bonds and that monomers and oligomers containing amide segments were released from the material and became solubilized, thus preventing accumulation of amide segments in the residual polymer.



Scheme 2.14: Segmented poly(ester amide)s based on 1,4-diaminobutane, ϵ -caprolactone, 1,4-butanediol and dimethyl adipate.

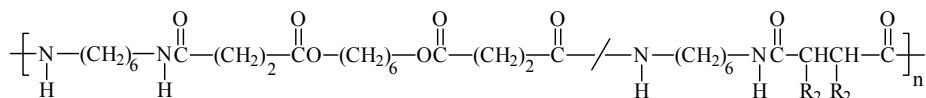
In vivo studies on high molecular weight segmented poly(ester amide)s indicate that these polymers are biocompatible and degrade to some extent (scheme 2.15B) ⁶³. A comparison with alternating poly(ester amide) oligomers (scheme 2.15A) showed that after 30 days of subcutaneous implantation in a rat, polymer films prepared from the alternating poly(ester amide) oligomer were completely fragmented while the segmented poly(ester amide) films were encapsulated. However, it should be emphasized that the alternating poly(ester amide)s have a much lower molecular weight. Both films from oligomer and polymer were resorbed after three months of implantation.



Scheme 2.15: An alternating poly(ester amide) (A) based on 1,6-diaminohexane, γ -butyrolactone and 1,10-decanedicarboxylic acid and a segmented poly(ester amide) (B) based on 1,6-diaminohexane, γ -butyrolactone, 1,2-ethanediol and adipic acid.

Random poly(ester amide)s

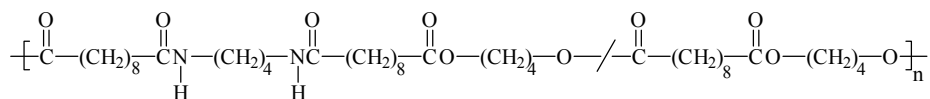
The hydrolytic degradation of poly(ester amide)s based on tartaric acid (scheme 2.16) in PBS (pH 7.4) at 37 °C showed a noticeable decrease in molecular weight and tensile properties in time (8 h to 70 days) ⁴⁵. Variations in glass and melting temperatures appeared to be minor, whereas the crystallinity increased with incubation time. In another study poly(ester amide)s based on tartaric and succinic acid (scheme 2.16) have been investigated for their hydrolytic degradation over a period of 0-25 wks ⁶⁸. The molecular weight decreased rapidly in the first two months of incubation and complete erosion was found for both polymers. The degradation takes place essentially through cleavage of the ester bonds, and is accompanied by formation of cyclic succinimide units due to an intramolecular imidation.



Scheme 2.16: Random poly(ester amide)s based on 1,6-diaminohexane, succinic acid, 1,6-hexanediol and tartaric or succinic acid ($\text{R}_2 = \text{H}, \text{OCH}_3$).

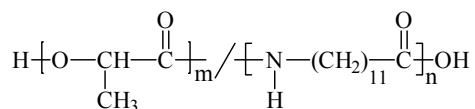
Random poly(ester amide)s based on a bisester-diamine (1,6-hexanediol and glycine or L-alanine), 1,12-dodecanediamine and sebacoyl chloride were exposed to a buffer solution at 37 °C containing papain and proteinase K. Fastest degradation was observed for the polymers derived from L-alanine. The same polymers exposed to buffer solutions (pH 7.4) at 37 °C degraded very slowly which confirmed the enzymatic catalysis ¹³.

As concluded above, degradation rates are generally faster at high ester content, but also the opposite has been observed. Lee *et al.* showed that the rate of hydrolytic degradation of random copolymers with amide contents ranging from 10 to 30 mol% (scheme 2.17) in a buffer solution (pH 11) at 35 °C increased with increasing amide content due to the enhanced hydrophilicity ⁴⁷.



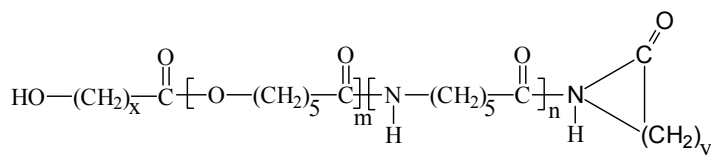
Scheme 2.17: Random poly(ester amide)s prepared from 1,4-diaminobutane, 1,4-butanediol and sebacic acid.

Random poly(ester amide)s based on 11-amino undecanoic acid and lactic acid (scheme 2.18) were exposed to PBS buffer (pH 7.2) at 37 °C up to a period of one year ^{50, 51}. The hydrolytic degradation proceeded mainly through cleavage of ester bonds and decreased with increasing amide content. The melting temperature and crystallinity of the polymers initially increased while after 135 days they started to decrease.



Scheme 2.18: A random poly(ester amide) based on 11-amino undecanoic acid and lactic acid.

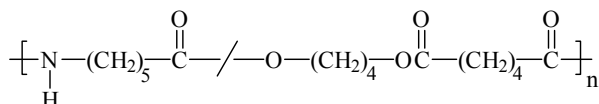
Random poly(ester amide)s (amide content 19-46 wt%) (scheme 2.19) films based on ϵ -caprolactam and ϵ -caprolactone were incubated with buffer solutions (pH 7.4) at 37 °C containing protease, collagenase, α -chymotrypsin or pancreatin ⁶⁹. The first three enzymes mentioned had no visible effect on any of the polymer films, and there was no significant evidence, with any enzyme or substrate, of the formation of amino acids as a product of amide bond splitting. In contrast, incubation with pancreatin caused surface erosion of these poly(ester amide)s, with depletion of the ester group content in the surface layer and the development of an amide rich striated surface morphology.



Scheme 2.19: A block poly(ester amide) based on ϵ -caprolactam and ϵ -caprolactone.

Comparative studies

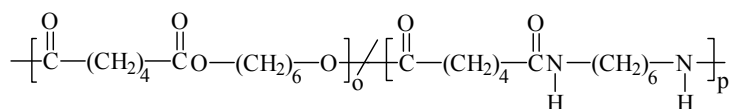
In a recent paper Botines *et al.* compared the hydrolytic and enzymatic degradation of two types of polymers both derived from 1,4-butanediol, adipic acid and 1,6-aminohexanoic acid or ϵ -caprolactam¹⁸. Alternating poly(ester amide)s very similar to Puiggali *et al.* were prepared by using 1,6-aminohexanoic acid instead of an α -amino acid (analogous as given in scheme 2.11). The other polymer was a random poly(ester amide) (scheme 2.20) from Bayer under the trade name BAK1095. An important conclusion was that the alternating poly(ester amide) was more stable than the random poly(ester amide)s to hydrolytic as well as enzymatic degradation. The regular sequence as found in alternating poly(ester amide)s leads to an increase in crystallinity and consequently the degradation rate decreases.



Scheme 2.20: A random poly(ester amide) (BAK1095) based on 1,4-butanediol, adipic acid and 1,6-aminohexanoic acid.

In another study, both hydrolytic degradation and degradation by fungi of random poly(ester amide)s prepared by interfacial polymerization of 1,6-hexanediamine, adipoyl chloride and 1,6-hexanediol (scheme 2.21) and diblock poly(ester amide)s prepared by ring-opening polymerization of ϵ -caprolactone and ϵ -caprolactam (scheme 2.19) has been investigated⁴⁹. Both poly(ester amide)s, with an amide content of ~ 55 mol%, were subjected to buffer solutions (pH 7.4) at 37 °C for 6-8 months. After 165 days of degradation the random poly(ester amide)s showed a weight loss of $\sim 7\%$ and a molecular weight reduction of $\sim 50\%$ while the diblock poly(ester amide) showed a

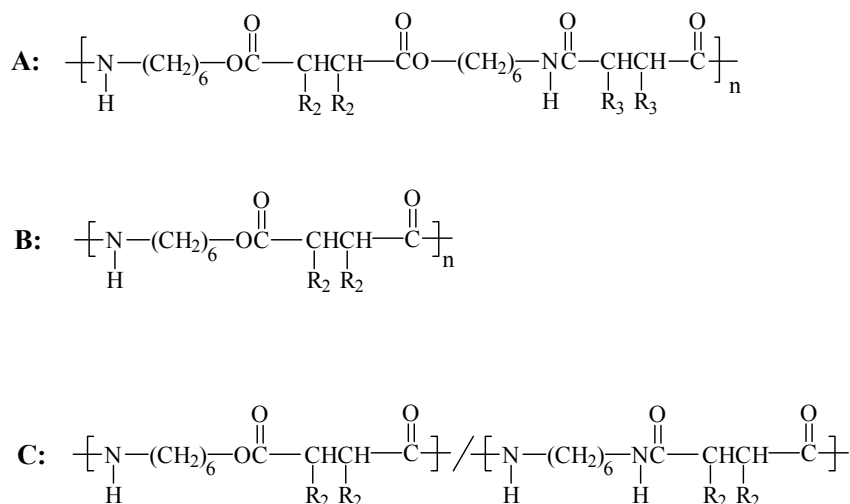
weight loss of $\sim 2.5\%$ and a molecular weight reduction of $\sim 15\%$. Similar to Botines *et al.* the presence of regular sequences as found in diblock poly(ester amide)s decreases the rate of degradation. The polymers were also subjected to solid agar media containing either the microorganism *Fusarium Moniliforme* or *Aspergillus Niger* (incubated at $25\text{ }^{\circ}\text{C}$). After 60 days, polymer films exposed to *Fusarium Moniliforme* were eroded and bulk degraded while polymer films exposed to *Aspergillus Niger* only showed a slight surface erosion. The degraded polymer samples were analyzed with IR to discover structural changes. Both polymers, degraded in the presence of *Fusarium Moniliforme*, showed a significant decrease in ester absorption intensity while no significant decrease in intensities of both amide I and II bands was observed thus indicating degradation via cleavage of ester bonds. The hydrolytic degradation in buffer solution (pH 7.4) at $37\text{ }^{\circ}\text{C}$ is much slower than the degradation in a solid agar media containing *Fusarium Moniliforme*. Both polymer films were also subjected to a basal mineral broth containing yeast, *Cryptococcus Laurentii* at $20\text{ }^{\circ}\text{C}$ ⁷⁰. The diblock copolymer showed a weight loss of $\sim 50\%$ after 19 days while the random poly(ester amide) showed a weight loss of $\sim 55\%$ after 28 days. The random poly(ester amide) was melt spun into polymer fibres and also subjected to a broth containing *Cryptococcus Laurentii* for 30 days. The tensile strength of the polymer decreased from 3.1 to 2.0 kPa while the elongation at break decreased from 500 to 10%. The mechanical properties of fibres remained unchanged after 40 days of treatment in buffer solution (pH 7.4) at $22\text{ }^{\circ}\text{C}$.



Scheme 2.21: Random poly(ester amide)s prepared from 1,6-diaminohexane, adipoyl chloride and 1,6-hexanediol.

Villuendas *et al.* investigated the influence of chemical composition and microstructure on the degradability of poly(ester amide)s derived from amino alcohols and/or diamines and diacids (scheme 2.22) ^{1, 2}. Poly(ester amide) films were exposed to a buffer solution (pH 7.4) at $37\text{ }^{\circ}\text{C}$ for 190 days. The rate of degradation increased significantly by increasing the ester content and by incorporation of di-O-methyl-L-tartaric acid units.

Only poly(ester amide)s containing diacid units with 4 methylene groups degraded in a buffer solution. It was demonstrated that the regicity, i.e. the relative orientation of the monomeric units along the main chain, is critical in the degradation behaviour of the poly(ester amide)s (scheme 2.22). The sample weight and molecular weight of alternating syndioregic poly(ester amide)s, prepared from preformed bisester-diamines and di-O-methyl-L-tartaric or succinic acid, were found essentially unaltered after eight months. On the contrary, the molecular weight of the alternating isoregic poly(ester amide)s, prepared from 6-aminohexanol and di-O-methyl-L-tartaric or succinic acid, decreased to less than one-third of its initial value after two months. The random aregic poly(ester amide), prepared from 1,6-hexane diamine, 6-aminohexanol and di-O-methyl-L-tartaric or succinic acid, degraded faster than the isoregic variant, despite the lower content of ester linkages. This effect is probably caused by the lower crystallinity of the aregic polymer. Both isoregic and aregic poly(ester amide)s containing four-carbon diacid units degrade through a mechanism implying cyclization to imides, probably by an intra-molecular amidolysis reaction. This mechanism is unable to operate if the polymer chain has an entirely syndioregic microstructure.



Scheme 2.22: Syndioregic (A), isoregic (B) and aregic (C) poly(ester amide)s comprising tartaric or succinic acid moieties ($R_2 = \text{H}, \text{OCH}_3$; $R_3 = \text{H}, \text{OCH}_3$).

Conclusions

Poly(ester amide)s distinguish themselves from aliphatic polyesters, which are biodegradable but often lack good mechanical and physical properties. Moreover, aliphatic polyamides do have good mechanical properties but are not biodegradable. The combination of ester and amide groups in poly(ester amide)s affords polymers with adequate properties and the required biodegradability. In this respect a wide variety of aliphatic poly(ester amide)s have been developed in the last decade. The placement of amide and ester groups along the polymer chain can be regulated and alternating, segmented (block) and random polymers have been prepared depending on the starting compounds and procedures applied. Two different strategies have been followed; placing the amide groups randomly in the polymer chain or incorporate well-defined bisamide containing blocks or segments. The latter strategy can give alternating or segmented poly(ester amide)s which are generally prepared from preformed monomers like bisester-diamines, bisamide-diols and bisamide-diesters.

A series of alternating, segmented and random poly(ester amide)s were prepared in the past two decades. In most cases, these poly(ester amide)s show melting temperatures in between those of the corresponding polyester and polyamide which increase with increasing amide content. However, some segmented (block) poly(ester amide)s show one crystalline phase independent of the amide content. Segmented and random polymers with a high ester content possess two crystalline phases with characteristic melting temperatures of the corresponding polyester and polyamide. The crystallinity depends on the regularity of the units in the polymer chain and is lower in random poly(ester amide)s as compared to segmented and alternating poly(ester amide)s. Alternating poly(ester amide)s prepared from bisester-diamines based on amino acids and random poly(ester amide)s based on ϵ -caprolactone or lactic acid crystallize very similar to nylons. Poly(ester amide)s, which are poorly phase separated, have one glass transition temperature which increases with increasing amide content. Most poly(ester amide)s show structural organization through hydrogen bonding with H-bonds present between amide groups and amide-ester groups. In general, the modulus and tensile strength of the poly(ester amide)s increase while the elongation decreases with increasing amide content.

The hydrolysis of ester linkages in poly(ester amide)s in buffer solution (pH 7.4) at room temperature was found to take place at a low rate. This degradation rate increases at elevated temperatures, low or high pH values and in the presence of enzymes. Alternating poly(ester amide)s based on amino acids show a high susceptibility to degradation in the presence of papain. In addition, the L-amino acid based polymers degrade faster in the presence of papain and α -chymotrypsin compared to polymers comprising D-amino acid residues. Alternating and segmented poly(ester amide)s were more stable to hydrolytic and enzymatic degradation than random poly(ester amide)s. Environmental degradation studies on poly(ester amide)s in the presence of lipases or when exposed to composted soil or activated sludge revealed that these polymers were readily degraded.

It can be concluded that incorporation of amide units in the polyester chain is a way to improve their physical and mechanical properties. Such polymers may fulfil the necessary requirements to be applicable as environmentally degradable materials or as implants in the biomedical field. Therefore, the development of new poly(ester amide)s that combine good mechanical performance and physical properties, low prize, safe manufacturing and processing methods and complete (controlled) biodegradability, all in relation to the intended applications, remains necessary. A strategy that can be followed is the design of poly(ester amide)s with a well-defined structure that allows a detailed analysis of the relationship between properties and structure. In addition, a better understanding of the relationships between polymer structure, polymer morphology and biodegradation properties could be achieved by carefully investigating the complete biodegradation process using well characterized polymer materials. Comparative studies using well-controlled and standardized conditions are of utmost importance.

References

1. I. Villuendas, *Macromol. Chem. Phys.*, **2001**, 202, (2), 236.
2. I. Villuendas, *Macromolecules*, **1999**, 32, 8033.
3. S.M. Aharoni, *Macromolecules*, **1988**, 21, (7), 1941.
4. M. Nagata, *Macromol. Chem. Phys.*, **1999**, 200, (9), 2059.
5. J. Montane, J. Puiggali, *J. Appl. Polym. Sci.*, **2002**, 85, 1815.
6. N. Paredes, J. Puiggali, *J. Polym. Sci. Part A: Polym. Phys.*, **2001**, 39, 1036.

7. N. Paredes, M.T. Casas, J. Puiggali, *Macromolecules*, **2000**, 33, (24), 9090.
8. N. Paredes, J. Puiggali, B. Lotz, *J. Polym. Sci. Part A: Polym. Phys.*, **1999**, 37, 2521.
9. N. Paredes, J. Puiggali, *J. Polym. Sci. Part A: Polym. Chem.*, **1998**, 36, 1271.
10. N. Paredes, J. Puiggali, *J. Appl. Polym. Sci.*, **1998**, 69, 1537.
11. L. Asin, J. Puiggali, *J. Polym. Sci Part A: Chem.*, **2001**, 39, 4283.
12. N. Arabuli, R. Katsarava, *Macromol. Chem. Phys.*, **1994**, 195, 2279.
13. E. Armelin, J. Puiggali, *Polymer*, **2001**, 42, 7923.
14. S. Han, S.S. Im, *Biomaterials*, **2003**, 24, 3453.
15. R. Katsarava, *J. Polym. Sci. Part A: Polym. Chem.*, **1999**, 37, 391.
16. Z. Gomurashvili, R. Katsarava, *J. Mat. Sci.: Pure Appl. Chem.*, **2000**, A37, (3), 215.
17. M. Okada, *J. Appl. Polym. Sci.*, **2001**, 81, 2721.
18. E. Botines, J. Puiggali, *Polymer*, **2002**, 43, 6073.
19. H.R. Stapert, A.M. Bouwens, P.J. Dijkstra, J. Feijen, *Macromol. Chem Phys.*, **1999**, 200, (8), 1921.
20. H.R. Stapert, P.J. Dijkstra, J. Feijen, *Macromol. Symp*, **1998**, 130, 91.
21. S. Katayama, T. Murakami, *J. Appl. Polym. Sci.*, **1976**, 20, 975.
22. S. Katayama, H. Horikawa, *J. Appl. Polym. Sci.*, **1971**, 15, 775.
23. K. Brandt, T. Latawiec, *Bull. Polish Academy Sci. Chem.*, **1989**, 37, (3-4), 141.
24. S. Bera, Z. Jedlinski, *J. Polym. Sci. Part A: Polym. Chem.*, **1993**, 31, (3), 731.
25. S. Bera, Z. Jedlinski, *Polymer*, **1992**, 33, (20), 4331.
26. T.H. Barrows, **1980**, *patent EP 030822*
27. J.D. Sudha, C.K.S. Pillai, S. Bera, *J. Polym. Mat.*, **1996**, 13, (4), 317.
28. J.D. Sudha, *J. Polym. Sci. Part A: Polym. Chem.*, **2000**, 38, 2469.
29. T.H. Barrows, The design and synthesis of bioabsorbable poly(ester-amides), in *Polymers in medicine II*. **1986**, Plenum: New York. p. 85.
30. F. de Candia, G. Maglio, *Polym. Bull.*, **1982**, 8, 109.
31. L. Castaldo, F. de Candia, G. Maglio, *J. Appl. Polym. Sci.*, **1982**, 27, 1809.
32. J.M. Bezemer, P. Oude Weme, D.W. Grijpma, P.J. Dijkstra, C.A. van Blitterswijk, J. Feijen, *J. Biomed. Mater. Res.*, **2000**, 52, (1), 8.
33. H.R. Stapert, P.J. Dijkstra, J. Feijen, *Macromol. Symp.*, **2000**, 152, 127.

34. Y. Fan, *J. Polym. Sci. Part A: Polym. Chem.*, **2002**, 40, 385.
35. Y. Fan, *J. Polym. Sci. Part A: Polym. Chem.*, **2001**, 39, 1318.
36. A. Rodriguez-Galan, L. Fuentes, J. Puiggali, *Polymer*, **2000**, 41, (15), 5967.
37. A. Rodriguez-Galan, J. Puiggali, *Macromol. Chem. Phys.*, **2003**, 204, 2078.
38. L. Castaldo, G. Maglio, *Polym. Bull.*, **1992**, 28, 301.
39. T. Ferre, J. Puiggali, *Polymer*, **2003**, 44, 6139.
40. B. Kaczmarczyk, D. Sek, *Polymer*, **1995**, 36, (26), 5019.
41. B. Kaczmarczyk, *Polymer*, **1998**, 39, (23), 5853.
42. S. Pivsa-Art, *J. Appl. Polym. Sci.*, **2002**, 85, (4), 774.
43. S. Andini, *Makromol. Chem. Rapid Commun.*, **1988**, 9, 119.
44. V. de Simone, *J. Appl. Polym. Sci.*, **1992**, 46, 1813.
45. A. Perez-Rodriguez, *J. Appl. Polym. Sci.*, **2000**, 78, 486.
46. A. Alla, *Polymer*, **1997**, 38, (19), 4935.
47. S.Y. Lee, *Polym. Degrad. Stab.*, **2002**, 78, 63.
48. N. Kawasaki, *Macromol. Chem. Phys.*, **1998**, 199, 2445.
49. K.E. Gonsalves, *Macromolecules*, **1992**, 25, 3309.
50. Z.Y. Qian, *Colloid Polym. Sci.*, **2003**, 281, 869.
51. Z.Y. Qian, *Polym. Degrad. Stab.*, **2003**, 81, 279.
52. R. Timmermann, R. Jardin, R. Koch, **1995**, patent EP 4327024
53. R. Timmermann, R. Dujardin, R. Koch, **1997**, patent US 5644020
54. R. Timmermann, E. Grigat, R. Koch, *Polym. Degrad. Stab.*, **1998**, 59, (1-3), 223.
55. S. Wiegand, *J. Environm. Polym. Degrad.*, **1999**, 7, (3), 145.
56. I. Goodman, A. Valavanidis, *Eur. Polym. J.*, **1984**, 20, (3), 241.
57. I. Goodman, R.N. Vachon, *Eur. Polym. J.*, **1984**, 20, (6), 529.
58. I. Goodman, R.N. Vachon, *Eur. Polym. J.*, **1984**, 20, (6), 539.
59. I. Goodman, *Eur. Polym. J.*, **1984**, 20, (6), 549.
60. I. Goodman, M.T. Rodriguez, *Macromol. Chem. Phys.*, **1996**, 197, (3), 881.
61. I. Goodman, R.J. Sheahan, *Eur. Polym. J.*, **1990**, 26, (10), 1081.
62. I. Goodman, R.J. Sheahan, *Eur. Polym. J.*, **1990**, 26, (10), 1089.
63. S. Bera, Z. Jedlinski, *Polymer*, **1993**, 34, (16), 3545.

64. M. van der Zee, *PhD thesis*, **1997**, University of Twente, The Netherlands: p. 147.
65. L. Stryer, **1995**, *Biochemistry*, W.H. Freeman and Company, New York.
66. A. Rodriguez-Galan, *J. Appl Polym. Sci.*, **1999**, 74, 2312.
67. H.R. Stapert, *PhD thesis*, **1998**, University of Twente, The Netherlands: p. 259.
68. A. Alla, *Polymer*, **2000**, 41, 6995.
69. I. Goodman, D.A. Starmer, *Macromol. Chem. Phys.*, **1999**, 200, (4), 881.
70. X. Chen, J.A. Gonsalves, *J. Appl. Polym. Sci.*, **1993**, 50, 1999.

Chapter 3

Crystallization behaviour of symmetrical bisamide-diols

P.A.M. Lips¹, M.J.M van Heeringen², R. Broos², P.J. Dijkstra¹, J. Feijen¹

¹ *Institute for Biomedical Technology (BMTI) and Department of Polymer Chemistry and Biomaterials, Faculty of Science and Technology, University of Twente, P.O. Box 217, 7500 AE Enschede, The Netherlands.*

² *Core R&D, Dow Benelux N.V., PO Box 48, 4530 AA, Terneuzen, The Netherlands.*

Abstract

Symmetrical bisamide-diol monomers can be incorporated into the backbone of aliphatic polyesters, to enhance their thermal and mechanical properties. The bisamide-diols, synthesized through ring-opening of ϵ -caprolactone or γ -butyrolactone with 1,4-diaminobutane or 1,2-diaminoethane, were studied as model compounds to elucidate the crystallization behaviour of the corresponding poly(ester amide)s.

DSC, optical microscopy, temperature dependent FT-IR and WAXD were used to investigate the crystallization behaviour of the bisamide-diols. The monomer prepared from 1,4-diaminobutane crystallizes predominantly in an α -type phase while bisamide-diols prepared from 1,2-diaminoethane afforded a mixture of α - and γ -type crystals. During heating, multiple endothermic transitions were detected in the DSC thermograms of the bisamide-diols. By crossing the lower endothermic transitions, melting of crystals and/or crystal-to-crystal transformations, were observed.

Introduction

The incorporation of uniform bisamide-diol monomers into the backbone of aliphatic polyesters, to enhance their thermal and mechanical properties, has gained much interest¹⁻¹¹. The resulting poly(ester amide)s contain crystallizable amide segments which partly resemble chain segments present in nylons. Assuming that the methylene chains between the amide and ester groups are incorporated in the crystal structure, the crystalline structure of the amide segments would most resemble even-odd nylons. Even-odd, odd-even and odd-odd nylons crystallize into a γ -phase while even-even nylons crystallize into an α -phase. The α - and γ -phases represent the two stable crystal structures present in nylons with all polymorphs classified as variations of these crystalline phases¹².

Even-even nylons form chain folded planar sheets in which H-bonds are present between amide groups in adjacent anti-parallel fully extended chains¹²⁻²⁰. The almost linear H-bonds within the sheets generate a progressive shear of the chains, so that the chain segments tilt relative to the surfaces created by the chain folds. The H-bonded sheets are held together by van der Waals forces and are stacked upon one another with a progressive shear (α -phase) or with an alternating shear (β -phase)¹⁴. The β crystalline phase amounts to only a slight disturbance of the α -phase and does not constitute a separate class of crystals. Both the α - and β -crystals give two strong diffraction signals at spacings of 0.44 and 0.37 nm, which represents a projected inter-chain distance within a H-bonded sheet and the inter-sheet spacing, respectively. At room temperature, the α -phase is the thermodynamically most stable crystalline form²¹. The crystal symmetry is triclinic with one chemical repeat unit per unit cell.

In the γ -phase, H-bonds are formed between parallel pleated chains^{12-15, 17, 19, 22}. The chain axis is shorter compared to the chain axis in the α -phase due to 30° tilting of the amide groups with respect to the chain axis which brings the hydrogen and oxygen atoms of the amide groups closer to each other in the chain axis direction. The tilting allows all H-bonds to be formed without strain. The energy needed to twist the amide group in γ -crystals is compensated by the higher stability of the fully (linear) H-bonded structure. The structure is termed pseudo-hexagonal because the H-bonds prohibit the hexagonal symmetry normally found in a hexagonal packing. The γ -form has restricted rotation in the methylene chain, which causes it to retain the planar zig-zag structure.

The pseudo-hexagonal phase, which is more disordered than the triclinic α -phase, is favoured at high temperatures^{14, 15}.

A number of nylons show a crystal-to-crystal transformation on heating, which is known as the Brill transition²³. This transition can be displayed by wide angle X-ray diffraction. On heating, the inter-chain distance within a H-bonded sheet and the inter-sheet distance move together and merge typically at a spacing of 4.0-4.2 Å. A “Brill temperature” is defined as the lowest temperature for which these specific distances are equal. The crystals of some nylons melt before the diffraction signals actually meet. A pseudo-hexagonal phase is not fully achieved prior to melting. A Brill temperature is not fixed for a particular nylon, but it can vary with the perfection of the crystals^{15, 16}. However, the mechanism of this transition is still not fully understood^{12-17, 19, 20, 24-28}. Early work suggests that the two-dimensional H-bonded sheets in the α -crystalline phase at room temperature change to a three-dimensional H-bonded network at higher temperatures. From later investigations it was suggested that local “melting” of the methylene segments occurred, whereas the integrity of the H-bonded sheet structure was maintained up to the melting temperature. It is commonly accepted that the Brill transition takes place at elevated temperatures due to conformational motion and that the transition is associated with changes in packing within the crystals.

Yoshioka *et al.* investigated the structural changes in the Brill transition of nylon 6 10, 6 12 and 10 10 and its model compounds with temperature dependent IR^{20, 29-32}. In the Brill transition region, the conformation of the methylene segments was found to change remarkably from the all-trans zigzag form to the disordered conformation consisting of shorter trans zigzag segments and gauche bonds. The methylene segments on the NH side are more disordered because of a lower torsional energy barrier than those on the CO side. During this order-to-disorder transition of molecular conformation, the inter-molecular H-bonds were maintained although they gradually weakened with increasing temperature. The conformational disordering occurs in a wide temperature region even for the model compounds.

Recently, Cooper *et al.*³³⁻³⁵ used monodisperse oligoamides as model systems to study the crystallization behaviour of nylons. Such monodisperse oligoamides form extended chain crystals, so that the crystallinity is essentially 100% and any effects due to chain

folding are absent. Nylon 6,6 oligoamides containing 3, 4, 8, 12 or 16 amide units appeared to have crystalline structures similar to that of polymeric nylon 6,6. In addition, the 3-amide nylon 6,6 oligomer crystal structure is analogous to the polymeric nylon 6,6 α -crystalline phase structure, found both in fibres and in chain-folded crystals, and consists of progressive H-bonded sheets, which stack with a progressive shear. The essential difference between the 3-amide nylon 6,6 structure and the chain-folded polymer crystal structure is the precise crystallographic register of the lamellar layers stacking in the c-direction. Upon heating, all nylon 6,6 oligomers exhibited Brill transformations prior to melting, which occurred 20 to 70 °C below the melting temperature. The occurrence of a Brill transition at the same temperature for the 4-, 8-, 12- and 16-amide nylon 6,6 oligomers and the nylon 6,6 polymer, despite a substantial relative change in chain length within the series, suggests that the chain length has little effect on the Brill temperature.

These model studies provide insight in the complex crystallization behaviour of nylons, which may be extrapolated to poly(ester amide)s. Similar to monodisperse oligoamides, bisamide-diols may be used as model systems for elucidating the crystal structure of the corresponding poly(ester amide)s.

Bisamide-diols are generally prepared by reacting a linear aliphatic diamine with a lactone or hydroxy acid in the melt or in solution^{4, 6, 8, 10}. Stapert *et al.*^{3, 4} prepared a series of bisamide-diols by ring-opening of γ -butyrolactone, δ -valerolactone and ϵ -caprolactone with diaminoalkanes containing two to seven methylene groups in THF. In most cases the reaction was accompanied by successive oligomerization through the formed hydroxyl end groups even in the absence of a catalyst. Almost no oligomerization occurred using glycolide, as the formed hydroxyl group is less reactive than the amine group still present after the ring opening of the glycolide in the first step. Barrows prepared bisamide-diols from glycolic acid or lactic acid and diaminoalkanes containing two to sixteen methylene groups in isopropanol at reflux conditions and obtained a yield of ~ 75%^{10, 11}. Sudha *et al.*^{1, 2, 7-9, 36} prepared similar bisamide-diols by the aminolysis of γ -butyrolactone, δ -valerolactone and ϵ -caprolactone with diaminoalkanes containing two to six methylene groups. Oligomerization of ϵ -caprolactone was partly suppressed by using isopropanol as a solvent and performing the reaction at 5 °C. Katayama *et al.*⁶ studied the influence of the reaction conditions on the

preparation of bisamide-diols from ϵ -caprolactone and 1,2-diaminoethane or 1,6-diaminohexane. The synthesis was performed in the melt or in acetonitrile at reflux and 0 °C. The highest yield was obtained for bisamide-diols prepared from either 1,2-diaminoethane or 1,6-diaminohexane in the melt at 100 °C.

Although the researchers mentioned above have attempted to improve yield and purity of the bisamide-diol synthesized, the melting temperatures of corresponding bisamide-diols differ, indicating that purification is difficult (table 3.1).

Table 3.1: Melting temperatures of bisamide-diols according to literature.

bisamide-diol	author	T _m (°C)
1,4-diaminobutane + ϵ -caprolactone	Stapert ⁴	140
bisamide-diol 4,5	Sudha ^{1, 2}	88
1,2-diaminoethane + ϵ -caprolactone	Stapert ⁴	117
bisamide-diol 2,5	Sudha ^{1, 2}	126
	Katayama ⁶	157
1,4-diaminobutane + γ -butyrolactone	Stapert ⁴	140
bisamide-diol 4,3	Sudha ^{1, 2}	116
γ -butyrolactone + 1,2-diaminoethane	Sudha ^{1, 2}	132
bisamide-diol 2,3		

In this chapter the synthesis of bisamide-diols from either 1,4-diaminobutane or 1,2-diaminoethane and ϵ -caprolactone or γ -butyrolactone is described. N,N'- α,ω alkanediyl-bis[hydroxy-alkanamide]s are referred to as bisamide-diols throughout this chapter. The characterization of these bisamide-diols was performed with NMR, IR, MS and elemental analysis. Thermal properties were investigated using TGA and DSC. The crystallization behaviour of the bisamide-diols was studied with DSC, optical microscopy and temperature dependent FT-IR and WAXD.

Experimental

Materials

1,4-Diaminobutane, ϵ -caprolactone (synthetic grade) and DMSO-d₆ (100.0%) were obtained from Aldrich, the Netherlands. 1,4-Diaminobutane was purified by distillation (b.p 60-70°C at 2-3 mmHg). 1,2-Diaminoethane was purchased from Acros, the Netherlands. γ -Butyrolactone and methanol-d₄ (99.8%) were purchased from Merck, the Netherlands. All other solvents used were of analytical grade (Biosolve, the Netherlands).

Synthesis

N,N'-1,4-butanediyl-bis[6-hydroxy-hexanamide] (bisamide-diol **4,5**)

ϵ -Caprolactone (77.7 g, 0.68 mol) was added in approximately 10 h to a solution of freshly distilled 1,4-diaminobutane (30.0 g, 0.34 mol) in 375 ml of tetrahydrofuran (THF). Subsequently the solution was stirred at room temperature for 16 h. The solvent was removed at reduced pressure and the product was dried in vacuum. The product was dissolved in a mixture of acetonitrile and water (7:1, v:v) or toluene and ethanol (9:1 v:v) at 55 °C, left to crystallize over night, filtered and dried in vacuum. This procedure was repeated 5 to 6 times to yield ~25% of pure product (mp. 142-143 °C).

¹H-NMR (300 MHz, DMSO-d₆): δ = 7.7 (*bt*, 2H, *NH*), 4.3 (*t*, 2H, *OH*), 3.3-3.4 (*dt*, 4H, CH₂CH₂OH), 3.0 (*dt*, 4H, CH₂NH), 2.0 (*t*, 4H, CH₂CONH), 1.4-1.5 (*m*, 4H, CH₂CH₂OH), 1.3-1.4 (*m*, 4H, CH₂CH₂CONH), 1.3-1.4 (*m*, 4H, CH₂CH₂NH), 1.2-1.3 (*m*, 4H, CH₂CH₂CH₂OH).

¹³C-NMR (75.26 MHz, methanol-d₄): δ = 174.2 (CONH), 60.8 (CH₂OH), 38.0 (CH₂NHCO), 35.2 (CH₂CONH), 31.4 (CH₂CH₂OH), 25.9 (CH₂CH₂NHCO), 24.9 (CH₂CH₂CONH), 24.6 (CH₂CH₂CH₂OH).

IR (KBr): 3304 cm⁻¹ (ν N-H H-bonded and ν O-H H-bonded), 1633 cm⁻¹ (ν C=O amide I), 1542 cm⁻¹ (ν C-N + δ N-H amide II).

Elemental analysis: Calc. C: 60.73, N: 8.85, H: 10.19; found: C: 60.26, N: 8.76, H: 10.23.

Crude *N,N'*-1,2-ethanediyl-bis[6-hydroxy-hexanamide] (bisamide-diol **2,5**) was provided by Dow Benelux N.V. (Terneuzen, the Netherlands) and was prepared by condensing 1 mole of 1,2-diaminoethane with 2 moles of ϵ -caprolactone according to a modified procedure of Katayama ⁶. The product was purified by recrystallization from a mixture of acetonitrile/water (7:1, v:v). The solution was left to crystallize over night, filtered and dried in vacuum. This procedure was repeated 3 times to yield ~ 50% of pure product (mp. 161-162 °C).

¹H-NMR (300 MHz, DMSO-d₆): δ = 7.8 (*bt*, 2H, NH), 4.3 (*t*, 2H, OH), 3.3-3.4 (*dt*, 4H, CH₂CH₂OH), 3.0 (*dt*, 4H, CH₂NH), 2.0 (*t*, 4H, CH₂CONH), 1.4-1.5 (*m*, 4H, CH₂CH₂OH), 1.3-1.4 (*m*, 4H, CH₂CH₂CONH), 1.2-1.3 (*m*, 4H, CH₂CH₂CH₂OH).

¹³C-NMR (75.26 MHz, methanol-d₄): δ = 174.6 (CONH), 60.8 (CH₂OH), 38.1 (CH₂NHCO), 35.2 (CH₂CONH), 31.5 (CH₂CH₂OH), 24.8 (CH₂CH₂CONH), 24.6 (CH₂CH₂CH₂OH).

IR (KBr): 3300 cm⁻¹ (ν N-H H-bonded and ν O-H H-bonded), 1640 cm⁻¹ (ν C=O amide I), 1560 cm⁻¹ (ν C-N + δ N-H amide II).

Elemental analysis: Calc. C: 58.31, N: 9.71, H: 9.79; found: C: 58.42, N: 9.67, H: 9.88.

N,N'-1,2-ethanediyl-bis[4-hydroxy-butanamide] (bisamide-diol **2,3**)

A solution of γ -butyrolactone (50.0 g, 0.58 mol) in 75 ml of THF was added in 2 h to a solution of 1,2-diaminoethane (17.5 g, 0.29 mol) in 150 ml of THF. Subsequently, the solution was stirred at room temperature for 36 h. The solvent was removed at reduced pressure. The product was dissolved in ethanol and precipitated in diethyl ether. The product was washed with acetone and diethyl ether and dried in vacuum to give a pure product in ~80% yield (mp. 147-148 °C).

¹H-NMR (300 MHz, DMSO-d₆): δ = 7.8 (*bt*, 2H, NH), 4.4 (*bt*, 2H, OH), 3.3-3.4 (*dd*, 4H, CH₂CH₂OH), 3.0-3.1 (*dt*, 4H, CH₂NH), 2.1 (*t*, 4H, CH₂CONH), 1.6 (*m*, 4H, CH₂CH₂OH).

¹³C-NMR (75.26 MHz, methanol-d₄): δ = 174.3 (CONH), 60.3 (CH₂OH), 38.1 (CH₂NHCO), 31.7 (CH₂CONH), 27.7 (CH₂CH₂CONH).

IR (KBr): 3298 cm⁻¹ (ν N-H H-bonded and ν O-H H-bonded), 1642 cm⁻¹ (ν C=O amide I), 1560 cm⁻¹ (ν C-N + δ N-H amide II).

Elemental analysis: Calc. C: 51.71, N: 12.06, H: 8.68; found: C: 51.95, N: 12.00, H: 8.73.

Methods

NMR: ^1H - and ^{13}C -NMR spectra were recorded on a Varian Inova 300 MHz Nuclear Magnetic Resonance Spectrometer using DMSO- d_6 and methanol- d_4 as solvents.

Element analysis: Elemental analysis was performed with a Micro-Elemental Analyzer EA 1108 (Carlo Erba).

Mass spectrometry: Mass Spectra were recorded on a Finnigan MAT95 double focused Mass Spectrometer with fast atomic bombardment ionisation. Data were recorded in the range $m/z = 160$ to 1200 .

TGA: Thermal gravimetric analysis was carried out on 5-10 mg samples under a nitrogen atmosphere in the 50-700 $^{\circ}\text{C}$ range at a heating rate of $10\text{ }^{\circ}\text{C}\cdot\text{min}^{-1}$, using a Perkin-Elmer Thermal gravimetric analyser TGA 7.

DSC: Thermal analysis was carried out using a Perkin-Elmer DSC-7 Differential Scanning Calorimeter equipped with a PE7700 computer and TAS-7 software. Calibration was performed with pure indium. Melting (T_m) and crystallization (T_c) temperatures were taken from the peak maxima, melt (ΔH_m) and crystallization enthalpies (ΔH_c) were obtained from the area under the curve. The data presented are from the second heating step, unless stated otherwise. In a standard run the monomers (5-10 mg) were heated from 25 to 180 $^{\circ}\text{C}$ at a heating rate of $20\text{ }^{\circ}\text{C}\cdot\text{min}^{-1}$, annealed for 5 min, cooled to $-20\text{ }^{\circ}\text{C}$ at $20\text{ }^{\circ}\text{C}\cdot\text{min}^{-1}$, and subsequently heated from -20 to 180 $^{\circ}\text{C}$.

The crystallization behaviour was studied by heating the monomers (5-10 mg) from 25 to 180 $^{\circ}\text{C}$ at a heating rate of $20\text{ }^{\circ}\text{C}\cdot\text{min}^{-1}$, annealing for 5 min and cooling to $-20\text{ }^{\circ}\text{C}$ with cooling rates of 5, 10, 20, 30, 50, 70 and 90 $^{\circ}\text{C}\cdot\text{min}^{-1}$. The samples were subsequently heated from -20 to 180 $^{\circ}\text{C}$ at a rate of $20\text{ }^{\circ}\text{C}\cdot\text{min}^{-1}$.

Optical microscopy: Optical microscopy was performed using an Olympus BX60 microscope equipped with a camera. The samples were heated using a Mettler hot stage FP82 equipped with a Mettler FP80 central processor. Samples were placed in between two glass slides and molten at 170 $^{\circ}\text{C}$, annealed for 5 min, cooled to 30 $^{\circ}\text{C}$ at $5\text{ }^{\circ}\text{C}\cdot\text{min}^{-1}$.

and subsequently heated to 170 °C at 5 °C.min⁻¹. Crystallization and melting were observed using crossed polarizers and a magnification of 20x.

FT-IR: Fourier Transform Infra-red spectra were recorded on a Biorad FTS 175 spectrometer utilizing a wide band MCT detector at 4 cm⁻¹ spectral resolution. Samples were placed between sodium chloride windows and transferred to a heatable infra-red cell from Specac Inc. The data were collected between 4000 and 500 cm⁻¹. The first data collection was performed at 30 °C after which the solution crystallized sample was heated to 190 °C at 45 °C.min⁻¹, kept for 10 min at 190 °C and cooled to 30 °C with an average rate of 5 °C.min⁻¹. Subsequently a second spectrum was collected. The sample was then heated to 190 °C in steps of 10 °C at a heating rate of 45 °C.min⁻¹. After each step the temperature was kept constant for 5 min before data collection. Subsequently, the sample was cooled at 5 °C.min⁻¹ to 30 °C, after which the last data points were collected to check for decomposition of the sample. Bisamide-diol **2,3** was heated to maximally 160 °C because of its thermal instability.

WAXD: Wide angle X-ray diffraction spectra were recorded using fine powder samples. X-ray diffraction data were collected with a Philips PW3710 X'Pert-1 diffractometer in Bragg-Brentano geometry, using a Θ compensating divergence slit (12.5 mm). Experiments were performed at room temperature using a low-background spinning (1 r/s) specimen holder. A Cu-anode was used, together with a curved graphite monochromator, giving CuK α_1 radiation of 1.5406 Å. The data were collected in the range of $2\Theta = 2.5$ -75 °.

X-ray diffraction patterns at different temperatures were obtained using a Philips X'Pert-MPD diffractometer in Bragg-Brentano geometry, with a Θ compensating divergence slit (10.0 mm). The sample (powder) was mounted on a Pt filament in an Anton Paar HTK-16 temperature chamber. A Cu-anode was used, together with a curved graphite monochromator, giving CuK α_1 radiation of 1.5406 Å. Prior to measurements the chamber was flushed with nitrogen.

The peak position at angles of 2θ correspond to interplanar d-spacings according to Bragg's law (eq. 3.1)

$$d = \frac{n\lambda}{2 \sin \theta} \quad (\text{eq. 3.1})$$

with n is an integer and λ is the applied wavelength (1.5406 Å).

Bisamidediol 4,5 and 2,5

The data were collected in a range of $2\Theta = 4-75^\circ$ over a 60 min period of time. The first data collection was performed at 30°C on a solution-crystallized sample, after which the sample was heated to 190°C , annealed for 10 min and cooled down at $20^\circ\text{C}\cdot\text{min}^{-1}$ to 30°C . Subsequently the second data set was collected. The sample was then heated to 190°C in steps of 10°C with a heating rate of $5^\circ\text{C}\cdot\text{min}^{-1}$. After each step the temperature was kept constant for 10 min before data collection. Subsequently, the sample was cooled at $20^\circ\text{C}\cdot\text{min}^{-1}$ to 30°C , after which the last data points were collected.

Bisamide-diol 2,3

The data were collected in a range of 2Θ is $4-26^\circ$ over a 20 min period of time.

Cooling cycle: The first data collection was performed at 30°C on a solution-crystallized sample. The sample was then heated to 180°C , annealed for 5 min and cooled to 30°C at $5^\circ\text{C}\cdot\text{min}^{-1}$. Data points were collected during cooling at $130, 125, 115, 105$ and 30°C .

Heating cycle: Before data collection the sample was heated to 180°C , annealed for 5 min, cooled down at $5^\circ\text{C}\cdot\text{min}^{-1}$ to 30°C . The sample was then heated to 160°C with a heating rate of $20^\circ\text{C}\cdot\text{min}^{-1}$ and data points were collected at $120, 135$ and 140°C . Subsequently, the sample was cooled down at $20^\circ\text{C}\cdot\text{min}^{-1}$ to 30°C , after which the last data points were collected.

Results and Discussion

The synthesis of poly(ester amide)s described in this thesis is based on the use of bisamide-diols partially replacing α,ω -diols in the condensation with diesters like dimethyl adipate. The symmetrical bisamide-moieties in these poly(ester amide)s can crystallize and serve as physical crosslinks. This results in a considerable improvement of the thermal and mechanical properties of aliphatic poly(ester amide)s, depending on the molar content of bisamide-diol segments, as compared to corresponding polyesters^{37, 38}.

Bisamide-diols were synthesized (fig. 3.1) and after purification extensively characterized as model compounds for the crystallization behaviour of the corresponding poly(ester amide)s. It is known that the reaction is accompanied by oligomerization through ring-opening of the lactone by the hydroxyl groups generated. By decreasing the lactone ring size from seven to five, the ring strain decreases which makes the lactone less reactive ¹⁸.

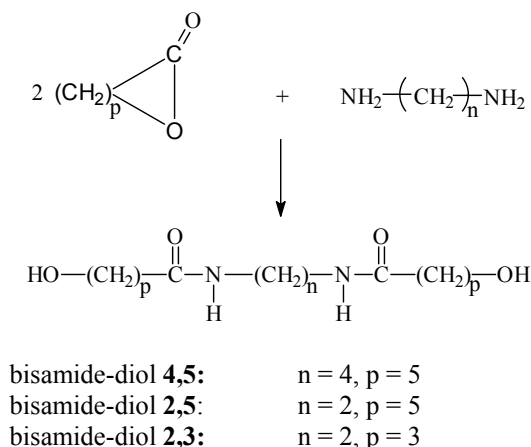


Figure 3.1: Synthesis of bisamide-diols.

The presence of oligomeric side products was clear from ¹H-NMR spectra of bisamide-diols **4,5** and **2,5** and could be as high as 20% of the total amount of product. In addition to the expected signal of the methylene protons next to the amide carbonyl at δ 2.05 a signal was present at δ 2.28 due to methylene protons next to the ester carbonyl group of the oligomers. Also, an additional signal was present at δ 3.98 of the methylene protons next to the acyl oxygen group. Moreover, mass spectrometry revealed the presence of products with molar masses of oligomeric side products. A major peak at a mass of 316, corresponding to the expected molar mass of bisamide-diol **4,5**, and five additional signals at 430, 544, 658, 772 and 886, clearly showed the presence of oligomeric side products with one to five additional caprolactoyl units, respectively. Mass spectra of crude bisamide-diol **2,5** showed a major peak at a mass of 288, corresponding to the expected molar mass, and two additional signals at 402 and 516. These additional peaks are in accordance with the presence of oligomeric side products with one or two

additional caprolactoyl units, respectively. Apparently less successive oligomerization occurred during the synthesis of bisamide-diol **2,5** as compared to bisamide-diol **4,5**. Attempts to suppress oligomerization by performing the reaction in water or isopropanol at 5 °C were unsuccessful ^{8, 36}. The crude bisamide-diol **2,3**, prepared from γ -butyrolactone and 1,2-diaminobutane, showed no additional ^1H -NMR signals resulting from oligomeric side products. Obviously the hydroxyl groups generated are not capable of ring-opening the more stable γ -butyrolactone. The mass spectra of bisamide-diol **2,3** revealed only a peak at a mass of 232 corresponding with the expected molar mass. Repetitive recrystallization was necessary to purify bisamide-diols **4,5** and **2,5** and this drastically decreased the yield of the products to less than 50%. The ^1H -NMR spectrum of pure bisamide-diol **4,5** is presented in figure 3.2. Signals from amide and hydroxyl protons, found at δ 7.74 and δ 4.34 respectively, are characteristic for these bisamide-diols. No signals of methylene protons next to an ester carbonyl were present in the purified bisamide-diols **4,5** and **2,5**. Mass spectra of the purified bisamide-diols **4,5** and **2,5** showed only one peak corresponding with the expected molar mass.

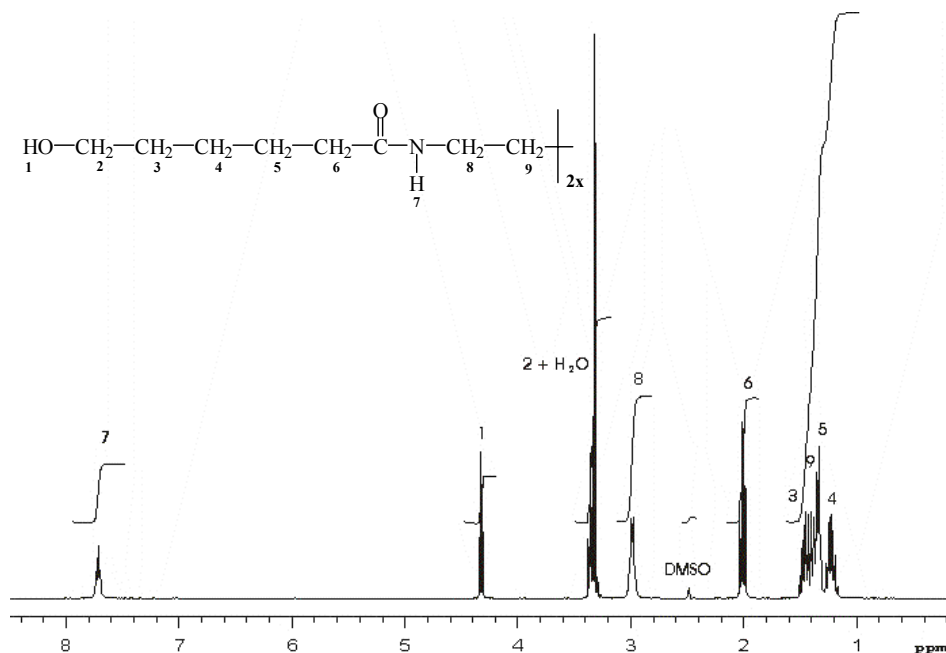


Figure 3.2: ^1H -NMR spectrum of pure bisamide-diol **4,5** in $\text{DMSO-}d_6$

Thermal properties

The thermal stability of the bisamide-diols **4,5**, **2,5** and **2,3** was determined by TGA analysis (fig. 3.3). The decomposition temperatures (T_d) taken at the inflection point, are listed in table 3.2. Bisamide-diols **4,5** and **2,5** both have a decomposition temperature of ~ 380 °C whereas bisamide-diol **2,3** has a decomposition temperature of 278 °C. During an isothermal measurement at 180 °C, bisamide-diol **2,3** decomposed completely in ~ 7 h.

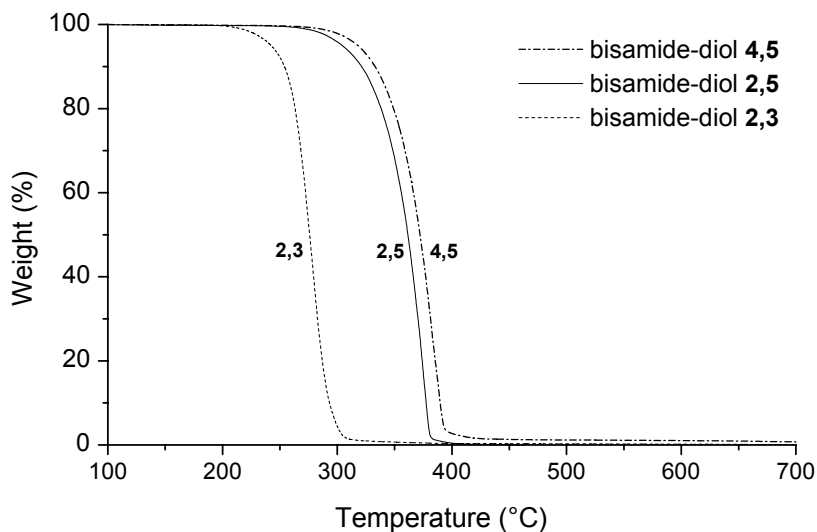


Figure 3.3: TGA thermograms of bisamide-diols.

The bisamide-diols show a complex melting and crystallization behaviour (table 3.2 and fig. 3.4). During cooling from the melt, the bisamide-diols crystallize with a main crystallization exotherm followed by a secondary (and third) crystallization to more imperfect crystals formed after the initial solidification. Upon heating, bisamide-diols **4,5** and **2,5** show two and three endothermic transitions respectively, while bisamide-diol **2,3** shows a bimodal transition. Multiple melt and crystallization transitions, observed for these bisamide-diols, have not been reported before. The highest melting temperatures ($T_{m,2}$) were 144, 163 and 143 °C for bisamide-diol **4,5**, **2,5** and **2,3**, respectively. The melting temperature of bisamide-diol **4,5** is much higher compared to

that of the corresponding bisamide-diol as prepared by Sudha while it is similar to the melting temperature of the same bisamide-diol found by Stapert (table 3.1). Both bisamide-diols **2,5** and **2,3** have much higher melting temperatures as compared to those of the corresponding bisamide-diols prepared by Sudha and Stapert.

Table 3.2: Thermal properties of bisamide-diols.

bisamide-diol	T_d^a (°C)	$T_{m,1}$ (°C)	$\Delta H_{m,1}$ (J.g ⁻¹)	$T_{c,1}$ (°C)	$\Delta H_{c,1}$ (J.g ⁻¹)	$T_{m,2}$ (°C)	$\Delta H_{m,2}$ (J.g ⁻¹)	$T_{c,2}$ (°C)	$\Delta H_{c,2}$ (J.g ⁻¹)
4,5	386	87	18	75	-3	144	126	124	-133
2,5 ^b	377	67/87	18/31	33/76	-16/-37	163	118	145	-114
2,3	278	-	-	105	-64	142/144 ^c	169	120	-80

^a taken at the inflection point; ^b bisamide-diol **2,5** has two lower melt/crystallization transitions ($T_{m,1}$ and $T_{c,1}$) ^c bimodal transition

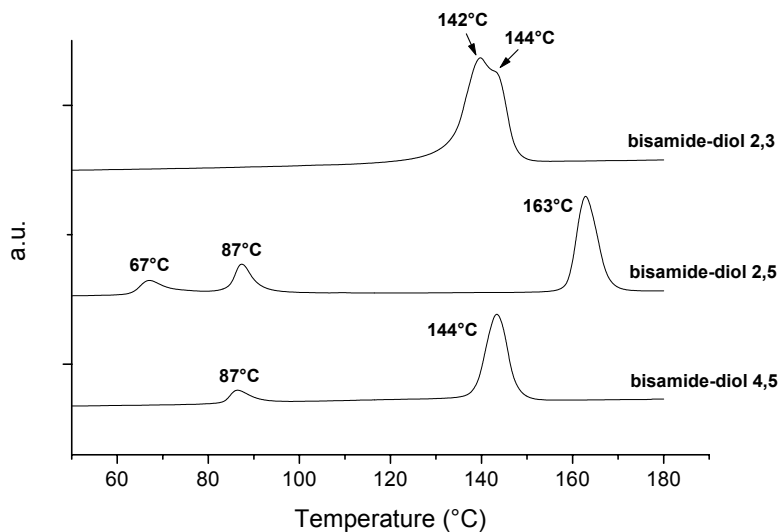


Figure 3.4: DSC thermograms of bisamide-diols (second heating scans).

Crystallization behaviour

Optical microscopy and temperature dependent FT-IR and WAXD were performed to study the crystal structure of these bisamide-diols. To remove the thermal history, all bisamide-diols were heated to the melt and subsequently cooled at a controlled rate to room temperature. Bisamide-diols **4,5**, **2,5** and **2,3** were subjected to various cooling/heating cycles using different cooling rates. The melting temperatures and melting enthalpies obtained (second scan) were independent of the previous cooling rate for all bisamide-diols. The high ($T_{c,2}$) and low ($T_{c,1}$) crystallization temperatures and thus also the undercooling, were dependent on cooling rates as depicted in figure 3.5. The higher the cooling rate, the larger the supercooling. The crystallization enthalpies ($\Delta H_{c,1}$ and $\Delta H_{c,2}$) for all bisamide-diols studied here were independent of the cooling rate.

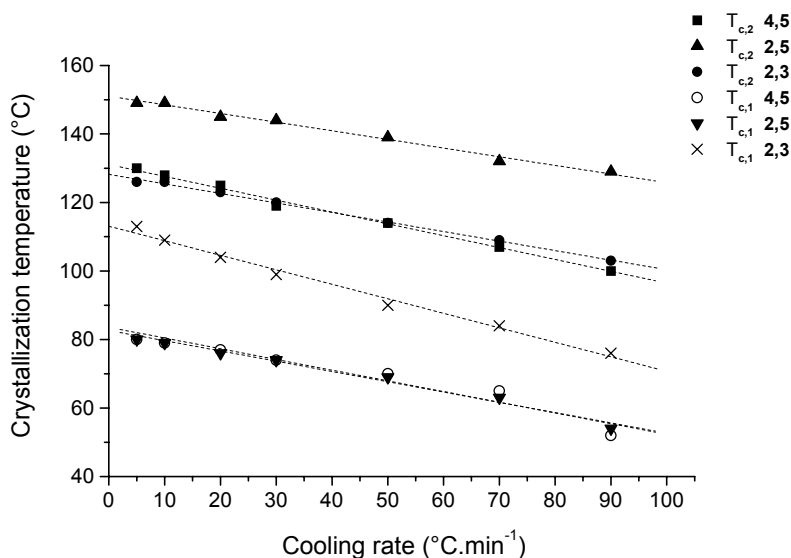


Figure 3.5: Effect of cooling rate on crystallization temperature of bisamide-diols **4,5**, **2,5** and **2,3**. $T_{c,2}$ is the high crystallization temperature and $T_{c,1}$ the low crystallization temperature.

Optical microscopy

Phase transitions of the bisamide-diols **4,5**, **2,5** and **2,3** were also studied with optical microscopy, using crossed polarizers. Samples were heated above their melting temperature, annealed for 5 min, cooled to 30 °C at 5 °C.min⁻¹ and subsequently heated till melting at 5 °C.min⁻¹. Micrographs of the crystalline structure of bisamide-diol **4,5** and **2,5** at room temperature are shown in figure 3.6 (A and B). Bisamide-diols **4,5** and **2,5** crystallized at 130 and 149 °C, respectively, which is in accordance with DSC measurements (fig. 3.5) but additional crystallization at $T_{c,1}$ was not observed by optical microscopy. Apparently, the first and main crystallization sets the morphology such that the secondary crystallization was not observed under the microscope. The onset of the highest melt transition ($T_{m,2}$) for bisamide-diols **4,5** and **2,5** was observed at 137 and 156 °C, respectively, but changes in the micrographs related to the lower melt transition ($T_{m,1}$) were not detected.

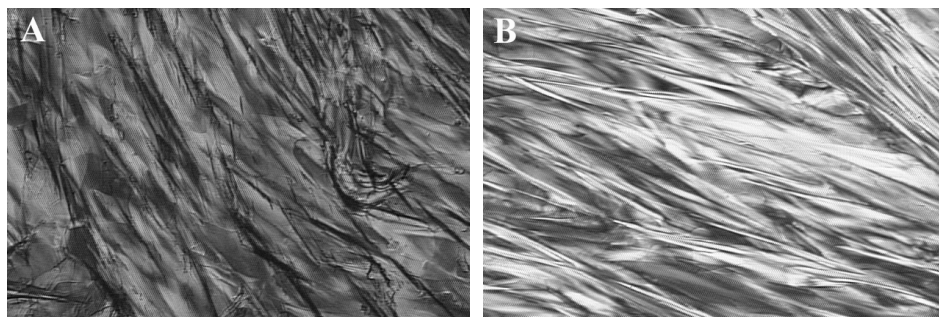


Figure 3.6: Micrographs (20x) of bisamide-diol **4,5** (A) and bisamide-diol **2,5** (B) taken at room temperature using crossed polarizers.

Surprisingly bisamide-diol **2,3** showed two distinct crystallization and melt transitions. When cooled from the melt, bisamide-diol **2,3** crystallized at 130 °C (fig. 3.7A). Upon further cooling, additional crystallization occurred at 110 °C (fig. 3.7B). Both crystallization temperatures are in accordance with the higher ($T_{c,2}$) and lower ($T_{c,1}$) crystallization temperatures as obtained with DSC measurements (fig. 3.5). Upon heating also two melt transitions were observed for bisamide-diol **2,3**. The crystalline structure present at room temperature (fig. 3.7B) melts at 134 °C and crystals with a different texture appear (similar to fig. 3.7A). The residual crystals melt at 140 °C.

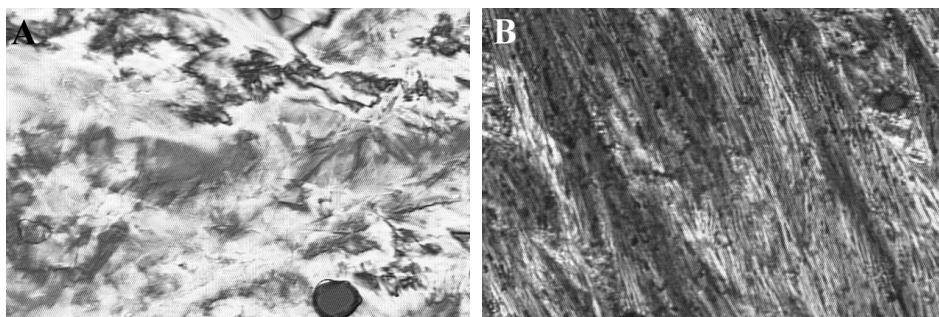


Figure 3.7: Micrographs (20x) of bisamide-diol **2,3** taken during cooling using crossed polarizers: first crystallization at 130 °C (A) and second crystallization at 110 °C (B).

Modelling of the crystalline structure

Modelling reveals that bisamide-diols may crystallize similarly to α - and γ -crystalline structures present in nylons¹². The bisamide-diols described are structurally similar to chain segments present in even-odd nylons. As only part of the chemical structure of the bisamide-diols resemble those present in nylons, the crystalline structures are denoted here as α - or γ -type. Figure 3.8 represents a picture of a framework molecular model (Prentice-Hall, Inc.) of bisamide-diol **4,5** crystallized in an α -type crystalline structure.

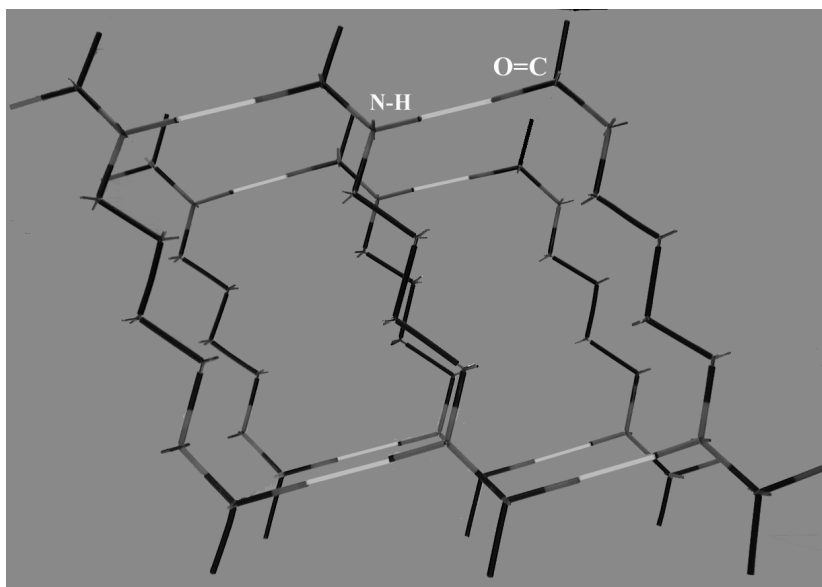
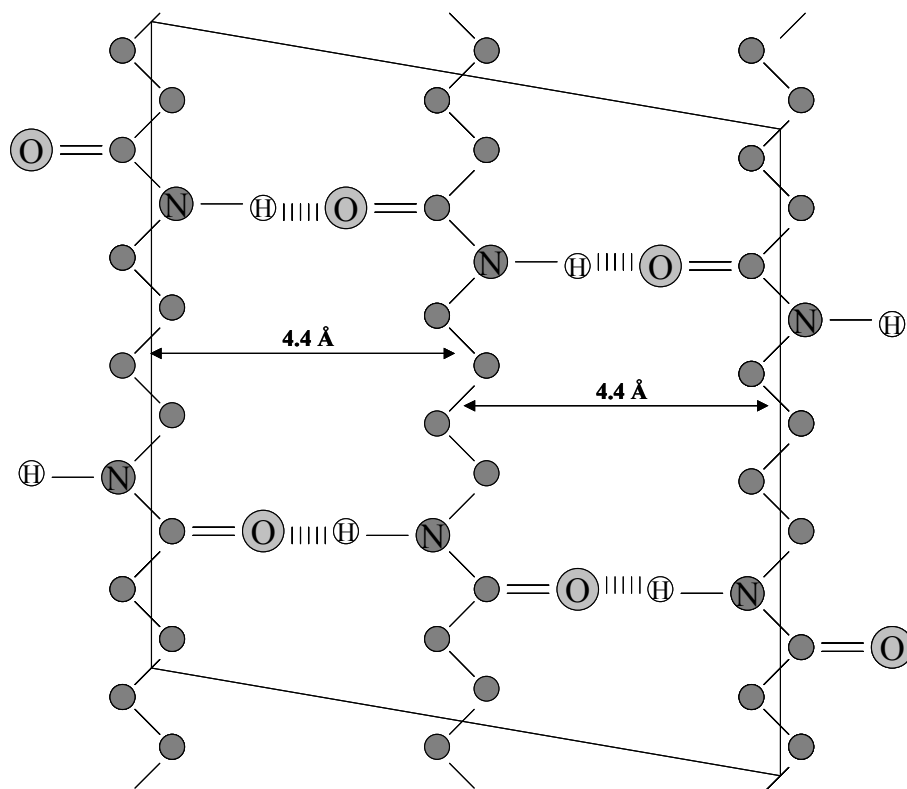


Figure 3.8: Picture of a framework molecular model of bisamide-diol **4,5** crystallized in an α -type crystalline structure.

Figure 3.9 shows the front and top view of bisamide-diol **4,5** crystallized in an α -type crystalline structure. The projected inter-chain distance within a H-bonded sheet (4.4 Å) and the inter-sheet distance (3.7 Å) are indicated (see also section WAXD).

A:



B:

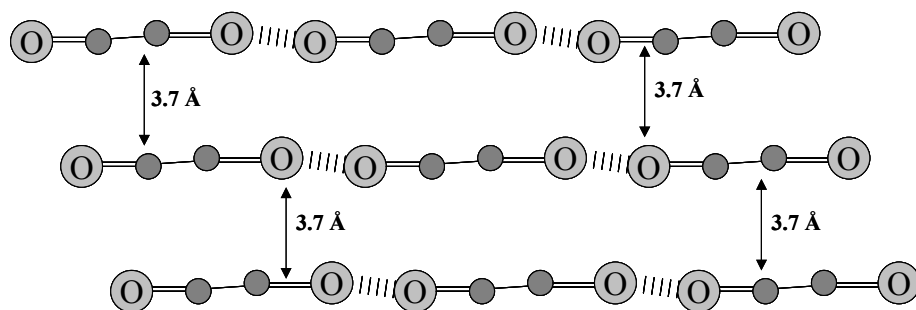
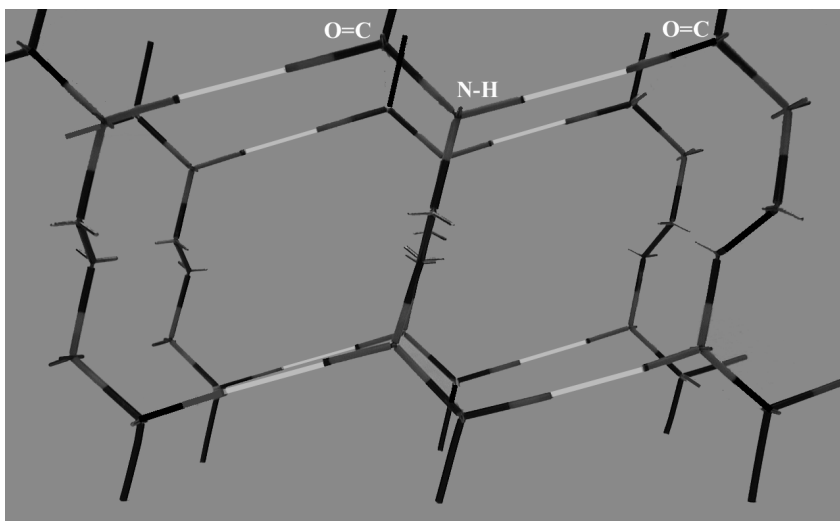


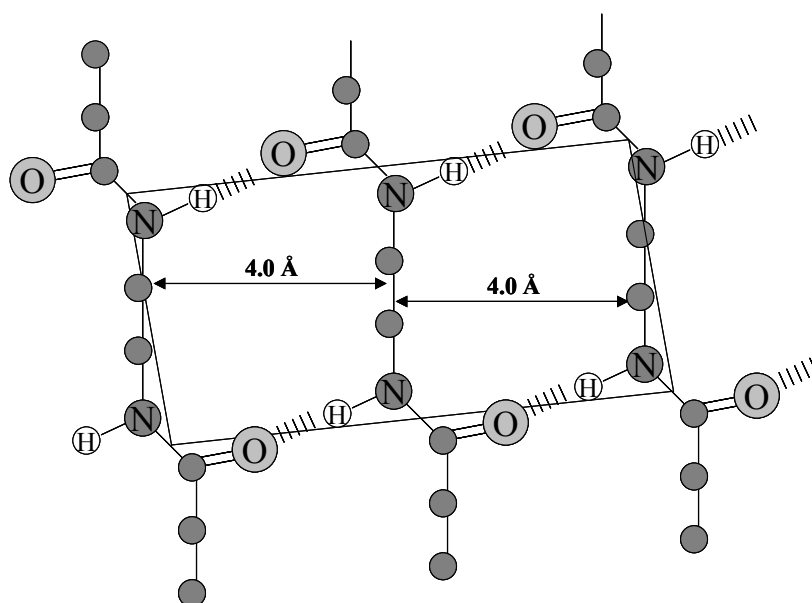
Figure 3.9: Projection of bisamidediol **4,5**, prepared from 1,4-diaminobutane and ϵ -caprolactone, in an α -type crystalline phase: (A) front view and (B) top view.

Figure 3.10 represents a picture of a framework molecular model (Prentice-Hall, Inc.) of bisamide-diol **2,5** crystallized in a γ -type crystalline structure. A model of bisamide-diol **2,5**, crystallized in a γ -type crystalline structure, is presented in figure 3.11. The inter-chain (within a H-bonded sheet) and inter-sheet distances both are ~ 4.0 Å.



*Figure 3.10: Picture of a framework molecular model of bisamide-diol **2,5** crystallized in a γ -type crystalline structure.*

A:



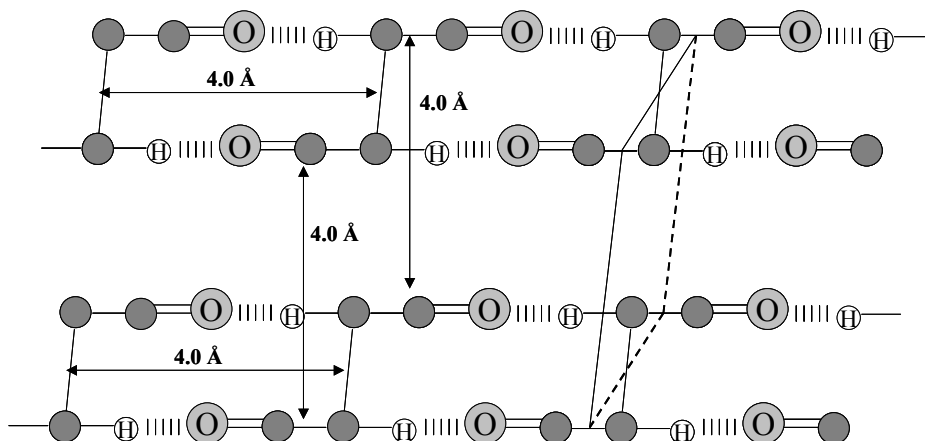
B:

Figure 3.11: Projection of bisamidediol **2,5**, prepared from 1,2-diaminoethane and ϵ -caprolactone, in an γ -type crystalline phase: (A) front view and (B) top view.

FT-IR

Nylons are characterized by IR bands at ~ 3300 (ν N-H H-bonded), ~ 1640 (amide I, ν C=O) and ~ 1545 cm^{-1} (amide II, ν C-N + δ N-H), which represent the trans, planar conformation of the amide group¹². Variations in position and intensity of the (usually sharp) bands from the crystalline phase and broader bands from the amorphous phase permit identification of the crystal structure and determination of the sample crystallinity. In table 3.3 the most important IR bands for the bisamide-diols **4,5**, **2,5** and **2,3** and for nylon 6 consisting either of an α - or γ -type crystalline phase are listed.

Table 3.3: Assignment of most important IR bands of bisamide-diols 4,5, 2,5 and 2,3 and an α or γ phase as present in nylon 6 ¹².

assignment ^a	α	γ	4,5	2,5	2,3
v N-H H-bonded (amide A)			3302	3300	3291
amide I (v C=O)			1631	1637	1639
amide II	~1540	~1560	1544 (α)	1559 (γ)	1560 (γ)
(v C-N or δ N-H)					
NH vic. δ CH ₂	~1475		1475 (α)	1474 ^b (α)	
δ CH ₂	1464	1463	1465 ^d	1465	
δ CH ₂	1436	1442		1448 (γ)	1448 (γ)
CO vic. δ CH ₂	~1420		1423 (α)	1422 ^b (α)	1419 ^a (α)
amide III	1265/1279 ^c	1269	1261		1277 (γ)
amide III coupled	~1201		1205 (α)	1209 ^b (α)	
with skel. carbon					
v C-C(O)	959	977	952 (α)	960 (α)	
CH ₂ wag	731	730		724	725
amide V, δ NH	~691	~712	697 (α)	686 (\square)	
amide VI, δ C=O	~580	~623	588 (α)	590 ^b (α)	586 ^b (α)

^a v = stretching mode, δ = in-plane bending or scissoring, ^b low intensity, ^c nylon 4,6
^d shoulder

In figure 3.12 the FT-IR spectra of the bisamide-diols **4,5**, **2,5** and **2,3** taken at room temperature are presented for the wave number regions, 3600-2700, 1700-1300, 1300-800 and 800-550 cm⁻¹. The samples were heated to the melt and cooled down to room temperature at 5 °C.min⁻¹. Note that the bisamide-diols also show bands at ~3400 (v O-H H-bonded, broader than N-H) and 1060 (v C-O) cm⁻¹ originating from their end groups. The H-bonded N-H stretching band is found at 3302, 3300 and 3291 cm⁻¹ for bisamide-diol **4,5**, **2,5** and **2,3**, respectively, which indicates that the H-bond strength increases.

The amide II band is especially sensitive to the type of crystalline structure and appears in nylons at ~ 1540 and $\sim 1560\text{ cm}^{-1}$ for the α - and γ -phase, respectively. In the spectrum of bisamide-diol **4,5** the amide II band is found at 1544 cm^{-1} revealing the presence of an α -type crystalline phase. In contrast, the amide II band in the spectra of compounds **2,5** and **2,3** is found at 1559 and 1560 cm^{-1} , respectively, showing the presence of a γ -type crystalline phase.

More evidence for the different crystalline structures is found in the fingerprint region in between 1800 and 500 cm^{-1} . The IR bands for the out-of-plane bends of the N-H (amide V) and C=O (amide VI) groups are also polymorph sensitive. In nylons, the amide V and VI bands appear as relatively sharp peaks at ~ 690 and $\sim 580\text{ cm}^{-1}$, respectively, when an α -crystalline phase is present, but are shifted to ~ 712 and 623 cm^{-1} , respectively, in case of a γ -crystalline phase. Care should be taken as the in-plane bending or rocking of $(\text{CH}_2)_n$ overlaps with the amide V band. For bisamide-diol **4,5** and **2,5**, the amide V band was present $\sim 690\text{ cm}^{-1}$ which, indicates the presence of α -type crystals. The amide V band was not observed for bisamide-diol **2,3**. The amide VI band was observed for all bisamide-diols at $\sim 588\text{ cm}^{-1}$.

Other strong bands specific for an α -phase are the NH vicinal CH_2 bending mode in all trans conformation at $\sim 1475\text{ cm}^{-1}$, the CO vicinal CH_2 bending mode at $\sim 1420\text{ cm}^{-1}$ and the amide III coupled with skeleton carbon at $\sim 1209\text{ cm}^{-1}$, which are all present in bisamidediol **4,5**. From these results it can be concluded that bisamide-diol **4,5** crystallizes into an α -type phase similar to the α -phase found in even-even nylons.

As described above the amide II band of bisamide-diol **2,5** and **2,3** found at $\sim 1560\text{ cm}^{-1}$ reflects the presence of a γ -type crystalline phase similar to the γ -phase found in even-odd nylons. For both monomers, a band at 1448 cm^{-1} is present corresponding with the CH_2 in the bending mode in a γ -phase. However, also small absorption bands at ~ 1474 , ~ 1420 , ~ 1209 , 686 and $\sim 590\text{ cm}^{-1}$, reflecting an α -type phase were detected for bisamide-diol **2,5**. It can be concluded that bisamidediol **2,5** is mainly crystallized in a γ -type crystalline phase, however, α -type crystals also appear to be present. The IR spectrum of bisamide-diol **2,3** also shows α -related bands at 1420 and 586 cm^{-1} . Other specific bands indicative for an α -type crystalline phase, like 1474 , 1209 and 690 cm^{-1} ,

were not observed. Based on these results it is concluded that bisamidediol **2,3** mainly crystallizes in a γ -type crystalline phase.

Compared to the ν C-O bands of bisamide-diol **4,5** and **2,5** located at $\sim 1060\text{ cm}^{-1}$, the ν C-O band of bisamide-diol **2,3** shifted to 1010 and 1030 cm^{-1} , which suggest stronger OH H-bonds and as a consequence the non H-bonded band present at 3445 cm^{-1} shifted beneath the H-bonded ν N-H band.

Crystallization of nylons into a mixture of crystals at room temperature has also been reported by Jones *et al.*¹⁴. Single crystals prepared from nylon 4,8 even showed the presence of α - and β -crystals and small amounts of the pseudo-hexagonal γ -phase at room temperature.

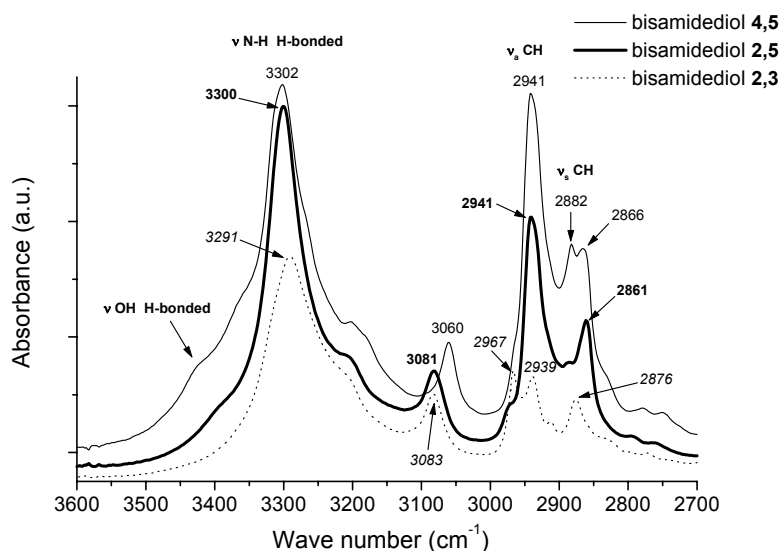


Figure 3.12a: FT-IR spectra of bisamide-diols **4,5**, **2,5** and **2,3** at room temperature for the wave number region $3600\text{-}2700\text{ cm}^{-1}$.

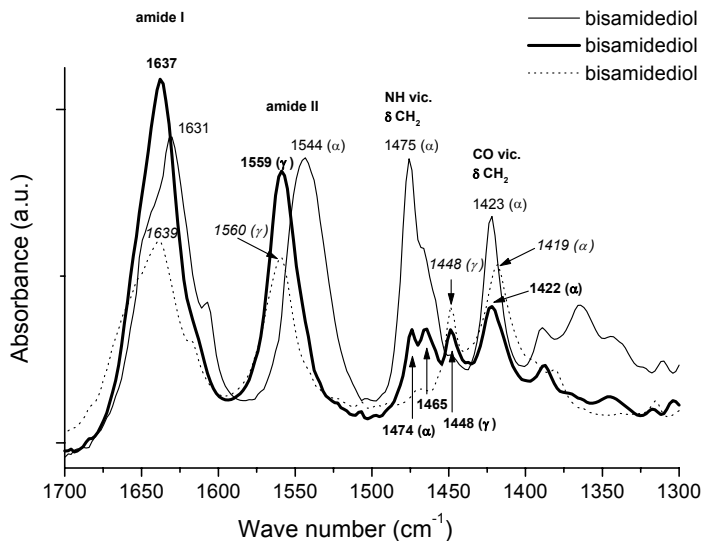


Figure 3.12b: FT-IR spectra of bisamide-diols 4,5, 2,5 and 2,3 at room temperature for the wave number region 1700-1300 cm^{-1} .

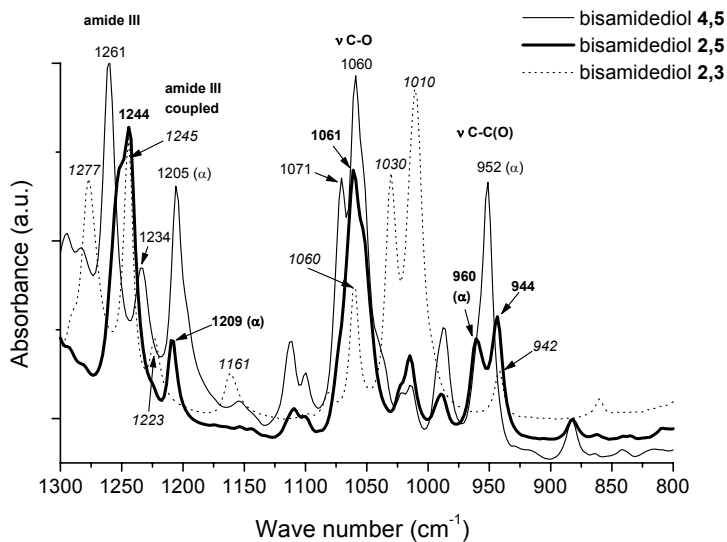


Figure 3.12c: FT-IR spectra of bisamide-diols 4,5, 2,5 and 2,3 at room temperature for the wave number region 1300-800 cm^{-1} .

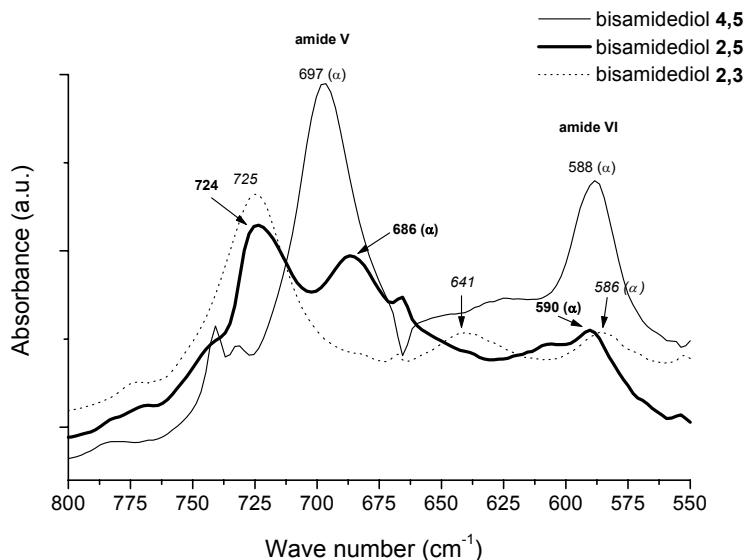


Figure 3.12d: FT-IR spectra of bisamide-diols **4,5**, **2,5** and **2,3** at room temperature for the wave number region 800-550 cm^{-1} .

The multiple transitions found in the DSC thermograms are likely due to the formation of different crystal structures. The FT-IR data obtained underline this picture, although no definitive conclusions can be drawn. Therefore temperature dependent FT-IR measurements were performed, which for the different bisamide-diols, will be discussed separately. To exclude differences due to thermal history, the bisamide-diols were all heated to the melt at $45\text{ }^{\circ}\text{C}\cdot\text{min}^{-1}$ and subsequently cooled to $30\text{ }^{\circ}\text{C}$ at $\sim 5\text{ }^{\circ}\text{C}\cdot\text{min}^{-1}$. Upon reheating to the melt at $45\text{ }^{\circ}\text{C}\cdot\text{min}^{-1}$ FT-IR spectra were recorded at different temperatures. As previously described the cooling rate for the sample has no effect on the subsequent melting temperature and corresponding melt enthalpies which allows us to relate the DSC to the FT-IR data.

Upon heating, bisamide-diol **4,5** reveals endothermic transitions at 87 and $144\text{ }^{\circ}\text{C}$ (fig. 3.4). Passing the first transition at $87\text{ }^{\circ}\text{C}$, the intensity of all amide related bands in the FT-IR spectrum decreases to a certain extent but do not broaden (fig. 3.13). The ν N-H stretch band at 3302 cm^{-1} characteristic for amide-amide H-bonds shifts to 3306 cm^{-1} due

to thermal expansion. Small bands, attributed to specific conformations of the methylene segments, disappeared around this transition. In addition, a small band at 882 cm^{-1} disappears while two new bands arise at 888 and 877 cm^{-1} . This suggests a change in the crystal packing in which the methylene segments change their conformation without affecting the H-bonded sheet structure. It has to be emphasized that the presence and mobility of the hydroxyl groups may allow a different crystal packing with similar amide-amide H-bonds. The minor changes observed at this first transition, allow the conclusion that α -type crystals melt and/or reorganize into a different α -type crystalline structure.

While increasing the temperature from $90\text{ }^{\circ}\text{C}$ up to the melting point, the $\nu\text{ N-H}$ band is shifted gradually from 3306 cm^{-1} to 3310 cm^{-1} . At $150\text{ }^{\circ}\text{C}$, when α -type crystals melt, a broad band emerges with a maximum at $\sim 3320\text{ cm}^{-1}$, which indicates that in the melt still substantial H-bonding is present.

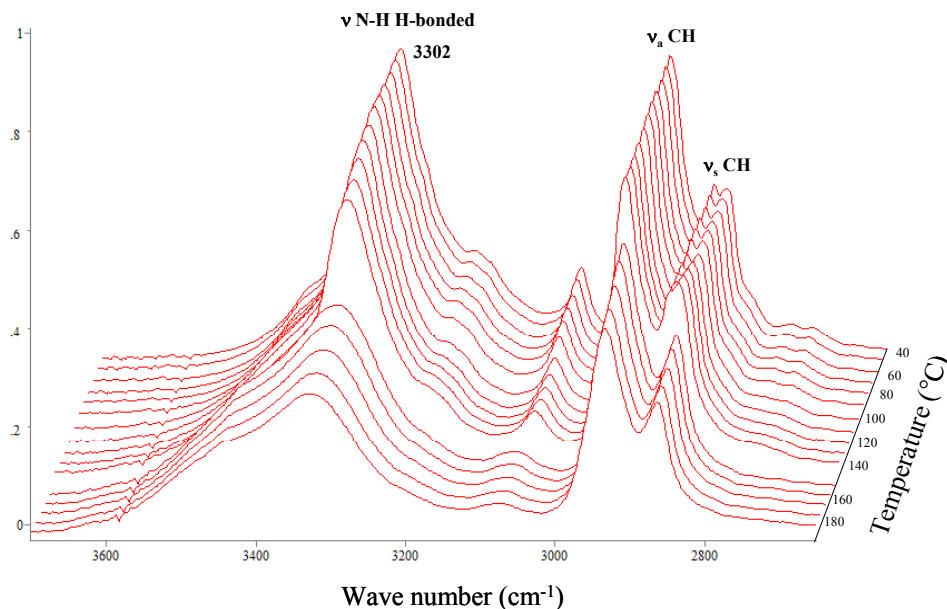


Figure 3.13a: FT-IR spectra of bisamide-diol 4,5 in the range of 40 to $190\text{ }^{\circ}\text{C}$ for the wave number region $3700\text{--}2700\text{ cm}^{-1}$.

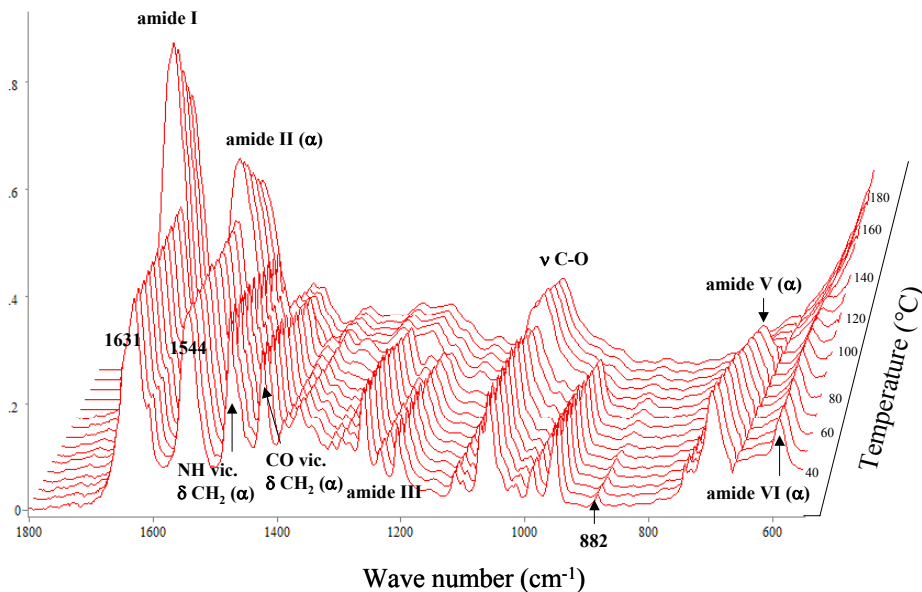


Figure 3.13b: FT-IR spectra of bisamide-diol 4,5 in the range of 40 to 190 °C for the wave number region 1800-550 cm^{-1} .

In the DSC scans of bisamide-diol 2,5 endothermic transitions at 67, 87 and 163 °C, were found. Going through the first transition at 67 °C the main amide related bands like ν N-H, amide I, II, III, V and VI only show a small decrease in intensity in the FT-IR spectra (fig. 3.14). The band at 1474 cm^{-1} corresponding with the NH vicinal CH_2 bend disappeared almost completely while the band at 1420 cm^{-1} of the CO vicinal CH_2 bend and the amide III band coupled with skeleton carbon at 1209 cm^{-1} have significantly decreased in intensity without broadening. Other bands disappeared around this transition, which are fully associated with methylene segments. Additionally, the band at 881 cm^{-1} diminished significantly at 70 °C. Because the bands at 1474, 1420 and 1209 cm^{-1} are associated with an α -type crystalline phase it can be concluded that at this transition these crystals melt or rearrange into a different crystalline structure.

Crossing the second transition between 80 and 90 °C several spectral changes are observed. The intensity of ν N-H band drops significantly and shifts from 3305 to 3301 cm^{-1} , which indicates shorter stronger H-bonds (γ -crystals). Most prominent changes are the disappearance of bands at 1420 and 1209 cm^{-1} , which are associated with melting of

α -type crystals. The amide V and VI bands, started to shift their peak position, suggesting a change in the twisting angles around the amide-CH₂ bonds. The band at 2941 cm⁻¹ belonging to the asymmetrical stretch CH₂ shows broadening and a major shift to 2937 cm⁻¹, which indicates more gauche conformations of the methylene sequences. The generation of gauche bonds could also be detected at ~1440²⁰ and ~1462 cm⁻¹²⁷. Similarly, Yoshioka *et al.* found that at the Brill temperature of even-even nylons the methylene sequence in the fully extended all-trans zigzag form changes to the geometry consisting of short trans zigzag segment and gauche bonds^{20, 30-32}. The large structural changes at 87 °C for bisamide-diol **2,5** suggest a gradual change of the methylene packing mode from the triclinic to the pseudo-hexagonal structure, which corresponds to the so-called Brill transition of nylons.

Additionally, the band at 882 cm⁻¹ disappeared at 80 °C while the bands at 887 and 877 cm⁻¹ emerge at 90 °C. The appearance of these bands, was also observed when crossing the first melt transition at 87 °C of bisamide-diol **4,5**. A second pair of bands (956 and 946 cm⁻¹) appeared at 90 °C while the band at 943 cm⁻¹ disappeared (fig. 3.12c). At 90 °C, a shoulder emerged (~1540 cm⁻¹) on the low wave number side of the amide II band, which is the characteristic band for α -type crystals. In addition to the formation of a pseudo-hexagonal phase maybe also α -type crystals are transformed into a different α -type crystalline structure.

The ν C-O of the hydroxyl groups at 1061 cm⁻¹ decreases and severely broadens, a process that continues up to complete melting around 170 °C whereas the H-bonded ν OH has disappeared at 90 °C. In conclusion, α -related bands at 1420, 1209 and 686 cm⁻¹ completely disappear at 90 °C. These changes correspond with those found for bisamide-diol **4,5**. New bands appeared at 956, 946, 887 and 877 cm⁻¹ and methylene sequences appeared more in gauche conformations, indicating a possible rearrangement of crystals (Brill). Thus at 87 °C, probably α -type crystals melt and/or reorganize into γ -type crystals. At the main transition around 170 °C γ -type crystals melt.

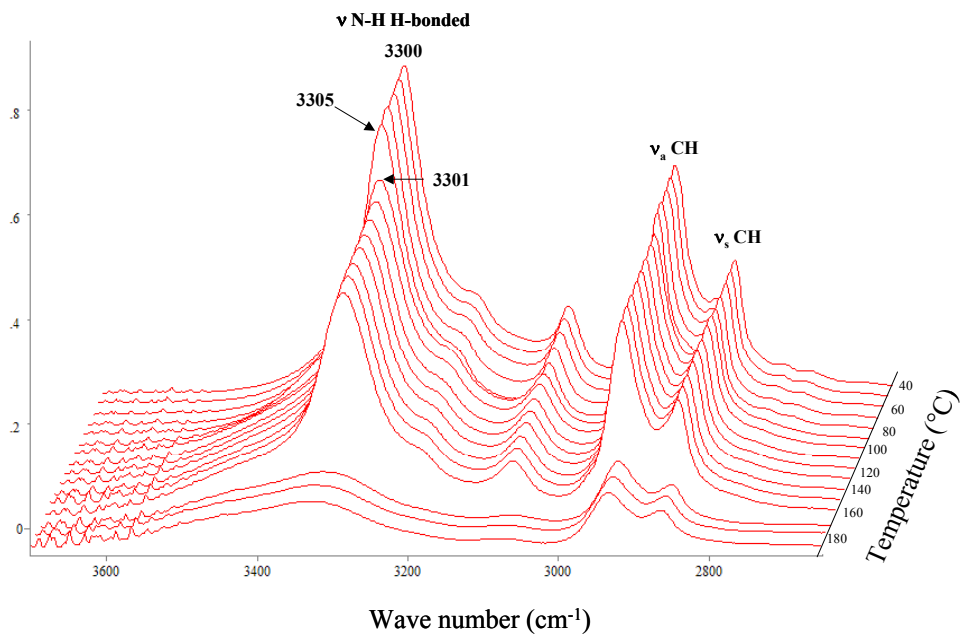


Figure 3.14a: FT-IR spectra of bisamide-diol 2,5 in the range of 40 to 190 $^{\circ}\text{C}$ for the wave number region 3700-2700 cm^{-1} .

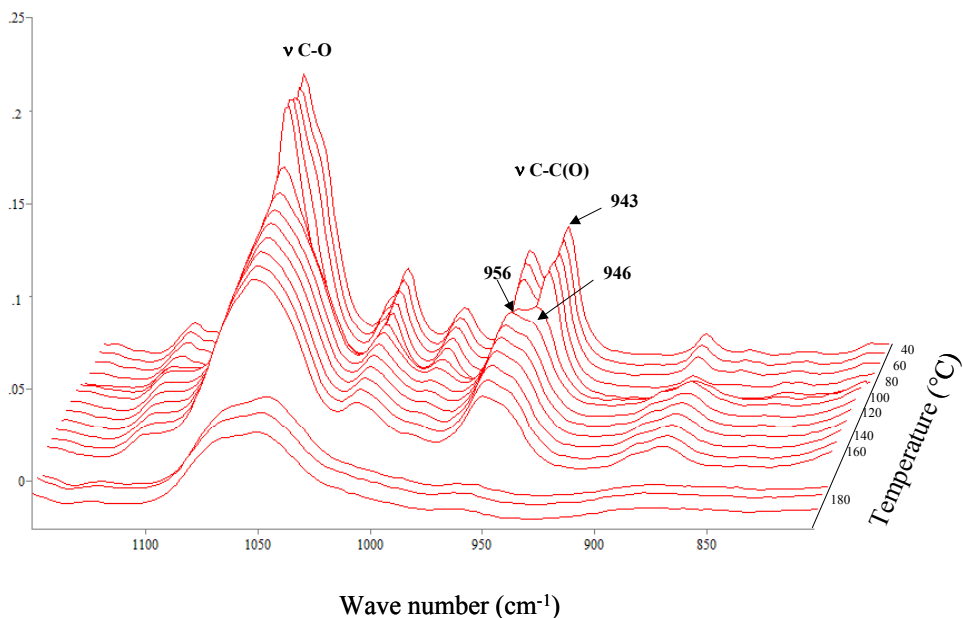


Figure 3.14b: FT-IR spectra of bisamide-diol 2,5 in the range of 40 to 190 $^{\circ}\text{C}$ for the wave number region 1150-810 cm^{-1} .

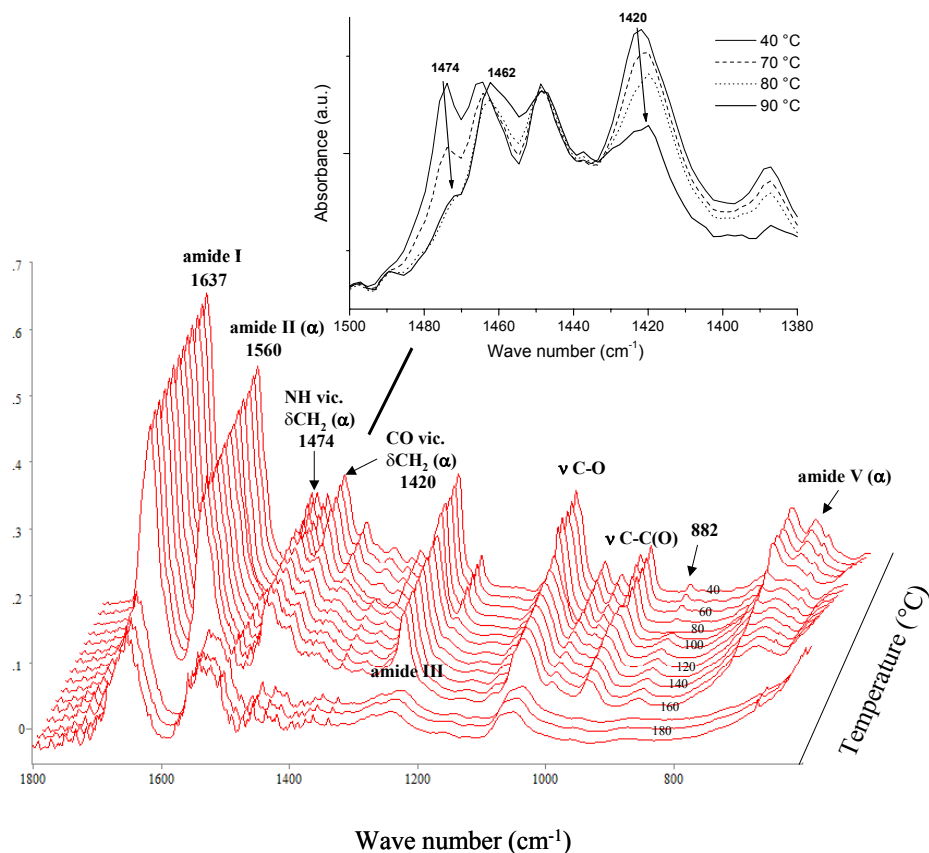


Figure 3.14c: FT-IR spectra of bisamide-diol **2,5** in the range of 40 to 190 °C for the wave number region 1800-550 cm^{-1} .

The DSC thermograms of bisamide-diol **2,3** show one bimodal melt transition with maxima at 142 and 144 °C. For all amide related bands a small decrease in intensity was observed in the FT-IR spectra with increasing temperature up to 134 °C (fig. 3.15). The ν N-H band at 3290 cm^{-1} shifts to 3302 cm^{-1} due to thermal expansion. Passing the melt transition at 134 °C, as observed with optical microscopy, small bands disappear or broaden in the FT-IR spectrum.

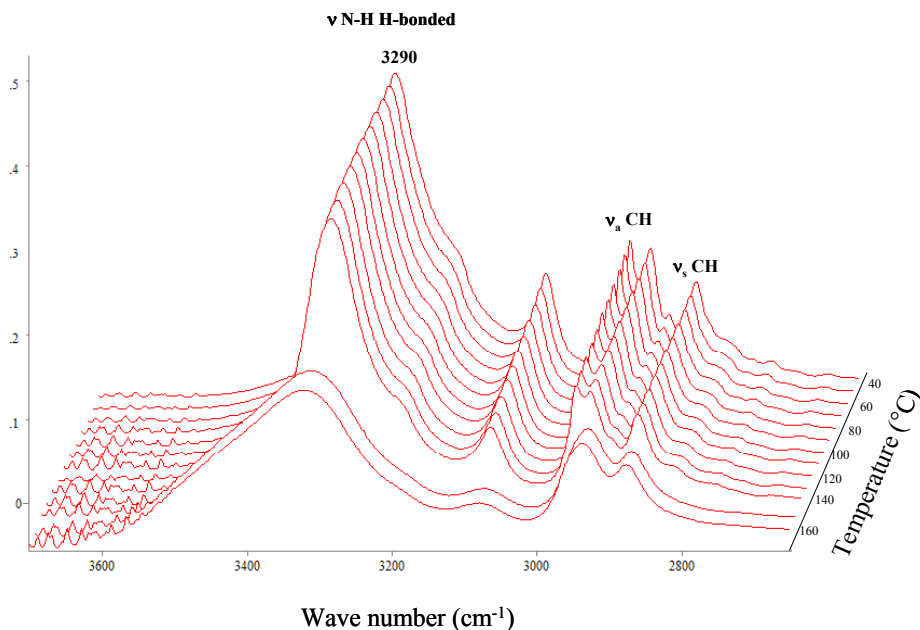


Figure 3.15a: FT-IR spectra of bisamide-diol 2,3 in the range of 30 to 160 $^{\circ}\text{C}$ for the wave number region 3700-2650 cm^{-1} .

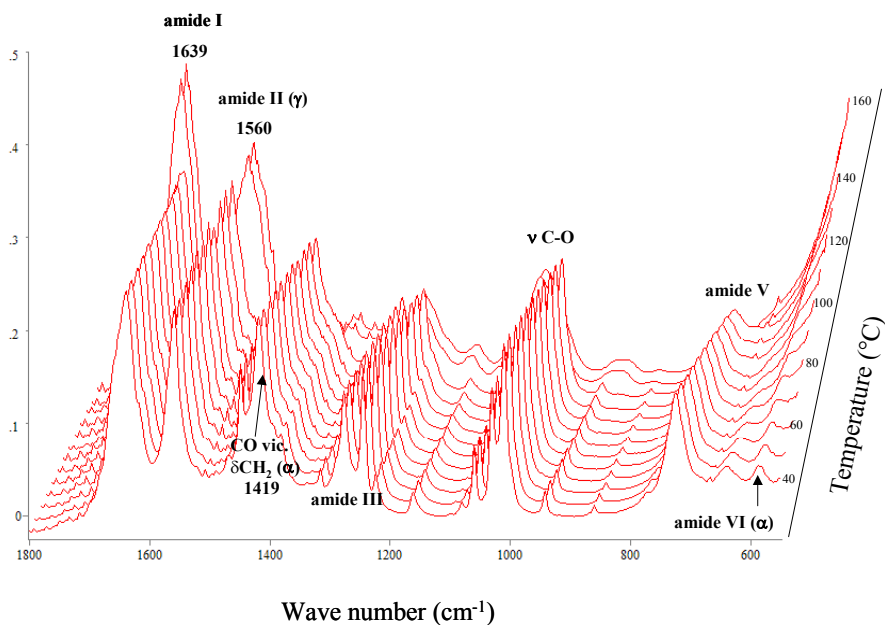


Figure 3.15b: FT-IR spectra of bisamide-diol 2,3 in the range of 30 to 160 $^{\circ}\text{C}$ for the wave number region 1800-550 cm^{-1} .

Regarding the temperature dependent FT-IR data the following conclusions can be made: Bisamide-diols crystallize similar to nylons either in an α - or a γ -type phase or in a mixture of the two phases. Bisamide-diol **4,5** crystallizes in an α -type phase. Crossing the first transition at 87 °C small IR-bands disappear while new IR-bands emerge which indicate a crystal-to-crystal transformation on heating. However, the amide related bands do not change which suggests rearrangement only in the methylene sequences. At room temperature bisamide-diol **2,5** shows the presence of a mixture of α - and γ -type crystals. Passing the first transition at 67 °C, probably α -type crystals melt or reorganize into a different crystalline phase. At 87 °C, going through the second transition, new IR-bands emerge belonging to methylene segments (in gauche conformation) while α -related bands disappear. The ν N-H band shifts to lower wave number, which suggests stronger H-bonds (γ -crystals). Thus, at 87 °C α -type crystals reorganize into a γ -type crystalline phase, which is known as the Brill transition. Bisamide-diol **2,3** crystallizes preferably into a γ -type phase, however α -related IR-bands are also present. The C-O stretch bands shifted to lower wave number compared to bisamide-diol **4,5** and **2,5**, which suggest that the OH H-bonds are stronger.

WAXD

The complex crystallization behaviour prompted us to perform also temperature dependent wide angle X-ray diffraction (WAXD) experiments. The diffraction profile is too complicated to obtain the concrete crystal structure. Some characteristic peaks can be evaluated, which are considered to reflect a packing mode of methylene segments. The WAXD data can hopefully confirm the type of crystalline structure of bisamide-diol **4,5**, **2,5** and **2,3** as determined by FT-IR and also give more insight in the melting and/or rearrangements of crystals during the lower endothermic transitions.

In nylons, the well-defined α -crystals are characterized by two reflections at about 4.4 Å for α (002) and 3.7 Å for α (200)¹². These reflections represent the distance between two amide-amide intermolecular H-bonded chains (4.4 Å) and the distance between two van der Waals packed sheets (3.7 Å). It is known that when polyamide crystals are heated, the spacing of the two characteristic diffraction signals shift toward one another and merge at the Brill temperature (T_b) to a spacing of 4.0-4.2 Å. The high temperature

crystalline phase between T_b and T_m , for which the interchain and the intersheet distances have become equal, is often referred to as pseudohexagonal.

In the following experiments, bisamide-diols **4,5**, **2,5** and **2,3** were heated to the melt, annealed for 10 min and subsequently cooled to 30 °C at 20 °C.min⁻¹ before WAXD data were recorded (fig. 3.16). These data can be related to the structural analysis from the FT-IR data as both samples were crystallized from the melt.

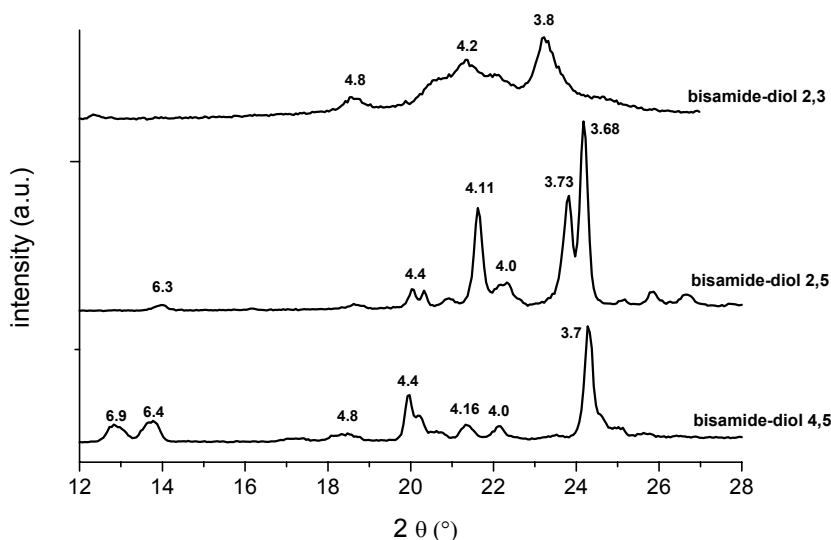


Figure 3.16: WAXD spectra of bisamide-diols **4,5**, **2,5** and **2,3** at room temperature that were heated to the melt, annealed for 10 min and subsequently cooled to 30 °C at 20 °C.min⁻¹. The data represent the *d*-spacings in Å.

All bisamide-diols show a broad spectrum of diffraction peaks indicating the presence of different crystalline phases. Strong diffraction peaks at 3.7 and 4.4 Å are observed for bisamide-diol **4,5**, which confirms the presence of α -type crystals. Additional reflections at 4.3 and 3.6 Å indicate the presence of another α -type crystal at room temperature. In addition, the small diffraction peaks in the range 4.0–4.2 Å are characteristic of the pseudo-hexagonal phase, which was not observed in the FT-IR spectra. However, Jones *et al.*¹⁴ reported that the nylons in the β -phase usually show a weak diffraction peak at 4.2 Å, which might indicate that bisamide-diol **4,5** crystallize in a mixture of α - and β -

type crystals. Bisamide-diol **2,5** reveals a strong diffraction peak at 4.1 Å, suggesting crystals in a γ -type crystalline phase. Additionally, two diffraction peaks close to each other are present at 3.7 Å and 4.4 Å. These data suggest the co-existence of two slightly different α -type phases and a γ -type phase, which is in accordance with the IR data. For bisamide-diol **2,3**, a very broad diffraction peak (trimodal) is present at ~ 4.2 Å and two broad diffraction peaks are observed at 3.8 and 4.8 Å. Similar to bisamide-diol **2,5**, bisamide-diol **2,3** shows the presence of a mixture of α - and γ -type crystals at room temperature.

To investigate the nature of the lower melt transitions as observed in DSC scans, temperature dependent WAXD spectra were recorded. The bisamide-diols were heated to the melt at 20 °C.min⁻¹, annealed for 10 min and subsequently cooled to 30 °C at 20 °C.min⁻¹ similarly as performed in DSC and FT-IR experiments. Upon reheating to the melt (5 °C.min⁻¹) WAXD spectra at different temperatures were recorded.

Bisamide-diol **4,5** shows a change in crystal packing when increasing the temperature from 70 to 90 °C thus going through the lower melt transition (fig. 3.17a). At 80 °C the diffraction lines at 3.68, 4.4 and 6.9 Å increase substantially while the diffraction lines at 3.70, 4.3 and 6.5 Å disappear completely at 90 °C. These changes can be associated with the transition of an α -type crystal into a different α -type crystalline phase and confirms conclusions drawn from the FT-IR study. Above the first transition at 87 °C a mixture of α - and γ - (or β -) type crystals remains. At 90 °C the structure is fixed and the only effect is the increase of sheet-to-sheet distance with temperature (fig. 3.17b).

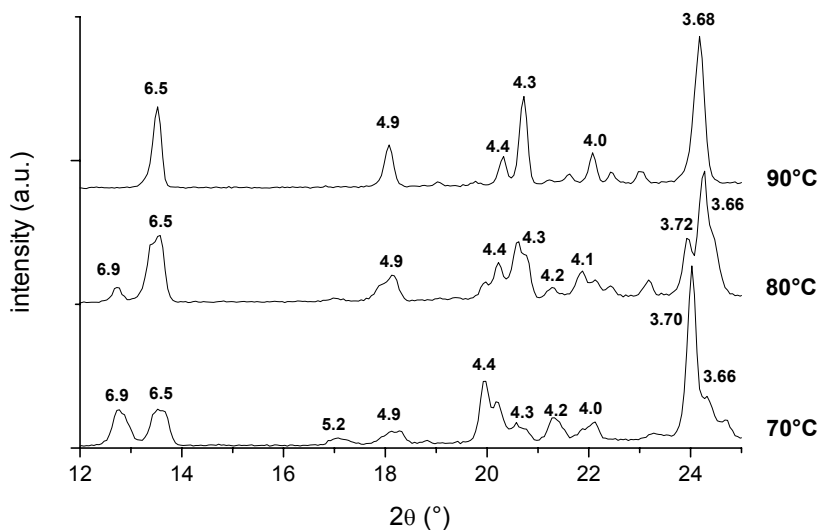


Figure 3.17a: WAXD spectra of bisamide-diol 4,5 at 70, 80 and 90 °C. The data represent the d-spacings in Å.

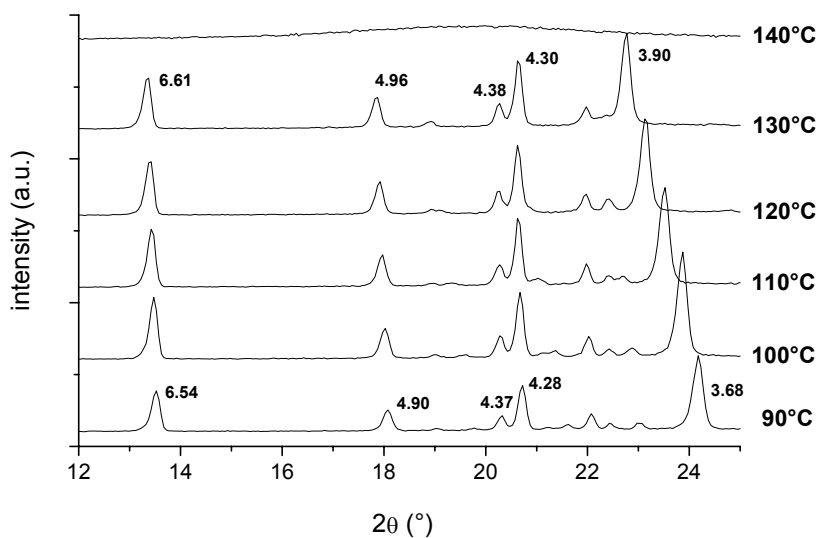


Figure 3.17b: WAXD spectra of bisamide-diol 4,5 in the range of 90 to 140 °C. The data represent the d-spacings in Å.

The temperature dependent WAXD spectra of bisamide-diol **2,5** in between 50 and 90 °C are presented in figure. 3.18. Two endothermic transitions at 67 and 87 °C have to be considered in this temperature region. Crossing the transition at 67 °C, α -related diffraction lines at 3.70 and 4.37 Å disappear. The diffraction line at 3.77 Å becomes more intense. This might indicate transformation of an α -type structure into a different α -type crystalline structure. Additionally, the diffraction line at 4.12 Å remains unchanged while a diffraction line at 4.06 Å emerges (fig. 3.18a). When increasing the temperature from 70 to 90 °C the α -related diffraction lines at 3.80 and 4.46 Å disappear while an intensive diffraction line emerges at 4.02 Å. This confirms the conclusions drawn from the IR data that at 87 °C α -type crystals melt and/or reorganize into well-defined γ -type crystals (Brill transition). Additionally, the diffraction lines at 4.17 and 4.13 Å remain present at 90 °C. The remaining γ -type crystalline structure melts at 150 °C, but mobility within this crystalline form already starts at 90 °C as is illustrated by the gradual peak shift from 4.02 to 4.16 Å (fig. 3.18b).

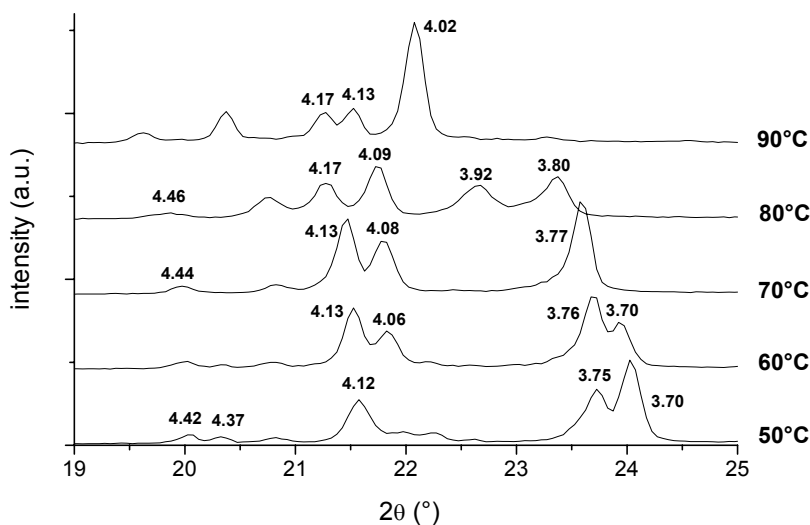


Figure 3.18a: WAXD spectra of bisamide-diol **2,5** in the range of 50 to 90 °C. The data indicate the d-spacings in Å.

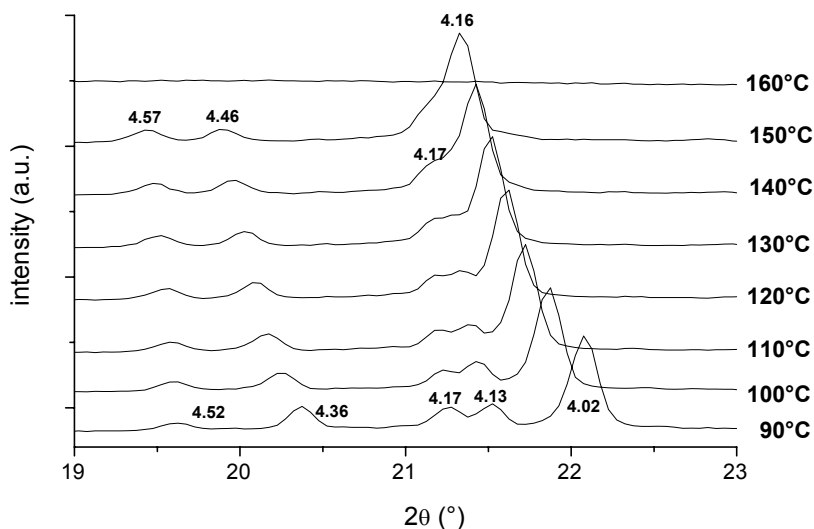


Figure 3.18b: WAXD spectra of bisamide-diol **2,5** in the range of 90 to 160 °C. The data represent the *d*-spacings in Å.

When bisamide-diol **2,3** is heated above its melting temperature and cooled down with 5 °C.min⁻¹ the WAXD spectra recorded at 130, 125, 115, 105 and 30 °C revealed a rather low resolution (fig. 3.19). At 130 °C, bisamide-diol **2,3** crystallized from the melt into a γ -type phase, indicated by the broad diffraction line at 4.2-4.0 Å. Upon further cooling, at 125 °C, the intensity of diffraction peak at 4.0 Å is increasing. At 105 °C, the diffraction lines at 3.8 and 4.8 Å are becoming more pronounced, due to additional crystallization into an α -type phase. During cooling from the melt, the appearance of first crystallization (γ -type) was observed at 130 °C with the optical microscope. Upon further cooling at 105 °C a second crystallization (α -type) was observed which showed a crystalline phase with a different texture (fig. 3.7).

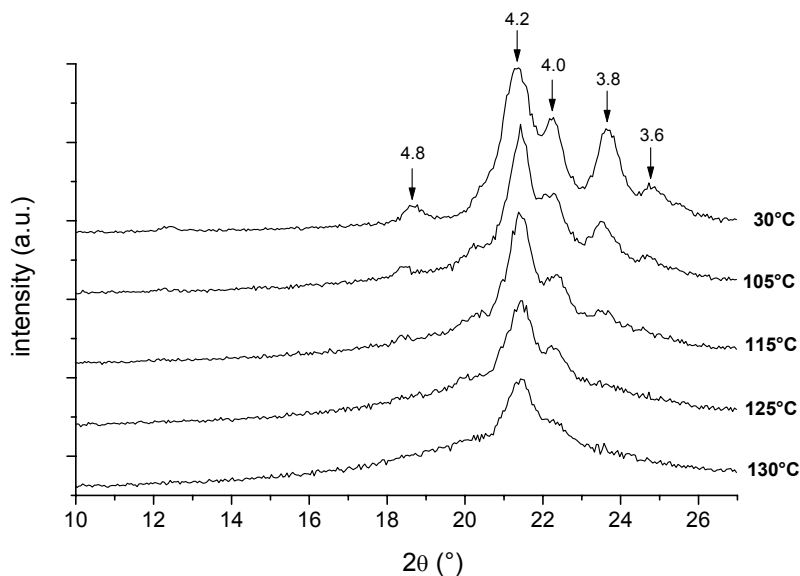


Figure 3.19: WAXD spectra of bisamide-diol **2,3** cooled from the melt to 30 °C at a rate of 5 °C.min⁻¹. The data represent the d-spacings in Å.

Subsequently, bisamide-diol **2,3** is heated to 160 °C with a rate of 20 °C.min⁻¹ and data points are collected at 30, 120 and 135 °C (fig. 3.20). Additionally, the melted sample was cooled down to 30 °C with a rate of 20 °C.min⁻¹ to check for thermal decomposition. The spectra at 30 °C before and after the measurement are similar indicating no thermal decomposition. Note that the different cooling rates also have no influence on the crystal structure. When the sample was heated to 160 °C, the diffraction line at 3.8 Å disappeared at ~120 °C indicating the melting of α -type crystals or the reorganization of these crystals into γ -type crystals. Up to the melt at ~140 °C, the diffraction peak at 4.2 Å, although broad, remained clearly present and represents the γ -type phase. With optical microscopy a similar melting behaviour was observed. At 134 °C, a layer of crystals (α -type) disappeared while different crystals (γ -type) appeared underneath (fig. 3.7d). The remaining crystals melted at 140 °C.

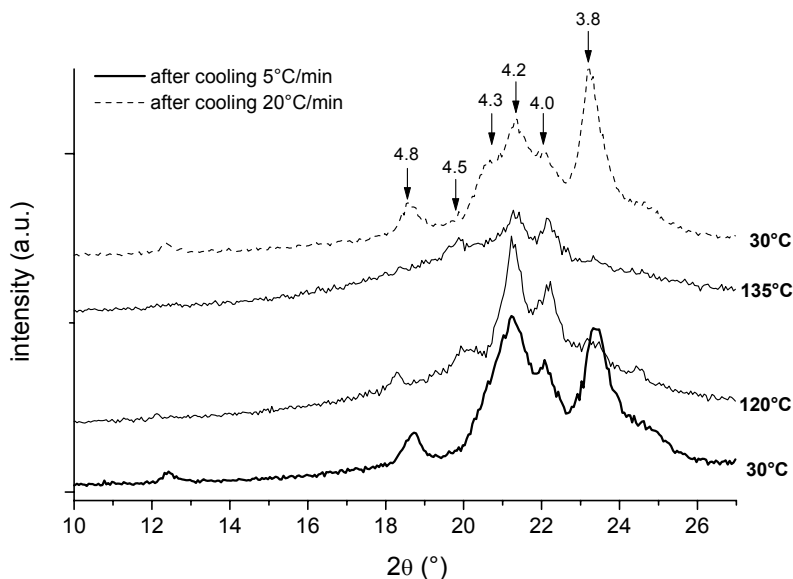


Figure 3.20: WAXD spectra of bisamide-diol **2,3** heated from 30 to 140 °C with a rate of 20 °C.min⁻¹. Before heating, the samples were cooled from the melt with a rate of 5 °C.min⁻¹. The data represent the d-spacings in Å.

Conclusions

Chemically pure and monodisperse bisamide-diols were prepared through ring-opening of ϵ -caprolactone or γ -butyrolactone with 1,4-diaminobutane or 1,2-diaminoethane. As these bisamide-diols will be incorporated in poly(butylene adipate) to form segmented poly(ester amide)s they are used as model compounds to elucidate the crystalline structure in the corresponding polymer. Combined temperature dependent FT-IR and WAXD allows, as we are not able to produce a single crystal, a qualitative description of the crystalline structure of the bisamide-diols. At room temperature, bisamide-diols are present in an α - or γ -type crystalline phase or a mixture of both, similar to those found in nylons. Bisamide-diols prepared from 1,4-diaminobutane crystallize predominantly in an α -type phase while bisamide-diols prepared from 1,2-diaminoethane crystallize into a mixture of α - and γ -type crystals. While heating the bisamide-diols to the melt, multiple endothermic transitions were observed. By crossing the lower endothermic transitions,

crystals melt and/or reorganize in to a different crystalline phase (crystal-to-crystal transformation).

Acknowledgements

Marc Ankoné is acknowledged for the bisamide-diol synthesis. The authors thank Herman Koster for the WAXD measurements and Siebolt Harkema and Gerrit van Hummel for valuable discussions. This study was financially supported by the European Commission, project: QLK5-1999-01298.

References

1. J.D. Sudha, *J. Polym. Sci. Part A: Polym. Chem.*, **2000**, 38, 2469.
2. J.D. Sudha, C.K.S. Pillai, S. Bera, *J. Polym. Mater.*, **1996**, 13, (4), 317.
3. H.R. Stapert, A.M. Bouwens, P.J. Dijkstra, J. Feijen, *Macromol. Chem. and Phys.*, **1999**, 200, (8), 1921.
4. H.R. Stapert, P.J. Dijkstra, J. Feijen, *Macromol. Symp.*, **1998**, 130, 91.
5. S. Katayama, T. Murakami, *J. Appl. Polym. Sci.*, **1976**, 20, 975.
6. S. Katayama, H. Horikawa, *J. Appl. Polym. Sci.*, **1971**, 15, 775.
7. S. Bera, Z. Jedlinski, *Polymer*, **1993**, 34, (16), 3545.
8. S. Bera, Z. Jedlinski, *J. Polym. Sci. Part A: Polym. Chem.*, **1993**, 31, (3), 731.
9. S. Bera, Z. Jedlinski, *Polymer*, **1992**, 33, (20), 4331.
10. T.H. Barrows, V.L. Horton, Comparison of bioabsorbable poly(ester-amide) monomers and polymers in vivo using radiolabeled homologs, in *Progress in biomedical polymers*. **1988**: Los Angeles.
11. T.H. Barrows, **1986**, *The design and synthesis of bioabsorbable poly(ester-amides)*, plenum publ. corp., New York.
12. M.I. Kohan, **1995**, *Nylon plastics handbook*, Hansers Publisher, New York.
13. J. Puiggali, L. Franco, C. Aleman, J.A. Subirana, *Macromolecules*, **1998**, 31, 8540.
14. N.A. Jones, E.D.T. Atkins, M.J. Hill, J. Cooper, L. Franco, *Polymer*, **1997**, 38, (11), 2689.
15. N. Jones, E. Atkins, *Macromolecules*, **1996**, 29, 6011.
16. C. Ramesh, A. Keller, *Polymer*, **1994**, 35, (12), 2483.

17. S. Rhee, J. White, *Polymer*, **2002**, 43, 5903.
18. W. Saiyasombat, *Polymer*, **1998**, 39, (23), 5581.
19. B. Vanhaecht, C.E. Koning, *Macromolecules*, **2004**, 37, (2), 421.
20. Y. Yoshioka, K. Tashiro, C. Ramesh, *Polymer*, **2003**, 44, 6407.
21. Y. Li, W.A. Goddard, *Macromolecules*, **2002**, 35, 8440.
22. N. Paredes, M.T. Casas, J. Puiggali, B. Lotz, *J. Polym. Sci.: Part B: Polym. Phys.*, **1999**, 37, 2521.
23. R. Brill, *J. Prakt. Chem.*, **1942**, 161, 49.
24. Y. Li, D. Yan, E. Zhou, *Colloid Polym. Sci.*, **2002**, 280, 124.
25. N. Vasanthan, N. Sanjeeva Murthy, R.G. Bray, *Macromolecules*, **1998**, 31, 8433.
26. D. Yan, Y. Li, X. Zhu, *Macromol. Rapid. Commun.*, **2000**, 21, 1040.
27. X. Yan, X. Zhu, L. Chen, P. He, D. Yan, X. Wang, *J Polym. Sci.: Part B: Polym. Phys.*, **2004**, 42, 60.
28. G. Zhang, Y. Li, D. Yan, *Polym. Int.*, **2003**, 52, 795.
29. Y. Yoshioka, K. Tashiro, *J. Phys. Chem. B*, **2003**, 107, 11835.
30. Y. Yoshioka, K. Tashiro, *Polymer*, **2003**, 44, 7007.
31. K. Tashiro, Y. Yoshioka, *Polymer*, **2004**, 45, 6349.
32. K. Tashiro, Y. Yoshioka, *Polymer*, **2004**, 45, 4337.
33. S.J. Cooper, M. Coogan, N. Everall, I. Priestnall, *Polymer*, **2001**, 42, 10119.
34. S.J. Cooper, E.D.T. Atkins, M.J. Hill, *Macromolecules*, **1998**, 31, 8947.
35. S.J. Cooper, E.D.T. Atkins, M.J. Hill, *J. Polym. Sci.: Part B: Polym. Phys.*, **1998**, 36, 2848.
36. K. Brandt, T. Latawiec, *Bulletin of the Polish Academy of Sci-Chem.*, **1989**, 37, (3-4), 141.
37. P.A.M. Lips, chapter 4, in *this thesis*. **2004**.
38. P.A.M. Lips, chapter 5, in *this thesis*. **2004**.

Chapter 4

Synthesis and characterization of poly(ester amide)s containing crystallizable amide segments

P.A.M. Lips¹, R. Broos², M.J.M van Heeringen², P.J. Dijkstra¹, J. Feijen¹

¹ *Institute for Biomedical Technology (BMTI) and Department of Polymer Chemistry and Biomaterials, Faculty of Science and Technology, University of Twente, P.O. Box 217, 7500 AE Enschede, The Netherlands.*

² *Core R&D, Dow Benelux N.V., PO Box 48, 4530 AA, Terneuzen, The Netherlands.*

Abstract

High molecular weight segmented poly(ester amide)s were prepared by melt polycondensation of 1,4-butanediol, dimethyl adipate and a preformed bisamide-diol based on 1,4-diaminobutane and ϵ -caprolactone. By varying the ratio of the bisamide-diol and 1,4-butanediol a series of polymers was obtained with a hard segment content between 10 and 85 mol%. FT-IR and WAXD analysis revealed that the poly(ester amide)s crystallize in an α -type phase similar to the α -phase of nylon 6,6. These polymers all have a micro-phase separated structure with an amide-rich hard phase and an ester-rich flexible soft phase. The polymers have a low and a high melt transition, corresponding with the melting of crystals comprising single ester amide sequences and 2 or more ester amide sequences, respectively. The low melt transition is between 50 and 70 °C and is independent of polymer composition. By increasing the hard segment content from 10 to 80 mol% the high melt transition increased from 80 to 140 °C while the glass transition temperature increased from -52 to -8 °C. Likewise, the elastic modulus increased from 70 to 550 MPa, the stress at break increased from 8 to 28 MPa

while the strain at break decreased from 850 to 350%. Thermal and mechanical properties can thus be tuned for specific applications by varying the hard segment content in these segmented polymers.

Introduction

Aliphatic polyesters, such as poly(ϵ -caprolactone) and poly(butylene adipate) are biodegradable, but lack the physical and mechanical properties necessary for a broad range of applications. Synthetic aliphatic polyamides are generally not biodegradable but have favourable crystallization properties, good solvent and heat stability and high moduli and tensile strength. Combination of the characteristics of both groups of polymers may be achieved by the synthesis of aliphatic poly(ester amide)s in which amide groups are randomly distributed in the polymer chain ¹⁻¹³ or in which well-defined amide group containing blocks or segments are incorporated in the polymer ^{11, 14-20}.

Segmented poly(ester-amide)s consisting of rigid amide segments and amorphous flexible ester segments are thermoplastic elastomers ²¹. These polymers have a micro-phase separated structure with an amide-rich hard phase and an ester-rich soft phase (fig. 4.1). The amide-rich phase usually contains crystalline lamellae and acts as a thermo-reversible physical crosslinker for the amorphous phase. The soft phase has a sub-ambient glass transition temperature (T_g) and contributes to the flexibility and extensibility of the polymer. Heating above the melting temperature of the hard domains usually results in phase mixing of hard and soft segments. Without the reinforcing tie points, the polymer will flow as a thermoplastic material and can easily be melt processed. Upon cooling, the hard and soft segments become incompatible, which leads to phase separation into micro-domains and crystallization and thus to reformation of the physical crosslinks. Previous research revealed that an effective way to improve phase separation is using short, symmetrical and uniform amide blocks ²²⁻²⁵. The hard segments almost completely crystallize which results in a T_g independent of hard segment content. If the hard segments crystallize only partially, the non-crystallizing units are either mixed with the amorphous segments or form a separate amorphous phase. If the hard segments are miscible with the amorphous soft segments, only one T_g is found and the T_g increases with the hard segment content in the amorphous phase.

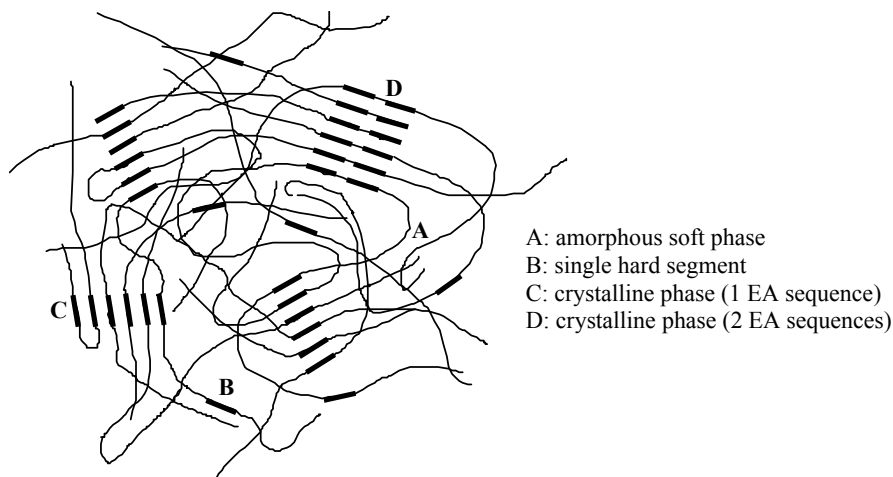


Figure 4.1: Schematic picture of the different phases in a segmented poly(ester amide) with ester-amide sequences abbreviated as EA ²⁶.

Aliphatic segmented poly(ester amide)s containing uniform hard blocks have received limited attention. Segmented poly(ester-amide)s (fig. 4.2B) prepared from preformed bisamide-diols and oligoesters were synthesized by Bera *et al.* ^{19, 20}. The bisamide-diol prepared from 1,6-diaminohexane and γ -butyrolactone, was first reacted with adipic acid to form a hard alternating poly(ester amide) oligomer (fig. 4.2A). The oligoester (soft block) was prepared from 1,2-ethanediol and dimethyl adipate. A series of high molecular weight polymers was obtained by reacting various ratios of hard and soft oligomers. By increasing the hard oligomer content from 20 to 80 mol% the modulus increased from 70 to 600 MPa and the yield stress increased from 0.04 to 15 MPa. All polymers have two glass transition temperatures (-40 to -50 °C and 40 to 50 °C) and one melting temperature at ~ 200 °C, indicating the presence of two separate amorphous domains and a crystalline phase. Hydrogen bonding, studied with temperature dependent IR, showed that amide-amide and ester-amide H-bonds were formed in all polymers ^{27, 28}. It was concluded that the ester-amide H-bonds are stable up to 210 °C whereas the amide-amide H-bonds disappear at 170 °C. However, Aleman *et al.* showed that computed interaction energies of ester-amide H-bonds were similar in strength as the amide-amide H-bonds in polypeptides and related polymers ²⁹.

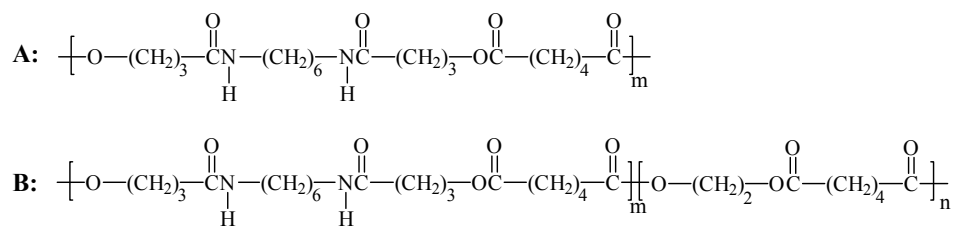


Figure 4.2: An alternating poly(ester amide) (A) based on 1,6-diaminohexane, γ -butyrolactone and adipic acid and a segmented poly(ester amide) (B) based on 1,6-diaminohexane, γ -butyrolactone, 1,2-ethanediol and adipic acid¹⁹.

Another way to prepare segmented poly(ester amide)s is to react oligoesters with a diacid chloride and a diamine by interfacial polymerization (fig. 4.3)^{11, 17, 18}. These polymers have two crystalline phases, with characteristic melting temperatures of the corresponding linear polyesters (75-77 °C) and polyamides (242-248 °C).

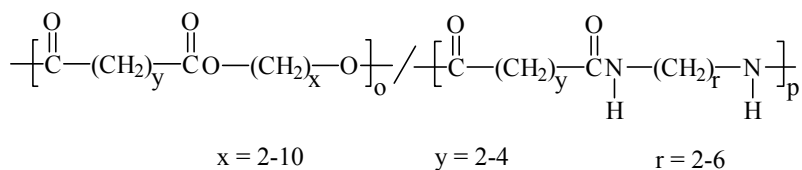


Figure 4.3: A segmented poly(ester amide) based on an alkanediamine, a diacid chloride and a diol terminated oligoester¹¹.

Stapert *et al.* prepared segmented block poly(ester amide)s by condensation of preformed bisamide-diols (fig. 4.4A) or bisamide-diester (fig. 4.4B), 1,4-butanediol and dimethyl adipate in the melt^{14-16, 30}. The uniform amide blocks were randomly distributed in the polymer chain and during the polycondensation reaction no or little ester-amide interchange occurred between segments of the polymer chain. These polymers show an endothermic transition between 50 and 70 °C followed by a melting temperature, which increased from 80 to 140 °C by increasing the hard segment content from 10 to 100 mol%. The higher transition corresponds to the melting of a crystalline phase consisting of crystals composed of 2 or more subsequent uniform ester amide (EA) sequences. The first melt transition, which is independent of the amide content of

the polymer, is attributed to melting of crystals comprising single uniform EA sequences. This crystalline phase is meta stable with respect to the higher melting crystalline phase. The glass transition temperature increases with increasing hard segment content, indicating a homogenous amorphous phase.

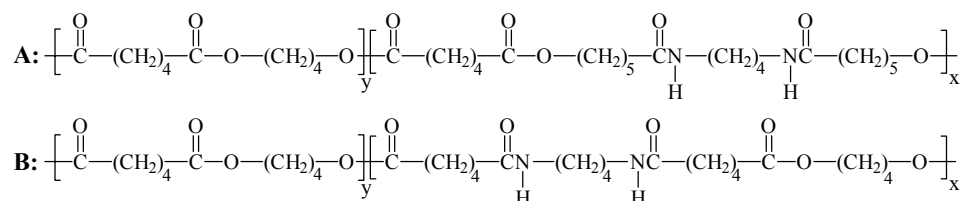


Figure 4.4: A segmented poly(ester amide) with a soft block (y) based on 1,4-butanediol and dimethyl adipate and a hard block (x) based on (A) ϵ -caprolactone, 1,4-diaminobutane and dimethyl adipate¹⁵ or (B) 1,4-diaminobutane, dimethyl adipate and 1,4-butanediol¹⁴.

The ratio of hard to soft segments, affects the properties of segmented poly(ester amide)s as the polymer changes from a more soft polyester to a hard polyamide. In this chapter the influence of the amount of hard segment in segmented poly(ester amide)s based on a N,N'-1,4-butanediyl-bis[6-hydroxy-hexanamide], dimethyl adipate and 1,4-butanediol, on the thermal, physical and mechanical properties is described.

Experimental

Materials

1,4-Butanediol, dimethyl adipate (synthetic grade) chloroform-d1 and the catalyst tetrabutylorthotitanate (Ti(OBu)₄) were purchased from Merck, Germany. The anti-oxidant Irganox 1330 was kindly provided by Ciba Geigi, Switzerland. Trifluoroacetic acid-d1 was obtained from Aldrich, The Netherlands. All other solvents were obtained from Biosolve, the Netherlands. The synthesis of N,N'-1,4-butanediyl-bis[6-hydroxy-hexanamide] is described in chapter 3 ($T_m = 144\text{ }^\circ\text{C}$)³¹.

Poly(ester amide) synthesis

The synthesis of the copolymer based on N,N'-1,4-butanediyl-bis[6-hydroxy-hexanamide], 1,4-butanediol and dimethyl adipate (DMA) was carried out as previously described¹⁵. Small adjustments were implemented to scale up the polymerization to ~100 g.

The molar ratio of hard (x) and soft (y) segments in the poly(ester amide) is varied by changing the ratio of N,N'-1,4-butanediyl-bis[6-hydroxy-hexanamide] and 1,4-butanediol.

A typical procedure for the preparation of PEA4,5-25 containing 25 mol% of hard segment is described hereafter in detail. Dimethyl adipate (70.00 g, 0.402 mol), N,N'-1,4-butanediyl-bis[6-hydroxy-hexanamide] (31.79 g, 0.101 mol) and a twofold excess of 1,4-butanediol (54.07 g, 0.602 mol) were placed in a polymerisation tube. To the mixture ~1 ml of a stock solution (0.15 g.ml⁻¹) of Ti(OBu)₄ in toluene and Irganox 1330 (1.55 g = 1.0 wt% of total mass) were added. The amount of catalyst used was always 2 mg Ti(OBu)₄ / g DMA. The mixture was stirred for 15 min at room temperature under an argon atmosphere. The pressure was reduced to 500 mbar and subsequently the mixture was slowly heated to 180 °C over a period of 3 h. The methanol distilled off during this period and was collected in a trap, cooled with ice water. Subsequently, the pressure was slowly decreased to ~100 mbar. The reaction vessel was cooled to room temperature under vacuum and left to stand over night. An additional 0.14 g of catalyst was added. The reaction mixture was heated to 180 °C under reduced pressure (500 mbar). In the next 2 h the pressure was decreased to 5 mbar. The temperature was increased to 190 °C and the pressure was very slowly decreased to 0.15 mbar. The trap was cooled with liquid nitrogen, which reduced the pressure to 0.1 mbar. The excess of 1,4-butanediol was distilled off during the next 5 h. The final pressure was 0.04 mbar. The reaction mixture was then cooled to room temperature under vacuum. The polymer was dissolved in 100 ml of chloroform at 55 °C for 2 h and subsequently precipitated in 4 L of diethyl ether. The polymer was filtered, washed with cold diethyl ether and dried overnight at room temperature at reduced pressure.

The polymers PBA, PEA4,5-10, PEA4,5-25, PEA4,5-50, PEA4,5-75 and PEA4,5-85 with a hard segment content x of 0, 10, 28, 56, 78 and 85 mol%, respectively, were prepared according to the method described above.

Methods

NMR: ^1H (300 MHz) and ^{13}C (75.26 MHz) NMR spectra were recorded on a Varian Inova Nuclear Magnetic Resonance Spectrometer using chloroform- d_1 or trifluoroacetic acid- d_1 as a solvent.

Viscometry: Intrinsic viscosities $[\eta]$ were determined by a single point measurement using a capillary Ubbelohde type 0C at 25 °C and a polymer solution with a concentration of 0.1 g.dl $^{-1}$ in chloroform-methanol (1:1 vol/vol) ^{32, 33}. The following empirical equation was applied:

$$[\eta] = \frac{\sqrt{2}}{c} \sqrt{\eta_{\text{spec}} - \ln \eta_{\text{rel}}} \quad (\text{eq. 4.1})$$

where $\eta_{\text{spec}} = \eta_{\text{rel}} - 1$ and c is the polymer concentration in g.dl $^{-1}$.

The intrinsic viscosity of PEA4,5-25 was also determined by extrapolation of η_{rel} and η_{inh} to $c = 0$.

FT-IR: Fourier Transform Infrared spectra were recorded with a Biorad FTS 175 spectrometer utilizing a wide band MCT detector at 4 cm $^{-1}$ spectral resolution. Thin polymer films were placed between sodium chloride windows and transferred to a heatable infrared cell from Specac Inc. The sample was heated to 190 °C at 45 °C.min $^{-1}$, kept for 10 min at 190 °C, cooled to 30 °C with an average rate of 5 °C.min $^{-1}$. Subsequently, data points were collected between 4000 and 550 cm $^{-1}$.

Temperature dependent FT-IR spectra of poly(butylene adipate) (PBA) were performed on melt-crystallized materials. The polymer film was first heated to 100 °C (45 °C.min $^{-1}$), kept for 10 min at 100 °C and cooled to 30 °C with an average rate of 5 °C.min $^{-1}$. The sample was then heated to 100 °C in steps of 10 °C at a heating rate of 45 °C.min $^{-1}$. After each step the temperature was kept constant for 5 min before data collection.

The crystallinity w_c (in mol%) of the poly(ester amide)s was calculated according to:

$$w_c = \frac{b_1}{b_1 + b_2 + b_3} * x \quad (\text{eq. 4.2})$$

with b_1 the band area of the amide I band at 1634 cm^{-1} (H-bonded, ordered, crystalline domains), b_2 the band area of the amide I band at $\sim 1651 \text{ cm}^{-1}$ (H-bonded disordered, amorphous domains), b_3 the band area of the amide I band at $\sim 1673 \text{ cm}^{-1}$ (non-H-bonded, amorphous domains) and x the hard segment content in mol%. Curve fitting was used to resolve the selected IR-band areas.

WAXD: Wide angle X-ray diffraction spectra were recorded using a Philips X'Pert-MPD diffractometer in Bragg-Brentano geometry, with a Θ compensating divergence slit (10.0 mm). The polymer film (15 x 10 x 1mm) was mounted on a Pt filament in an Anton Paar HTK-16 temperature chamber. A Cu-anode was used, together with a curved graphite monochromator, giving $\text{CuK}\alpha_1$ radiation of 1.5406 \AA . Prior to measurement the chamber was flushed with nitrogen.

The sample was heated to $190 \text{ }^\circ\text{C}$, annealed for 10 min and subsequently cooled at $20 \text{ }^\circ\text{C}.\text{min}^{-1}$ to $30 \text{ }^\circ\text{C}$. Data points were collected in the range of 2Θ is $4\text{--}90 \text{ }^\circ$.

The peak position at angles of 2θ correspond to interplanar d-spacings according to Bragg's law (eq. 4.3)

$$d = \frac{n\lambda}{2 \sin \theta} \quad (\text{eq. 4.3})$$

with n is an integer and λ is the applied wavelength (1.5406 \AA).

TGA: Thermal gravimetric analysis was carried out with 5-10 mg samples under a nitrogen atmosphere in the $50\text{--}700 \text{ }^\circ\text{C}$ range at a heating rate of $10 \text{ }^\circ\text{C}.\text{min}^{-1}$, using a Perkin-Elmer Thermal gravimetric analyser TGA 7.

DSC: Thermal analysis of the polymers was carried out using a Perkin-Elmer DSC-7 Differential Scanning Calorimeter equipped with a PE7700 computer and TAS-7 software. Calibration was performed with pure indium. Measurements were performed on isolated precipitated polymers. Samples (5-10 mg) were heated from 25 to $180 \text{ }^\circ\text{C}$ at a rate of $20 \text{ }^\circ\text{C}.\text{min}^{-1}$, annealed for 5 min, cooled to $-80 \text{ }^\circ\text{C}$ at a rate of $20 \text{ }^\circ\text{C}.\text{min}^{-1}$, and subsequently heated from -80 to $180 \text{ }^\circ\text{C}$ at a rate of $20 \text{ }^\circ\text{C}.\text{min}^{-1}$. Melting (T_m) and crystallization (T_c) temperatures were obtained from the peak maxima, melt (ΔH_m) and

crystallization (ΔH_c) enthalpies were determined from the area under the curve and the glass transition temperature (T_g) was taken at the inflection point. The data presented are from the second heating step, unless stated otherwise.

Processing: Polymer bars were prepared both by compression moulding and injection moulding. Compression moulded bars (75x4x2 mm) were prepared with a hot press (THB 008, Fontijne Holland BV, the Netherlands). Polymers were heated for 6-8 min at 20 °C above their T_m as measured by DSC, pressed for 3 min at 300 kN, and cooled in approximately 5 min under pressure to room temperature. Injection moulded bars (70x9x2 mm) were prepared with an Arburg-H manual injection moulding machine. The barrel was set to 40 °C above the T_m of the polymer as determined by DSC.

DMA: Differential mechanical analysis was performed with a Myrenne ATM3 torsion pendulum at a frequency of approximately 1 Hz. The storage modulus (G') and the loss modulus (G'') were measured as a function of temperature. Samples (75x4x2 mm) were first cooled to -100 °C and then heated at a rate of 1 °C.min⁻¹. The temperature at which the loss modulus reached a maximum was taken as the T_g . The flow temperature (T_{flow}) was defined as the temperature at which the storage modulus reached 1 MPa.

Tensile tests: Tensile tests were conducted with compression moulded and injection moulded bars and tensile set measurements were performed with compression moulded bars, cut to dumbbells (ISO 37). A Zwick Z020 universal machine equipped with a 500 N load cell and extensometers was used to measure the stress as a function of strain at a strain rate of 500 mm.min⁻¹ and a preload of 3 N. Measurements were performed on at least 6 different polymer bars.

Compression set: Polymer samples (10x10x2 mm) cut from injection moulded bars were placed between two metal plates at 25 °C (ASTM 395 B standard) and compressed to 75% of their original thickness for 24 h. The sample thickness was determined half an hour after the load was released. The measurements were performed in triplo. The compression set (C.S.) is calculated according to:

$$CS = \frac{d_0 - d_2}{d_0 - d_1} \times 100\% \quad (\text{eq. 4.4})$$

where d_0 , d_1 , and d_2 are the sample thicknesses before, during, and after compression respectively.

Rheology: Melt viscosities were measured with a TA Instruments ARES-2 with parallel plates. The viscosity was determined at 190 °C as a function of the frequency (0.1-100 rad.s⁻¹).

Water uptake: The polymer water absorption was determined by placing polymer bars (75x4x2 mm) in a dessicator at room temperature at 100% relative humidity (RH) for 28 days. Samples (10x10x2 mm) were also immersed in demineralised water at 37 °C for 28 days. Compression moulded samples were predried at 30 °C under reduced pressure for at least 2 days. The water absorption (wt %) is calculated from:

$$\text{wt \%} = \frac{w_0 - w}{w_0} \times 100\% \quad (\text{eq. 4.5})$$

where w_0 and w are the sample weights before and after treatment, respectively.

Results and Discussion

Segmented poly(ester amide)s were prepared by copolymerisation of a bisamide-diol, dimethyl adipate and 1,4-butanediol in the melt (fig. 4.5). The trans-esterification was performed at 180 °C at atmospheric pressure under argon for 2 h. The polycondensation started by increasing the temperature to 190 °C and reducing the pressure to ~0.1 mbar with distillation of 1,4-butanediol. The molar ratio of hard (x) and soft (y) segment of the poly(ester amide) was varied by changing the ratio of bisamide-diol to 1,4-butanediol in the monomer feed. A series of poly(ester amide)s PEA4,5-10, PEA4,5-25, PEA4,5-50, PEA4,5-75 and PEA4,5-85 with a hard segment content x of 10, 28, 56, 78 and 85 mol%, respectively, were prepared in this way. The homopolymer poly(butylene adipate) (PBA) was added to the series.

Previously it has been shown that the symmetrical and uniform structure of the hard bisamide segments was retained in the polymer^{15, 30}. Less than 5 mol% of the symmetrical amide segments is lost due to alcoholysis of the amide bonds during the first hours of the reaction.

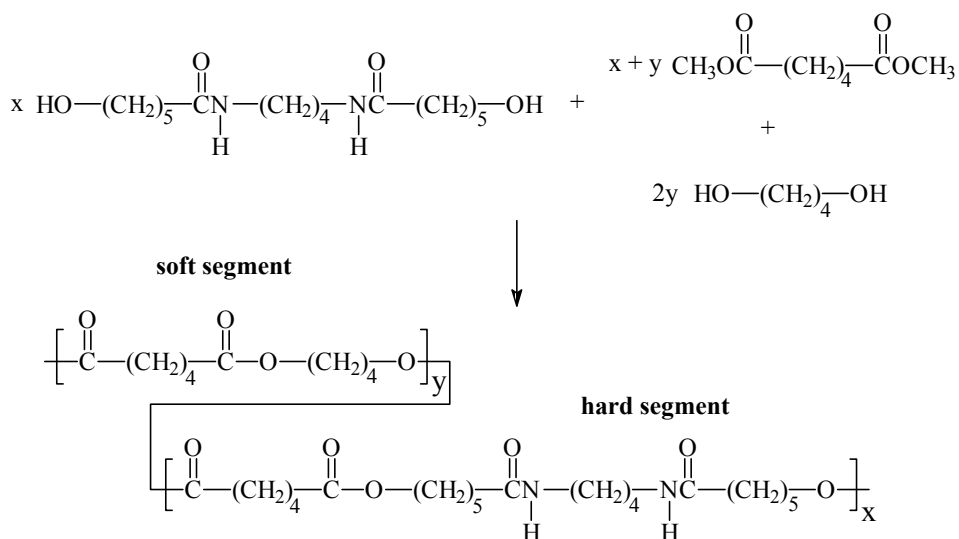


Figure 4.5: Reaction scheme for the synthesis of a poly(ester amide) based on bisamide-diol **4,5**, 1,4-butanediol and dimethyl adipate (PEA4,5).

A ^1H -NMR spectrum of PEA4,5-25 is presented in figure 4.6. The polymer composition (x/y) was determined from the ratio of the signal of the methylene groups next to the amide NH at δ 3.26 (**11**) and the signal of the methylene groups next to the ester acyl oxygen at δ 4.10 (**3** + **5**). The ^1H -NMR spectra were also used to estimate the molecular weights (M_n) of the polymers. Assuming that the polymer chains have hydroxyl end groups, molecular weights were calculated from the signals of the $\text{CH}_2\text{-OH}$ endgroups at δ 3.67 (**3^e** + **5^e**) and the signals of the methylene groups next to the ester acyl oxygen at δ 4.10 (**3** + **5**).

The composition of the poly(ester amide)s determined from the ^1H -NMR spectra in almost all cases deviates slightly from the intended composition (table 4.1). The deviation is becoming more pronounced at higher hard segment content. This deviation is caused by distillation of a small amount of dimethyl adipate during the polymerization, which disturbs the stoichiometry. The molecular weights (M_n), as determined from ^1H -NMR, are denoted as $>50 \text{ kg.mol}^{-1}$ for the poly(ester amide)s with a hard segment content up to 50 mol%, due to the inaccuracy in the measurement of the integrals of the small signals corresponding to the end-groups. Poly(ester amide)s with a

hard segment content of 78 and 85 mol% have a M_n of 39 and 20 $\text{kg}\cdot\text{mol}^{-1}$, respectively. These results show that the increasing deviation from the intended composition, by disturbing the stoichiometry, leads to a substantial decrease in M_n ^{30, 34}.

The ^{13}C -NMR spectra confirmed the structure of the poly(ester amide)s. Amide carbonyls at δ 182.2 and the carbon next to the amide NH at δ 41.0 are typical signals found. No additional signals due to interchange reactions were observed.

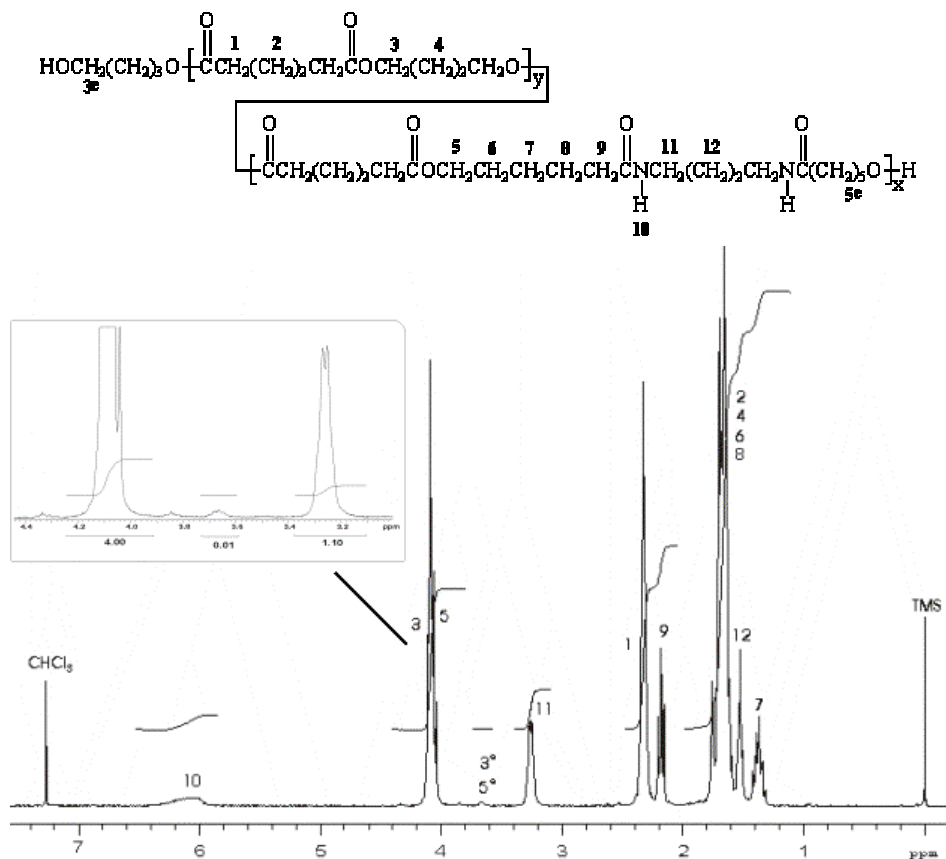


Figure 4.6: ^1H -NMR spectrum of PEA4,5-25 in chloroform- d_1 .

A standard GPC measurement was performed on PEA4,5-25 using a Waters Styragel column and chloroform as the eluent. An additional measurement without column was performed on PEA4,5-25 to exclude column interactions. The areas, as detected with refractive index (RI), of both measurements were compared and a discrepancy of 16% was observed. The area, detected with RI, was lower for the measurement with the

column indicating that some polymer remained on the column. Thus GPC measurements, performed with polymers dissolved in chloroform, were not reliable.

Previous work³⁵⁻³⁷ has shown that a mixture of chloroform-methanol (1:1 vol/vol) is a suitable solvent for poly(ether ester amide)s. It was not possible to perform GPC analyses on the poly(ester amide)s at 25 °C, using this solvent. Alternatively, the intrinsic viscosity of the polymer (chloroform-methanol 1:1 vol/vol) was evaluated by capillary viscometry by extrapolation of the reduced ($\eta_{\text{red}} = \eta_{\text{spec}} \cdot c^{-1}$) and inherent ($\eta_{\text{inh}} = \ln(\eta_{\text{rel}}) \cdot c^{-1}$) viscosities to $c = 0$ ³⁸. A linear relationship was observed for PEA4,5-25, suggesting that the chloroform-methanol mixture is a good solvent even at relatively high polymer concentrations (fig. 4.7). Extrapolating the reduced and inherent viscosities of PEA4,5-25 to $c = 0$ gives an intrinsic viscosity of $0.59 \pm 0.01 \text{ dl.g}^{-1}$. The reduced viscosity measured at $c = \sim 0.1 \text{ g.dl}^{-1}$ is 0.59 dl.g^{-1} , indicating that the single point measurement of the reduced viscosity is representative of the intrinsic viscosity for PEA4,5-25. Care should be taken when extrapolating these results to poly(ester amide)s with other compositions. In addition, since the Mark-Houwink constants are not known for the systems, the resulting intrinsic viscosities could not be converted to molecular weights.

The intrinsic viscosities of poly(ester amide)s before and after compression moulding are shown in table 4.1. The synthesized poly(ester amide)s have intrinsic viscosities of 0.5 – 0.6 dl.g^{-1} . The intrinsic viscosity decreased significantly upon compression moulding indicating that small amounts of absorbed moisture in poly(ester amide)s can already lead to hydrolytic chain scissions at elevated processing temperatures.

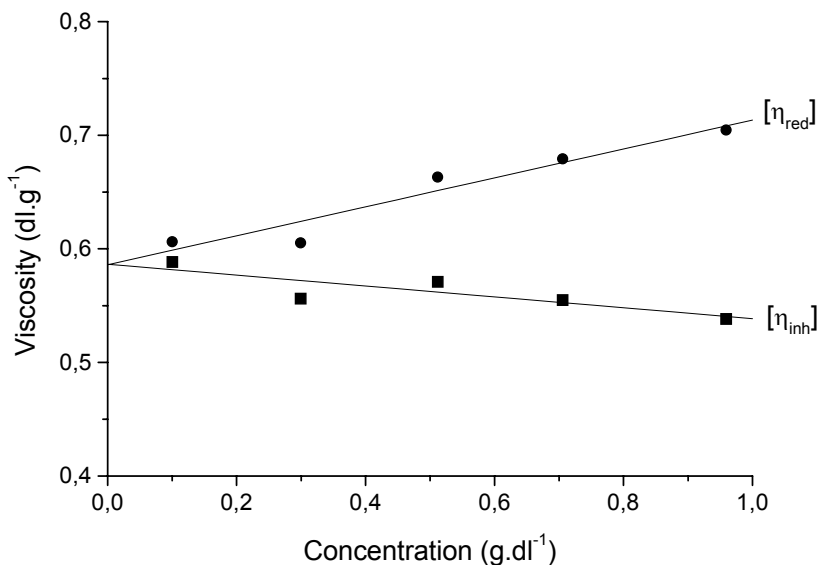


Figure 4.7: Reduced and inherent viscosities of PEA4,5-25, solvent CHCl_3 / MeOH (1:1 vol/vol) at 25 °C, as a function of concentration.

Table 4.1: Chemical composition and physical properties of PEA4,5 polymers with different hard segment content x .

polymer code	hard segment, x^a (mol %)	composition, x^b (mol %)	M_n^b (kg.mol ⁻¹)	$[\eta]^c$ (dl.g ⁻¹)	$M_n^{b,d}$ (kg.mol ⁻¹)	$[\eta]^{c,d}$ (dl.g ⁻¹)
PBA	0	0	27	0.43	27	0.39
PEA4,5-10	10	10	> 50	0.55	18	0.39
PEA4,5-25	25	28	> 50	0.59	20	0.52
PEA4,5-50	50	56	> 50	0.61	19	0.52
PEA4,5-75	70	78	39	0.52	13	0.44
PEA4,5-85	75	85	20	0.45	8	0.42

^a theoretical value, ^b according to ¹H-NMR, ^c CHCl_3 / MeOH (1:1 vol/vol) at 25 °C,

^d after compression moulding.

In figure 4.8 the FT-IR spectra of the PEA4,5 copolymers at room temperature are presented for the selected wave number regions, 3600-2700 and 1800-650 cm^{-1} .

Characteristic IR-bands are found at 3305 (ν N-H H-bonded), ~ 1730 (ν C=O ester), 1634 (amide I, ν C=O) and 1540 cm^{-1} (amide II, ν C-N + δ N-H). Several weaker IR-bands were observed at 1476, 1420 and 693 cm^{-1} belonging to the NH vicinal CH_2 bend, CO vicinal CH_2 bend and amide V, respectively. These latter IR-bands in combination with the amide II band provide important structural information. In polyamides like nylon 6,6 these bands are found at similar wave numbers, and are characteristic of a so-called α -crystalline phase. As only part of the structure of the bisamide-diol resembles the structure of nylon 6,6 the crystalline phase is denoted here as an α -type phase. Moreover, these bands are located at the same wave numbers as in the IR-spectra of the bisamide-diol monomer. It thus seems that the α -type crystalline structure of the bisamide-diol is preserved in the poly(ester amide).

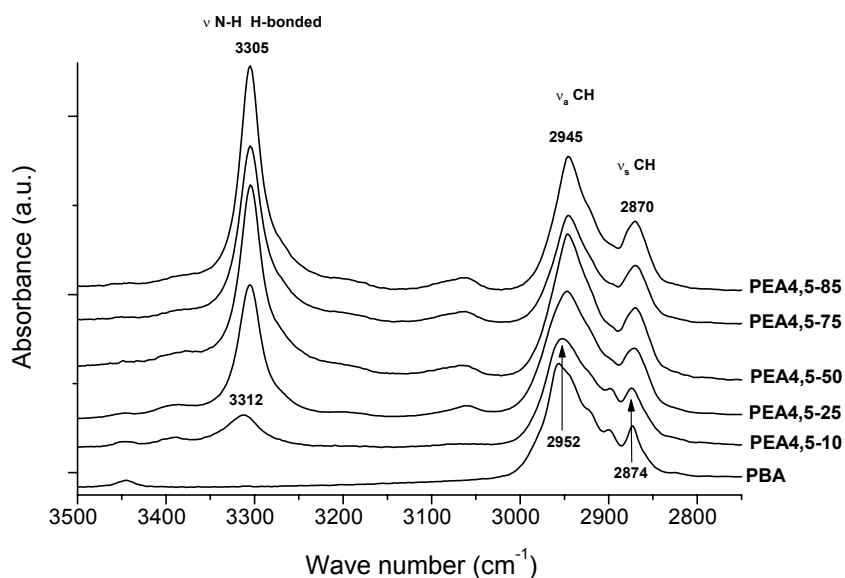


Figure 4.8a: FT-IR spectra of PBA and PEA4,5 polymers with different hard segment content (10-85 mol%) at room temperature for the wave number region $3600\text{-}2700\text{ cm}^{-1}$.

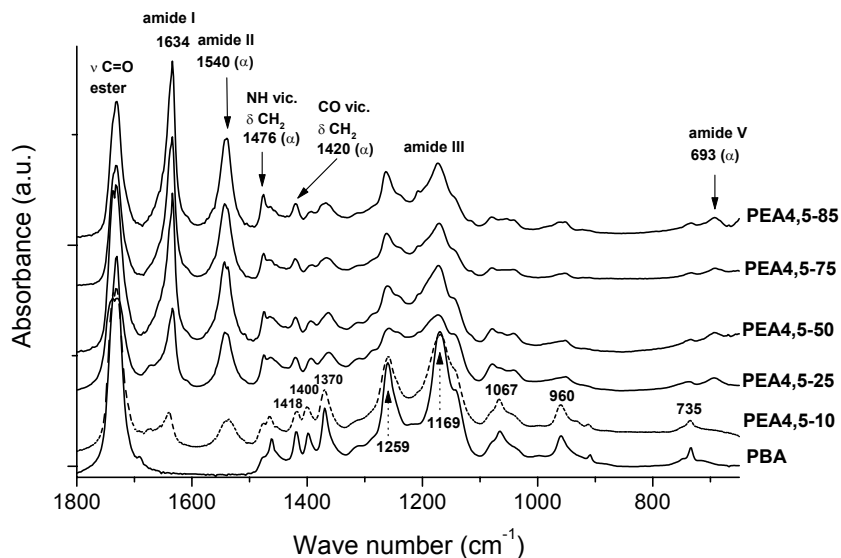


Figure 4.8b: FT-IR spectra of PBA and PEA4,5 polymers with different hard segment content (10-85 mol%) at room temperature for the wave number region 1800-650 cm^{-1} .

In a previous study it was shown that only at a low amide content of ~ 10 mol% crystallization of butylene adipate segments takes place¹⁵. This is illustrated by the change in FT-IR spectra of poly(butylene adipate) (PBA) at elevated temperatures (fig. 4.9). Upon heating PBA to the melt (60 °C), the IR-bands at 1419, 1398, 1370, 1260, 1170, 959 and 735 cm^{-1} (fig. 4.9A), which are related to the crystalline part, disappear or decrease drastically in intensity. FT-IR spectra of PEA4,5-10 also contain characteristic bands of crystalline PBA (fig. 4.8b), which show that besides hard segments also polyester segments crystallize.

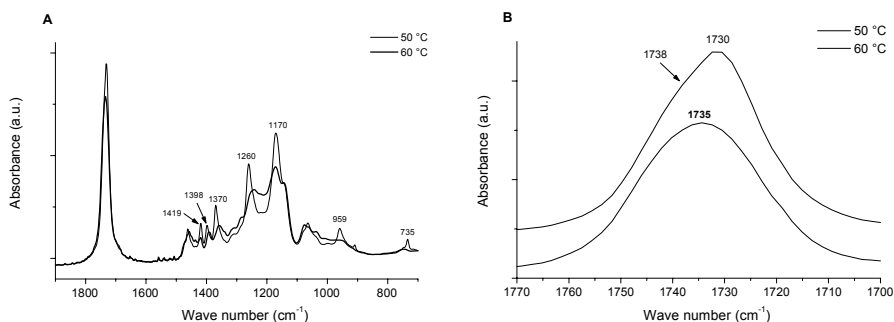


Figure 4.9: FT-IR spectra of PBA at 50 and 60 °C for the wave number region 1900-700 cm^{-1} (A) and 1770-1700 cm^{-1} (B).

The carbonyl band of PBA at room temperature is highly asymmetric with a narrow top at 1730 cm^{-1} and a shoulder around 1738 cm^{-1} (fig. 4.9B). Above 50 °C, the crystals melt and one broad band centred around 1735 cm^{-1} remains. This suggests that the absorption band at 1730 and 1738 cm^{-1} are associated with carbonyl groups in crystalline domains whereas the band at $\sim 1735 \text{ cm}^{-1}$ is associated with carbonyl groups in the amorphous phase ³⁹. However, care should be taken because curve fitting of this band is extremely difficult.

The band in the ester $\nu \text{C=O}$ region of the PEA4,5 polymers consists of two bands at ~ 1730 and $\sim 1738 \text{ cm}^{-1}$ (fig. 4.10). Since the soft polyester segments crystallize only in poly(ester amide)s with a hard segment content $\leq 10 \text{ mol\%}$, these results suggest that ester sequences in the hard segment of poly(ester amide)s with higher ($>10 \text{ mol\%}$) hard segment content are incorporated in the crystals.

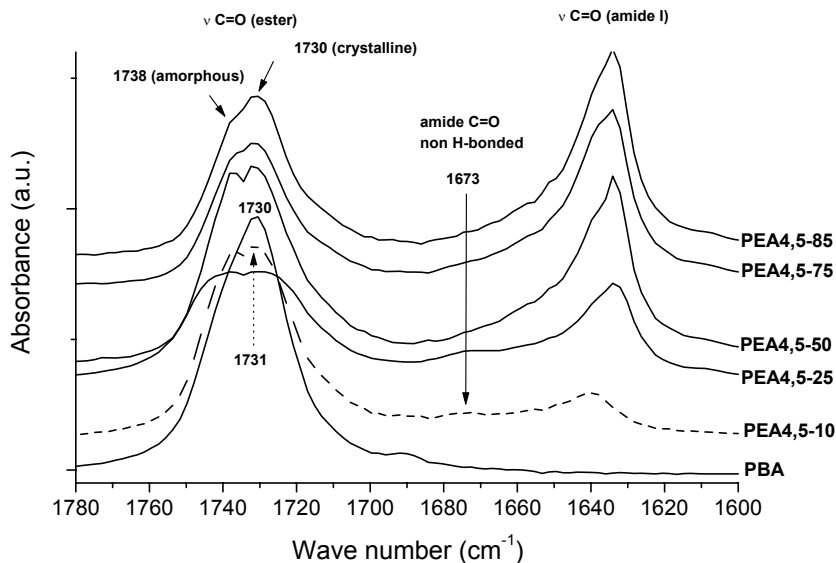


Figure 4.10: FT-IR spectra of PBA and PEA4,5 polymers with different hard segment content (10-85 mol%) at room temperature for the wave number region 1780-1600 cm^{-1} .

The WAXD spectra (fig. 4.11) of the PEA4,5 polymers show typical reflections of an α -type crystalline phase similar to the well-defined α -crystalline phase in nylon 6,6. These reflections represent the distance between two amide-amide intermolecular H-bonded chains (4.4 Å) and the distance between two van der Waals packed sheets (3.7 Å). In the WAXD spectra of the poly(ester amide)s the d-spacing (4.34-4.41 Å) representing the distance between two amide-amide intermolecular H-bonded chains is found at almost similar d-spacing as of nylon 6,6. The distance between the two van der Waals packed sheets (3.98-3.87 Å) in the poly(ester amide)s is somewhat larger than in nylon 6,6. The comparable values of the d-spacing in the PEA4,5 polymers and nylon 6,6 and the structural data obtained from FT-IR lead to the conclusion that the chains are in the fully extended planar zig-zag conformation forming H-bonded planar sheets typical for an α -crystalline phase.

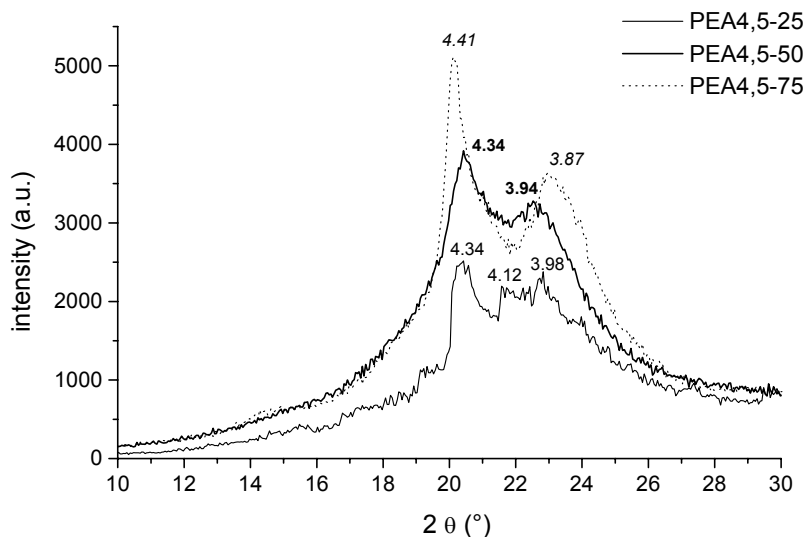


Figure 4.11: WAXD spectra of PEA4,5-25, PEA4,5-50 and PEA4,5-75 at room temperature. Polymers were heated to the melt, annealed for 10 min and subsequently cooled to 30 °C at 20 °C.min⁻¹. The data represent the d-spacings in Å.

Thermal properties

The thermal stability of the segmented poly(ester amide)s under non-oxidative conditions was investigated by thermal gravimetric analysis (TGA). PBA is stable up to 380 °C and segmented poly(ester amide)s are stable up to ~340 °C. The TGA trace of PBA is characterized by a single degradation step, whereas the poly(ester amide)s show a more complex degradation pattern, consisting of two main steps (fig. 4.12). For all polymers the decomposition temperatures are considerably higher than the melting temperature, which is important for the processing of these materials.

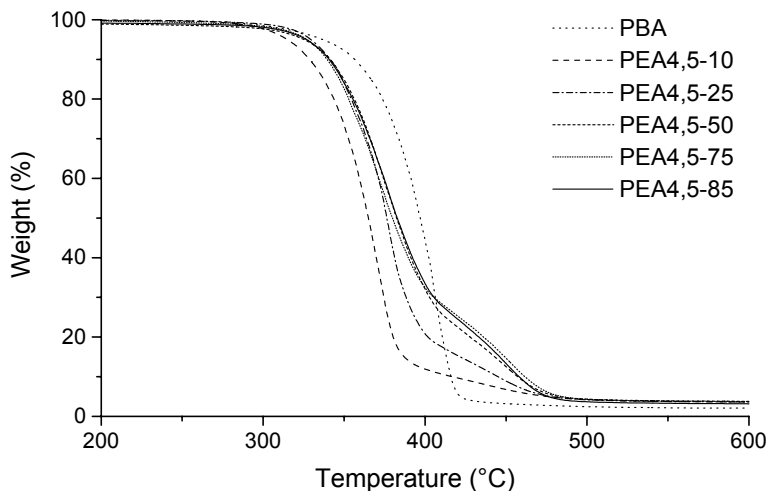


Figure 4.12: TGA thermograms of PBA and PEA4,5 polymers with different hard segment content x (10-85 mol%).

The crystallization and melting temperatures and corresponding enthalpies of the poly(ester amide)s were taken from the first cooling and second heating scan as measured by DSC (table 4.2). All PEA4,5 polymers show 2 melt transitions denoted as $T_{m,1}$ and $T_{m,2}$ for the low and high melt transition, respectively.

Table 4.2: Thermal properties of PEA4,5 polymers with different hard segment content x (10-85 mol%).

polymer code	$T_{m,1}$ (°C)	$\Delta H_{m,1}$ (J.g ⁻¹)	$T_{c,1}$ (°C)	$\Delta H_{c,1}$ (J.g ⁻¹)	$T_{m,2}$ (°C)	$\Delta H_{m,2}$ (J.g ⁻¹)	$T_{c,2}$ (°C)	$\Delta H_{c,2}$ (J.g ⁻¹)
PBA					63	58	24	-57
PEA4,5-10	59 ^a	35	-	-	83	1	-7, 22 ^b	-39
PEA4,5-25	70	24	-	-	108	9	37	-23
PEA4,5-50	67	16	-	-	126	32	54, 56, 79 ^c	-34
PEA4,5-75	58	4	22	-4	136	45	104	-42
PEA4,5-85	59	4	32	-4	140	58	111	-47

^a $T_{m,1} + T_{m,ester}$, ^b 2 peaks, ^c trimodal

Upon cooling from the melt, the poly(ester amide)s show a complex crystallization pattern with one or even multi-modal transitions depending on the hard segment content (fig. 4.13). Only in the poly(ester amide) with a high ester content (PEA4,5-10) crystallization of PBA is possible. However, the corresponding exotherm at $-7\text{ }^{\circ}\text{C}$, is found at a somewhat lower temperature compared to that of the homopolymer PBA ($24\text{ }^{\circ}\text{C}$). The exotherm at $22\text{ }^{\circ}\text{C}$ is due to the presence of crystals comprising EA segments.

Statistically, at low hard segment content, the number average ester amide (EA) sequence length k increases from 1.1 for PEA4,5-10 to 1.4 for PEA4,5-25^{26, 40}. This value is approximately 2.2 for PEA4,5-50 and 4.2 for the PEA4,5-75. This suggests that the crystalline phase at low amide content constitutes single EA sequences whereas the crystalline phase at high amide content contains 2 or more EA sequences. Moreover, in the IR-spectra of PEA4,5 polymers ($x > 10\text{ mol}\%$) a band was found at 1730 cm^{-1} corresponding with ester carbonyl groups in the crystalline phase, which confirms the formation of crystals comprising 2 or more EA sequences.

During cooling, a multi-modal exotherm was observed in the DSC scan of PEA4,5-50 which might be due to the presence of a mixture of crystals with different EA sequence lengths. At high EA content the T_c eventually shifts to temperatures of $111\text{ }^{\circ}\text{C}$, but also a small transition still can be observed at $\sim 30\text{ }^{\circ}\text{C}$ due to a crystalline phase containing single EA sequences.

Upon reheating, the poly(ester amide)s show an endothermic transition ($T_{m,1}$) between 50 and $70\text{ }^{\circ}\text{C}$ followed by a second transition ($T_{m,2}$) (fig. 4.14). PEA4,5-10 shows a broad melt transition at $59\text{ }^{\circ}\text{C}$, which is attributed to melting of crystalline PBA segments and of crystals that consist of single EA sequences. PEA4,5-25 shows an exotherm directly after the first melt transition, at which probably crystals are rearranged into a more stable crystalline structure.

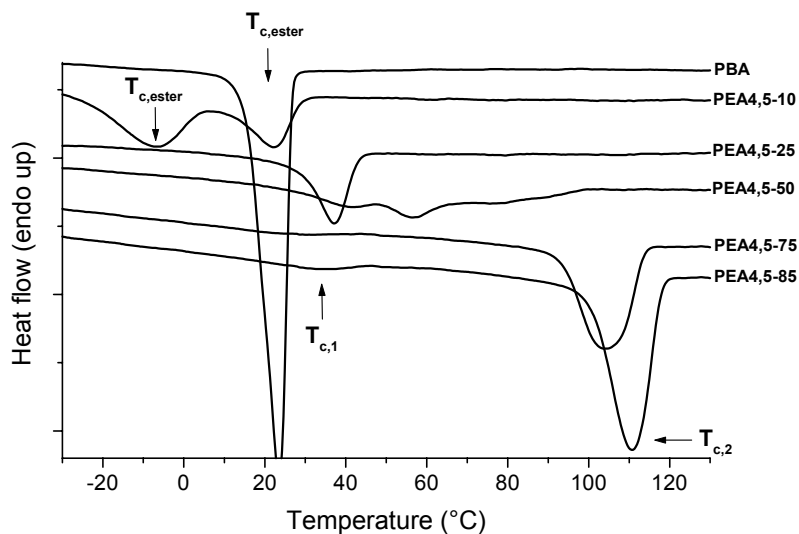


Figure 4.13: DSC cooling scans ($20\text{ }^{\circ}\text{C}.\text{min}^{-1}$) of PBA and PEA4,5 polymers with different hard segment content (10-85 mol%).

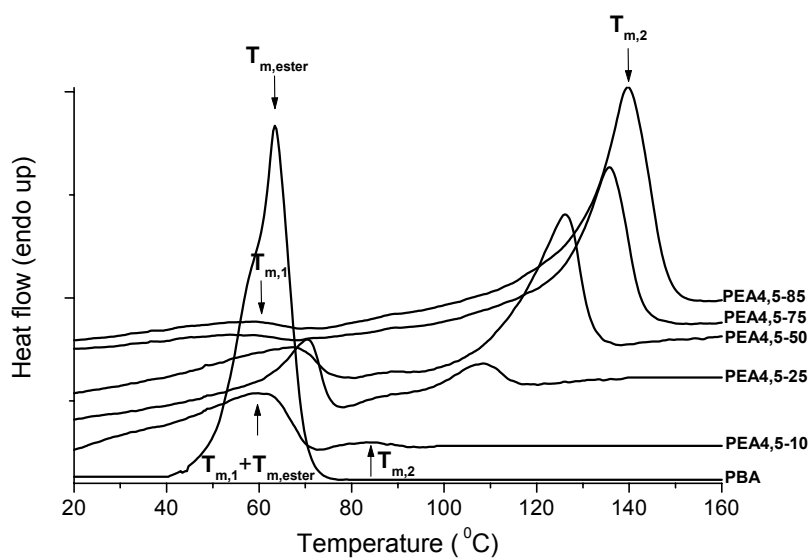


Figure 4.14: DSC heating scans ($20\text{ }^{\circ}\text{C}.\text{min}^{-1}$) of PBA and PEA4,5 polymers with different hard segment content x (10-85 mol%).

The first melting temperature was almost independent of the polymer hard segment content (fig. 4.15) ¹⁵. However, the corresponding melt enthalpies decreased with increasing hard segment (fig. 4.16). The higher probability of having crystals consisting of more successive EA sequences at higher hard segment content explains the decreasing melt enthalpy ($\Delta H_{m,1}$) ⁴⁰. The second melting temperature ($T_{m,2}$), at which crystals comprising 2 or more EA sequences melt, increases with decreasing soft segment content. This is a general trend observed for segmented copolymers and is explained by the solvent effect proposed by Flory ⁴¹. Upon dilution of the crystallizable hard segment thus increasing the molar fraction of soft segment, the size of the crystals will become smaller and hence its melting temperature decreases. Also with increasing hard segment content the average length of the hard segment and thus the crystal lamellar size increases, resulting in a higher melting temperature ⁴². Probably, the increasing melting temperature with increasing hard segment content is a consequence of both effects although $T_{m,2}$ is levelling off at higher hard segment contents to ~ 140 °C. The corresponding enthalpies still increase with increasing hard segment content. The crystallinity of the poly(ester amide)s, calculated by deconvolution of the IR-band of the amide I, increased with increasing hard segment content (table 4.3).

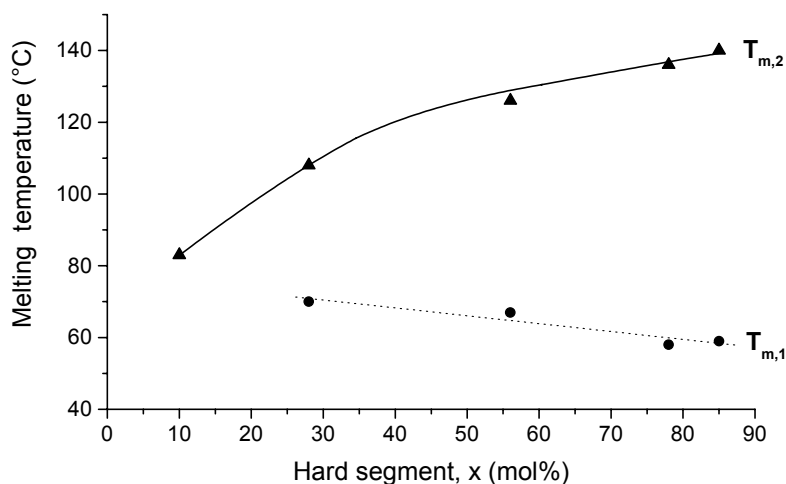


Figure 4.15: Low ($T_{m,1}$) and high ($T_{m,2}$) melting temperatures of PEA4,5 polymers as a function of hard segment content x .

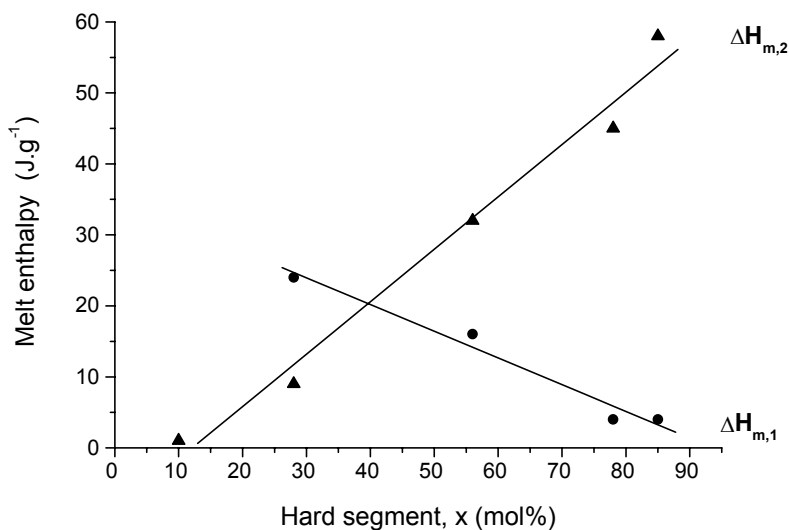


Figure 4.16: Melting enthalpies $\Delta H_{m,1}$ and $\Delta H_{m,2}$ for the low and high T_m transitions of PEA4,5 polymers as a function of hard segment content x .

Table 4.3: Thermal properties of PEA4,5 polymers with different hard segment content x , as obtained from DMA and DSC.

polymer code	x (wt %)	T_{flow} ^a (°C)	$T_{m,2}$ ^b (°C)	w_c ^c (mol%)	$G'_{25\text{ °C}}$ (MPa)	T_g ^a (°C)
PBA		60	63		140	-52
PEA4,5-10	14	70	83	5 ± 2.5	34	-45
PEA4,5-25	33	105	108	12.5 ± 2.5	62	-40
PEA4,5-50	53	130	126	27.5 ± 2.5	103	-20
PEA4,5-75	65	146	136	42.5 ± 2.5	203	-8
PEA4,5-85	68	145	140	42.5 ± 2.5	274	-5

^a from DMA, ^b from DSC, ^c crystallinity according to amide I band in FT-IR spectra.

Dynamic mechanical properties

Similar to $T_{m,2}$, the flow temperature as obtained from DMA measurements increased with increasing hard segment content (table 4.3). This transition is very sharp for all poly(ester amide)s.

Poly(ester amide)s with a hard segment content >25 mol% show a transition in the rubber plateau (fig. 4.17). This transition is found at temperatures corresponding with the lower melting temperature ($T_{m,1}$) obtained from DSC measurements.

DSC traces only showed weak transitions at the polymer T_g , which made their evaluation rather imprecise. For this reason, only T_g data obtained from DMA measurements are reported here. The T_g of the poly(ester amide)s is linearly increasing with increasing hard segment content (fig. 4.18) ¹⁵. This suggests that the phase separation is not complete and that hard segments are molecularly dispersed throughout the amorphous soft phase forming a homogeneous amorphous phase ²⁶.

The storage modulus at 25 °C, which is a measure for the crystallinity, increased with increasing hard segment content x (table 4.3 and fig. 4.20). This increase is due to an increased physical crosslink density at higher hard segment content as described by Wegner ⁴³.

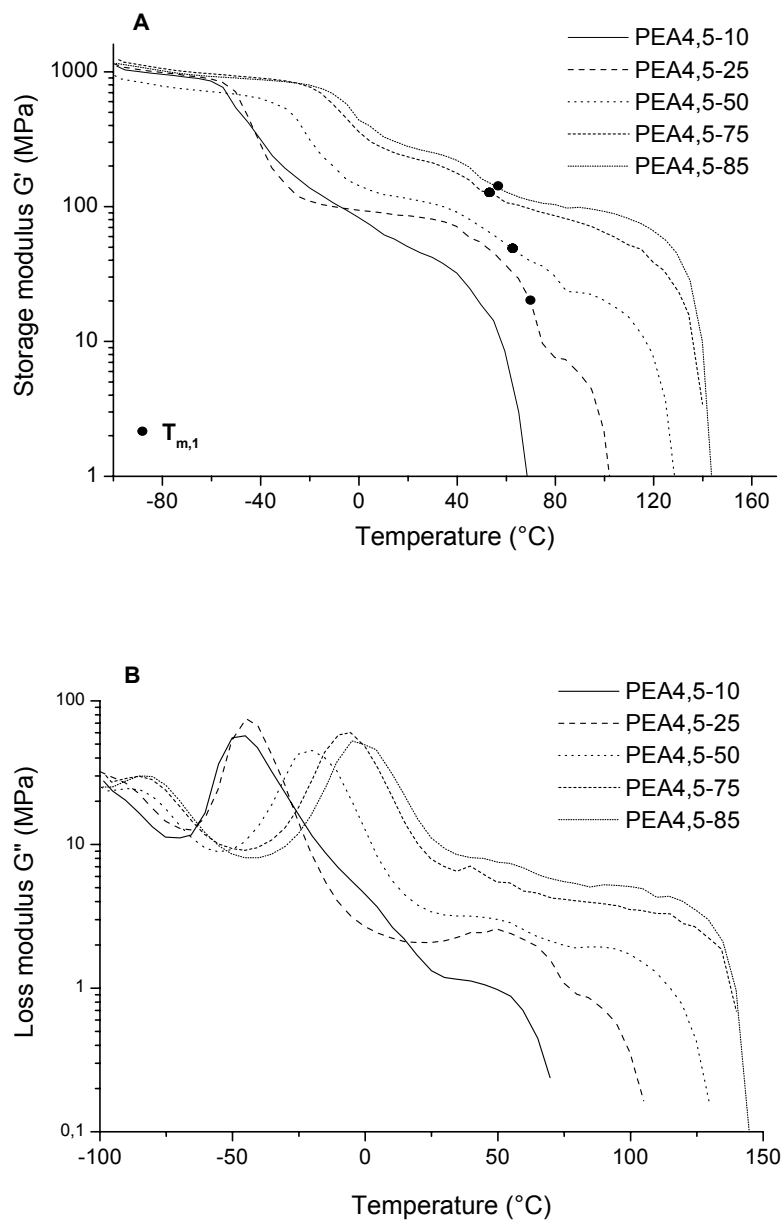


Figure 4.17: Storage modulus (A) and loss modulus (B) as a function of temperature for PEA4,5 polymers with different hard segment content x (10–85 mol%).

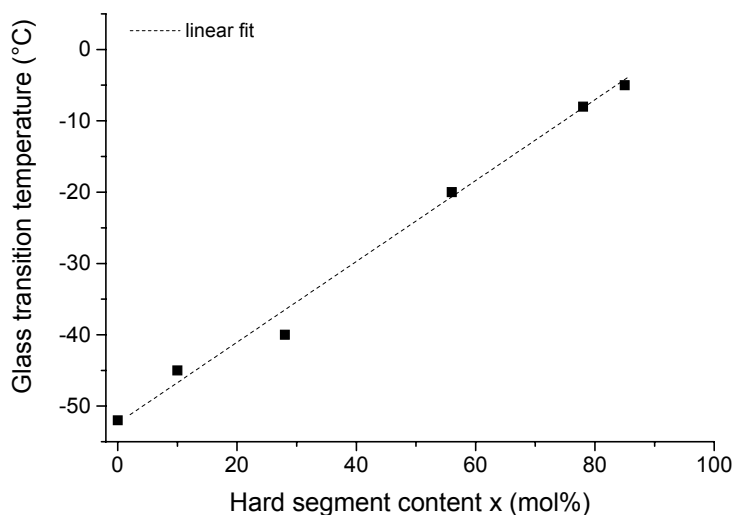


Figure 4.18: Glass transition temperature (T_g) as a function of hard segment content x in PEA4,5 polymers.

Mechanical properties

Typical stress-strain curves for the segmented poly(ester amide)s are presented in figure 4.19. The E modulus is determined at small deformations (0.1%) where stress increases linearly with strain (Hooke's law). At the yield point, the cross sectional area of the polymer bar starts to decrease in a localized region of the specimen, instead of over its entire length. This necking is associated with slip planes formed within the material. The plateau in the stress-strain curve reflects the growing of the neck, at the expense of the material at either end, eventually consuming the entire specimen after which the stress goes up again. Accompanying these macroscopic changes in the shape of the tensile bar are molecular processes. During straining of a segmented copolymer, the soft segments are stretched, thereby exercising forces on the crystalline structure. Above the yield point reorganization takes place and the material is permanently deformed (plastic deformation). Several research groups described a similar deformation process for segmented copolymers⁴⁴⁻⁴⁶. Just above the yield point, the network of crystalline lamellar stacks is disrupted but also individual stacks of lamellae start to break up in their lateral direction. At the same time, the chain axis of the hard segment begins to

orient preferentially transverse to the deformation axis. Upon further elongation and thus further disruption of the lamellae, the molecular axes become aligned parallel to the draw direction. At even higher strains, the amorphous soft segments start to deform until they approach their fully extended lengths, at which point the stress level becomes high enough to cause chain breakage and sample failure.

The PEA4,5 polymers with a high hard segment content display a stress-strain curve typical of glassy or crystalline homopolymers with a pronounced yield point followed by break at relatively low strains.

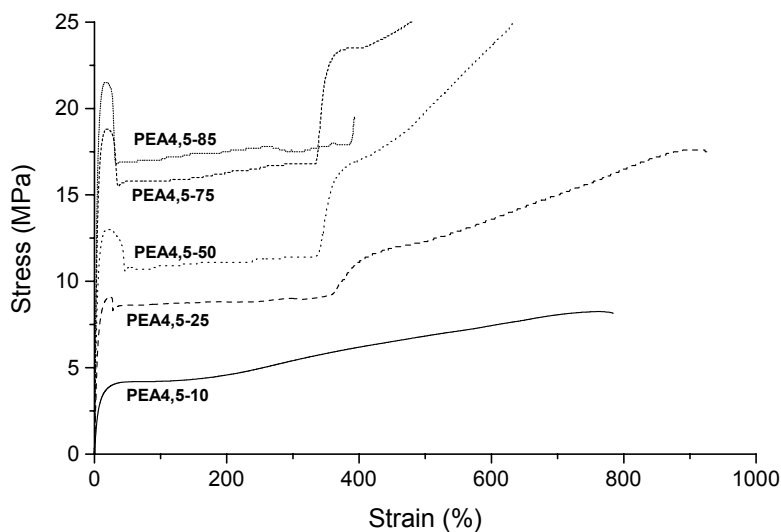


Figure 4.19: Stress strain curves for injection moulded samples of PEA4,5 polymers with different hard segment content x (10-85 mol%).

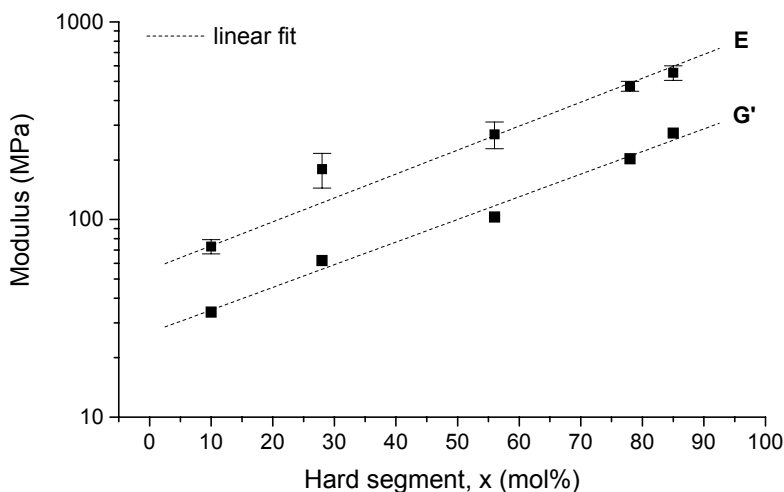


Figure 4.20: Elastic (E) and storage (G') modulus as a function of hard segment content x in PEA4,5 polymers.

According to Wegner ⁴³, the logarithm of the modulus of a segmented copolymer follows a linear relationship with the crystalline volume fraction. Plotting the logarithm of the tensile and storage modulus of the poly(ester amide)s against the hard segment content (fig. 4.20), confirms this empirical relationship. As a high preload was necessary to straighten the samples in between the clamps, the E moduli only indicate a trend.

By increasing the hard segment content from 10 to 85 mol%, the E modulus increases from 70 to 550 MPa, the yield stress increases from 4 to 26 MPa while the strain at break decreases from 870 to 350% (table 4.4). The homopolymer PBA has a high E modulus and tensile strength but is very brittle. By the incorporation of bisamide-diols moieties into the backbone of PBA the elastic modulus, yield stress and stress at break remained high but the strain at break increased to a large extent. Thus these poly(ester amide)s are tough materials with a high stiffness. The mechanical properties of these segmented poly(ester amide)s are similar to low density polyethylene ($T_g \sim -25^\circ\text{C}$, T_m 98-115 $^\circ\text{C}$), which has an elastic modulus in the range of 170-280 MPa, a stress at break in the range of 8-30 MPa and a strain at break in the range of 100 to 650%. The mechanical properties also correspond well with segmented poly(ester amide)s based on 1,6-

diaminohexane, γ -butyrolactone, 1,2-ethanediol and dimethyl adipate which revealed an elastic modulus up to 600 MPa and a yield stress up to 10 MPa with increasing hard segment content ²⁰.

Table 4.4: Mechanical properties of PBA and PEA4,5 polymers with different hard segment content x (10-85 mol%).

x (%)	E modulus (MPa)		yield stress (MPa)		stress at break (MPa)		strain at break (%)	
	com ^a	inj ^b	com ^a	inj ^b	com ^a	inj ^b	com ^a	inj ^b
0	415 ± 24	477 ± 20	15 ± 0.5	-	15 ± 0.5	17 ± 1.5	150 ± 20	10 ± 5
10	73 ± 6	70 ± 11	4 ± 0.5	-	8 ± 0.5	8 ± 0.5	870 ± 35	820 ± 45
25	180 ± 36	180 ± 35	9 ± 0.5	9 ± 0.5	15 ± 1	16 ± 1	810 ± 100	840 ± 60
50	270 ± 42	274 ± 30	14 ± 0.5	13 ± 0.5	25 ± 1	26 ± 0.5	680 ± 30	660 ± 10
75	473 ± 27	432 ± 36	23 ± 1	18 ± 1	24 ± 1.5	28 ± 2	420 ± 20	580 ± 25
85	553 ± 47	524 ± 59	26 ± 1	22 ± 1	25 ± 2	22 ± 1	50 ± 15	370 ± 25

^a compression moulded bars

^b injection moulded bars

Polymer samples were processed by compression as well as injection moulding in order to determine the influence of these processing steps on the mechanical properties. Overall, the mechanical properties of both series of polymer are comparable. In general, injection moulded samples have a lower crystallinity compared to compression moulded samples because the latter is cooled down at lower rate. This is reflected in the somewhat higher modulus and yield stress for the compression moulded samples. The strain at break for the compression moulded film of PEA4,5-85 is significantly lower compared to that of the injection moulded film, which might be due to their low molecular weight.

Table 4.5: Compression set of injection moulded samples of PEA4,5 polymers with different hard segment content x (10-85 mol%).

polymer code	x (wt %)	σ at yield (MPa)	ϵ at yield (%)	CS _{25%} (%)
PEA4,5-10	14	-	- ^a	35 ± 2
PEA4,5-25	33	9 ± 0.5	24 ± 2	39 ± 5
PEA4,5-50	53	13 ± 0.5	18 ± 2	49 ± 6
PEA4,5-75	65	18 ± 1	16 ± 1	30 ± 5
PEA4,5-85	68	22 ± 1	16 ± 0.5	5 ± 2

^ano yield point

Complete elastic recovery is hardly observed for thermoplastic elastomers (TPE's) ²¹. During deformation polymer chains in a network held together by entanglements and other physical interactions are stretched. Above the yield point reorganization takes place, the crystalline network as well as the crystalline lamellae start to disrupt. After release of the external stress the polymer chains retract to their original position with a gain in entropy as the driving force for the recovery. However, only part of the material recovers. The non-recoverable plastic deformation is due to permanent viscous flow of the polymer chains. Relaxation in semi-crystalline polymers is associated with the amorphous component, the crystalline component or an interaction whereby the crystalline component constrains the motion of the amorphous phase ^{42, 47}. In TPE's the soft segments usually relax to the non-oriented state while the hard domains remain oriented which leads to a considerable amount of permanent set ^{44, 45}. Long soft segments are less influenced by the restricting behaviour of the hard domains and will accordingly be better capable of accommodating deformation without breaking and will retract more readily, resisting set. In general, a higher hard segment content leads to a higher permanent set in segmented copolymers ^{48, 49}.

To measure the compression set (CS) at room temperature, polymer bars are compressed to 75% of their original thickness and thus the polymers are strained above their yield point (table 4.5). During the compression test the polymer is deformed to some state of strain (25 % of compression) and secured in such a way that it retains the initial deformation. Since the material behaves visco-elastic, the stress level is lowered

(relaxation) during the experiment (in time). After release of the external stress, the polymer system will show a time-dependent strain relaxation. The compression set of the PEA4,5 polymers increases with increasing hard segment content up to 50 mol%. Surprisingly, the compression set starts to decrease by increasing the hard segment content to 85 mol%. However, PEA4,5 polymers with a high hard segment content have a higher stiffness (higher modulus and yield stress) compared to PEA4,5 polymers with a low hard segment content (table 4.5) and thus the initial force (stress) to sustain a similar deformation will be higher. It is thus understandable that PEA4,5 polymers with a high hard segment content respond differently with respect to relaxation (elastic recovery) as compared to PEA4,5 polymers with a low hard segment. In addition, the elastic recovery is time dependent and relaxation time in our experiment (30 min.) is probably not enough to reach a state of equilibrium.

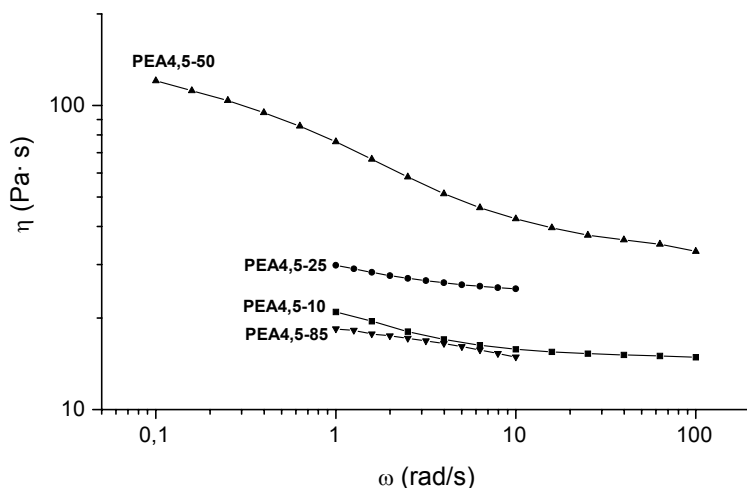


Figure 4.21: Melt viscosity at 190 °C as a function of shear rate for PEA4,5 polymers with different hard segment content x .

Upon heating the poly(ester amide)s to the melt, the physical crosslinks are removed and the polymer can easily be melt processed. The melt viscosity is an important parameter in polymer processing and is dependent on the molecular weight of the polymer and the temperature. The melt viscosity at 190 °C of poly(ester amide)s with different hard segment contents (fig. 4.21) decreased with increasing shear rate, which is known as

“shear thinning”⁴². This viscosity reduction is caused by the reduced number of chain entanglements as the chains orient along the lines of flow.

At all shear rates, the melt viscosity increases with increasing hard segment content, except for PEA4,5-85 which has a very low melt viscosity due to its low molecular weight.

Water uptake

The polymer water absorption was determined by placing polymer samples in a dessicator at room temperature at 100% relative humidity (RH) or immersing polymer samples in water at 37 °C. The water absorption of poly(ester amide) samples was followed in time over a period of 3 wks. Polymers show an increase in water absorption in time, which is levelling off at prolonged times (equilibrium). PBA shows a low water absorption of 0.7% at equilibrium. Polyamides are known to have high water absorption⁵⁰, and it was expected that with increasing bisamide content the water absorption will increase.

Table 4.6: Equilibrium water uptake of PEA4,5 polymers with different hard segment content, conditioned at 100% relative humidity at room temperature or immersed in water at 37 °C.

x (%)	time _{equilibrium} (days)	water uptake _{RH = 100%} (%)	time _{equilibrium} (days)	water uptake _{37°C} (%)
0	3	0,7	1	1.0 ± 0,2
10	6	3,8	5 ^a	14.7 ± 0.2
25	6	5,7	3	11.7 ± 0.1
50	6	7,5	2	9.4 ± 0.1
75	6	6,1	5	8.8 ± 0.1
85	6	5,9	3	7.8 ± 0.2

^a not at equilibrium

Water absorption of polymers at 100% RH, is maximal at a hard segment content of ~50 mol% (table 4.6). The polymers PEA4,5-75 and PEA4,5-85 show a lower water absorption than expected based on their amide content, which can be ascribed to the

higher crystallinity of these materials. The polymers immersed in water at 37 °C show a decreasing water absorption with increasing hard segment content. Apparently the increasing crystallinity is more important than the increasing amide content. The very high water uptake of PEA4,5-10 is probably caused by partial melting of the polymer at 37 °C (fig. 4.14), which decreases the crystallinity.

Conclusions

High molecular weight segmented poly(ester amide)s comprising different ester to amide ratios have been successfully prepared by melt polycondensation of a preformed bisamide-diol, 1,4-butanediol and dimethyl adipate. The polymers have melt transitions between 50 and 70 °C and between 80 and 140 °C, depending on the hard segment content, and a sub-ambient glass transition temperature (–52 to –8 °C). The poly(ester amide)s have a micro-phase separated structure with an amide-rich hard phase and an ester-rich flexible soft phase. The poly(ester amide)s crystallize in an α -type phase similar to nylon 6,6. The presence of α -related bands in the IR- and WAXD-spectra of the bisamide-diol monomer indicates that the α -type crystalline structure of the bisamide-diol is preserved in the poly(ester amide).

By increasing the hard segment content from 10 to 80 mol% the elastic modulus increased from 70 to 550 MPa, the stress at break increased from 8 to 28 MPa while the strain at break decreased from 850 to 350%. It can be concluded that the incorporation of well-defined amide segments in the poly(butylene adipate) backbone results in improved thermal and mechanical properties compared to the homopolymer poly(butylene adipate). Furthermore, these properties can be tuned for specific applications by varying the hard segment content in these segmented polymers.

Acknowledgements

Dow Benelux NV (Terneuzen) is acknowledged for the rheology and FT-IR measurements. The authors thank Herman Koster for the WAXD measurements. This study was financially supported by the European Commission, project: QLK5-1999-01298.

References

1. R. Timmermann, E. Grigat, R. Koch, *Polym. Degrad. Stab.*, **1998**, 59, (1-3), 223.
2. T. Ferre, J. Puiggali, *Polymer*, **2003**, 44, 6139.
3. S. Wiegand, *J. Env. Polym. Degrad.*, **1999**, 7, (3), 145.
4. K.E. Gonsalves, *Macromolecules*, **1992**, 25, 3309.
5. S.Y. Lee, *Polym. Degrad. Stab.*, **2002**, 78, 63.
6. Z.Y. Qian, *Polym. Degrad. Stab.*, **2003**, 81, 279.
7. Z.Y. Qian, *Colloid Polym. Sci.*, **2003**, 281, 869.
8. A. Alla, *Polymer*, **1997**, 38, (19), 4935.
9. A. Perez-Rodriguez, *J. Appl. Polym. Sci.*, **2000**, 78, 486.
10. S. Andini, *Macromol. Chem. Rapid Commun.*, **1988**, 9, 119.
11. L. Castaldo, F. de Candia, G. Maglio, *J. Appl. Polym. Sci.*, **1982**, 27, 1809.
12. E. Armelin, J. Puiggali, *Polymer*, **2001**, 42, 7923.
13. N. Kawasaki, *Macromol. Chem. Phys.*, **1998**, 199, 2445.
14. H.R. Stapert, P.J. Dijkstra, J. Feijen, *Macromol. Symp.*, **2000**, 152, 127.
15. H.R. Stapert, P.J. Dijkstra, J. Feijen, *Macromol. Symp.*, **1998**, 130, 91.
16. H.R. Stapert, M. van der Zee, P.J. Dijkstra, J. Feijen, *Abstracts Papers ACS*, **1997**, 213, 253.
17. S. Pivsa-Art, *J. Appl. Polym. Sci.*, **2002**, 85, (4), 774.
18. L. Castaldo, G. Maglio, *Polym. Bull.*, **1992**, 28, 301.
19. S. Bera, Z. Jedlinski, *J. Polym. Sci. part A: Polym. Chem.*, **1993**, 31, (3), 731.
20. S. Bera, Z. Jedlinski, *Polymer*, **1992**, 33, (20), 4331.
21. G. Holden, N.R. Legge, R. Quirk, H.E. Schroeder, **1996**, *Thermoplastic elastomers*, Hanser, New York.
22. J.A. Miller, S.B. Lin, K.S. Kirk, K.S. Hwang, K.S. Wu, P.E. Gibson, S.L. Cooper, *Macromolecules*, **1985**, 18, (1), 32.
23. R.J. Gaymans, J.L. de Haan, *Polymer*, **1993**, 34, (20), 4360.
24. H.N. Ng, A.E. Allegrezza, R.W. Seymour, S.L. Cooper, *Polymer*, **1973**, 14, 255.
25. L.L. Harrell, *Macromolecules*, **1969**, 2, (6), 607.
26. R.J. Cella, *J. Polym. Sci.*, **1973**, 42, 727.

27. B. Kaczmarczyk, *Polymer*, **1998**, 39, (23), 5853.
28. B. Kaczmarczyk, D. Sek, *Polymer*, **1995**, 36, (26), 5019.
29. C. Aleman, J.J. Navas, S. Munoz-Guerra, *J. Phys. Chem.*, **1995**, 99, 17653.
30. H.R. Stapert, A.M. Bouwens, P.J. Dijkstra, J. Feijen, *Macromol. Chem. Phys.*, **1999**, 200, (8), 1921.
31. P.A.M. Lips, chapter 3, in *this thesis*. **2004**.
32. O.F. Solomon, I.Z. Ciuta, *J. Appl. Polym. Sci.*, **1962**, VI, 683.
33. R.N. Shroff, *J. Appl. Polym. Sci.*, **1965**, 9, 1547.
34. F. Pilati, B. Manaresi, B. Fortunato, A. Munari, P. Monari, *Polymer*, **1983**, 24, 1479.
35. A.A. Deschamps, D.W. Grijpma, J. Feijen, *J. Biomater. Sci. Polym. Edn.*, **2002**, 13, (12), 1337.
36. F. Signori, R. Solaro, E. Chiellini, P.A.M. Lips, P.J. Dijkstra, J. Feijen, *Macromol. Chem. and Phys.*, **2003**, 204, (16), 1971.
37. F. Signori, R. Solaro, P.A.M. Lips, P.J. Dijkstra, J. Feijen, E. Chiellini, *Macromol. Chem. and Phys.*, **2004**, 204, (16), 1299.
38. F.W. Billmeyer, Structure and properties of polymers, in *Textbook of polymer science*. **1962**, Wiley-Interscience: New York. p. 79.
39. B. Fei, C. Chen, H. Wu, S. Peng, X. Wang, L. Dong, *Eur. Polym. J.*, **2003**, 39, 1939.
40. H.R. Stapert, *PhD thesis*, **1998**, University of Twente, The Netherlands: p. 121.
41. P.J. Flory, *Trans. Faraday Soc.*, **1955**, 51, 848.
42. L.H. Sperling, **2001**, *Introduction to physical polymer science*, Wiley-Interscience, New York.
43. G. Wegner, Model studies toward a molecular understanding of the properties of segmented block copolyetheresters, in *Thermoplastic elastomers*. **1987**, Hanser: New York.
44. R.M. Versteegen, *PhD thesis*, **2003**, Technische Universiteit Eindhoven, The Netherlands: p. 65.
45. M.C.E.J. Niesten, S. Harkema, E. van der Heide, R.J. Gaymans, *Polymer*, **2001**, 42, 1131.
46. R. Bonart, *J. Macromol. Sci. Phys.*, **1968**, B2, (1), 115.

47. N.G. McCrum, C.P. Buckley, C.B. Bucknall, **1991**, *Principles of polymer engineering*, Oxford university press, Oxford.
48. M.C.E.J. Niesten, R.J. Gaymans, *J. Appl. Polym. Sci.*, **2001**, *81*, 1372.
49. J. Krijgsman, D. Husken, R.J. Gaymans, *Polymer*, **2003**, *44*, 7573.
50. M.I. Kohan, **1995**, *Nylon plastic handbook*, Hanser, New York.

Chapter 5

Incorporation of different crystallizable amide blocks in segmented poly(ester amide)s

P.A.M. Lips¹, R. Broos², M.J.M van Heeringen², P.J. Dijkstra¹, J. Feijen¹

¹ *Institute for Biomedical Technology (BMTI) and Department of Polymer Chemistry and Biomaterials, Faculty of Science and Technology, University of Twente, P.O. Box 217, 7500 AE Enschede, The Netherlands.*

² *Core R&D, Dow Benelux N.V., PO Box 48, 4530 AA, Terneuzen, The Netherlands.*

Abstract

High molecular weight segmented poly(ester amide)s were prepared by melt polycondensation of dimethyl adipate, 1,4-butanediol and a symmetrical bisamide-diol based on ϵ -caprolactone and 1,2-diaminoethane or 1,4-diaminobutane. FT-IR and WAXD analysis revealed that segmented poly(ester amide)s based on the 1,4-diaminobutane (PEA4,5) give an α -type crystalline phase whereas polymers based on the 1,2-diaminoethane (PEA2,5) give a mixture of α - and γ -type crystalline phases with the latter being similar to γ -crystals present in odd-even nylons. PEA2,5 and PEA4,5 polymers with a hard segment content of 25 or 50 mol% have a micro-phase separated structure with an amide-rich hard phase and an ester-rich flexible soft phase. All polymers have a glass transition temperature below room temperature and melt transitions are present at 60 to 70 °C ($T_{m,1}$) and at 110 to 130 °C ($T_{m,2}$) with the latter being highest at higher hard segment content. The two melt transitions are ascribed to melting of crystals comprising single ester amide sequences and 2 or more ester amide sequences, respectively. These polymers have an elastic modulus in the range of 160-350 MPa, a stress at break in the range of 15-25 MPa combined with a high strain at break

(600-800%). The thermal and mechanical properties are not influenced by the different crystalline structures of the polymers, only by the amount of crystallizable hard segment present.

Introduction

Aliphatic poly(ester amide)s, which are biodegradable and have good processing- and end-use properties, are interesting materials for environmental and biomedical applications. Several groups have devoted their research to this class of materials and showed that starting from commercial or synthesized monomers, amide groups can be randomly distributed in the polymer chain or be incorporated in the polymer as well-defined blocks or segments, leading to a wide variety of materials ¹⁻²¹.

In our previous research it was shown that the incorporation of well-defined amide blocks or segments in the polyester main chain results in materials with a relatively high melting temperature, a low glass transition temperature and sufficient mechanical properties ^{5, 21-24}. A strategy to ensure the uniformity of the amide blocks, is the polycondensation of preformed bisamide-diols with aliphatic diesters and diols to obtain segmented poly(ester amide)s.

Bisamide-diols are conveniently synthesized through ring-opening of lactones by α,ω -diamines ^{4, 5, 21, 25-28}. Polycondensation of such bisamide-diols with dimethyl adipate and aliphatic diols has been intensively investigated ^{5, 7, 21, 23, 29, 30}. Poly(ester amide)s are easily prepared but it appeared that bisamide-diols synthesized from diamines and lactide or glycolide are unreactive or decompose at the high polycondensation temperatures. Contrary, bisamide-diols prepared from 1,4-diaminobutane and ϵ -caprolactone (bisamide-diol **4,5**) can be easily incorporated in the polymer chain with hardly any ester amide interchange reactions taking place ²¹. The conservation of the bisamide moiety leads to an extraordinary crystallization behaviour of the poly(ester amide)s. The FT-IR and WAXD spectra of these polymers revealed that the crystalline phase shows high spectral similarities to the α -crystalline phase present in nylon 6,6. Moreover, the structural analysis of the bisamide-diol monomer revealed a similarity in crystalline structure of the monomer and polymer, which led to the conclusion that a well-defined segmented polymer is obtained. Because a full structural analysis can not

be made because e.g. a crystal structure of the monomer or polymer is not available the crystalline phase has been ascribed as an α -type crystalline phase.

Poly(ester amide)s with a hard segment content > 10 mol% show two distinct melting transitions at relative low (60-70 °C) and high (130-140 °C) temperatures which are assigned to the melting of crystals composed of single ester amide sequences and 2 or more ester amide sequences, respectively.

A bisamide-diol prepared from 1,2-diaminoethane and ϵ -caprolactone (bisamide-diol **2,5**) has a completely different crystalline structure than that prepared from 1,4-diaminobutane. The FT-IR and WAXD spectra of this monomer revealed a crystalline structure with structural characteristics of a γ -crystalline phase present in even-odd and even nylons like nylon 6³¹. The characteristic IR-band of the amide II at 1559 cm⁻¹ and the diffraction peak at a d-spacing of ~4.2 Å are typical for the structure of even-odd nylons and are found also in the spectra of bisamide-diol **2,5**. This prompted us to compare poly(ester amide)s based on these two bisamide-diols and study the relation between their crystalline structure and material properties.

In this chapter the synthesis and properties of segmented poly(ester amide)s prepared from bisamide-diols **4,5** or **2,5**³¹ are described. The molar ratio of hard (x) and soft (y) segment of the poly(ester amide) has been varied by changing the ratio of the alkanediyl-bis[6-hydroxy-hexanamide] to 1,4-butanediol in the condensation with dimethyl adipate. Poly(ester amide)s with a hard segment content of 25 and 50 mol% were selected and their thermal, crystallization and mechanical behaviour were studied.

Experimental

Materials

1,4-Butanediol, dimethyl adipate (synthetic grade) chloroform-d1 and the catalyst tetrabutylorthotitanate (Ti(OBu)₄) were purchased from Merck, Germany. The anti-oxidant Irganox 1330 was kindly provided by Ciba Geigi, Switzerland. Trifluoroacetic acid-d1 was obtained from Aldrich, The Netherlands. All other solvents were obtained from Biosolve, the Netherlands. The synthesis of N,N'-1,4-butanediyl-bis[6-hydroxy-hexanamide] (T_m = 144 °C) and N,N'-1,2-ethanediyl-bis[6-hydroxy-hexanamide] (T_m = 163 °C) was described previously³¹.

Poly(ester amide) synthesis

Copolymerisations of N,N'- α , ω alkanediyl-bis[6-hydroxy-hexanamide], 1,4-butanediol and dimethyl adipate were performed in the presence of Ti(OBu)₄ as a catalyst. The molar ratio of hard (x) and soft (y) segments in the poly(ester amide) is varied by changing the ratio of N,N'- α , ω alkanediyl-bis[6-hydroxy-hexanamide] and 1,4-butanediol (fig. 5.1).

A typical procedure for the preparation of a PEA_{2,5-25} containing 25 mol% of N,N'-1,2-ethanediyl-bis[6-hydroxy-hexanamide] is described hereafter in detail. Dimethyl adipate (70.00 g, 0.402 mol), N,N'-1,2-ethanediyl-bis[6-hydroxy-hexanamide] (29.94 g, 0.100 mol) and a twofold excess of 1,4-butanediol (54.07 g, 0.602 mol) were placed in a polymerization tube. To the mixture ~1 ml of a stock solution (0.15 g.ml⁻¹) of Ti(OBu)₄ in toluene and Irganox 1330 (1.55 g = 1.0 wt% of total mass) were added. The amount of catalyst used was always 2 mg Ti(OBu)₄ / g DMA. The mixture was stirred for 15 min at room temperature under an argon atmosphere. The pressure was reduced to 500 mbar and subsequently the mixture was slowly heated to 180 °C over a period of 3 h. The methanol distilled off during this period and was collected in a trap, cooled with ice water. Subsequently, the pressure was slowly decreased to ~100 mbar. The reaction vessel was cooled to room temperature under vacuum and left to stand over night. An additional 0.14 g of catalyst was added. The reaction mixture was heated to 180 °C under reduced pressure (500 mbar). In the next 2 h the pressure was decreased to 5 mbar. The temperature was increased to 190 °C and the pressure was very slowly decreased to 0.15 mbar. The trap was cooled with liquid nitrogen, which reduced the pressure to 0.1 mbar. The excess of 1,4-butanediol was distilled off during the next 5 h. The final pressure was 0.04 mbar. The reaction mixture was then cooled to room temperature under vacuum. The polymer was dissolved in 100 ml of chloroform at 55 °C for 2 h and subsequently precipitated in 4 L of diethyl ether. The polymer was filtered, washed with cold diethyl ether and dried overnight at room temperature at reduced pressure.

The polymers PEA_{4,5-25}, PEA_{4,5-50} with 28 and 56 mol% of N,N'-1,4-butanediyl-bis[6-hydroxy-hexanamide], respectively and PEA_{2,5-25} and PEA_{2,5-50} with 26 and 51 mol% of N,N'-1,2-ethanediyl-bis[6-hydroxy-hexanamide], respectively, were prepared according to the method described above.

Methods

NMR: ^1H (300 MHz) and ^{13}C (75.26 MHz) NMR spectra were recorded on a Varian Inova Nuclear Magnetic Resonance Spectrometer using chloroform- d_1 or trifluoroacetic acid- d_1 as a solvent.

Viscometry: Intrinsic viscosities $[\eta]$ were determined by a single point measurement using a capillary Ubbelohde type 0C at 25 °C and a polymer solution with a concentration of 0.1 g.dl $^{-1}$ in chloroform-methanol (1:1 vol/vol) ^{32, 33}. The following empirical equation was applied:

$$[\eta] = \frac{\sqrt{2}}{c} \sqrt{\eta_{\text{spec}} - \ln \eta_{\text{rel}}} \quad (\text{eq. 5.1})$$

where $\eta_{\text{spec}} = \eta_{\text{rel}} - 1$ and c is the polymer concentration in g.dl $^{-1}$.

The intrinsic viscosity of PEA2,5-25 was also determined by extrapolation of η_{rel} and η_{inh} to $c = 0$.

FT-IR: Fourier Transform Infrared spectra were recorded with a Biorad FTS 175 spectrometer utilizing a wide band MCT detector at 4 cm $^{-1}$ spectral resolution. Thin polymer films were placed between sodium chloride windows and transferred to a heatable infrared cell from Specac Inc. The sample was heated to 190 °C at 45 °C.min $^{-1}$, kept for 10 min at 190 °C, cooled to 30 °C with an average rate of 5 °C.min $^{-1}$. Subsequently, data points were collected between 4000 and 550 cm $^{-1}$.

The crystallinity w_c (in mol%) of the poly(ester amide)s was calculated according to:

$$w_c = \frac{b_1}{b_1 + b_2 + b_3} * x \quad (\text{eq 5.2})$$

with b_1 the band area of the amide I band at 1634 cm $^{-1}$ (H-bonded, ordered, crystalline domains), b_2 the band area of the amide I band at ~1651 cm $^{-1}$ (H-bonded disordered, amorphous domains), b_3 the band area of the amide I band at ~1673 cm $^{-1}$ (non-H-bonded, amorphous domains) and x the hard segment content in mol%. Curve fitting was used to resolve the selected IR-band areas.

WAXD: Wide angle X-ray diffraction spectra were recorded using a Philips X'Pert-MPD diffractometer in Bragg-Brentano geometry, with a Θ compensating divergence slit (10.0 mm). The polymer film (15 x 10 x 1mm) was mounted on a Pt filament in an

Anton Paar HTK-16 temperature chamber. A Cu-anode was used, together with a curved graphite monochromator, giving $\text{CuK}\alpha_1$ radiation of 1.5406 Å. Prior to measurement the chamber was flushed with nitrogen.

The sample was heated to 190 °C, annealed for 10 min and subsequently cooled at 20 °C.min⁻¹ to 30 °C. Data points were collected in the range of 2θ is 4-90 °.

The peak position at angles of 2θ correspond to interplanar d-spacings according to Bragg's law (eq. 5.3)

$$d = \frac{n\lambda}{2 \sin \theta} \quad (\text{eq. 5.3})$$

with n is an integer and λ is the applied wavelength (1.5406 Å).

TGA: Thermal gravimetric analysis was carried out with 5-10 mg samples under a nitrogen atmosphere in the 50-700 °C range at a heating rate of 10 °C.min⁻¹, using a Perkin-Elmer Thermal gravimetric analyser TGA 7.

DSC: Thermal analysis of the polymers was carried out using a Perkin-Elmer DSC-7 Differential Scanning Calorimeter equipped with a PE7700 computer and TAS-7 software. Calibration was performed with pure indium. Measurements were performed on isolated precipitated polymers. Samples (5-10 mg) were heated from 25 to 180 °C at a rate of 20 °C.min⁻¹, annealed for 5 min, cooled to -80 °C at a rate of 20 °C.min⁻¹, and subsequently heated from -80 to 180 °C at a rate of 20 °C.min⁻¹. Melting (T_m) and crystallization (T_c) temperatures were obtained from the peak maxima, melt (ΔH_m) and crystallization (ΔH_c) enthalpies were determined from the area under the curve and the glass transition temperature (T_g) was taken at the inflection point. The data presented are determined from the second heating run, unless stated otherwise.

Processing: Compression moulded bars (75x4x2 mm) were prepared with a hot press (THB 008, Fontijne Holland BV, the Netherlands). Polymers were heated for 6-8 min at 20 °C above their T_m as measured by DSC, pressed for 3 min at 300 kN, and cooled in approximately 5 min under pressure to room temperature. Upon compression moulding the intrinsic viscosity of PEA4,5 and PEA2,5 polymers decreased from ~0.60 to ~0.52 dl.g⁻¹ and from ~0.95 to ~0.65 dl.g⁻¹, respectively.

DMA: Differential mechanical analysis was performed with a Myrenne ATM3 torsion pendulum at a frequency of approximately 1 Hz. The storage modulus (G') and the loss

modulus (G'') were measured as a function of temperature. Samples (75x4x2 mm) were first cooled to $-100\text{ }^{\circ}\text{C}$ and then heated at a rate of $1\text{ }^{\circ}\text{C}\cdot\text{min}^{-1}$. The temperature at which the loss modulus reached a maximum was taken as the T_g . The flow temperature (T_{flow}) was defined as the temperature at which the storage modulus reached 1 MPa.

Tensile test: Tensile tests were conducted with compression moulded bars, cut to dumbbells (ISO 37). A Zwick Z020 universal machine equipped with a 500 N load cell and extensometers was used to measure the stress as a function of strain at a strain rate of $500\text{ mm}\cdot\text{min}^{-1}$ and a preload of 3 N. Measurements were performed on at least 6 different polymer bars.

Tensile set: Polymer samples (10x10x2 mm), cut from compression moulded bars, were placed between two metal plates at $25\text{ }^{\circ}\text{C}$ (ASTM 395 B standard) and compressed to 75% of their original thickness for 24 h. The sample thickness was determined half an hour after the load was released. The measurements were performed in triplo. The compression set (CS) is calculated according to:

$$\text{CS} = \frac{d_0 - d_2}{d_0 - d_1} \times 100\% \quad (\text{eq. 5.4})$$

where d_0 , d_1 , and d_2 are the sample thicknesses before, during, and after compression, respectively.

Water uptake: The polymer water absorption was determined by immersing polymer bars (10x10x2 mm) in demineralised water at $37\text{ }^{\circ}\text{C}$ for 28 days. Compression moulded samples were predried at $30\text{ }^{\circ}\text{C}$ under reduced pressure for at least 2 days. The water absorption (wt %) is calculated from:

$$\text{wt \%} = \frac{w - w_0}{w_0} \times 100\% \quad (\text{eq. 5.5})$$

where w_0 and w are the sample weights before and after treatment, respectively.

Results and Discussion

In previous research it was shown that segmented poly(ester amide)s are conveniently synthesized by melt polycondensation of dimethyl adipate, 1,4-butanediol and N,N'-1,4-butanediyl-bis[6-hydroxy-hexanamide], abbreviated as bisamide-diol **4,5** (fig. 5.1) ^{21, 22, 34}. The incorporation of amide groups in the poly(butylene adipate) main chain has proven to be an excellent method to obtain polymers with enhanced physical and mechanical properties as compared to the polyesters. Similarly, polycondensation of dimethyl adipate and 1,4-butanediol and bisamidediol **2,5** afforded high molecular weight polymers. The molar ratio of hard (x) and soft (y) segment in the poly(ester amide)s was varied by changing the molar ratio of the bisamide-diol and 1,4-butanediol in the monomer feed. The poly(ester amide)s are abbreviated as PEA4,5 and PEA2,5, having 4 and 2 methylene units between the amide groups, respectively.

The thermal and mechanical properties of PEA4,5 polymers with a hard segment content of at least 25 mol% are comparable to those of low density polyethylene and are considerably improved compared to the relatively low melting and brittle poly(butylene adipate) ^{21, 22, 34}. Therefore we focussed our research on the poly(ester amide)s PEA4,5-25, PEA4,5-50, PEA2,5-25 and PEA2,5-50. The last numbers refer to the molar percentages of hard segment in the corresponding polymers.

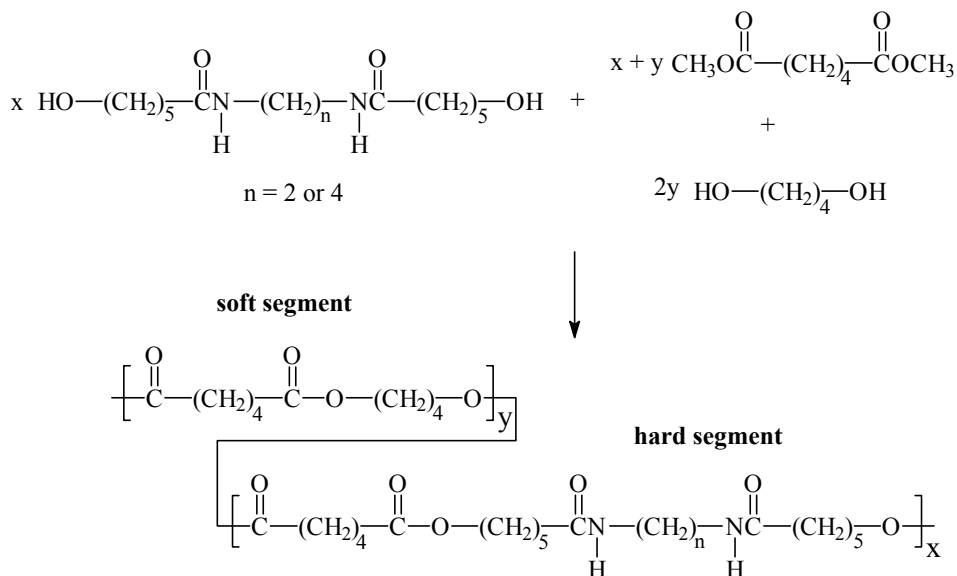


Figure 5.1: Reaction scheme for a poly(ester amide) based on bisamide-diol 4,5 or 2,5, 1,4-butanediol and dimethyl adipate (PEA4,5 or PEA2,5).

A representative ^1H -NMR spectrum of PEA2,5-25 is presented in figure 5.2. The hard to soft segment ratio (x/y) was determined from the ratio of the signal of the methylene groups next to the amide NH at δ 3.26 (**11**) and the signal of the methylene groups next to the ester acyl oxygen at δ 4.10 (**3** + **5**). The ^1H -NMR spectra were also used to estimate the molecular weights (M_n) of the polymers. Assuming that polymer chains have hydroxyl end groups, molecular weights were calculated from the signals of the $\text{CH}_2\text{-OH}$ endgroups at δ 3.67 (**3^e** + **5^e**) and the signals of the methylene groups next to the ester acyl oxygen at δ 4.10 (**3** + **5**). Due to the inaccuracy in the determination of the integrals of ^1H -NMR signals corresponding to the end-groups M_n values presented in table 5.1 are denoted $>50 \text{ kg.mol}^{-1}$ for the PEA4,5 polymers. PEA2,5-25 and PEA2,5-50 have a M_n of 50 and 25 kg.mol^{-1} , respectively.

The ^{13}C -NMR spectra confirmed the structure of the poly(ester amide)s and no additional signals due to interchange reactions²² could be detected.

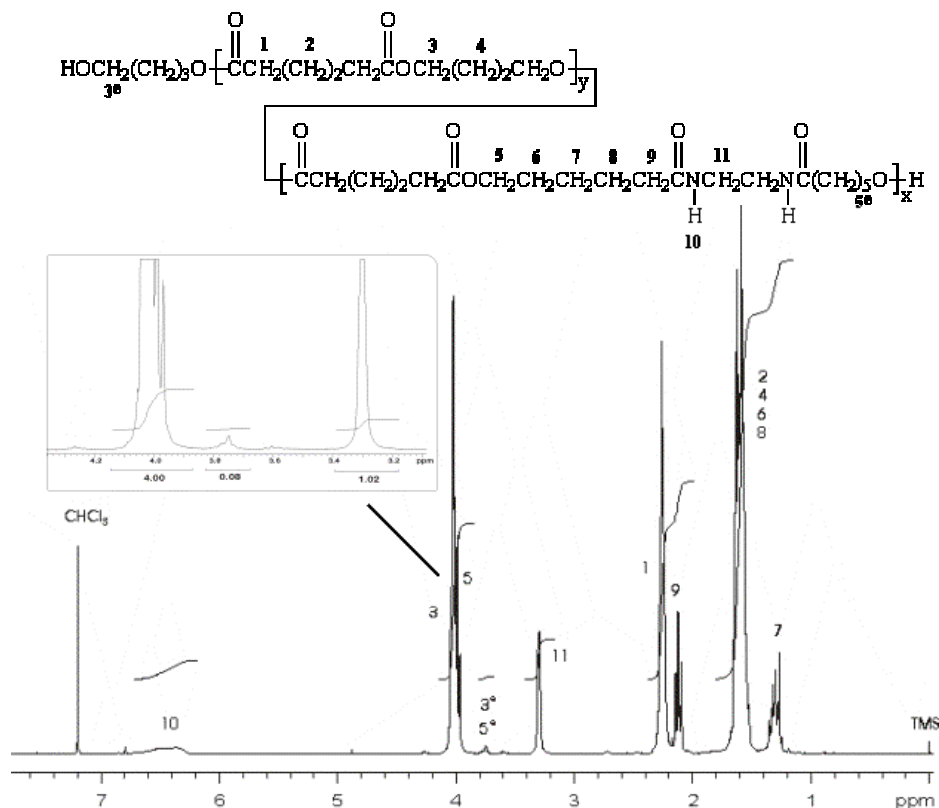


Figure 5.2: ^1H -NMR spectrum of PEA2,5-25 in chloroform- d_1 .

The composition of the poly(ester amide)s, as determined from the ^1H -NMR spectra, deviates slightly from the intended composition (table 5.1). This deviation is caused by distillation of a small amount of dimethyl adipate during the polymerization, which disturbs the stoichiometry.

The polymers PEA4,5 and PEA2,5 are insoluble in diethyl ether, acetonitrile, toluene and acetone but were soluble in chloroform and DMSO. At elevated temperatures the polymers are soluble in THF and slightly soluble in methanol and ethanol.

As previously reported, polymer molecular weights could not be determined with GPC due to polymer interaction with the column material ³⁴. Instead, intrinsic viscosities of the polymers were measured by capillary viscometry using chloroform-methanol (1:1

vol/vol) as a solvent (table 5.1). This solvent mixture is a good solvent for the PEA4,5-25 and PEA2,5-25 polymers even at high concentrations, as determined by the reduced ($\eta_{\text{red}} = \eta_{\text{spec}} \cdot c^{-1}$) and inherent ($\eta_{\text{inh}} = \ln(\eta_{\text{rel}}) \cdot c^{-1}$) viscosity ^{32, 33}. As the Mark-Houwink constants are not known for the systems, the resulting intrinsic viscosities could not be converted to molecular weights.

Table 5.1: Chemical composition and physical properties of PEA4,5 and PEA2,5 polymers.

polymer code	hard segment, x ^a (mol %)	composition, x ^b (mol %)	Mn ^b (kg.mol ⁻¹)	[η] ^c (dl.g ⁻¹)
PEA4,5-25	25	28	> 50	0.59
PEA2,5-25	25	26	50	1.02
PEA4,5-50	50	56	> 50	0.61
PEA2,5-50	50	51	25	0.93

^a theoretical value, ^b according to ¹H-NMR, ^c CHCl₃/MeOH (1:1 vol/vol) at 25 °C

In figure 5.3 the FT-IR spectra of PEA4,5-50 and PEA2,5-50 at room temperature are presented for the wave number regions, 3500-2700, 1800-1000 and 850-525 cm⁻¹. Previous work showed that characteristic IR-bands of PEA4,5-50 located at 1540, 1476, 1420 and 693 cm⁻¹ can be related to an α -type crystalline phase similar to that of the α -crystalline phase of nylon 6,6 ³⁴. Moreover, for bisamide-diol **4,5** these characteristic IR-bands are located at the same wave numbers ³¹, which led to the conclusion that the crystalline structure of the bisamide-diol **4,5** is preserved in PEA4,5-50 ³⁴.

In contrast to PEA4,5-50 which shows an amide II band at 1540 cm⁻¹, the amide II band for PEA2,5-50 appears at 1557 cm⁻¹. This IR-band is also found for nylon 6 and even-odd nylons and is characteristic of a so-called γ -crystalline phase. Compared to PEA4,5-50 (693 cm⁻¹), also the phase sensitive amide V band of PEA2,5-50 is shifted to ~710 cm⁻¹, which is characteristic for a γ -type crystalline phase. However, this relatively broad band indicates that an α -type phase is also present, which is confirmed by the presence of a characteristic band of an α -type phase at 1419 cm⁻¹. In addition, the amide

II band is very broad which could be due to the presence of the α -related IR-band at $\sim 1540\text{ cm}^{-1}$.

All these characteristic IR-bands are located at almost exactly the same wave numbers as in the IR-spectra of the bisamide-diol **2,5** monomer³¹. The bisamide-diol **2,5** monomer showed IR-bands at 1559, 1474, 1422, 686 and 590 cm^{-1} belonging to the amide II, NH vicinal CH_2 bend, CO vicinal CH_2 bend, amide V and VI, respectively. From these results and the WAXD data³¹, it was found that bisamide-diol **2,5** consists of a mixture of α - and γ -type crystals and it thus seems that the crystalline structures are preserved in PEA2,5-50.

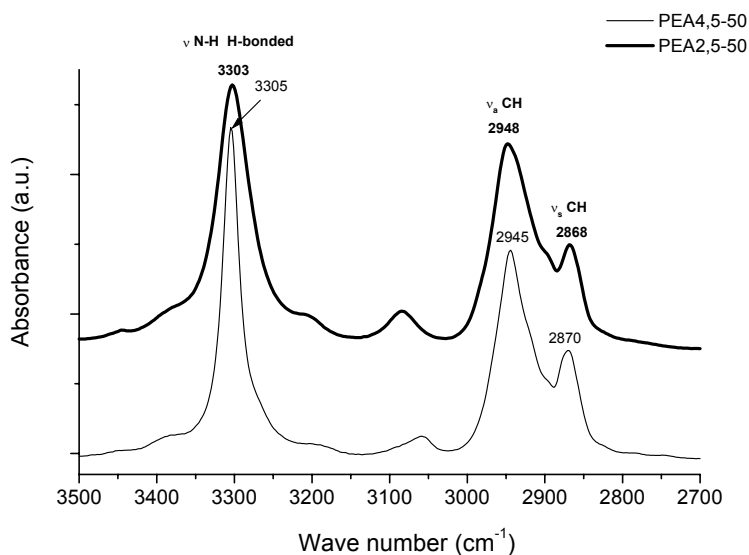


Figure 5.3a: FT-IR spectra of PEA4,5-50 and PEA2,5-50 at room temperature for the wave number region $3500\text{--}2700\text{ cm}^{-1}$.

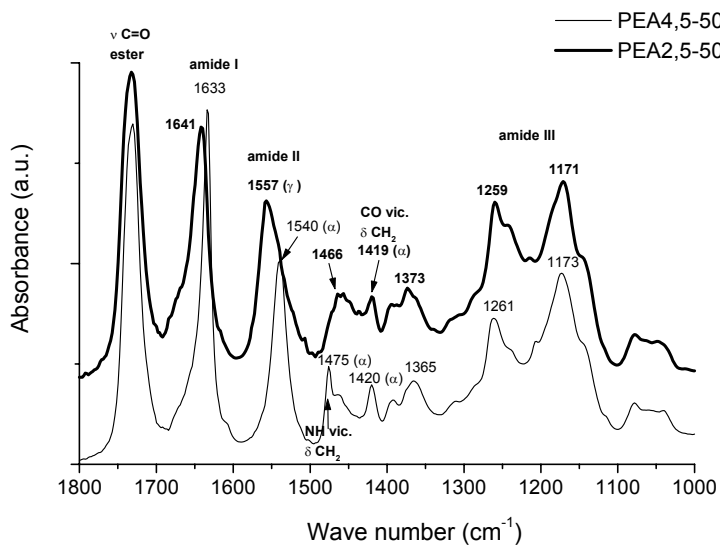


Figure 5.3b: FT-IR spectra of PEA4,5-50 and PEA2,5-50 at room temperature for the wave number region 1800-1000 cm^{-1} .

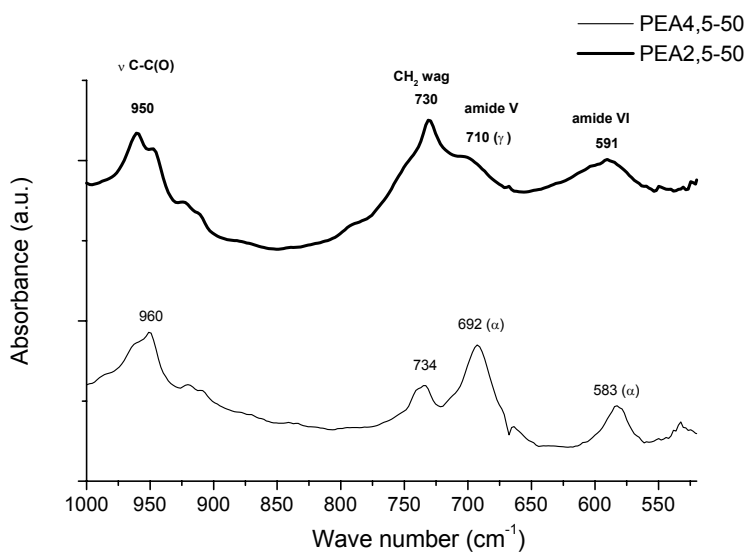


Figure 5.3c: FT-IR spectra of PEA4,5-50 and PEA2,5-50 at room temperature for the wave number region 1000-525 cm^{-1} .

The WAXD spectra of the poly(ester amide)s (fig. 5.4) confirm the conclusion that different type of crystalline phases are present. PEA4,5-50 shows two broad reflections at 3.94 and 4.34 Å and these reflections are characteristic of the α -crystalline phase as present in nylon 6,6 (4.4 and 3.7 Å). These reflections represent the distance between two amide-amide intermolecular H-bonded chains (4.4 Å) and the distance between two van der Waals packed sheets (3.7 Å). In the α -crystalline phase polymer chains are in an extended zigzag planar conformation and H-bonds are formed between adjacent anti-parallel chains that make up a sheet. These H-bonded sheets are stacked upon each other and held together by van der Waals forces. The WAXD spectrum of the PEA2,5-50 polymer shows a broad peak with a d-spacing of ~ 4.1 Å similar to a γ -crystalline phase as present in nylon 6. In such a γ -type crystalline phase the amide groups are tilted with respect to the chain axis and H-bonds are formed within the sheets, between parallel chains. It can be concluded, similarly as from the FT-IR data, that PEA2,5-50 mainly crystallizes in a γ -type crystalline phase. However, also the presence of α -type crystals can not be excluded in PEA2,5-50, because the resolution of the WAXD spectrum is too low.

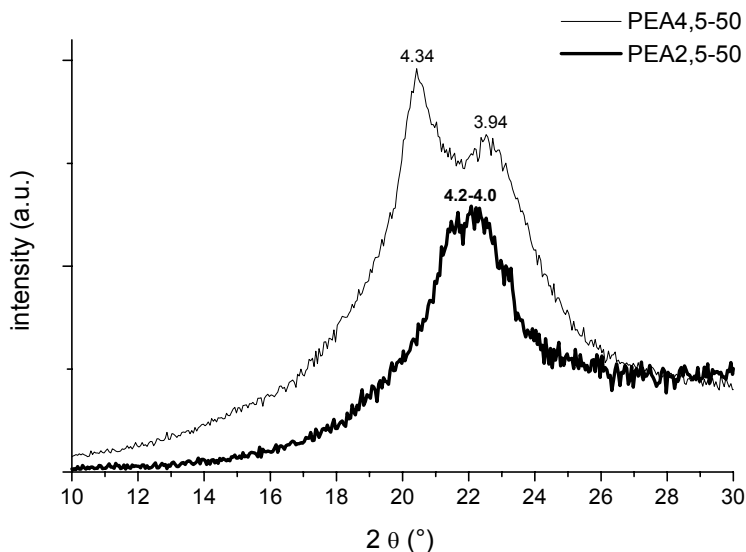


Figure 5.4: WAXD spectra of PEA4,5-50 and PEA2,5-50 at room temperature. Polymers were heated to the melt, annealed for 10 min and subsequently cooled to 30 °C at 20 °C.min⁻¹. The data represent the d-spacings in Å.

Thermal properties

The thermal stability of the segmented poly(ester amide)s under non-oxidative conditions was investigated by thermal gravimetric analysis. The PEA4,5 polymers show a degradation pattern, consisting of two steps while the PEA2,5 series degrade via a single degradation step (fig. 5.5). The decomposition temperature, taken at the (first) inflection point, is ~375 °C for the PEA4,5 polymers and ~400 °C for the PEA2,5 polymers. For all polymers the decomposition temperatures are considerably higher than the melting temperatures, which is necessary to process these materials by compression moulding.

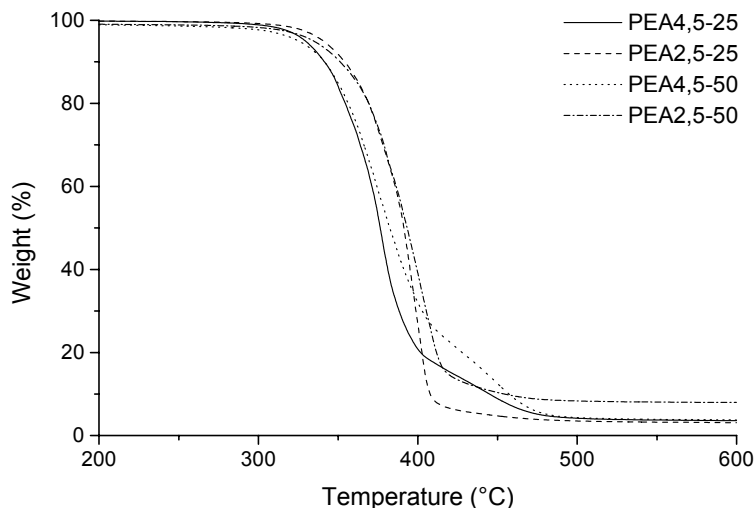


Figure 5.5: TGA thermograms of PEA4,5 and PEA2,5 polymers.

The thermal properties of the poly(ester amide)s were determined by DSC. The crystallization and melting temperatures and corresponding enthalpies of the polymers, obtained from the first cooling and second heating scan, are reported in table 5.2. All polymers show 2 endothermic transitions denoted as $T_{m,1}$ and $T_{m,2}$ for the low and high melt transition, respectively. These transitions in the poly(ester amide)s are ascribed to the melting of crystals comprising a single EA sequence ($T_{m,1}$) and crystals comprising 2 or more EA sequences ($T_{m,2}$)³⁵.

Table 5.2: Thermal properties of PEA4,5 and PEA2,5 polymers .

polymer code	$T_{m,1}$ (°C)	$\Delta H_{m,1}$ (J.g ⁻¹)	$T_{c,1}$ (°C)	$\Delta H_{c,1}$ (J.g ⁻¹)	$T_{m,2}$ (°C)	$\Delta H_{m,2}$ (J.g ⁻¹)	$T_{c,2}$ (°C)	$\Delta H_{c,2}$ (J.g ⁻¹)
PEA4,5-25	70	24	-	-	108	9	37	-23
PEA2,5-25	64	9	-	-	75-110 ^a	8	33	-14
PEA4,5-50	67	16	-	-	126	32	54/56/79 ^b	-34
PEA2,5-50	62	5	42	-5	130	25	86	-18

^a melting range, ^b trimodal.

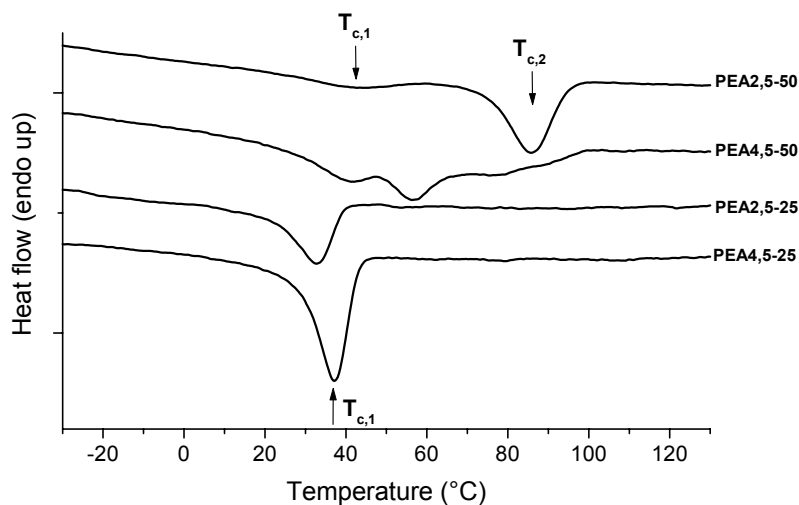


Figure 5.6: DSC cooling scans ($20\text{ }^{\circ}\text{C}.\text{min}^{-1}$) of PEA4,5 and PEA2,5 polymers.

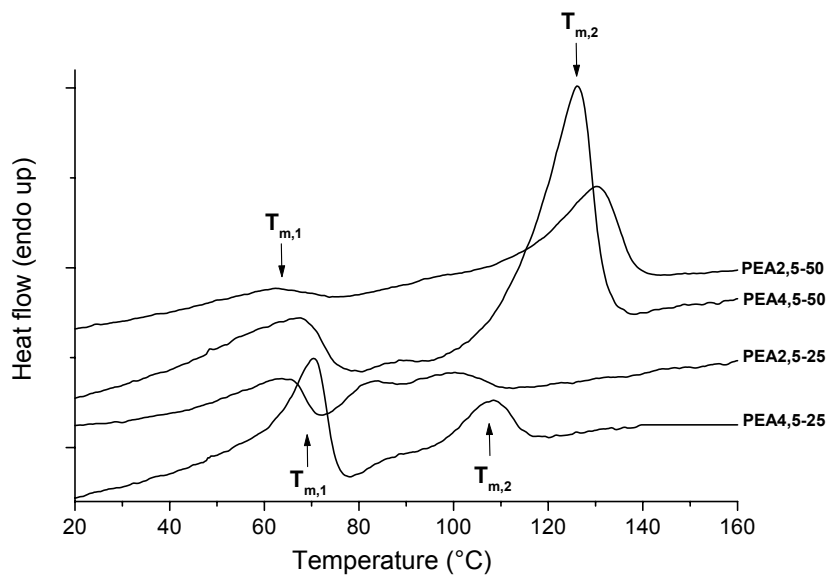


Figure 5.7: DSC heating scans of PEA4,5 and PEA2,5 polymers, after cooling at a rate of $20\text{ }^{\circ}\text{C}.\text{min}^{-1}$.

Upon cooling from the melt, the polymers with 25 mol% hard segment show an exothermic transition at ~ 35 °C (fig. 5.6). At this transition PEA4,5-25 and PEA2,5-25 crystals comprising single EA sequences are predominantly formed. Upon reheating PEA4,5-25 and PEA2,5-25 show an endothermic transition ($T_{m,1}$) between 64 and 70 °C, followed by a recrystallization exotherm and a second melt transition ($T_{m,2}$) (fig. 5.7). This exotherm can be ascribed to rearrangement of crystals into a more stable crystalline structure. Compared to PEA4,5-25, the transitions at $T_{m,1}$ and $T_{m,2}$ are broader and at a lower temperature for PEA2,5-25 which might be explained by melting of a mixture of α - and γ -type crystals at the transitions $T_{m,1}$ as well as $T_{m,2}$. The presence of this mixture of crystals probably suppresses the formation of well-defined crystals.

During cooling, PEA4,5-50 shows a multi modal transition which indicates that not only a crystalline phase containing single EA sequences is formed but also a crystalline phase comprising longer EA sequences. PEA2,5-50 shows two distinct exothermic transitions at 86 ($T_{c,1}$) and 42 °C ($T_{c,2}$) (fig. 5.6). At $T_{c,2}$, PEA2,5-50 crystallizes into a phase existing of 2 or more EA sequences and at $T_{c,1}$ PEA2,5-50 crystallizes into a phase comprising single EA sequences. Upon reheating PEA4,5-50 and PEA2,5-50 show an endothermic transition ($T_{m,1}$) at 67 and 62 °C, respectively, followed by a second melt transition ($T_{m,2}$) (fig. 5.7). The $T_{m,2}$ is 133 and 130 °C for PEA4,5-50 and PEA2,5-50, respectively, and the corresponding melt enthalpies are ~ 25 J.g⁻¹ for both polymers. Similar to PEA4,5-25 and PEA2,5-25, both transitions ($T_{m,1}$ and $T_{m,2}$) of PEA2,5-50 are broader and at a lower temperature as compared to PEA4,5-50. This can also be attributed to melting of a mixture of α - and γ -type crystals for PEA2,5-50 at the transitions $T_{m,1}$ and $T_{m,2}$.

Table 5.3: Thermal properties of PEA4,5 and PEA2,5 polymers as obtained from DMA and DSC.

polymer code	x (wt %)	T _{flow} ^a (°C)	T _{m,2} ^b (°C)	w _c ^c (%)	G' _{25 °C} ^a (MPa)	T _g ^a (°C)
PEA4,5-25	33	105	108	12.5 ± 2.5	62	-40
PEA2,5-25	30	94	75-110 ^d	12.5 ± 2.5	51	-40
PEA4,5-50	53	130	126	27.5 ± 2.5	103	-20
PEA2,5-50	49	130	130	27.5 ± 2.5	103	-25

^a from DMA, ^b from DSC, ^c crystallinity according to amide I band in FT-IR spectra,
^d melting range

In chapter 4 it was shown that the T_{m,2} and the corresponding enthalpies of the PEA4,5 polymers are dependent on the polymer hard segment content ³⁴. By increasing the amount of hard segment in the polymer the fraction of hard blocks comprising 2 or more EA sequences increases resulting in an increase in T_{m,2} (lamellar thickness) and ΔH_{m,2}. The number average EA sequence length k, calculated with a probability function, increases from 1.4 for PEA4,5-25 to 2.2 for PEA4,5-50 ^{35, 36}. Statistically, about 50% of all EA segments are present as single units in poly(ester amide)s with 25 mol% of amide content. In the poly(ester amide)s with 50 mol% of amide content about 20% of all EA segments are present as single units, whereas 80% have EA sequence lengths of 2 or more. This is reflected in the much lower ΔH_{m,2} of PEA-25 polymers compared to PEA-50 polymers. The crystallinity of the PEA-25 polymers was approximately 12.5 ± 2.5% and that of the PEA-50 polymers 27.5 ± 2.5% (table 5.3).

Dynamic mechanical properties

The flow temperature, as obtained from DMA measurements, was similar to $T_{m,2}$, for all polymers (table 5.3). All poly(ester amide)s show a transition in the rubber plateau (fig. 5.8), which is found at temperatures corresponding with the lower melting temperature ($T_{m,1}$, table 5.3).

The storage modulus (G') is a measure for the overall crystallinity of the polymers. The G' at 25 °C is ~50–60 and 103 MPa for the PEA-25 and PEA-50 polymers, respectively, indicating a similar crystallinity for PEA2,5 and PEA4,5 polymers.

Only T_g data obtained by DMA measurements are presented in table 5.3 since DSC traces only showed very weak transitions at the polymer T_g , which made their evaluation rather inaccurate. Similar T_g 's were found for the PEA2,5 and 4,5 polymers as was expected because a similar concentration of amide segments is present in the amorphous phase (table 5.3).

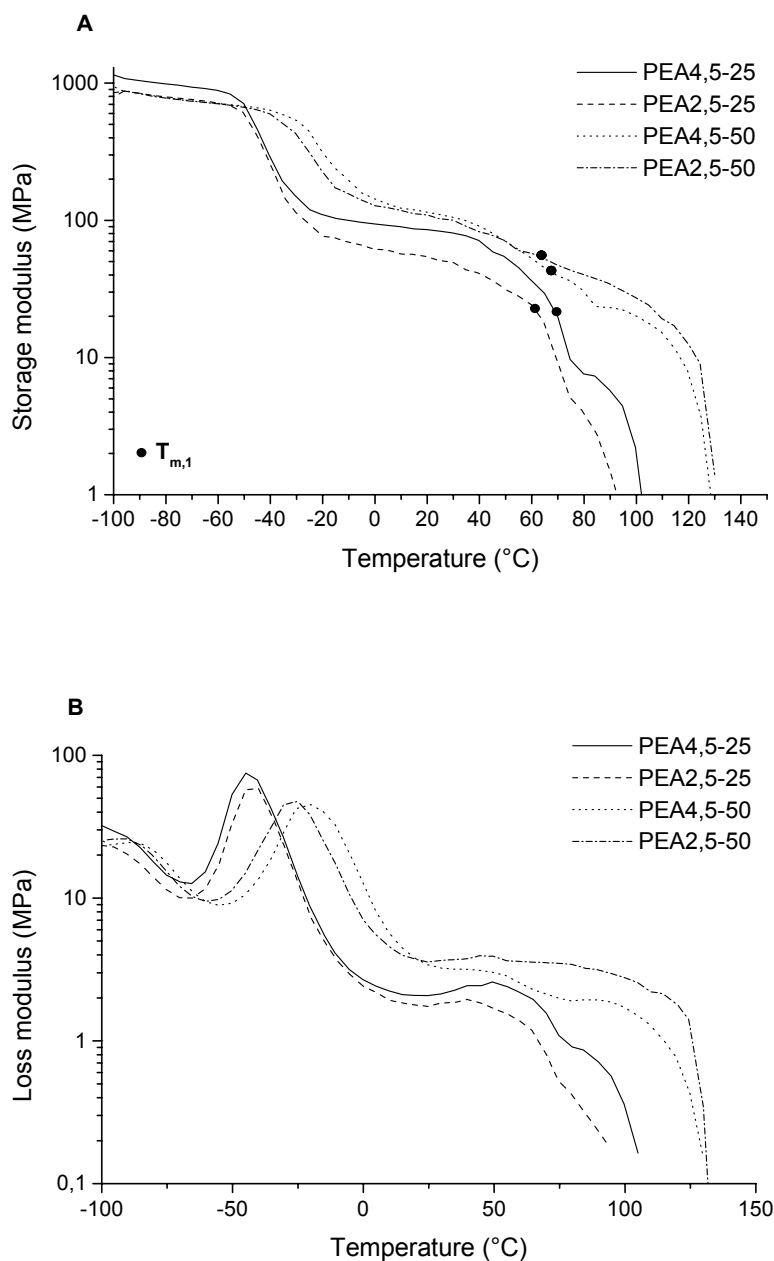


Figure 5.8: Storage modulus (A) and loss modulus (B) as a function of temperature for PEA4,5 and PEA2,5 polymers.

Mechanical properties

Typical stress-strain curves of PEA2,5 and PEA4,5 polymers are presented in figure 5.9. The stress-strain curves of poly(ester amide)s show a yield stress followed by strain softening, necking and stabilisation of the neck ³⁴.

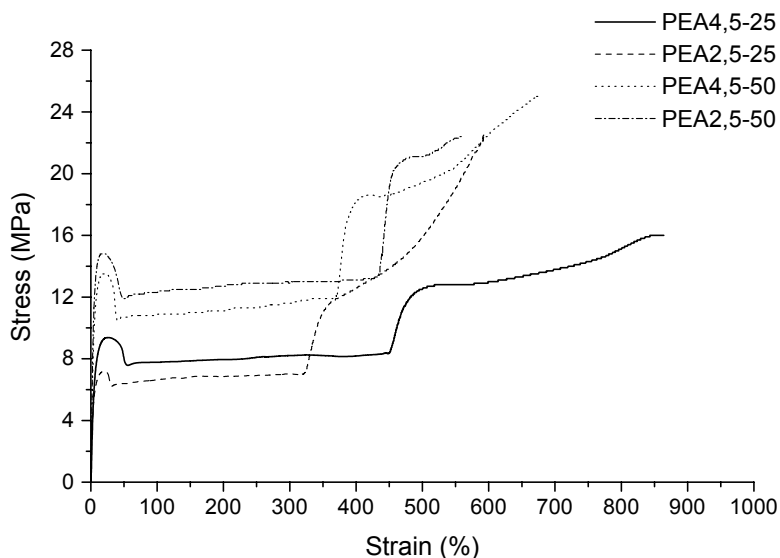


Figure 5.9: Stress strain curves for PEA4,5 and PEA2,5 polymers.

Increasing the hard segment content in the PEA4,5 and PEA2,5 polymers results in an increase of the elastic modulus, yield stress and stress at break as was expected because of the increased stiffness (table 5.4). The polymers have a strain at break between ~600 and 800%.

The PEA2,5 and PEA4,5 polymers have comparable tensile properties, although the stress at break is lower and strain at break is higher for PEA4,5-25 compared to PEA2,5-25. However, it should be taken into account that the stress and strain at break are sample properties rather than material properties. Apparently, the different crystalline structures (α - or γ -type) of the polymers have hardly any influence on their tensile properties.

Table 5.4: Mechanical properties of PEA4,5 and PEA2,5 polymers.

polymer code	E ^a (MPa)	σ_{yield} (MPa)	$\sigma_{\text{at break}}$ (MPa)	$\epsilon_{\text{at break}}$ (%)	ϵ_{yield} (%)	CS _{25%} (%)
PEA4,5-25	180 ± 36	9 ± 0.5	15 ± 1.0	810 ± 100	24 ± 1	39 ± 5
PEA2,5-25	159 ± 27	7 ± 0.2	23 ± 0.5	600 ± 10	20 ± 1	12 ± 5
PEA4,5-50	270 ± 42	14 ± 0.5	25 ± 1.0	680 ± 30	18 ± 1	49 ± 6
PEA2,5-50	359 ± 20	15 ± 0.5	22 ± 1.5	590 ± 90	16 ± 1	24 ± 6

^a E modulus only indicate a trend

The compression set (CS) at room temperature (table 5.4) was measured to determine the elasticity of the poly(ester amide)s. At 25% compression the poly(ester amide)s are strained above the yield point. In chapter 4 it was shown that the compression set of PEA4,5 polymers increased with increasing hard segment content up to a hard segment content of 50 mol%³⁴. Likewise, the compression set is increasing from 12 to 24% with increasing hard segment for the PEA2,5 polymers. However, the compression set of the PEA2,5 polymers is substantially lower compared to the PEA4,5 polymers. As the crystallinity and the morphology of PEA4,5 and PEA2,5 polymers with the same hard segment content is similar, the elastic recovery was expected to be the same. However, the visco-elastic recovery process of the PEA4,5 and PEA2,5 may differ significantly in time. If the recovery time, e.g. the time after the load was released, would have been extended the compression set values might be much closer together.

Water uptake

The water absorption of poly(ester amide) samples, immersed in water at 37 °C, was followed in time over a period of 3 wks. The polymers show an increase in water absorption in time, which levels off at 2 to 3 days (equilibrium). In table 5.5 the water uptake at equilibrium is listed for the PEA4,5 and PEA2,5 polymers.

Table 5.5: Equilibrium water uptake of PEA4,5 and PEA2,5 polymers, immersed in water at 37 °C.

polymer code	time _{equilibrium} (days)	water uptake _{37°C} (%)
PEA4,5-25	3	11.7 ± 0.1
PEA2,5-25	2	4.4 ± 0.1
PEA4,5-50	2	9.4 ± 0.1
PEA2,5-50	2	4.2 ± 0.2

The water absorption for the PEA4,5 polymers increased with decreasing hard segment content. However, the water absorption of the PEA2,5 polymers is low and seems independent of the hard segment content. From literature it is known that water uptake takes place exclusively in the amorphous regions. Polymers PEA4,5 and PEA2,5 with the same hard segment content (and thus crystallinity) are thus expected to have a similar water uptake. From IR-data it was concluded that PEA4,5 and PEA2,5 polymers both have amide-amide H-bonds present in the disordered amorphous phase ³⁷. PEA2,5 polymers mainly have a γ -type crystalline structure which is characterized by fully (linear) H-bonded structure which is more stable (shorter H-bonds) compared to the α -type crystalline structure. It is assumed that H-bonds in the amorphous phase of PEA2,5 are also shorter and thus stronger compared to those of PEA4,5. The more compact H-bonds of PEA2,5 are thus less accessible for solvation by water molecules. Water molecules might also be involved in breakage of the H-bonds between the amide-amide and ester-amide groups. This breakage is expected to be more difficult for the stronger H-bonds in the amorphous phase of PEA2,5.

Conclusions

Segmented poly(ester amide)s were prepared by melt polycondensation of dimethyl adipate, 1,4-butanediol and a symmetrical bisamide-diol with 2 (**2,5**) or 4 (**4,5**) methylene units between the amide groups, abbreviated as PEA2,5 and PEA4,5, respectively. All polymers have a sub-ambient glass transition temperature and two melt transitions, corresponding with the melting of crystals comprising single ester amide

sequences or 2 or more ester amide sequences. The poly(ester amide)s have a micro-phase separated structure with an amide-rich hard phase and an ester-rich flexible soft phase and crystallize into an α - or a γ -type crystalline phase, similar to α - or γ -crystals present in nylons. PEA4,5 polymers crystallize into an α -type crystalline phase, while a mixture of α - and γ -type crystalline phases was found for PEA2,5 polymers. In the IR- and WAXD-spectra of the bisamide-diol **2,5** monomer α - and γ -related bands were found which indicates that the crystalline structures present in the monomer are preserved in the corresponding poly(ester amide). The polymers have an elastic modulus in the range of 160-350 MPa, a stress at break in the range of 15-25 MPa combined with a high strain at break (600-800%). The thermal and mechanical properties are not influenced by the different crystalline structures of the polymers, only by the amount of crystallizable hard segment present. However, the compression set and water absorption are significantly lower for the PEA2,5 polymers compared to PEA4,5 polymers.

Acknowledgements

This study was financially supported by the European Commission, project: QLK5-1999-01298. DOW Benelux N.V. is acknowledged for the synthesis of N,N'-1,2-ethanediyl-bis[6-hydroxy-hexanamide].

References

1. A. Alla, *Polymer*, **1997**, 38, (19), 4935.
2. S. Andini, *Makromol. Chem. Rapid Commun.*, **1988**, 9, 119.
3. L. Asin, J. Puiggali, *J. Polym. Sci Part A: Chem.*, **2001**, 39, 4283.
4. T.H. Barrows, **1986**, *The design and synthesis of bioabsorbable poly(ester-amides)*, Plenum, New York.
5. S. Bera, Z. Jedlinski, *J. Polym. Sci. part A: Polym. Chem.*, **1993**, 31, (3), 731.
6. E. Botines, J. Puiggali, *Polymer*, **2002**, 43, 6073.
7. L. Castaldo, F. de Candia, G. Maglio, *J. Appl. Polym. Sci.*, **1982**, 27, 1809.
8. F. de Candia, G. Maglio, *Polym. Bull.*, **1982**, 8, 109.
9. V. de Simone, *J. Appl. Polym. Sci.*, **1992**, 46, 1813.
10. T. Fey, *Polym. Intern.*, **2003**, 52, 1625.

11. Z. Gomurashvili, R. Katsarava, *J. Mat Sci: Pure Appl. Chem.*, **2000**, A37, (3), 215.
12. I. Goodman, R.J. Sheahan, *Eur. Polym. J.*, **1990**, 26, (10), 1081.
13. S. Katayama, T. Murakami, *J. Appl. Polym. Sci.*, **1976**, 20, 975.
14. I. Goodman, D.A. Starmer, *Eur. Polym. J.*, **1991**, 27, (6), 515.
15. R. Katsarava, *J. Polym. Sci. Part A: Polym. Chem.*, **1999**, 37, 391.
16. N. Paredes, J. Puiggali, *J. Polym. Sci. Part A: Polym. Chem.*, **1998**, 36, 1271.
17. Z. Qian, Y, *Colloid Polym. Sci.*, **2003**, 281, 869.
18. A. Rodriguez-Galan, J. Puiggali, *Macromol. Chem. Phys.*, **2003**, 204, 2078.
19. I. Villuendas, *Macromol. Chem. Phys.*, **2001**, 202, (2), 236.
20. H.R. Stapert, P.J. Dijkstra, J. Feijen, *Macromol. Symp.*, **2000**, 152, 127.
21. H.R. Stapert, P.J. Dijkstra, J. Feijen, *Macromol. Symp.*, **1998**, 130, 91.
22. H.R. Stapert, A.M. Bouwens, P.J. Dijkstra, J. Feijen, *Macromol. Chem. Phys.*, **1999**, 200, (8), 1921.
23. S. Bera, Z. Jedlinski, *Polymer*, **1992**, 33, (20), 4331.
24. H.R. Stapert, M. van der Zee, P.J. Dijkstra, J. Feijen, *Abstracts Papers ACS*, **1997**, 213, 253.
25. J.D. Sudha, *J. Polym. Sci. Part A: Polym. Chem.*, **2000**, 38, 2469.
26. J.D. Sudha, C.K.S. Pillai, S. Bera, *J. Polym. Mater.*, **1996**, 13, (4), 317.
27. S. Katayama, H. Horikawa, *J. Appl. Polym. Sci.*, **1971**, 15, 775.
28. T.H. Barrows, V.L. Horton, **1988**, *progress in biomedical polymers*, Los Angeles.
29. L. Castaldo, G. Maglio, *Polym. Bull.*, **1992**, 28, 301.
30. S. Pivsa-Art, *J. Appl. Polym. Sci.*, **2002**, 85, (4), 774.
31. P.A.M. Lips, chapter 3, in *this thesis*. **2004**.
32. R.N. Shroff, *J. Appl. Polym. Sci.*, **1965**, 9, 1547.
33. O.F. Solomon, I.Z. Ciuta, *J. Appl. Polym. Sci.*, **1962**, VI, 683.
34. P.A.M. Lips, chapter 4, in *this thesis*. **2004**.
35. H.R. Stapert, *PhD thesis*, **1998**, University of Twente, The Netherlands: p. 121.
36. R.J. Cella, *J. Polym. Sci.*, **1973**, 42, 727.
37. P.A.M. Lips, chapter 6, in *this thesis*. **2004**.

Chapter 6

Crystallization behaviour of aliphatic segmented poly(ester amide)s

P.A.M. Lips¹, M.J.M van Heeringen², R. Broos², L.B. Li³, P.J. Dijkstra¹, J. Feijen¹

¹ *Institute for Biomedical Technology (BMTI) and Department of Polymer Chemistry and Biomaterials, Faculty of Science and Technology, University of Twente, P.O. Box 217, 7500 AE Enschede, The Netherlands.*

² *Core R&D, Dow Benelux N.V., PO Box 48, 4530 AA, Terneuzen, The Netherlands.*

³ *FOM-Institute of Atomic and Molecular Physics, Kruislaan 407, 1098 SJ Amsterdam, The Netherlands.*

Abstract

High molecular weight segmented poly(ester amide)s were prepared by melt polycondensation of preformed bisamide-diols, 1,4-butanediol and dimethyl adipate. These polymers, consisting of well-defined amide blocks and an amorphous polyester matrix, have thermal, physical and mechanical properties that can be readily tuned by varying the length of the methylene units between the amide groups and the bisamide content. FT-IR and WAXD analysis revealed that segmented poly(ester amide)s have crystalline phases very similar to those of nylons. Polymers based on the bisamide-diol N,N'-1,4-butanediyl-bis[6-hydroxy-hexanamide] (PEA4,5) give an α -type crystalline phase whereas polymers based on the bisamide-diol N,N'-1,2-ethanediyl-bis[6-hydroxy-hexanamide] (PEA2,5) give a mixture of α - and γ -type crystalline phases. The crystallization behaviour and morphological aspects as a function of polymer composition were studied with DSC, AFM, temperature dependent FT-IR, WAXD and

SAXS. All polymers have a sub-ambient glass transition temperature and two melt transitions, corresponding with the melting of crystals comprising single ester amide sequences ($T_{m,1}$) or 2 or more ester amide sequences ($T_{m,2}$). From the IR-data it was concluded that both $T_{m,1}$ and $T_{m,2}$ are associated with the melting of a crystalline structure comprising ordered hard segments. Moreover, H-bonds between amide groups remain present in the melt. WAXD measurements at room temperature of PEA4,5 polymers showed diffraction peaks at 3.7 and 4.4 Å which are characteristic for the α -crystalline phase of even-even nylons. These diffraction peaks shift significantly upon heating for the polymers PEA4,5 with 50 and 75 mol% of hard segment content but do not actually meet. Thus before the actual Brill transition is reached the polymers have melted. The SAXS data showed that the average lamellar thickness of the PEA4,5 polymers increased from 19 to 57 Å with increasing hard segment content, which is in line with the increasing ester amide sequence length. The average lamellar thickness of PEA2,5 with 50 mol% of hard segment is substantially lower compared to the corresponding PEA4,5 polymer.

Introduction

In the previous chapters it was shown that the incorporation of symmetrical bisamide-diol monomers into the backbone of aliphatic polyesters, enhanced their thermal and mechanical properties^{1, 2}. These segmented poly(ester amide)s, abbreviated as PEA4,5 and PEA2,5 were prepared by melt polycondensation of dimethyl adipate, 1,4-butanediol and either N,N'-1,4-butanediyl-bis[6-hydroxy-hexanamide] (bisamide-diol **4,5**) or N,N'-1,2-ethanediyl-bis[6-hydroxy-hexanamide] (bisamide-diol **2,5**), respectively (fig. 6.1). By varying the ratio of the bisamide-diol (x) and 1,4-butanediol (y) in the monomer feed a series of polymers was obtained. These poly(ester amide)s show a complex micro-phase separated structure comprising an amide-rich hard phase and an ester-rich flexible soft phase. The polymers have a sub-ambient glass transition temperature, which increases from -52 to -8 °C with increasing hard segment, and two melt transitions. The lower melt transition is ascribed to crystals composed of single H-bonded ester amide (EA) sequences and the higher transition is due to melting of crystals composed of 2 or more EA sequences. The FT-IR and WAXD spectra of these materials indicate that the crystalline phase resembles that of polyamides (nylons).

Depending on their structure and crystallization conditions nylons crystallize in either an α or γ stable crystalline phase^{3, 4}. Although additional polymorphs (β) exist, they can be classified as variations of these main structures. In the α -phase which is characteristic of both even nylons with a low number of methylene groups and even-even nylons, molecular chains are in a fully extended all-trans planar-zigzag conformation. Adjacent anti-parallel chains are packed together with the intermolecular H-bonds between the neighbouring amide groups to form a sheet structure. These sheets are stacked upon one another and held together by van der Waals forces. The crystal symmetry is triclinic with one chemical repeat unit per unit cell. The β -crystalline phase amounts to only a slight disturbance of the α -phase and does not constitute a separate class of crystals. The lateral packing of the chains is staggered up and down instead of the chains being successively displaced by one atom in the same direction on the c-axis (as in the α -phase). A γ -phase is expected for nylons derived from even diamines and odd diacids, since an unfavourable H-bond geometry derives from the extended zigzag conformation of the molecular chains in the α - and β -structures. The amide planes are tilted by 30° to the chain axis, allowing the formation of linear H-bonds between parallel molecular chains. The tilting allows all H-bonds to be formed without strain. The energy needed to twist the amide group in γ -crystals is compensated by the higher stability of the fully H-bonded structure. The structure is termed pseudo-hexagonal because the H-bonds prohibit the hexagonal symmetry normally found in hexagonal packing. The γ -form has restricted rotation in the methylene chain, which causes it to retain the planar zigzag structure. The pseudo-hexagonal γ -phase, which is more disordered than the triclinic α -phase, is favoured at high temperatures.

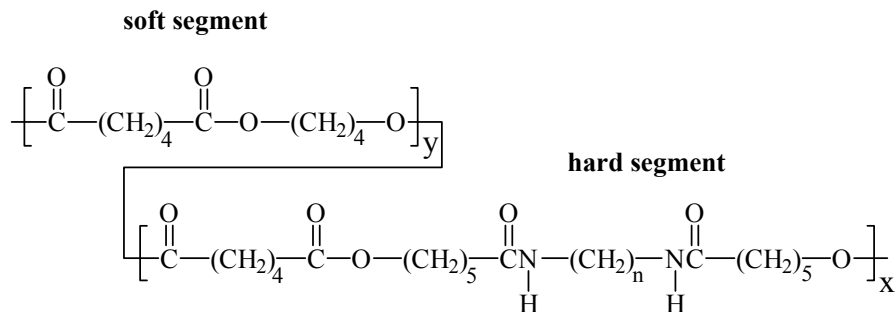
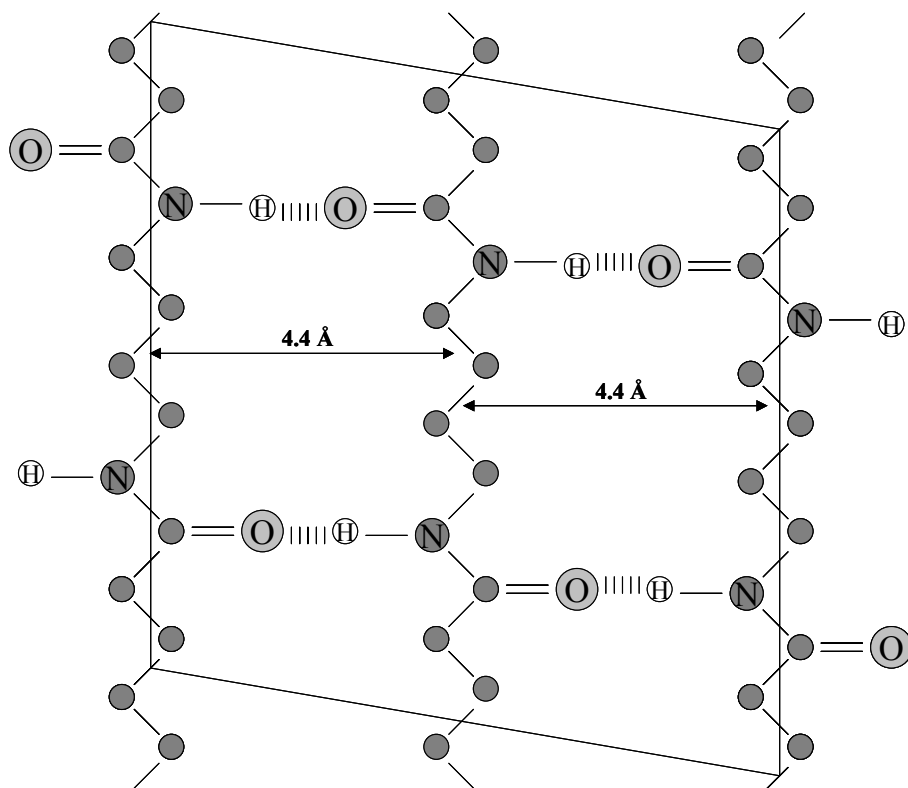


Figure 6.1: Segmented poly(ester amide) derived from a bisamide-diol, dimethyl adipate and 1,4-butanediol ($n=4$, PEA4,5 and $n=2$, PEA2,5).

Although the chemical structure of the hard segment in the polymers PEA4,5 and PEA2,5 only differs in the length of the bisamide-diol block, the crystalline structure of these polymers is different (fig. 6.1). PEA4,5 polymers crystallize predominantly in an α -type phase, very similar to the α -crystals present in even-even nylons² while PEA2,5 polymers consist of a mixture of α - and γ -type crystals in which the latter resembles the γ -crystals present in even-odd nylons¹. As only part of the chemical structure of the poly(ester amide)s resemble those present in nylons, the crystalline structures are denoted here as α - or γ -type. In the previous chapters^{1, 2} it was concluded that the crystalline structure of the bisamide-diols are preserved in the poly(ester amide)s. Models of the α - or γ -type crystalline structure, first presented in chapter 3, are thus also suitable models to illustrate the molecular organization of the crystalline phases of the PEA4,5 and PEA2,5 polymers⁵. In figure 6.2 the front and top view of the H-bonded part of the hard segment of PEA4,5 polymers crystallized in an α -type crystalline structure is depicted. The projected inter-chain distance within a H-bonded sheet (4.4 Å) and the inter-sheet distance (3.7 Å) are indicated (see also section WAXD). Figure 6.3 represents a picture of a framework molecular model (Prentice-Hall, Inc.) of the H-bonded part of the hard segment of PEA4,5 crystallized in an α -type crystalline structure.

A:



B:

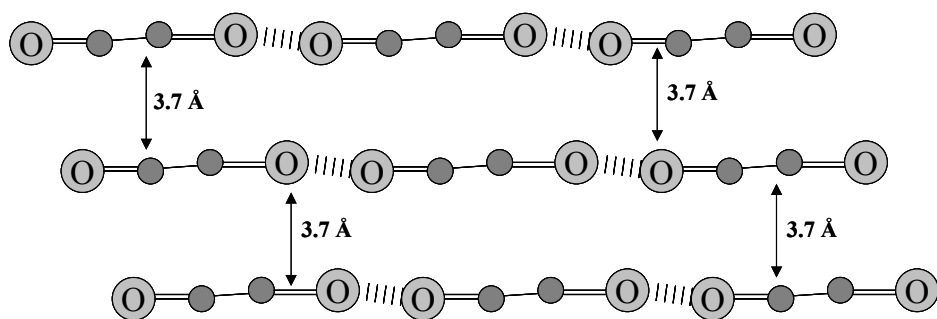


Figure 6.2: Projection of PEA4,5 in an α -type crystalline phase: (A) front view and (B) top view.

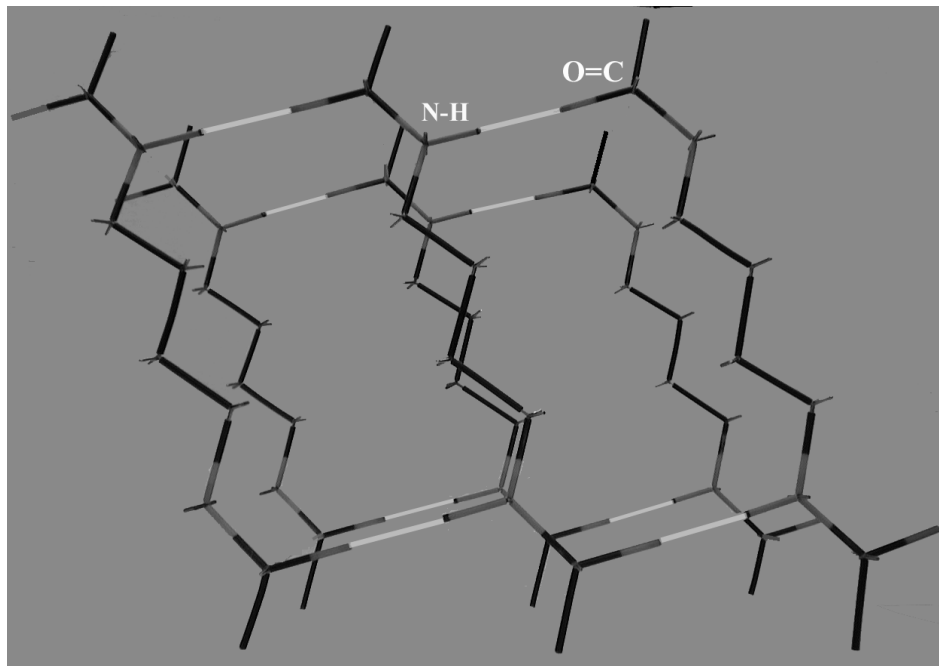
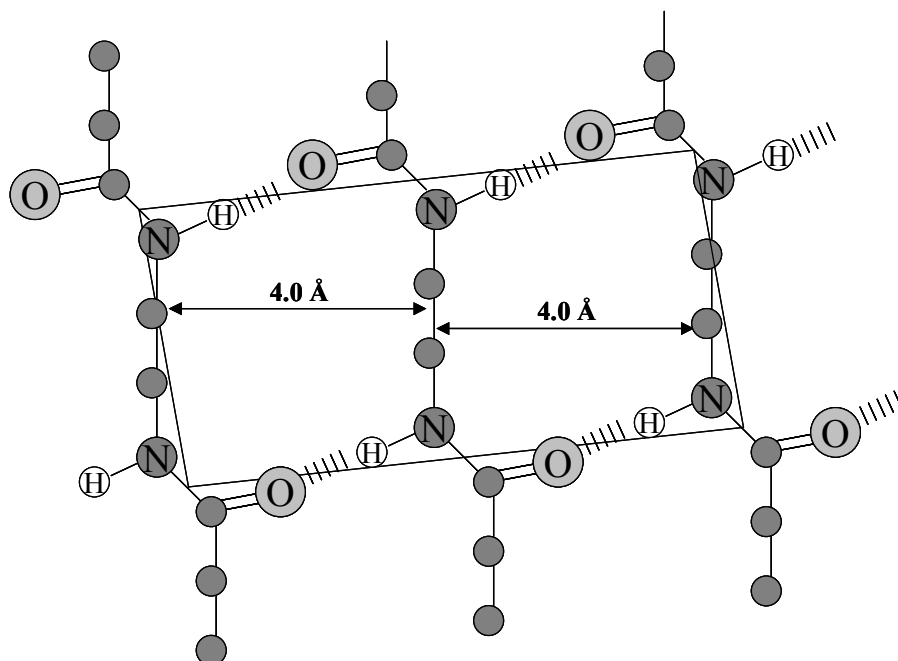


Figure 6.3: Picture of a framework molecular model of the H-bonded part of the hard segment of PEA4,5 crystallized in an α -type crystalline structure.

A model of the H-bonded part of the hard segment of PEA2,5 crystallized in a γ -type crystalline structure, is presented in figure 6.4. The inter-chain (within a H-bonded sheet) and inter-sheet distances both are ~ 4.0 Å. Figure 6.5 represents a picture of a framework molecular model (Prentice-Hall, Inc.) of the H-bonded part of the hard segment of PEA2,5 crystallized in a γ -type crystalline structure.

A:



B:

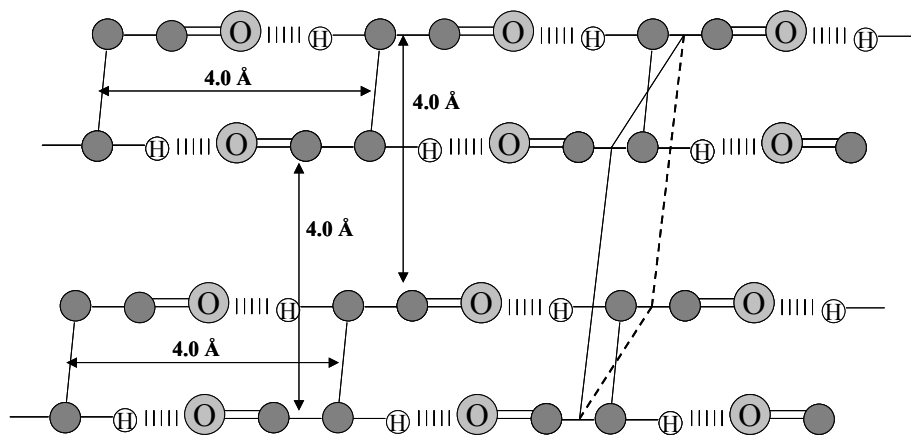


Figure 6.4: Projection of PEA2,5 in an γ -type crystalline phase: (A) front view and (B) top view.

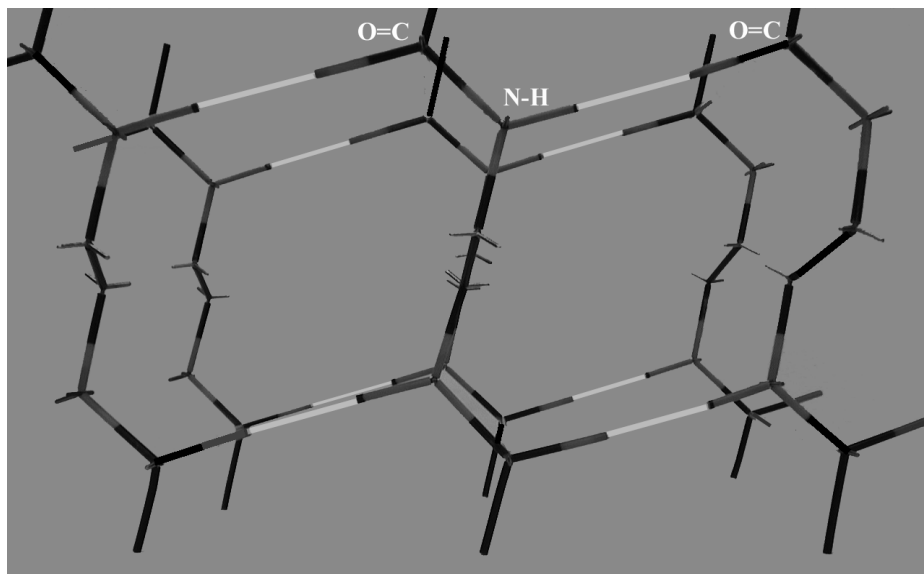


Figure 6.5: Picture of a framework molecular model of the H-bonded part of the hard segment of PEA2,5 crystallized in a γ -type crystalline structure.

On heating, most nylons show a crystal-to-crystal transition known as the Brill transition⁶. It is commonly accepted that the nature of the Brill transition is the effect of conformational motion at elevated temperatures and is associated with a packing change within the crystal. However, the mechanism is still controversial^{4, 7-18}. Early work suggested that the transition was related to the change from two-dimensional H-bonded sheets at room temperature to a three-dimensional H-bonded network at higher temperatures. Later investigations suggest that local “melting” of the methylene segments occurred, whereas the integrity of the H-bonded sheet structure was maintained up to the melting temperature. Usually, a Brill transition can be displayed by wide angle X-ray diffraction (WAXD). On heating, e.g. nylon 6, two strong diffraction peaks at the spacing of 4.4 and 3.7 Å move together and merge typically at a spacing of ~4.2 Å. A “Brill temperature” is defined as the lowest temperature for which the projected inter-chain distance within a H-bonded sheet and the inter-sheet spacing are equal. The triclinic structure at room temperature transforms into a pseudo-hexagonal structure at elevated temperatures, and the transition is reversible. It has to be emphasized that the Brill temperature strongly depends on the crystallization conditions.

IR spectroscopy has been used to study H-bonding between ester and amide or between amide groups in the ordered (crystalline) and disordered (amorphous) state in poly(ester amide)s^{19, 20}. In addition, unassociated groups can also be present in the ordered or disordered phase. Generally, the amide stretch (ν) band at $\sim 3304\text{ cm}^{-1}$ is characteristic of amide-amide H-bonds whereas the band at $\sim 3386\text{ cm}^{-1}$ originates from ester–amide H-bonds. The stretching vibrations of free N-H groups are located in the range $3440\text{--}3455\text{ cm}^{-1}$. Ester carbonyl groups are either in the free state or H-bonded^{21, 22}. Moreover, these groups may be in an ordered or disordered state and consequently several bands can be found. Also the amide I band is sensitive to ordered and disordered domains through dipole-dipole interaction between C=O and NH groups as well as H-bonding. Kaczmarczyk *et al.* studied H-bonding in aliphatic oligoesters, oligo(ester amide)s and segmented poly(ester amide)s with temperature dependent IR (fig. 6.6)²⁰. The bands at ~ 1745 and $\sim 1733\text{ cm}^{-1}$ were ascribed to vibrations of free C=O ester groups in the disordered and ordered form, respectively, whereas the bands at ~ 1712 and $\sim 1698\text{ cm}^{-1}$ were ascribed to H-bonded C=O ester groups in the disordered and ordered form, respectively. Thus H-bonding leads to a shift to lower wave numbers and this shift increases when the H-bonded carbonyl ester group is in the ordered state. Similar shifts are observed for the amide I band. The C=O amide group in the disordered state is found at 1676 cm^{-1} and shifts to 1649 cm^{-1} upon H-bonding. For the same group in the ordered state the band shifts from 1663 to 1636 cm^{-1} . In segmented poly(ester amide)s with a low hard segment content (m), H-bonding primarily takes place between ester and amide groups. However, in the crystalline (ordered) phase H-bonded amide groups are present to a greater extent than in the amorphous (disordered) state. Upon heating the polymers to the melt, a decrease in order occurs but in the melt some ester-amide and amide-amide H-bonds are still present. The ester-amide H-bonds are stable up to $210\text{ }^{\circ}\text{C}$ whereas the amide-amide H-bonds disappear at $170\text{ }^{\circ}\text{C}$.

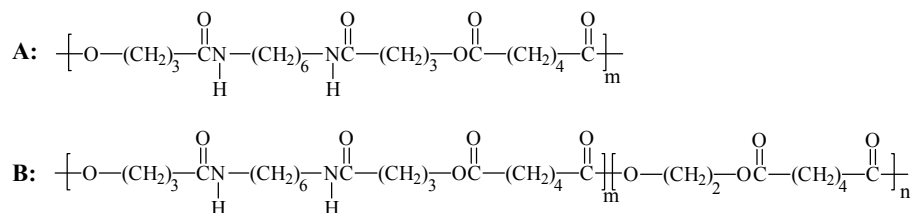


Figure 6.6: An oligo(ester amide) (A) based on 1,6-diaminohexane, γ -butyrolactone and adipic acid and a segmented poly(ester amide) (B) based on 1,6-diaminohexane, γ -butyrolactone, 1,2-ethanediol and adipic acid.

In this chapter the crystallization behaviour of segmented poly(ester amide)s comprising an ester amide hard segment and a butylene adipate soft segment is described. PEA4,5 polymers with a hard segment content of 25, 50 and 75 mol% and PEA2,5 with a hard segment content of 50 mol% were selected and studied with DSC and temperature dependent WAXD and SAXS. Temperature dependent FT-IR was performed on PEA4,5 polymers with a hard segment content of 25 and 50 mol% and PEA2,5 with a hard segment content of 50 mol%. PEA4,5-25 and PEA4,5-50 were subjected to AFM measurements.

Experimental

Polymer synthesis

The synthesis of the copolymers based on $\text{N,N}'$ - α, ω alkanediyl-bis[6-hydroxy-hexanamide]s, 1,4-butanediol and dimethyl adipate is described in chapter 5¹. The molar ratio of hard (x) and soft (y) segments in the poly(ester amide)s is varied by changing the ratio of $\text{N,N}'$ - α, ω alkanediyl-bis[6-hydroxy-hexanamide] and 1,4-butanediol.

Methods

DSC: Thermal analysis was carried out using a Perkin-Elmer DSC-7 Differential Scanning Calorimeter equipped with a PE7700 computer and TAS-7 software. Calibration was performed with pure indium. Melting (T_m) and crystallization (T_c) temperatures were taken from the peak maxima and melt (ΔH_m) and crystallization enthalpies (ΔH_c) were obtained from the area under the curve. The data presented are

from the second heating step, unless stated otherwise. In a standard run compression moulded films (5-10 mg) were heated from 25 to 180 °C at a rate of 20 °C.min⁻¹, annealed for 5 min, cooled to -80 °C at 20 °C.min⁻¹, and subsequently heated from -80 to 180 °C at a rate of 20 °C.min⁻¹.

FT-IR: Fourier Transform Infra-red spectra were recorded on a Biorad FTS 175 spectrometer utilizing a wide band MCT detector at 4 cm⁻¹ resolution. A polymer film was placed between sodium chloride windows and transferred to a heatable infra-red cell from Specac Inc. The data were collected between 4000 and 500 cm⁻¹. The first data collection was performed at 30 °C after which the polymer film was heated to 190 °C at 45 °C.min⁻¹, kept for 10 min at 190 °C and cooled to 30 °C at an average rate of 5 °C.min⁻¹. Subsequently, a second spectrum was collected. The sample was then heated to 190 °C in steps of 10 °C at a heating rate of 45 °C.min⁻¹. After each step the temperature was kept constant for 5 min before data collection. Subsequently, the sample was cooled at 5 °C.min⁻¹ to 30 °C, after which the last data points were collected to check for decomposition of the sample.

The relative band area of the amide I, associated with a H-bonded ordered state, at different temperatures was calculated according to:

$$b_{1 \text{ relative}} = \frac{b_1}{b_1 + b_2 + b_3} * 100\% \quad (\text{eq. 6.1})$$

with b_1 the band area of the amide I band at 1634 cm⁻¹ (H-bonded, ordered, crystalline domains), b_2 the band area of the amide I band at ~1651 cm⁻¹ (H-bonded, disordered, amorphous domains) and b_3 the band area of the amide I band at ~1673 cm⁻¹ (non-H-bonded, amorphous domains). Deconvolution was used to resolve the selected IR-band areas.

AFM: Atomic force microscope images were obtained using a MultiMode scanning probe microscope (SPM) (Veeco Metrology Group, Santa Barbara, CA) with a Nano-Scope IV controller running software version of 5.12b42. The nano-sensor tip was used for the entire study with the following parameters: 235 µm in length, 5-10 nm in tip ratio, and 37-55 N.m⁻¹ in force constant. A moderate tapping ratio of about 0.8 was used for all the samples. Height and phase images were recorded at various magnifications.

A polymer film was placed in a vacuum oven and heated to 190 °C for 10 min and subsequently cooled to room temperature in air. The free surface of the polymer film was subjected to an AFM measurement.

WAXD/SAXS: Simultaneous WAXD and SAXS measurements were made using an in-house set up with a rotating anode x-ray generator (Rigaku RU-H300, 18 kW) equipped with two parabolic multi-layer mirrors (Bruker, Karlsruhe), giving a highly parallel beam (divergence about 0.012°) of monochromatic CuK α radiation ($\lambda = 1.5406 \text{ \AA}$). The SAXS intensity was collected with a two-dimensional gas-filled wire detector (Bruker Hi-Star). A semi-transparent beamstop placed in front of the area detector allowed monitoring the intensity of the direct beam. The WAXD intensity was recorded with a linear position sensitive detector (PSD-50M, M. Braun, Germany), which could be rotated around the beam path to measure either in the meridional or in the equatorial direction. The SAXS and WAXD intensities were normalized to the intensity of the direct beam.

A Linkam CSS450 temperature controlled shear system was employed as sample stage. Samples were kept in a brass sample holder with kapton windows replacing the original glass windows of the system. For isothermal crystallization the sample was first heated to 170 °C, annealed for 10 min and subsequently cooled ($\sim 10 \text{ }^\circ\text{C.min}^{-1}$) to the crystallization temperature. A nitrogen atmosphere prevented possible degradation at high temperatures. SAXS and WAXD measurements were taken during isothermal crystallization with 30 s and 120 s per frame, respectively. After completion of the crystallization, as indicated by saturation of the SAXS intensity, the SAXS and WAXD data were collected over a 20 min period of time to obtain high-quality statistics. SAXS and WAXD data were also collected during further cooling of the sample to 30 °C ($\sim 10 \text{ }^\circ\text{C.min}^{-1}$) and subsequent heating to the melt ($\sim 10 \text{ }^\circ\text{C.min}^{-1}$). After each step the temperature was kept constant for 5 min before data collection.

The peak position at angles of 2θ correspond to interplanar d-spacings according to Bragg's law (eq. 6.2)

$$d = \frac{n\lambda}{2 \sin \theta} \quad (\text{eq. 6.2})$$

with n is an integer and λ is the applied wavelength (1.5406 Å).

The two-dimensional SAXS intensity was first integrated azimuthally to obtain the scattering pattern as a function of $q = 4\pi \sin \theta / \lambda$, the modulus of the momentum transfer vector q , λ being the x-ray wavelength and 2θ the scattering angle. To examine the lamellar structures linear correlation functions $\gamma(r)$ were calculated according to:

$$\gamma(r) = \frac{1}{Q} \int_0^\infty I(q) q^2 \cos(qr) dq \quad (\text{eq. 6.3})$$

$$Q = \int_0^\infty I(q) q^2 dq \quad (\text{eq. 6.4})$$

where I is the intensity and Q is the so-called invariant. The correlation functions contain the basic morphological information for a model of lamellar stacks. The long spacing L can be estimated from the position of the first maximum. Further analysis of the correlation function yields the average crystalline lamellar thickness l_c and the amorphous layer thickness l_a . From these results the linear crystallinity (w_{lc}) within the stacks can be calculated according to:

$$w_{lc} = l_c / L \quad (\text{eq. 6.5})$$

Results and Discussion

The poly(ester amide)s studied (fig. 6.1) are prepared by a two-step polycondensation of dimethyl adipate, 1,4-butanediol and N,N'- α, ω alkanediyl-bis[6-hydroxy-hexanamide]s as described previously¹. A series of segmented polymers containing 28, 56 and 78 mol% hard segment was synthesized starting from N,N'-1,4-butanediyl-bis[6-hydroxy-hexanamide]. These polymers are abbreviated as PEA4,5-25, PEA4,5-50 and PEA4,5-75. The polymer PEA2,5-50, starting from N,N'-1,2-ethanediyl-bis[6-hydroxy-hexanamide], was added to this series and contains actually 51 mol% hard segment. The crystallization behaviour as a function of polymer composition was studied with DSC and temperature dependent FT-IR and WAXD. The latter was also performed to display a possible Brill transition. Morphological aspects of polymers with different compositions and crystalline structures were examined with AFM and temperature dependent SAXS.

Thermal properties

The thermal properties of the poly(ester amide)s, as determined by DSC measurements, are summarized in table 6.1, and second heating scans are depicted in figure 6.7. The DSC thermograms are characterized by a low ($T_{m,1}$) and a high ($T_{m,2}$) melt transition. The lower transition, found in the temperature range 75-80 °C, is independent of the hard segment content. By increasing the hard segment content from 25 to 75 mol% the melt enthalpy corresponding with $T_{m,1}$ decreases from 24 to 4 J.g⁻¹. The temperature and enthalpy of the higher melt transition increased with increasing hard segment due to an increased crystal lamellar size and crystallinity, respectively. The two transitions are ascribed to the melting of crystals comprising single ester amide (EA) sequences at $T_{m,1}$ and crystals composed of 2 or more EA sequences at $T_{m,2}$ ².

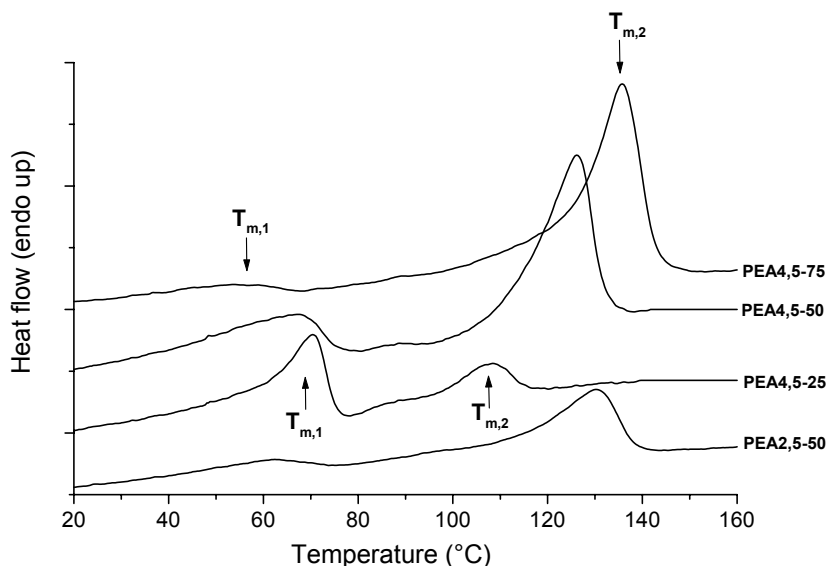


Figure 6.7: DSC heating scans of PEA4,5-25, PEA4,5-50, PEA4,5-75 and PEA2,5-50. Polymers were first heated to the melt, annealed for 10 min and subsequently cooled to 30 °C at 20 °C.min⁻¹.

Table 6.1: Physical and thermal properties of PEA4,5 and PEA2,5 polymers.

polymer code	$[\eta]^a$ (dl.g ⁻¹)	$T_{m,1}$ (°C)	$\Delta H_{m,1}$ (J.g ⁻¹)	$T_{c,1}$ (°C)	$\Delta H_{c,1}$ (J.g ⁻¹)	$T_{m,2}$ (°C)	$\Delta H_{m,2}$ (J.g ⁻¹)	$T_{c,2}$ (°C)	$\Delta H_{c,2}$ (J.g ⁻¹)
PEA4,5-25	0.59	70	24	-	-	108	9	37	-23
PEA4,5-50	0.61	67	16	-	-	126	32	54/56/79 ^b	-34
PEA4,5-75	0.52	58	4	22	-4	136	45	104	-42
PEA2,5-50	0.93	62	5	42	-5	130	25	86	-18

^a CHCl₃ / MeOH (1:1 vol/vol) at 25 °C, ^b trimodal.

FT-IR

Although structurally similar, it could be concluded from FT-IR and WAXD measurements that the poly(ester amide)s PEA4,5 and PEA2,5 show large differences in their crystalline structures. The FT-IR spectra of these polymers revealed that typical bands, especially the amide II and VI band, are found at different wave numbers. The resemblance between typical amide bands in these poly(ester amide)s and even-even and/or even-odd nylons led to the following conclusions: 1) PEA4,5 polymers crystallize in an α -type crystalline phase similar to that of the α -crystalline phase of even-even nylons ² and 2) PEA2,5 polymers give both α - and γ -type crystals with the latter similar to the so-called γ -crystalline phase found in even-odd nylons ¹.

The influence of chemical structure and composition on the thermal behaviour prompted us to investigate these changes in more detail. For this purpose, temperature dependent FT-IR spectra were recorded in between 30 and 170 °C. To exclude differences due to thermal history, the polymers were all first heated to the melt at 45 °C.min⁻¹ and subsequently cooled to 30 °C at ~5 °C.min⁻¹. Upon reheating to the melt FT-IR spectra were recorded at different temperatures. IR-bands in the regions 3200-3500 (ν N-H), 1700-1800 (ν C=O ester) and 1600-1700 cm⁻¹ (amide I) are of most interest because they depend on the state (free, bonded, ordered, disordered) of the ester and amide groups.

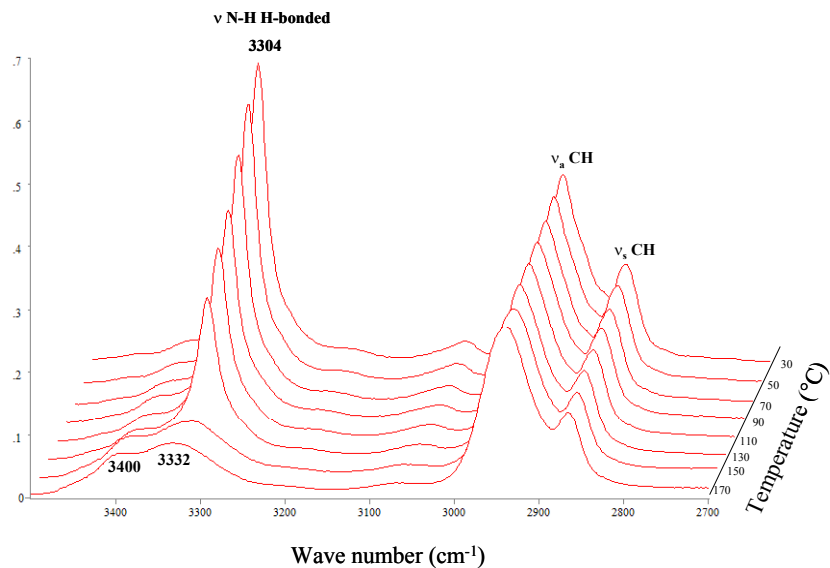


Figure 6.8a: FT-IR spectra of PEA4,5-50 at 30, 50, 70, 90, 110, 130, 150 and 170 °C for the wave number region 3500-2700 cm^{-1} .

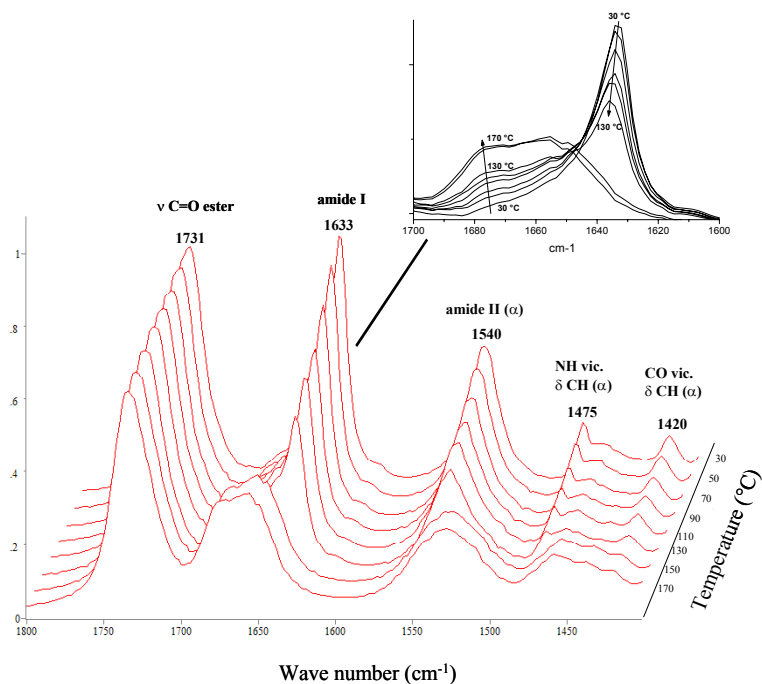


Figure 6.8b: FT-IR spectra of PEA4,5-50 at 30, 50, 70, 90, 110, 130, 150 and 170 °C for the wave number region 1800-1400 cm^{-1} .

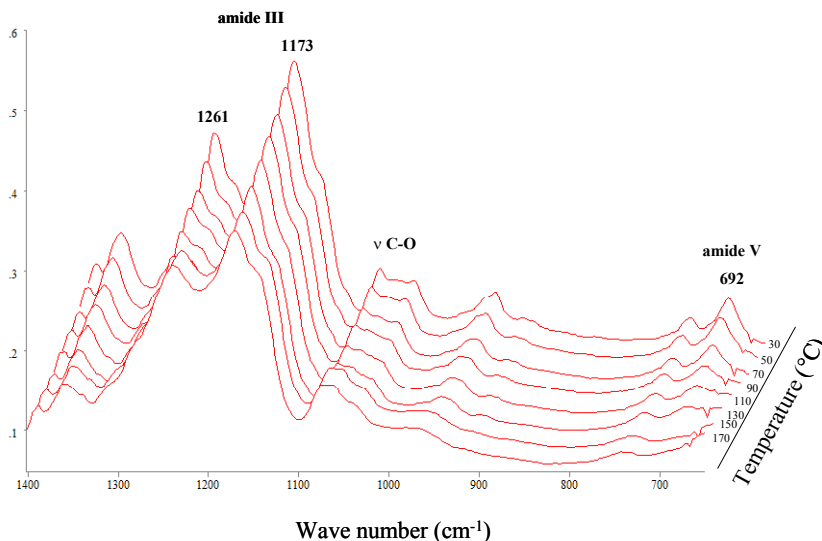


Figure 6.8c: FT-IR spectra of PEA4,5-50 at 30, 50, 70, 90, 110, 130, 150 and 170 °C for the wave number region 1400-650 cm^{-1} .

PEA4,5-50

As shown in figure 6.5, PEA4,5-50 reveals endothermic transitions at 81 and 135 °C. Upon heating to 90 °C, the ν NH band at $\sim 3304 \text{ cm}^{-1}$ characteristic of amide-amide H-bonds gradually shifts to 3309 cm^{-1} and crossing the first transition at 81 °C, the area of this band decreases but the width does not change (fig. 6.8a). In addition, the band at $\sim 3390 \text{ cm}^{-1}$ which originates from ester-amide H-bonds increases in width and shifts to $\sim 3400 \text{ cm}^{-1}$. A band at $\sim 3450 \text{ cm}^{-1}$, attributed to free (non H-bonded) N-H groups, is hardly visible²⁰. Above the melting temperature the ν NH band has drastically decreased. However, an extremely broad band centered around 3332 cm^{-1} remains even when the polymer is far above its melting temperature. Regarding its position and width, the presence of this new band is probably associated with H-bonded assemblies still present in the melt.

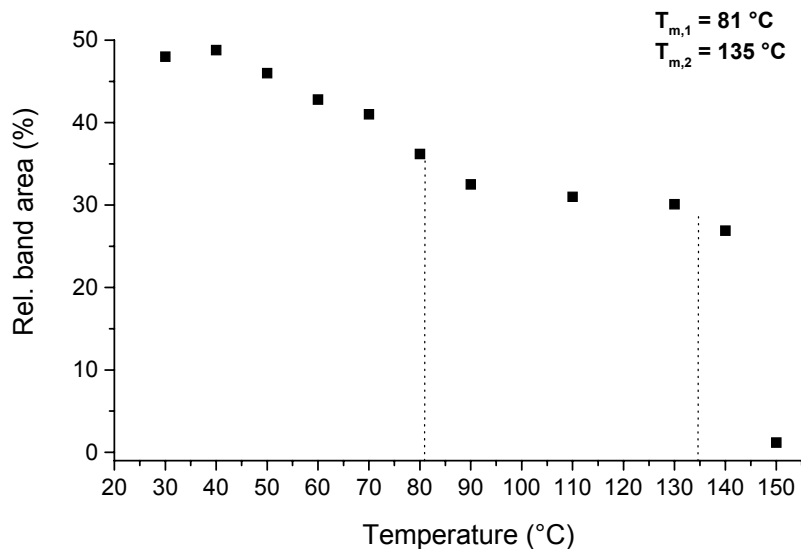


Figure 6.9: Relative band area of the amide I band at 1633 cm^{-1} of PEA4,5-50 as a function of temperature. The band areas are obtained by deconvolution of bands related to the H-bonded ordered phase at $\sim 1633\text{ cm}^{-1}$, the H-bonded disordered phase at $\sim 1651\text{ cm}^{-1}$ and the non-H-bonded disordered phase at $\sim 1673\text{ cm}^{-1}$.

By deconvolution of the amide I band, band areas of the H-bonded ordered phase at $\sim 1633\text{ cm}^{-1}$, the H-bonded disordered phase at $\sim 1651\text{ cm}^{-1}$ and the non-H-bonded disordered phase at $\sim 1673\text{ cm}^{-1}$ could be obtained. At room temperature, the relative band area of the band at $\sim 1633\text{ cm}^{-1}$ is $\sim 50\%$, which indicates that half of the amide groups are in the H-bonded ordered (crystalline) state. When the relative area of this band is plotted as a function of temperature two transitions corresponding to $T_{m,1}$ and $T_{m,2}$ are clearly observed (fig. 6.9). Moreover, up to $T_{m,1}$ a gradual decrease is found but in between $T_{m,1}$ and $T_{m,2}$ the area remains constant. It can be concluded that both transitions are associated with the melting of crystals comprising H-bonded ordered hard segments.

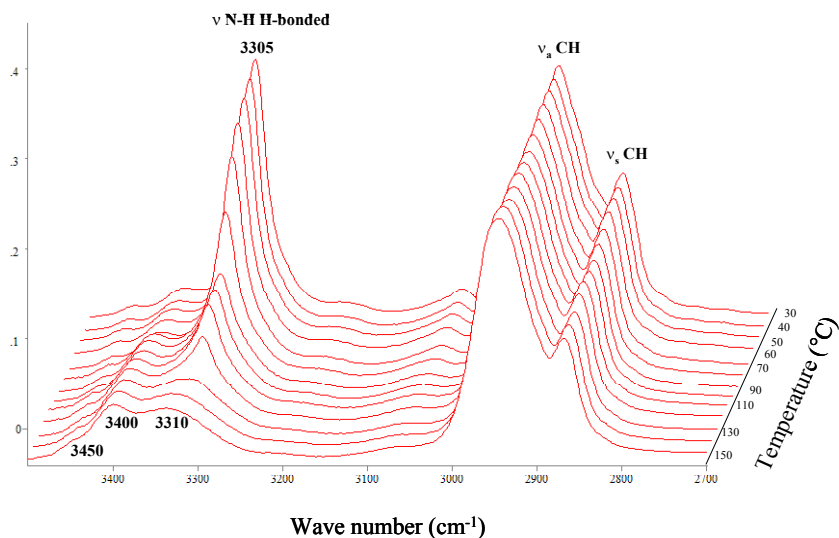


Figure 6.10a: FT-IR spectra of PEA4,5-25 at 30, 40, 50, 60, 70, 80, 90, 100, 110, 120, 130, 140 and 150 °C for the wave number region 3500-2700 cm^{-1} .

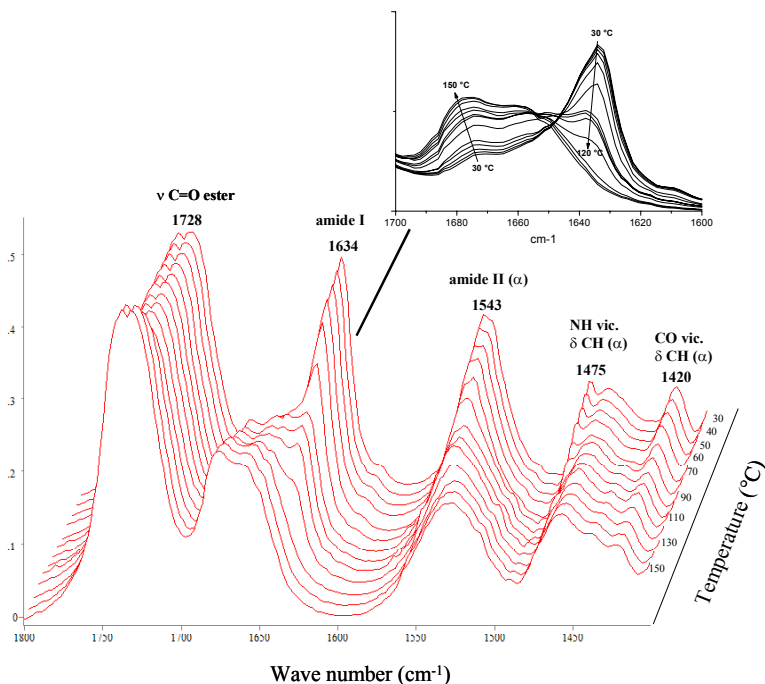


Figure 6.10b: FT-IR spectra of PEA4,5-25 at 30, 40, 50, 60, 70, 80, 90, 100, 110, 120, 130, 140 and 150 °C for the wave number region 1800-1400 cm^{-1} .

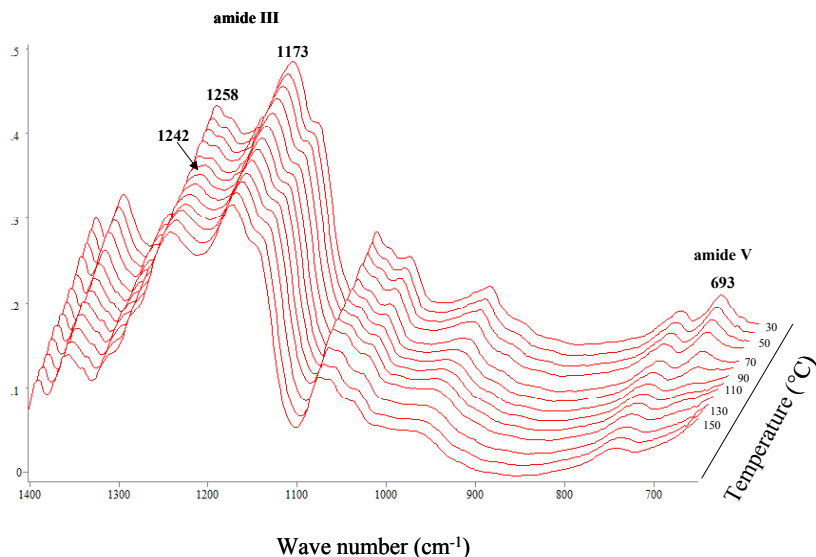


Figure 6.10c: FT-IR spectra of PEA4,5-25 at 30, 40, 50, 60, 70, 80, 90, 100, 110, 120, 130, 140 and 150 °C for the wave number region 1400-650 cm^{-1} .

PEA4,5-25

At room temperature, the IR-band at $\sim 3400 \text{ cm}^{-1}$ which is associated with ester–amide H-bonds, is much more pronounced for PEA4,5-25 (fig. 6.10a) as compared to PEA4,5-50 (fig. 6.8a). Kaczmarczyk *et al.* also found that segmented poly(ester amide)s with a low amount of hard segment content contained more ester-amide H-bonds as compared to those with a high hard segment content ²⁰.

The transition at $T_{m,1}$ of PEA4,5-25, located at 80 °C, has a much higher melt enthalpy than that of the transition at $T_{m,2}$. By increasing the temperature from room temperature to 90 °C the first melting transition is clearly observed in the FT-IR spectra (fig. 6.10). The $\nu \text{ NH}$ band at 3305 cm^{-1} associated with H-bonded groups in crystalline domains shifts to 3310 cm^{-1} with a substantial decrease in intensity. In addition, the bands at 3400 and $\sim 3450 \text{ cm}^{-1}$ increase in intensity with the former being more pronounced. These data indicate that at 80 °C some crystals melt and form disordered H-bonded N-H groups as well as unassociated groups. Increasing the temperature even further shows that at 130 °C when all remaining crystals had melted H-bonds between amide groups remain present as indicated by the broad band at $\sim 3323 \text{ cm}^{-1}$.

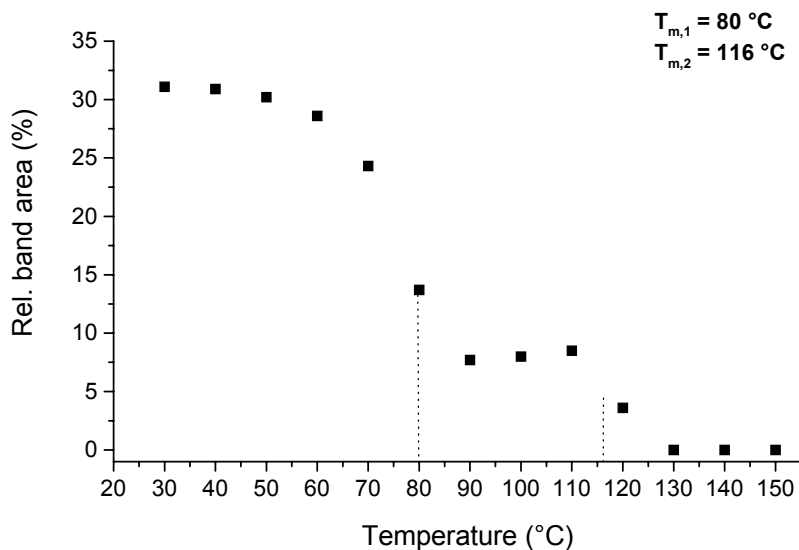


Figure 6.11: Relative band area of the amide I band at 1634 cm⁻¹ of PEA4,5-25 as a function of the temperature. The band areas are obtained by deconvolution of the bands related to the H-bonded ordered phase at ~1633 cm⁻¹, the H-bonded disordered phase at ~1651 cm⁻¹ and the non-H-bonded disordered phase at ~1673 cm⁻¹.

The amide I band in the H-bonded ordered (crystalline) state is situated at 1634 cm⁻¹. From figure 6.11 it is clear that ~ 30% of all the amide groups are present in this state, which is much less compared to PEA4,5-50. Crossing the first melt transition (T_{m,1}) the relative band area decreases to a large extent (fig. 6.11). This confirms the conclusion that the transition at T_{m,1} is associated with the melting of a crystalline structure comprising ordered hard segments. The relatively small decrease observed at T_{m,2} was expected because of the low melt enthalpy (3 J.g⁻¹) corresponding with this transition.

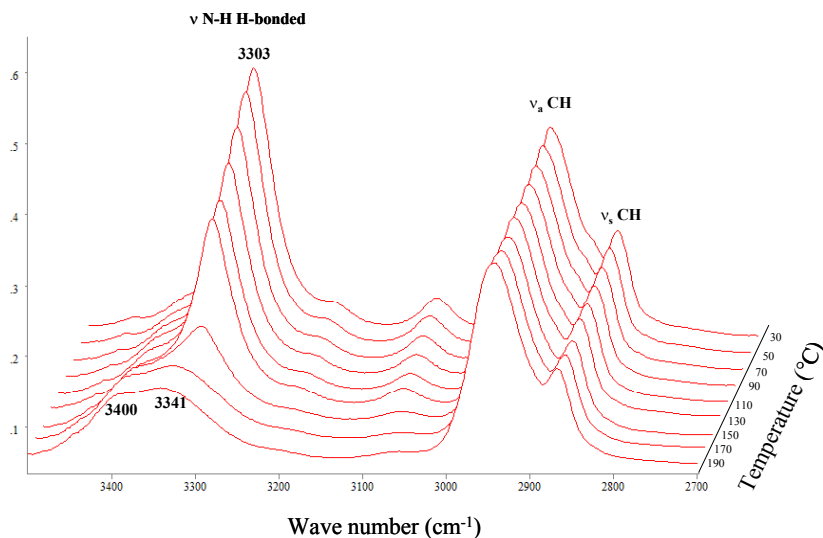


Figure 6.12a: FT-IR spectra of PEA2,5-50 at 30, 50, 70, 90, 110, 130, 150, 170 and 190 °C for the wave number region 3500-2700 cm^{-1} .

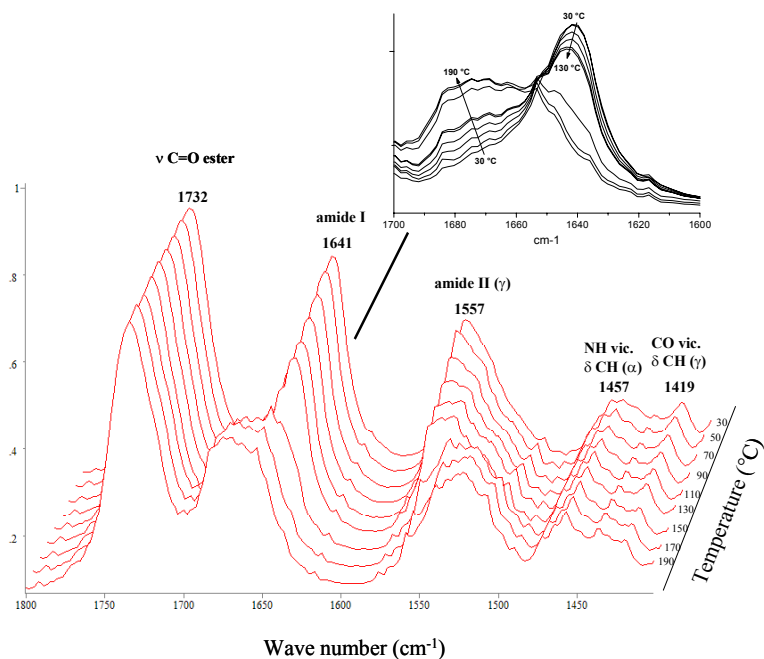


Figure 6.12b: FT-IR spectra of PEA2,5-50 at 30, 50, 70, 90, 110, 130, 150, 170 and 190 °C for the wave number region 1800-1400 cm^{-1} .

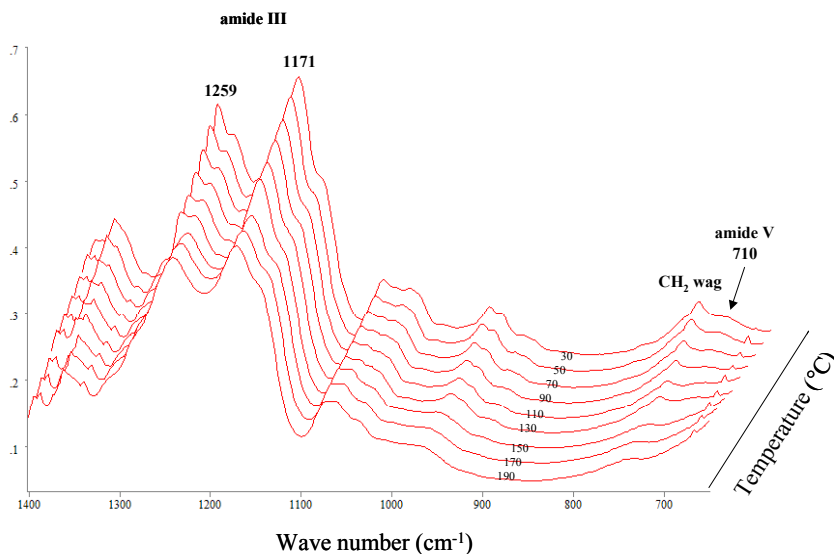


Figure 6.12c: FT-IR spectra of PEA2,5-50 at 30, 50, 70, 90, 110, 130, 150, 170 and 190 °C for the wave number region 1400-650 cm^{-1} .

PEA2,5-50

PEA2,5-50 shows two endothermic transitions at 74 and 136 °C, respectively, when heated to the melt (fig. 6.7). Similar as described for the PEA4,5 polymers at the first transition the ν NH band decreases and at the second transition becomes broad and shifts to higher wave numbers whereas H-bonded assemblies retain (fig. 6.12a). Also for the amide I band at 1641 cm^{-1} clear transitions are observed at $T_{m,1}$ and $T_{m,2}$ confirming that both transitions are associated with melting of H-bonded ordered hard segments.

AFM

The lamellar morphology for segmented copolymers, in which the crystalline phase consists of hard segments, which are embedded in a mixed amorphous phase, was first proposed by Cella ²³. Recently, the morphology of segmented copolymers like poly(ether ester amide)s and poly(ether urea)s has been investigated with AFM ^{24, 25}. The AFM images show the presence of ribbon-like structures of hard segments in a soft amorphous matrix. A similar morphology was assumed for the segmented poly(ester

amide)s described in this thesis (fig. 4.1) ². To verify this hypothesis, AFM and X-ray diffraction measurements were performed on PEA4,5-25 and PEA4,5-50 films.

Figures 6.13 - 6.15 show AFM height and phase images of PEA4,5-25 and PEA4,5-50 in which the lighter areas comprise the hard crystalline phase. Both phase images show bundles of ribbons of hard segments, which are embedded in the soft amorphous matrix. The estimated average thickness of the ribbons is ~ 160 Å for PEA4,5-25 and ~ 200 Å for PEA4,5-50. From the height image of PEA4,5-50 it appears that the ribbons are organized in spherulites. PEA4,5-85 (data not shown) showed a similar morphology as PEA4,5-50 with an estimated average thickness of the ribbons of ~ 300 Å.

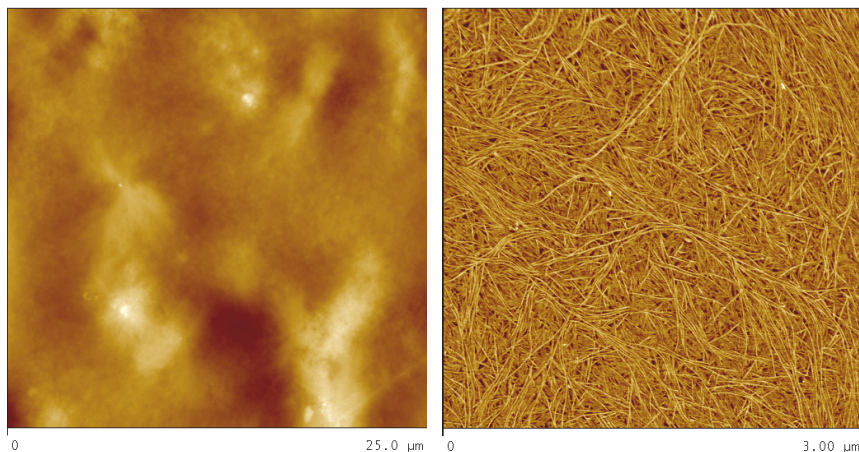


Figure 6.13: AFM image of PEA4,5-25: height image (left) and phase image (right).

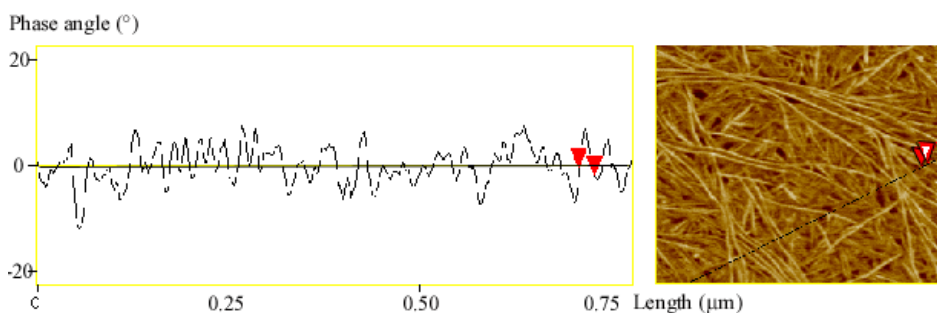


Figure 6.14: AFM phase image of PEA4,5-25.

Poly(ester amide)s with a low hard segment content, like PEA4,5-25, will likely have crystalline lamellae with no or hardly any development into the lateral directions. These polymers will be more inclined to form a micellar structure instead of a lamellar

structure. The thickness of the ribbons in the phase image of PEA4,5-25 show an almost monodisperse distribution which is an indication for the presence of a spherical (micellar) crystalline structure. The formation of more well-developed crystalline lamellae (in the lateral directions) is more likely for poly(ester amide)s with a higher hard segment content, like PEA4,5-50. This is confirmed by the AFM images (fig. 6.15), which clearly show spherulites (height image) and ordered ribbons of various dimensions (phase image).

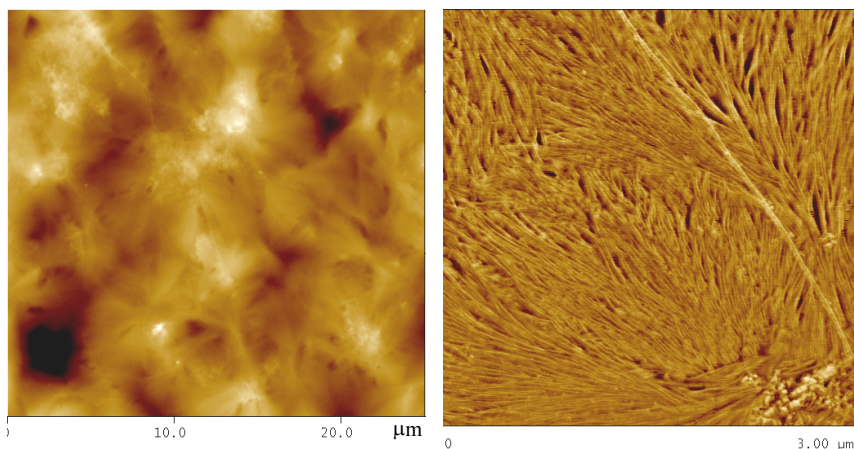


Figure 6.15: AFM image of PEA4,5-50: height image (left) and phase image (right).

WAXD / SAXS

Simultaneous WAXD and SAXS measurements were performed on the polymers PEA4,5-25, PEA4,5-50, PEA4,5-75 and PEA2,5-50. The polymers were heated to the melt, annealed for 10 min and subsequently cooled to 10-30 °C below $T_{m,2}$ and kept at that temperature for 20 min to complete the crystallization. PEA4,5-75 and PEA2,5-50 were cooled to 110 °C while PEA4,5-25 and PEA4,5-50 were cooled down to 85 and 120 °C, respectively. As an example the saturation of the SAXS intensity of PEA4,5-50 is shown in figure 6.16. The samples were then further cooled to 30 °C and subsequently heated to the melt (~ 10 °C.min⁻¹). The WAXD and SAXS data were collected during the cooling and subsequent heating scans.

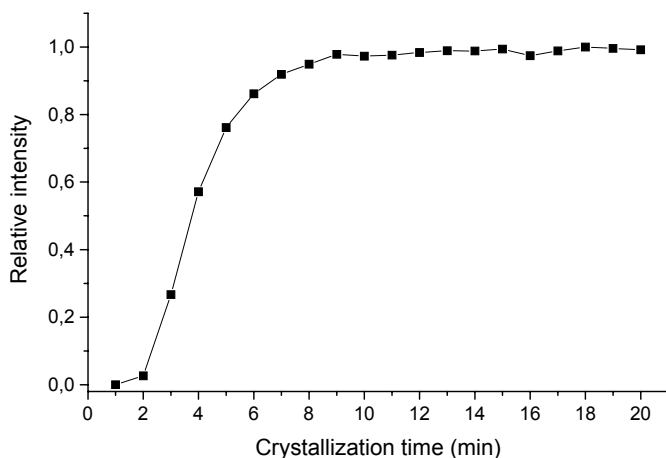


Figure 6.16: SAXS intensity of PEA4,5-50 as a function of crystallization time at a crystallization temperature of 110 °C.

As control experiments, DSC measurements were performed on polymers, which were isothermally crystallized. The thermal properties of the isothermally crystallized polymers were compared to those of the polymers, which were cooled at 20 °C.min⁻¹. Differences in melting temperatures and corresponding enthalpies due to different crystallization conditions were not observed. This indicates that the crystallization behavior of these segmented copolymers is controlled by chain architecture rather than crystallization conditions. The sequence length of the hard block sets a precondition for its phase behavior. This in fact is a general phenomenon observed for most of thermo elastomers such as poly(ethylene-1-octene)^{26, 27}.

WAXD

In previous chapters it was shown that the crystalline structure of segmented poly(ester amide)s is very similar to that of nylons. An α -crystalline phase as present in even-even nylons is characterized by two diffraction peaks at ~ 4.4 and ~ 3.7 Å whereas a γ -crystalline phase as present in odd-even nylons is found at a d-spacing of ~ 4.2 Å. The WAXD spectra of the polymers recorded at 30 °C (fig. 6.14) confirm the conclusions

drawn in chapter 5 that the crystalline phase of PEA4,5 polymers consists of α -type crystals and that a mixture of α - and γ -type crystals are present in PEA2,5-50^{1,2}.

A high intensity of the diffraction peak at 4.4 Å along with a relatively low intensity of the diffraction peak at 3.7 Å indicates that the crystal plane parallel with the H-bonds is highly developed and that the crystal plane parallel with the Van der Waals interactions is poorly developed. Thus PEA4,5-25, which has a relatively low hard segment content, contains crystals which preferably grow in the direction along the H-bonds and hardly in the direction perpendicular to that. At increasing hard segment concentration (PEA4,5-50 and PEA4,5-75) the intensity of the diffraction peak at 3.7 Å increases which indicates that more well-developed crystalline lamellae are formed thus also growth into the lateral direction.

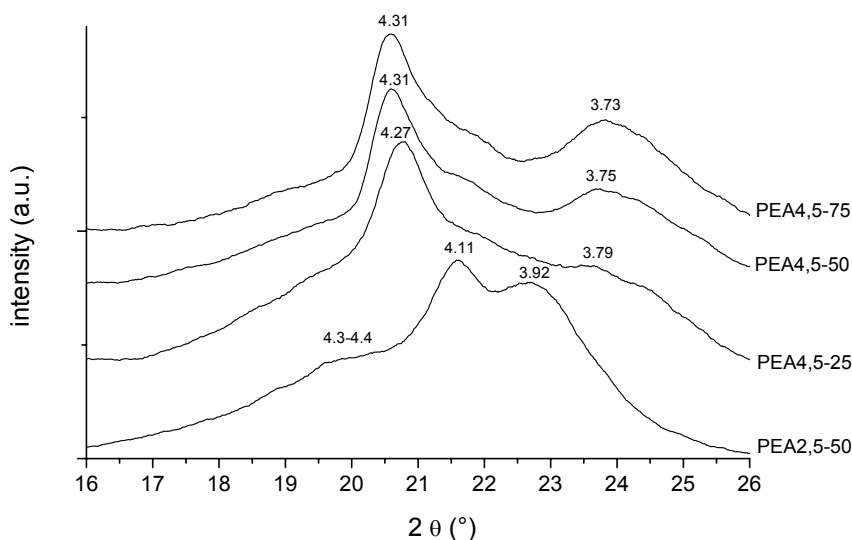


Figure 6.17: WAXD spectra at 30 °C of PEA4,5-25, PEA4,5-50, PEA4,5-75 and PEA2,5-50 after isothermal crystallization at 85, 120, 110 and 110 °C, respectively. The data represent the d -spacings in Å.

The temperature dependent WAXD measurements will be discussed separately for each polymer.

When PEA4,5-25 is cooled from the melt at $20\text{ }^{\circ}\text{C}.\text{min}^{-1}$ the polymer crystallizes at $37\text{ }^{\circ}\text{C}$ (table 6.1). Thus when PEA4,5-25 was isothermally crystallized it is not surprising that hardly any crystalline structure has formed at $85\text{ }^{\circ}\text{C}$ (fig 6.18). Upon further cooling to $30\text{ }^{\circ}\text{C}$, the polymer slowly formed its crystalline structure. By heating PEA4,5-25 to just below its $T_{m,2}$ ($108\text{ }^{\circ}\text{C}$) but above its $T_{m,1}$, only a minor amount of crystals is still present as indicated by the very low melt enthalpy of $T_{m,2}$. This corresponds well with the almost amorphous halo present at $90\text{ }^{\circ}\text{C}$ in the WAXD spectra.

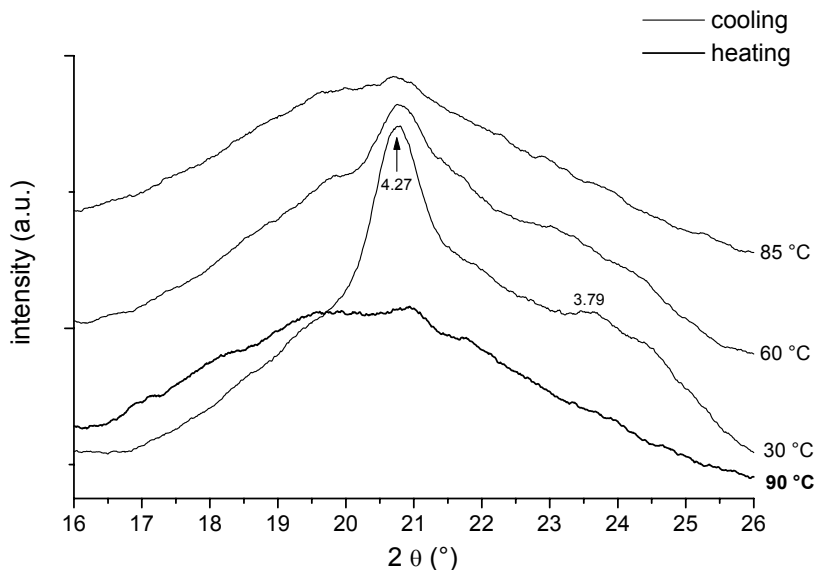


Figure 6.18: WAXD spectra of PEA4,5-25, isothermally crystallized at $85\text{ }^{\circ}\text{C}$, upon cooling to 60 and $30\text{ }^{\circ}\text{C}$ and subsequent heating to $90\text{ }^{\circ}\text{C}$.

On heating, many nylons show a Brill transition, i.e. a crystal-to-crystal transformation at which the triclinic structure transforms into a pseudo-hexagonal structure ⁶. The transition is known to be reversible and can be easily displayed by WAXD measurements ^{4, 7, 9, 13, 16}. Upon heating, e.g. nylon 6, the two diffraction peaks at 4.4 and 3.7 \AA converge and finally merge at a spacing of $\sim 4.2\text{ \AA}$. The crystals of some nylons melt before the diffraction signals actually meet and a pseudo-hexagonal phase is not fully achieved prior to melting. A similar behavior was observed for PEA4,5-50 (fig.

6.19) and PEA4,5-75 (6.20), i.e. the diffraction peaks do not actually meet, but prior to melting they have shifted significantly. Upon heating to just below the melting temperature, the inter-chain distance within a H-bonded sheet, which is fixed by H-bonds and hence less sensitive to temperature variations, decreases from a 4.31 Å to 4.22 and 4.17 Å for PEA4,5-50 and PEA4,5-75, respectively. On the other hand, the inter-sheet distance (~ 3.74 Å) shows a significant increase with temperature and prior to melting equals 3.92 and 3.99 Å for PEA4,5-50 and PEA4,5-75, respectively. Upon cooling, the two characteristic diffraction peaks of PEA4,5-50 and PEA4,5-75 diverge again, which shows that the transition is reversible.

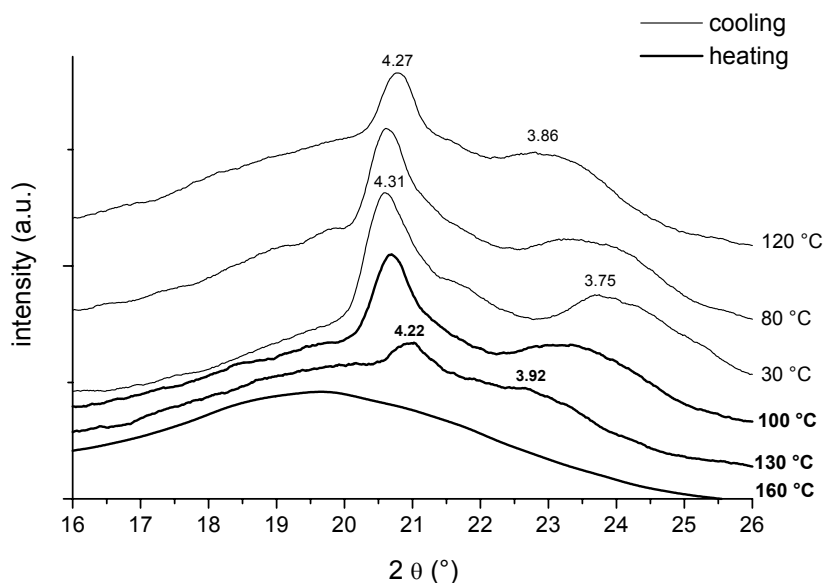


Figure 6.19: WAXD spectra of PEA4,5-50, isothermally crystallized at 120 °C, upon cooling to 80 and 30 °C and subsequent heating to 100, 130 and 160 °C.

Upon cooling from the melt, WAXD data of PEA2,5-50 were recorded at 110 °C and 50 °C (fig. 6.21). It appears that at 110 °C the crystalline structure is already fully developed. Upon further cooling, the peak positions of the characteristic diffraction peaks do not shift anymore, only the intensity of the α -related peaks (~ 4.4 and 3.9) changes.

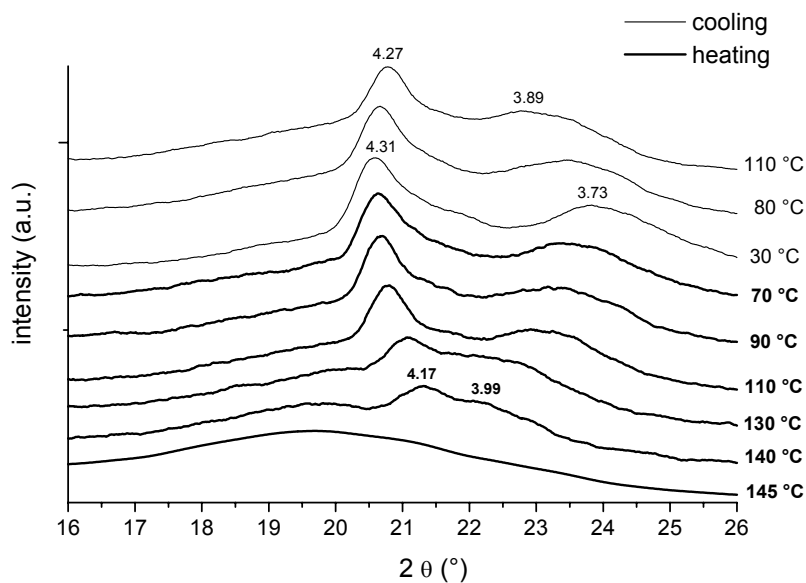


Figure 6.20: WAXD spectra of PEA4,5-75, isothermally crystallized at 110 °C, upon cooling to 80 and 30 °C and subsequent heating to 70, 90, 110, 130, 140 and 145 °C.

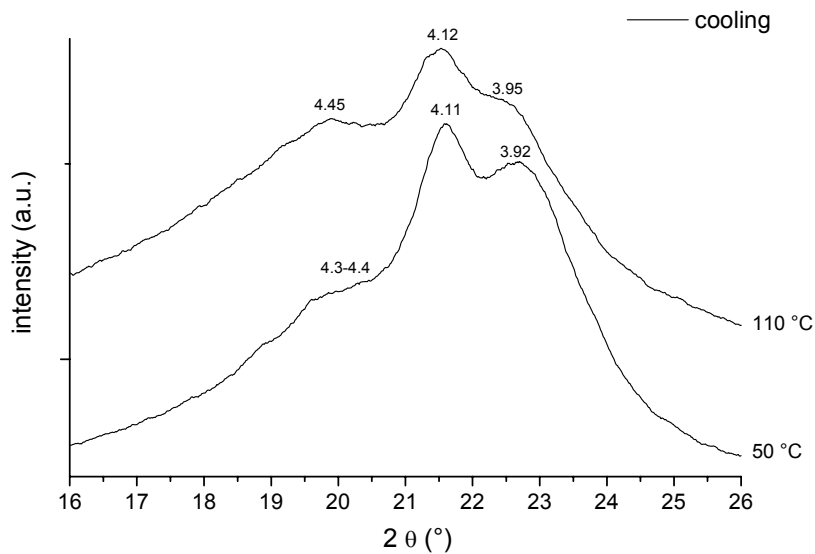


Figure 6.21: WAXD spectra of PEA2,5-50 during cooling at 110 and 50 °C.

SAXS

The so-called long spacing (period) L can be derived from SAXS measurements performed on semi-crystalline polymers that possess a lamellar structure. This spacing corresponds to the periodicity in a stack of lamellae and is equal to the lamellar thickness plus the thickness of the inter-lamellar (amorphous) region (fig. 6.22). The crystalline lamellae are generally much denser than the non-crystalline regions and hence possess a much higher electron density. It is assumed that in segmented poly(ester amide)s stacks of crystalline lamellae are formed. The presence of a scattering maximum (fig. 6.24) indicates that phase separation does occur in these poly(ester amide)s. However, the peaks are relatively broad, implying a large distribution of domain sizes.

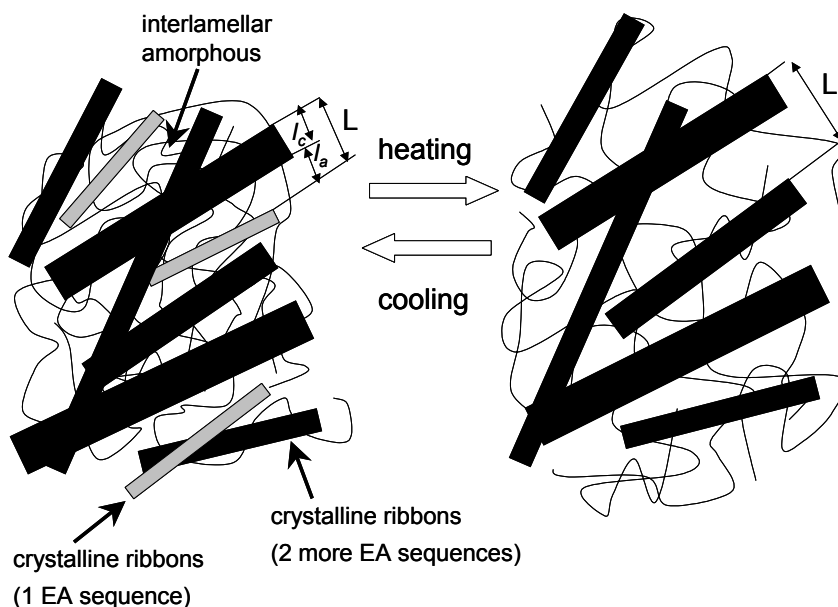


Figure 6.22: Schematic picture of poly(ester amide)s with stacks of lamellar crystals (ribbons) and interlamellar amorphous regions.

The long period, crystal and amorphous thickness are all calculated from the correlation function as presented in figure 6.23. This approach is based on a two-phase, lamellar morphology with sharp boundaries in which the width of the domains is much larger than their height. The long period is taken as the peak maximum. Further analysis of the

linear correlation functions $\gamma(r)$ (eq. 6.3), which contains the basic morphological information for a model of lamellar stacks, yields the average crystalline lamellar thickness l_c and the amorphous layer thickness l_a .

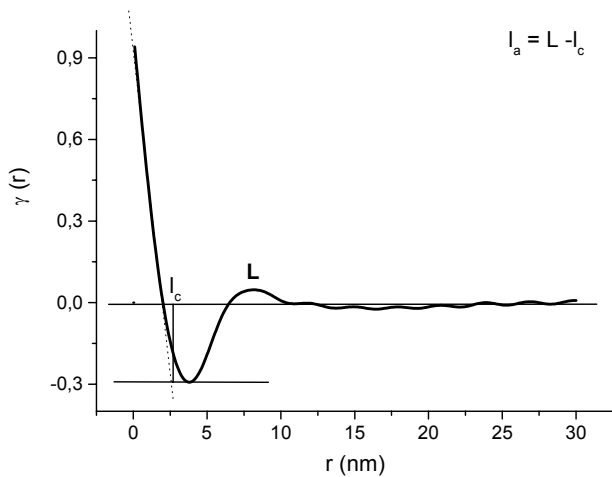


Figure 6.23: The correlation function with the dotted line being a linear fitting of the first part of the correlation function.

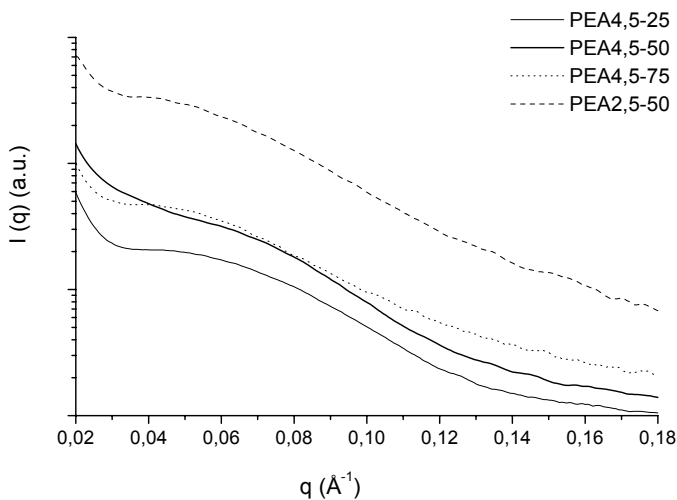


Figure 6.24: Intensity (I) as a function of the q vector for PEA4,5-25, PEA4,5-50, PEA4,5-75 and PEA2,5-50 at 30 °C.

Table 6.2: Crystallinity (w), long period (L), crystalline lamellar thickness (l_c) and amorphous layer thickness (l_a) at 30 °C for PEA4,5-25, PEA4,5-50, PEA4,5-75 and PEA2,5-50.

polymer code	w_c^a (mol%)	L (Å)	l_c (Å)	l_a (Å)	w_{ic}^b (v %)
PEA4,5-25	12.5 ± 2.5	89	19	70	21
PEA4,5-50	27.5 ± 2.5	85	25	60	29
PEA4,5-75	42.5 ± 2.5	82	57	25	70
PEA2,5-50	27.5 ± 2.5	89	19	70	21

^a crystallinity according to deconvolution of the amide I band in FT-IR spectra

^b linear crystallinity according to SAXS with the stacks calculated from l_c/L .

In chapters 4 and 5, it has been shown that the number average ester amide (EA) sequence length k increases with increasing hard segment content from 1.4 for PEA4,5-25 to 4.2 for PEA4,5-75^{23, 28}. Hence, with increasing hard segment content the average length of the hard segments increases, i.e. the crystal lamellar size increases which is in agreement with the increasing melting temperature (table 6.1). The increase of the average crystalline lamellar thickness l_c of the PEA4,5 polymers (table 6.2) from 19 to 57 Å with increasing hard segment content is in line with the increasing sequence length, although based on the molecular structure somewhat higher values were expected for PEA4,5-25, PEA4,5-50 and PEA2,5-50. It has to be noted that it is assumed that the hard segment that crystallizes and melts at $T_{m,1}$ comprises bisamide moieties including the caprolactone units, and crystals that melt at $T_{m,2}$ comprise ester amide sequences. Furthermore the lamellar model which is based on a lamellar morphology with sharp boundaries in which crystalline domains of infinite size in two dimensions are formed is not applicable for PEA4,5-25 because the crystalline lamellae have preferably grown in one direction (along the H-bonds). The model is better applicable for poly(ester amide)s with a higher hard segment content. The amorphous layer thickness l_a decreased from 70 to 25 Å with increasing hard segment while the long period L , which is a measure for the sum of the hard and soft segment size, remains relatively constant (80-90 Å). The average crystalline lamellar thickness l_c of PEA2,5-50 is substantially lower than the l_c of PEA4,5-50. This is probably due to the shorter alkyl chain length of PEA2,5-50 compared to that of PEA4,5-50. In addition, in the γ -crystalline phase (PEA2,5-50) the

chain axis is shorter compared to the chain axis in the α -phase (PEA4,5-50) due to 30° tilting of the amide groups with respect to the chain axis. The long period L of PEA2,5-50 is in the same range as that of the PEA4,5 polymers.

From the SAXS data the crystallinity in volume percentage (table 6.2) could be calculated according to equation 6.5. The lamellar model assumes that crystalline domains of infinite size in two dimensions are formed. As mentioned above the size of the crystalline domains of the poly(ester amide)s in the lateral dimension are finite ²⁵. The crystallinity, calculated from SAXS data, is thus overestimated.

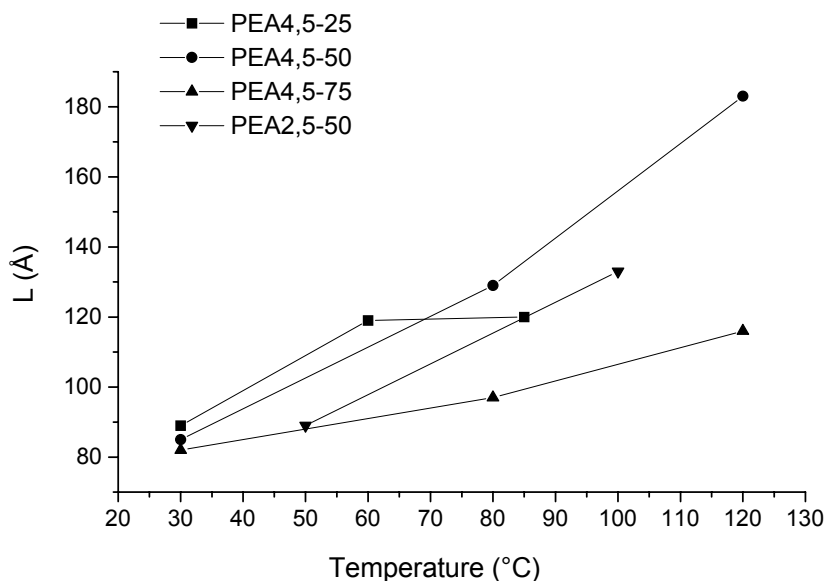


Figure 6.25: Long period (L) as a function of temperature for PEA4,5-25, PEA4,5-50, PEA4,5-75 and PEA2,5-50.

Temperature dependent SAXS measurements were performed to obtain information on the changes in crystal size upon heating. The long period L and average crystalline lamellar thickness l_c are presented as a function of temperature in figure 6.25 and 6.26, respectively. Above the flow temperature, no structural features were observed in the SAXS pattern, indicating a homogeneous melt in which the hard blocks are dissolved in the soft phase. It is assumed that poly(ester amide)s with 25 and 50 mol% of hard

segment have a pseudo two-phase morphology in which crystalline domains of rather limited size are dispersed in the amorphous matrix ²⁷. Poly(ester amide)s with a hard segment content of ≥ 75 mol% probably resemble a co-continuous hard and soft phase morphology.

The average crystalline lamellar thickness l_c of PEA4,5-25, PEA 4,5-50 and PEA2,5-50 slightly increased while their amorphous layer thickness l_a increased significantly with increasing temperature. Several phenomena contribute to this increase in amorphous lamellar thickness and long period L like thermal expansion, surface melting of crystals and melting of crystals composed of single ester amide (EA) sequences. The crystalline hard domains are in a first approximation insensitive to temperature while the amorphous domains expand with temperature. The most effective contribution is from the melting of defective crystals and crystals comprising single EA sequences, which causes a significant increase in long period and amorphous layer thickness but also the average crystalline lamellar thickness slightly increases. Surface melting of crystals also should be taken into account ²⁹. Upon heating, surface layers will melt before the whole crystal will collapse, which increases the long period and amorphous layer thickness while the average crystalline lamellar thickness is reduced.

The increase in long period and amorphous layer thickness with temperature is less for PEA4,5-75 when compared to PEA4,5-25, PEA4,5-50 and PEA2,5-50. A few possible explanations are given below. The volume fraction of amorphous soft domains in PEA4,5-75 is small and probably confined in the continuous amide hard domains and thus the amorphous soft domains can not dominate the thermal expansion. The low melt enthalpy of the lower melt transition $T_{m,1}$ indicates that only a minor fraction of crystals comprising single EA sequences, is present. Thus melting of crystals comprising single EA sequences will only contribute to a certain extent to an increase in long period and amorphous layer thickness. As the crystal thickness of PEA4,5-75 is much larger compared to PEA4,5-25, PEA4,5-50 and PEA2,5-50, the effect of surface melting of crystals is rather small and thus will contribute only slightly to an increase in long period and amorphous layer thickness. In contrast to PEA4,5-25, PEA4,5-50 and PEA2,5-50, the average crystalline lamellar thickness of PEA4,5-75 has increased significantly with temperature. Crystal thickening caused by an annealing effect might explain this increase.

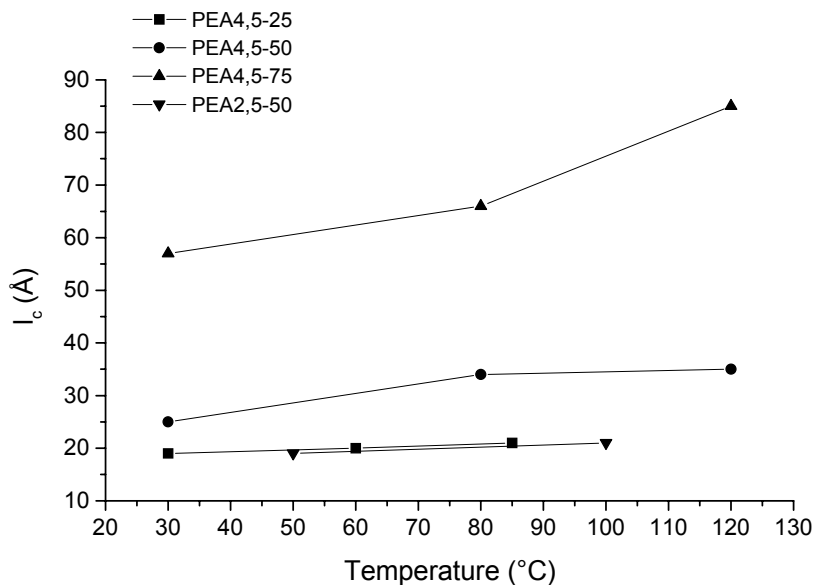


Figure 6.26: Crystalline lamellar thickness (l_c) as a function of temperature for PEA4,5-25, PEA4,5-50, PEA4,5-75 and PEA2,5-50.

Conclusions

Segmented poly(ester amide)s were prepared by melt polycondensation of dimethyl adipate, 1,4-butanediol and a symmetrical bisamide-diol with 2 or 4 methylene units between the amide groups, abbreviated as PEA2,5 and PEA4,5, respectively. All polymers have a sub-ambient glass transition temperature and two melt transitions, corresponding with the melting of crystals comprising single ester amide sequences or 2 or more ester amide sequences. The poly(ester amide)s have a micro-phase separated structure with an amide-rich hard phase and an ester-rich flexible soft phase and crystallize into an α - or a γ -type crystalline phase, similar to α - or γ -crystals present in nylons. PEA4,5 polymers crystallize into an α -type crystalline phase, while a mixture of α - and γ -type crystalline phases was found for PEA2,5 polymers. The crystallization behaviour and morphological aspects of PEA4,5 and PEA2,4 polymers with different hard segment content were studied with DSC, AFM, temperature dependent FT-IR, WAXD and SAXD. Upon heating to the first melt transition, IR-bands characteristic of

ordered H-bonded amide groups decrease which indicate that at $T_{m,1}$ some crystals melt and form disordered H-bonded N-H groups as well as unassociated groups. This decrease is much more pronounced for PEA4,5 and PEA2,5 with 25 mol% of hard segment as compared to these polymers with 50 mol% of hard segment. This confirms that also the transition at $T_{m,1}$ is associated with the melting of a crystalline structure comprising ordered hard segments. H-bonds between amide groups were still present in the melt. WAXD measurements at room temperature of PEA4,5 polymers showed diffraction peaks at 3.7 and 4.4 Å which are characteristic for the α -crystalline phase of even-even nylons. These diffraction peaks shift significantly upon heating for the polymers PEA4,5 with 50 and 75 mol% of hard segment content but do not actually meet. Thus the polymers have already melted before the actual Brill transition is reached. SAXD measurements showed that the average lamellar thickness of PEA4,5 polymers increased from 19 to 57 Å with increasing hard segment content. This is in line with the increasing $T_{m,2}$ i.e. the increasing average length of the hard segments. The average lamellar thickness of PEA2,5 with 50 mol% of hard segment is substantially lower compared to the corresponding PEA4,5 polymer.

References

1. P.A.M. Lips, chapter 5, in *this thesis*. **2004**.
2. P.A.M. Lips, chapter 4, in *this thesis*. **2004**.
3. S.M. Aharoni, **1997**, *n-nylons: Their synthesis, structure and properties*, John Wiley & Sons Ltd., Chichester.
4. M.I. Kohan, **1995**, *Nylon plastics handbook*, Hansers Publisher, New York.
5. P.A.M. Lips, chapter 3, in *this thesis*. **2004**.
6. R. Brill, *J. Prakt. Chem.*, **1942**, 161, 49.
7. Y. Li, D. Yan, E. Zhou, *Colloid Polym. Sci.*, **2002**, 280, 124.
8. N. Vasanthan, N. Sanjeeva Murthy, R.G. Bray, *Macromolecules*, **1998**, 31, 8433.
9. D. Yan, Y. Li, X. Zhu, *Macromol. Rapid. Commun.*, **2000**, 21, 1040.
10. X. Yan, X. Zhu, L. Chen, P. He, D. Yan, X. Wang, *J. Polym. Sci.: Part B: Polym. Phys.*, **2004**, 42, 60.
11. G. Zhang, Y. Li, D. Yan, *Polym. Int.*, **2003**, 52, 795.

12. Y. Yoshioka, K. Tashiro, C. Ramesh, *Polymer*, **2003**, *44*, 6407.
13. B. Vanhaecht, C.E. Koning, *Macromolecules*, **2004**, *37*, (2), 421.
14. S. Rhee, J. White, *Polymer*, **2002**, *43*, 5903.
15. J. Puiggali, L. Franco, C. Aleman, J.A. Subirana, *Macromolecules*, **1998**, *31*, 8540.
16. C. Ramesh, A. Keller, *Polymer*, **1994**, *35*, (12), 2483.
17. N.A. Jones, E.D.T. Atkins, M.J. Hill, J. Cooper, L. Franco, *Polymer*, **1997**, *38*, (11), 2689.
18. N. Jones, E. Atkins, *Macromolecules*, **1996**, *29*, 6011.
19. D.J. Skrovanek, P.C. Painter, M.M. Coleman, *Macromolecules*, **1986**, *19*, 699.
20. B. Kaczmarczyk, *Polymer*, **1998**, *39*, (23), 5853.
21. J. Jutier, E. Lumieux, R.E. Prud'homme, *J. Polym. Sci.: Part A: Polym. Phys.*, **1988**, *26*, 1313.
22. P. Iriondo, J.J. Iruin, M.J. Fernandez-Berridi, *Polymer*, **1995**, *36*, (16), 3225.
23. R.J. Cella, *J. Polym. Sci.*, **1973**, *42*, 727.
24. J. Krijgsman, D. Husken, R.J. Gaymans, *Polymer*, **2003**, *44*, 7573.
25. R.M. Versteegen, *PhD thesis*, **2003**, Technische Universiteit Eindhoven, The Netherlands: p. 65.
26. B. Goderis, H. Reynaers, M.H.J. Koch, V.B.F. Mathot, *J. Polym. Sci.: Part B: Polym. Phys.*, **1999**, *37*, 1715.
27. B. Goderis, H. Reynaers, M.H.J. Koch, *Macromolecules*, **2002**, *35*, 5840.
28. H.R. Stapert, *PhD thesis*, **1998**, University of Twente, The Netherlands: p. 121.
29. E.W. Fischer, *Pure. Appl. Chem.*, **1971**, *26*, 385.

Chapter 7

Biocompatibility and degradation of aliphatic segmented poly(ester amide)s: *in vitro* and *in vivo* evaluation

P.A.M. Lips¹, M. J. A. van Luyn², F. Chiellini³, L.A. Brouwer², I.W. Velthoen¹, P.J. Dijkstra¹, J. Feijen¹

¹ *Institute for Biomedical Technology (BMTI) and Department of Polymer Chemistry and Biomaterials, Faculty of Science and Technology, University of Twente, P.O. Box 217, 7500 AE Enschede, The Netherlands.*

² *Medical Biology, Pathology and Laboratory Medicine, University of Groningen, Hanzeplein 1, 9713 GZ Groningen, The Netherlands,*

³ *Department of Chemistry and Industrial Chemistry, University of Pisa, Via Risorgimento 35, 56127 Pisa, Italy.*

Abstract

Aliphatic segmented poly(ester amide)s, comprising a crystallizable amide phase and a flexible amorphous ester phase, were investigated for potential use in biomedical applications. By varying the amide content and the type of crystallizable amide segments the polymers thermal and mechanical properties can readily be tuned. Polymers with 25 and 50 mol% of amide content are non-cytotoxic and sustain growth of fibroblasts onto polymer films. The *in vitro* degradation of these polymers was followed in PBS (pH 7.4) at 37 °C up to 7 months. The poly(ester amide)s showed the characteristics of bulk degradation with a gradual decrease in molecular weight and almost no mass loss. The *in vivo* degradation of these polymers, followed by subcutaneous implantation in rats up to 6 wks, was slow and similar to the *in vitro* degradation. The tissue response upon

implantation was followed over 6 wks. A mild foreign body reaction, characterized by the presence of macrophages and sporadically a lymphocyte was observed in the first week of implantation. After 6 wks the implant site is characterized by fibrous encapsulation with no signs of inflammation. The poly(ester amide)s tested are biocompatible but their *in vitro* as well as *in vivo* degradation is very slow.

Introduction

Degradable polymers can be used in a wide range of pharmaceutical and biomedical applications such as drug delivery systems and temporary implant materials like sutures, scaffolds and barrier materials. Currently, a limited number of degradable and/or absorbable materials suitable for use in this field are applied, including poly(hydroxy acid)s, poly(ortho ester)s, poly(anhydride)s and poly(phospho ester)s. A considerable amount of research has been directed to the aliphatic polyesters, poly(lactic acid) (PLA), poly(glycolic acid) (PGA) and their copolymers (PLGA). Degradation, through hydrolysis, of these polyesters *in vivo* generates lactic acid and/or glycolic acid, which are converted to water and carbon dioxide in the tricarboxylic acid cycle¹. However, the acidic compounds released during the degradation of PGA and PLGA polymers and the potential crystalline remnants generated by PLA degradation can induce unwanted foreign body reactions¹⁻⁴.

The aliphatic polyester poly(butylene adipate) is a degradable polymer with potential use in the biomedical field. However, poly(butylene adipate) is a very brittle material with a low melting temperature (67 °C). Incorporation of amide segments in aliphatic polyesters leads to segmented polymers with improved thermal and mechanical properties with respect to polyesters. Segmented poly(ester amide)s are prepared by melt condensation of preformed bisamide-diols, 1,4-butanediol and dimethyl adipate (fig. 7.1). These polymers, consisting of well-defined amide blocks and an amorphous polyester matrix, have thermal, physical and mechanical properties that can be readily tuned by variation of the hard (x) to soft (y) block ratio^{5, 6}. By increasing the amide content (x) from 10 to 85 mol% the melting temperature (T_m) and glass transition temperature (T_g) of the poly(ester amide)s increased from 80 to 140 °C and from -45 to -8 °C, respectively. Correspondingly, the modulus (70-550 MPa) and the stress at break

(8-25 MPa) increased while the strain at break (850-400%) decreased. Initial degradation studies using lipases from *Aspergillus Niger* and *Rhizopus Arrhizus* showed that poly(ester amide)s with a hard block content of 10 to 30 mol% were fully degradable⁷. Within 8 days the residual weight of poly(ester amide) dense films (thickness = ~ 0.5 mm) with a hard block content of 10 and 20 mol% was less than 5%, while polymers with a hard block content of 30 mol% had a residual weight of 15 to 40%. This illustrates that degradation mainly proceeds through cleavage of ester bonds. A major advantage is that the bisamide-diol monomers and oligomers are water-soluble which prevents the formation of crystalline amide remnants.

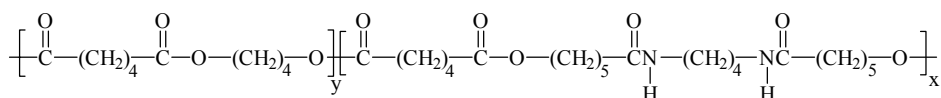


Figure 7.1: A segmented poly(ester amide) with a soft block (y) based on 1,4-butanediol and dimethyl adipate and a hard block (x) based on based on ϵ -caprolactone, 1,4-diaminobutane and dimethyl adipate.

One of the first studies on aliphatic poly(ester amide)s to be applied as bioresorbable sutures was performed by Barrows *et al.*^{8,9}. In this study alternating poly(ester amide)s were prepared by solution polymerization from symmetrical bisamide-diols and succinyl chloride and the fibre forming properties and *in vivo* resorption were investigated (fig. 7.2). Different water-soluble bisamide-diols were prepared from glycolic acid and diaminoalkanes containing two to twelve methylene groups. The degradation of the poly(ester amide)s was examined by the tensile strength retention after 4 wks of implantation. The tensile strength retention increased with decreasing water solubility of the bisamide-diol. To study the *in vivo* degradation behaviour of the poly(ester amide)s, a bisamide-diol based on 1,6-diaminohexane was labelled with carbon-14 in the hydroxyacetamide moiety. *In vivo* resorption of these radiolabeled poly(ester amide) monofilament fibres resulted in complete elimination of all radioactivity from the body after 9 months. The principal mechanism of *in vivo* degradation appeared to be hydrolysis of the ester bonds with the water-soluble bisamide-diol monomer as a non-toxic major metabolite excreted by the kidneys. More hydrophilic metabolites generated from these poly(ester amide)s are excreted faster and to a greater extent, whereas more

hydrophobic metabolites are excreted slower and to a greater degree in feces due to extensive biotransformation. In separate experiments the 1,6-diaminohexane based bisamide-diol monomer and the corresponding polymer showed no evidence of acute cytotoxicity.

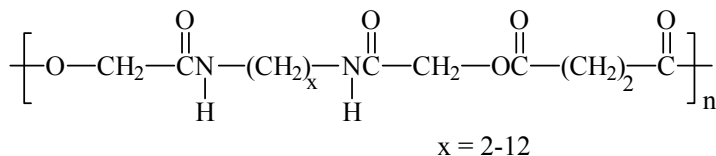


Figure 7.2: Alternating poly(ester amide) based on a diaminoalkane, glycolic acid and succinyl chloride ^{8,9}.

Bera *et al.* investigated the *in vivo* degradation of alternating and segmented poly(ester amide)s for possible biomedical applications ¹⁰. Low molecular weight alternating poly(ester amide)s ($M_n=1450$) were prepared from 1,10-decanedicarboxylic acid and a preformed bisamide-diol, based on 1,6-diaminohexane and γ -butyrolactone (fig. 7.3A). By replacing the 1,10-decanedicarboxylic acid with adipic acid in the alternating poly(ester amide) ($M_n=1050$) and reacting it with an oligoester ($M_n=2550$), prepared from 1,2-ethanediol and adipic acid, a high molecular weight segmented poly(ester-amide) was obtained (fig. 7.3B). By changing the molar fraction of amide segments (m) a series of polymers could be prepared with a T_m ranging from 50 to 215 °C and a T_g varying from -45 to -15 °C. In addition, the modulus (150-180 MPa), the stress at break (6-15 MPa) and the strain at break (1000-1500%) are also changing. After 30 days of subcutaneous implantation in rats, the alternating poly(ester amide) oligomer was completely fragmented while the segmented poly(ester amide) was encapsulated. Both oligomer and polymer were resorbed after three months of implantation. Bisamide-diols, tested on albino mice by intravenous administration of the monomer in an isotonic 1% saline solution, were found to be non-toxic with no mortality or morbidity.

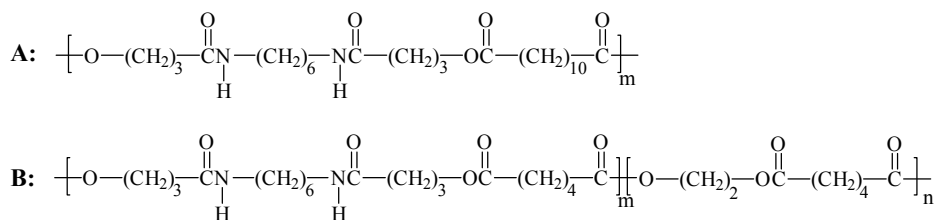


Figure 7.3: An alternating poly(ester amide) (A) based on 1,6-diaminohexane, γ -butyrolactone and 1,10-decanedicarboxylic acid and a segmented poly(ester amide) (B) based on 1,6-diaminohexane, γ -butyrolactone, 1,2-ethanediol and adipic acid ¹⁰.

Deschamps *et al.* ¹¹ prepared poly(ether ester amide)s, based on poly(ethylene glycol), 1,4-butanediol and a diamide-diester for tissue engineering applications (fig. 7.4A). By varying the x/y ratio and the M_w of the poly(ethylene glycol), the T_m and T_g could be tuned from 110 to 150 °C and from -50 to -20 °C, respectively. Similarly, the modulus ranged from 200 to 400 MPa, the stress at break from 10 to 25 MPa and the strain at break from 300 to 850%. To investigate the *in vivo* degradation, poly(ether ester amide)s films were implanted in rats for a period of 14 weeks. Depending on the x/y ratio and the M_w of the poly(ethylene glycol), a decrease in intrinsic viscosity of 20 to 30% and a mass loss of 7 to 12 wt% were measured. An important outcome of this study was the degradation, although slow, of the parent poly(ester amide) (fig 7.4B). In addition, endothelial cells were cultured onto poly(ether ester amide) and poly(ester amide) films. The growth rate of the cells was higher when the poly(ethylene glycol) content decreased.

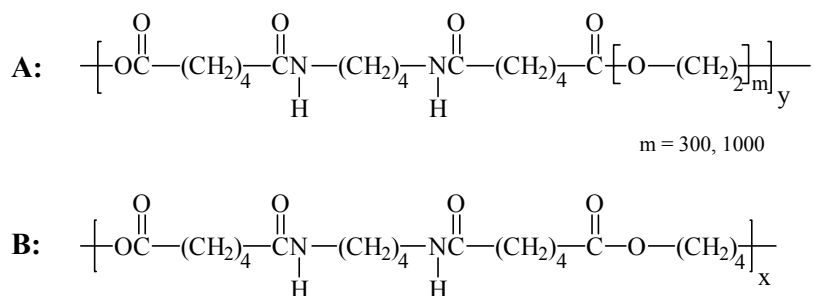


Figure 7.4: A segmented poly(ether ester amide) with a soft block (A) based on 1,4-diaminobutane, dimethyl adipate and poly(ethylene glycol) and a hard block (B) based 1,4-diaminobutane, dimethyl adipate and 1,4-butanediol ¹¹.

Based on previous studies ⁵⁻⁷, aliphatic segmented poly(ester amide)s comprising water-soluble bisamide-diols, dimethyl adipate and 1,4-butanediol (fig. 7.1), are expected to degrade and/or resorb in the body. In addition, the thermal and mechanical properties of these polymers can be tuned by changing the ratio of bisamide-diol to 1,4-butanediol in the monomer feed. To study their applicability in the biomedical field these poly(ester amide)s have been evaluated with respect to their mechanical properties in the hydrated state, cytotoxicity, adhesion and growth of fibroblasts, *in vitro* and *in vivo* degradation and tissue response.

Experimental

Polymer synthesis

A two-step polycondensation of dimethyl adipate, 1,4-butanediol and N,N'- α , ω alkanediyl-bis[6-hydroxy-hexanamide] (bisamide-diol) was performed in the presence of tetrabutyl(orthotitanate) as a catalyst (fig. 7.5). The molar ratio of hard (x) and soft (y) segments of the poly(ester amide) can be varied by changing the ratio of bisamide-diol and 1,4-butanediol. The polymers, PEA4,5-25, PEA4,5-50 and PEA4,5-85 with 28, 56 and 85 mol% of N,N'-1,4-butanediyl-bis[6-hydroxy-hexanamide], respectively, and PEA2,5-25 and PEA2,5-50 with 26 and 51 mol% of N,N'-1,2-ethanediyl-bis[6-hydroxy-hexanamide], respectively, were prepared as previously described ⁶.

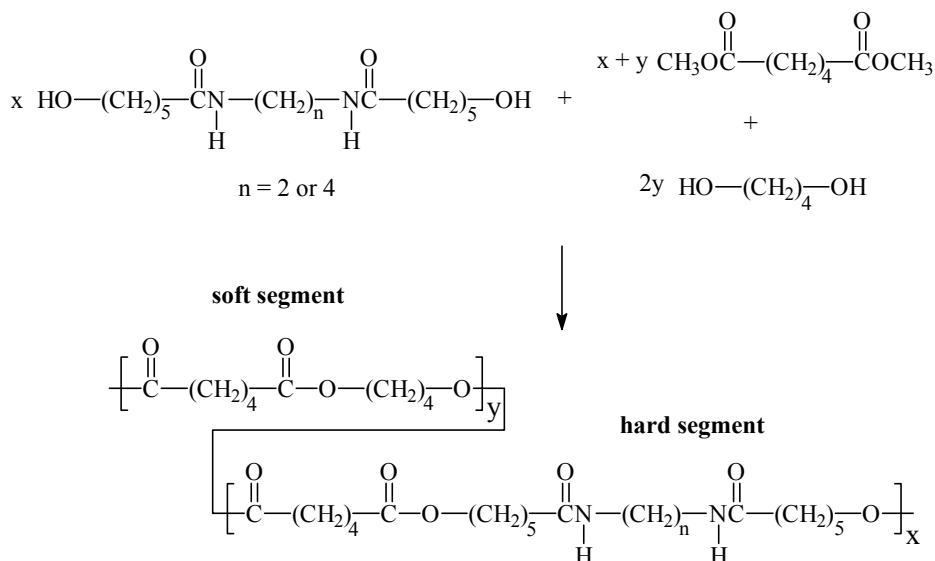


Figure 7.5: Synthesis of a segmented poly(ester amide) from a bisamide-diol, dimethyl adipate and 1,4-butanediol ($n=4$, PEA4,5 and $n=2$, PEA2,5).

Preparation of polymer films

Compression moulded polymer films with various thicknesses were prepared with a hot press (THB 008, Fontijne Holland BV, the Netherlands). Polymers were heated for 6-8 min at 20 °C above their T_m as measured by DSC, pressed for 3 min at 300 kN, and cooled in approximately 5 min under pressure to room temperature.

Water uptake

The water absorption was determined by immersing polymer bars (10x10x2 mm) in demineralised water at 37 °C for 2 days. Polymer bars were predried at 30 °C under reduced pressure for at least 2 days. The water absorption (wt %) was calculated using:

$$\text{wt \%} = \frac{w - w_0}{w_0} \times 100\% \quad (\text{eq. 7.1})$$

where w_0 and w are the sample weight before and after treatment, respectively.

Contact angle measurements

The water contact angle was determined using the sessile drop technique. A drop of demineralized water was put on a polymer film (0.4 mm thickness, 12 mm diameter). After 3 seconds the contact angle was measured using a Contact Angle System OCA 15. Results are averages of at least 10 measurements.

Tensile tests

Tensile tests were conducted on compression moulded bars (75x4x2 mm), cut to dumb bells (ISO 37). The dumb bell shaped samples were immersed in a water bath at 37 °C for 3 days. Before the measurement, samples are wiped off. A Zwick Z020 universal tensile tester equipped with a 500 N load cell and extensometers was used to measure the stress as a function of strain at a strain rate of 500 mm.min⁻¹ and a preload of 3 N.

In vitro degradation

Polymer discs (~ 350 µm thickness, 10 mm diameter) were placed in phosphate buffered saline (PBS) at 37 °C, containing 0.03 wt% sodium azide as anti-bacterial agent. Samples were removed from the water bath after 7 days and 1, 2, 3, 4, 5, 6 and 7 months, rinsed with demineralized water and dried under vacuum at room temperature. Subsequently, the dry weight, the molar composition, molecular weight and thermal properties of the specimen were determined.

Mass loss was expressed as:

$$\text{wt \%} = \frac{w_0 - w}{w_0} \times 100\% \quad (\text{eq. 7.2})$$

where w_0 and w are the sample weight before and after degradation, respectively.

NMR: ¹H-NMR (300 MHz) spectra were recorded on a Varian Inova Nuclear Magnetic Resonance Spectrometer using chloroform-d₁ as a solvent.

The polymer composition (x/y) was determined from the ratio of the signal of the methylene groups next to the amide NH at δ 3.26 and the signal of the methylene groups next to the ester acyl oxygen at δ 4.10. Assuming that the polymer chains have hydroxyl end groups, molecular weights were calculated from the signals of the CH₂-OH

endgroups at δ 3.67 and the signals of the methylene groups next to the ester acyl oxygen at δ 4.10.

Viscometry: Intrinsic viscosities $[\eta]$ were determined by a single point measurement using a capillary Ubbelohde type 0C at 25 °C and a polymer solution with a concentration of 0.1 g.dl⁻¹ in chloroform-methanol (1:1 vol/vol). The following empirical equation was applied:

$$[\eta] = \frac{\sqrt{2}}{c} \sqrt{\eta_{spec} - \ln \eta_{rel}} \quad (\text{eq 7.3})$$

where $\eta_{spec} = \eta_{rel} - 1$ and c is the polymer concentration in g.dl⁻¹.

DSC: Thermal analysis of the polymers was carried out with a Perkin-Elmer DSC-7 Differential Scanning Calorimeter equipped with a PE7700 computer and TAS-7 software. Calibration was performed with pure indium. Samples (5-10 mg) were heated from -20 to 180 °C at a rate of 20 °C.min⁻¹. Melting temperatures (T_m) were obtained from the peak maximum and melt enthalpies (ΔH_m) were determined from the area under the curve.

Cytotoxicity

Experiments were performed following the standards indicated by ISO-10993-5 "Biological Evaluation of Medical Devices: Cytotoxicity".

Polymer precipitates, obtained by precipitation of a polymer/chloroform solution into diethyl ether, were UV ($\lambda = 254$ nm, $P = 30$ W, $d = 50$ cm) sterilized for 15 min. Fluid extracts were prepared by incubating the polymer precipitate in cell culture medium (DMEM) (0.2 g.ml⁻¹) for 24 h at 37 °C. The fluid extracts were then filtered through a 0.2 μ m sterile filter and used undiluted as well as diluted 1:2 with DMEM.

Cytotoxicity tests of the PEA4,5-25, PEA4,5-85, PEA2,5-25 and PEA2,5-50 were carried out using a Balb/3T3 clone A31 mouse embryo fibroblast cell line (ATCC CCL-163). Cells were grown on tissue culture polystyrene (TCPS) in DMEM supplemented with 10% heat-inactivated fetal bovine serum, 4 mM glutamine, 100 U.ml⁻¹ penicillin-100 g.ml⁻¹ streptomycin at 37 °C and 5% CO₂. A subconfluent monolayer of the fibroblasts was trypsinized using a 0.25% trypsin-1mM EDTA solution. Cells were centrifuged at 200 g for 5 min, resuspended in growth medium and counted.

100 μl of cell suspension ($3 \times 10^4 \text{ cells.ml}^{-1}$) was added to each well of a 96 well plate. Cells were incubated at 37°C and $5\% \text{ CO}_2$ for 24 h resulting in 60-70% confluence. The medium from each well was removed and replaced with polymer extracts (undiluted and diluted 1:2 with DMEM) of the polymers. As a control, cells were grown on TCPS incubated with DMEM. After 24 h of incubation, cells were analyzed with a Cell Proliferation Reagent (WST-1), which is a colorimetric assay for the quantitative determination of mitochondrial dehydrogenases in viable cells by the cleavage of the tetrazolium salt WST-1 into formazan. Cells were incubated with WST-1 diluted 1:10 for 4 h at 37°C , $5\% \text{ CO}_2$. Plates were then analysed with a Biorad Microplate Reader. Measurement of formazan dye absorbance is carried out at 450 nm. The reference wavelength was 620 nm.

Cell adhesion and proliferation

The ability of PEA films to promote cell adhesion and proliferation was evaluated by using the ATCC CCL-163 cell line (see cytotoxicity). Samples were UV ($\lambda = 254 \text{ nm}$, $P = 30 \text{ W}$, $d = 50 \text{ cm}$) sterilized for 15 min and incubated in PBS for 15 min before cell seeding.

Qualitative analysis

Two ml of the cell suspension ($1.5 \times 10^4 \text{ cell.ml}^{-1}$) was placed onto the polymer films (0.4 mm thickness, 32 mm diameter) fitted in 6 wells TCPS plates. Cells were incubated at 37°C and $5\% \text{ CO}_2$ for 2 h. The culture medium was then removed and replaced with 2 ml of fresh growth media. Cells were allowed to grow for 72 h, representing the typical time needed by 3T3 cells to grow and reach confluence on TCPS i.e. the reference material. Next, the medium from each well was removed and adhered cells were washed 3 times with PBS (pH 7.3), fixed in 3.8% paraformaldehyde at room temperature for 2 h and finally carefully rinsed with PBS. Cells were stained with toluidine blue and analyzed under an inverted light microscope.

Quantitative analysis

One ml of cell suspension ($1.5 \times 10^4 \text{ cell.ml}^{-1}$) was placed onto the polymer films (0.4 mm thickness, 12 mm diameter) fitted in 24 wells TCPS plates. Cells were incubated at 37°C and $5\% \text{ CO}_2$ for 2 h. The culture medium was then removed and replaced with 1 ml fresh growth media. Cells were allowed to grow for 72 h, representing the typical

time needed by 3T3 cells to grow and reach confluence on TCPS. After 72 h, cells were analysed with Cell Proliferation Reagent WST-1, as described in the part 'Cytotoxicity'. Growth medium was used as a blank and cells grown on TCPS as a control.

In vivo experiments

To investigate the *in vivo* degradation and the tissue response of aliphatic poly(ester amide)s PEA4,5-50 and PEA2,5-50 discs were implanted subcutaneously in the back of rats.

Discs (1 mm thickness, 8 mm diameter) were sterilized by incubation in 70 vol% ethanol solution for 24 h followed by two times rinsing for 4 h in PBS buffer. The discs were stored in PBS overnight before implantation. Animal experiments were carried out according to the National Institute of Health (NIH) guidelines for care and use of laboratory animals (NIH publication # 85-23 rev. 1985). Male A.O. rats of approximately 3 months of age were anesthetized with a mixture of halothane, N₂O and O₂. After shaving and disinfection, subcutaneous pockets were made to the right and left of two 1 cm midline incisions on the back of the rat. Discs were placed in the pockets and implanted for respectively 5, 10 days and 6 wks (n=3). After surgery, the rats were housed in a temperature- and humidity-controlled room with 12 h light/dark cycles and access to water and standard rat food *ad libitum*.

After 5, 10 days and 6 wks of implantation, rats were anesthetized and the implants with the surrounding tissue were carefully explanted. Per implantation time, three discs of PEA4,5-50 and PEA2,5-50 were further processed for histology and three discs were used for chemical and physical characterization.

Histology

The explants were immediately fixed in 2 vol% glutaraldehyde in PBS (0.1 M, pH 7.4) for at least 24 h at 4 °C. After rinsing in distilled water and dehydration in graded alcohols (50, 70, 96 and 100 vol%), explants were cut in halve and each part was embedded in poly(hydroxyethyl methacrylate) (polyHEMA) (Kulzer Histo Technik, Heraeus Kulzer, Germany). Sections (2 µm) were cut using a microtome (Jung), stained with toluidine blue and evaluated by light microscopy.

The tissue response was independently rated by three persons according to the following scoring system: - = no infiltration, sp to +++ = sporadic to relatively high infiltration of

granulocytes, macrophages, multinucleated giant cells and lymphocytes. The sections were also examined for the presence of fibrin, the induction of vascularization, the formation of a fibrous capsule around the polymer discs and degradation of the polymers.

In vivo degradation

The explants were immediately immersed in PBS solution. Within 24 h the samples were freed from the surrounding tissue, rinsed with demineralized water and dried under vacuum at room temperature. Subsequently, the dry weight, the molar composition, molecular weight and thermal properties of the specimen were determined similar to the method described in the part '*in vitro* degradation'. In addition, Scanning Electron Microscopy (SEM) was carried out with a LEO Gemini 1550 field emission microscope at a voltage of 2 kV to investigate the surface of the polymers discs after degradation. Samples were mounted on an aluminium holder.

Results and Discussion

The nature of a biomaterials surface, such as wettability (hydrophilicity/hydrophobicity), chemistry, charge and roughness is critical to its biocompatibility. A large number of research groups have studied the effect of the surface wettability on the interaction of cells with solid substrates¹²⁻¹⁴. Lee *et al.* investigated the interaction of fibroblasts and endothelial cells on polymer surfaces (PE) with a wettability gradient¹⁵. It was observed that cells adhered, spread and grew better onto surfaces with moderate hydrophilicity than onto the more hydrophilic or hydrophobic surfaces. The maximum adhesion and growth of the cells appeared at a contact angle of $\sim 55^\circ$, regardless of the cell type used.

The contact angle of TCPS, which is an ideal surface for cells to adhere to, is $62 \pm 2^\circ$.

In an attempt to correlate cell growth with the surface characteristics of the substrate, static contact angle and water uptake measurements were performed (table 7.1). PEA4,5-25, PEA4,5-85 and PEA2,5-50 have a contact angle of $\sim 70^\circ$ whereas PEA2,5-25 has a much higher contact angle (106°). The hydrophobicity of PEA2,5-25 is reflected in its low water uptake. Increasing the amide content leads to an increase in crystallinity which lowers the water uptake of the PEA2,5-50 polymer.

Table 7.1: Crystallinity, water uptake and contact angle of PEA4,5 and PEA2,5.

polymer code	Crystallinity ^a (%)	Water uptake ^b (%)	Contact angle ^c (°)
PEA4,5-25	12.5 ± 2.5	11.7 ± 0.1	66 ± 2
PEA4,5-85	42.5 ± 2.5	7.8 ± 0.2	73 ± 2
PEA2,5-25	12.5 ± 2.5	4.4 ± 0.1	106 ± 6
PEA2,5-50	27.5 ± 2.5	3.9 ± 0.1	77 ± 2

^a crystallinity according to amide I band in FT-IR spectra, ^b at equilibrium, ^c sessile drop

Mechanical properties

As shown in table 7.1 the poly(ester amide)s can take up 4-12 wt% of water, which is lower than polyamides and much higher than polyesters. Considering the use of these materials as implants in the body where it will absorb body fluids and swell, the mechanical properties were also evaluated in the hydrated state. This is illustrated in table 7.2 which shows that the elastic modulus, stress at break, stress at yield and strain at break do decrease for the polymers in the hydrated state.

Both in the dry and the wet state, the elastic modulus and the tensile strength increase when increasing the hard segment content from 25 to 50 mol%, whereas the stress at break hardly changes.

Table 7.2: Water-uptake and tensile properties for dry and swollen PEA2,5-25 and PEA2,5-50 polymers.

property	dry state ⁶		wet state	
	PEA2,5-25	PEA2,5-50	PEA2,5-25	PEA2,5-50
water uptake (wt%)	-	-	4.4 ± 0.1	3.9 ± 0.1
E (MPa)	150 ± 18	313 ± 24	59 ± 5	234 ± 11
σ _{yield} (MPa)	8 ± 0.2	14 ± 0.5	5 ± 0.2	11 ± 0.5
σ _{break} (MPa)	21 ± 2	25 ± 2.5	13 ± 1.5	16 ± 3
ε _{break} (%)	745 ± 25	775 ± 25	675 ± 10	520 ± 40

Hydrolytic degradation

A long-term hydrolytic degradation test was performed on PEA2,5-25 and PEA2,5-50. Polymer discs were incubated in PBS buffer (pH 7.4) at 37 °C for 7 months. In time, changes in mass, intrinsic viscosity, molecular weight and compositional changes were measured.

The mass loss increases linearly with degradation time as depicted in figure 7.6. The first data points ($t=0$) are removed from the trend line as in the first days oligomers present in the polymer matrix might be released. The total mass loss after 7 months of degradation was 3.4% for PEA2,5-25 and 2.8% for PEA2,5-50. The weight loss of PEA2,5-50 as a result of hydrolytic degradation is most probably even lower because a weight loss of ~1.3% can be attributed to the release of oligomers.

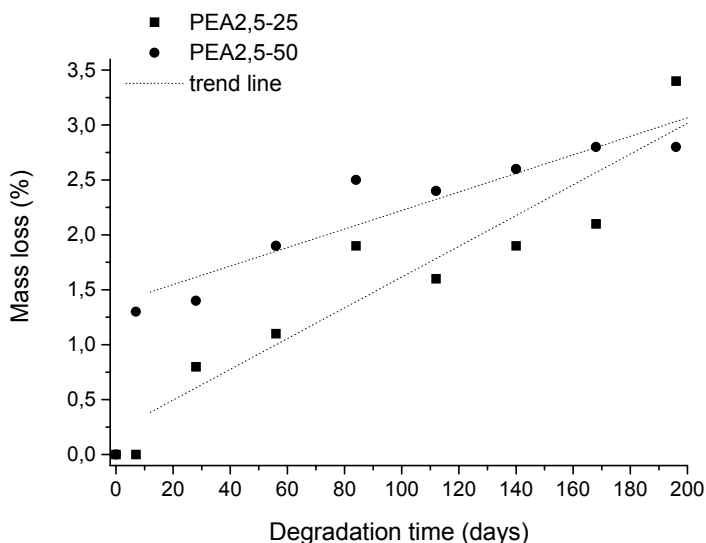


Figure 7.6: Mass loss as a function of degradation time for PEA2,5-25 and PEA2,5-50, in PBS (pH 7.4) at 37 °C.

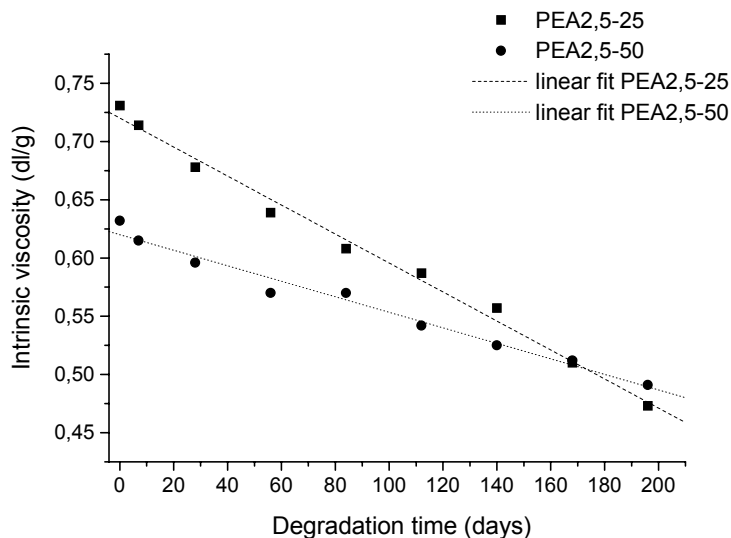


Figure 7.7: Intrinsic viscosity as a function of degradation time for PEA2,5-25 and PEA2,5-50, in PBS (pH 7.4) at 37 °C.

The intrinsic viscosity (chloroform-methanol 1:1 vol/vol) of PEA2,5-25 and PEA2,5-50 linearly decreases in time (fig. 7.7). The slope of the lines suggests that PEA2-25 degrades faster in time. However, care should be taken because the initial intrinsic viscosity and the composition of both polymers is different, which can both influence the degradation behaviour. The decrease in intrinsic viscosity with degradation time was confirmed by a decrease in molecular weight (M_n) in time. The M_n , as determined by end-group analysis, decreased from ~ 33 to ~ 18 kg.mol⁻¹ and from ~ 26 to ~ 11 kg.mol⁻¹ for PEA2,5-25 and PEA2,5-50, respectively. The hard segment content of PEA2,5-25 increased from 25.1 to 26.6% in time, which suggests that degradation takes place preferentially through ester bond cleavage. A similar trend is observed for PEA2,5-50 with a hard segment content increasing from 52.7 to 54.0% in time. These data reflect the characteristics of bulk degradation of polymers, a gradual decrease in molecular weight and almost no mass loss¹⁶⁻¹⁸. Due to ester bond cleavage mainly or exclusively taken place in the amorphous regions, additional crystallization can take place due to an increasing flexibility of the chain segments. To investigate if this also occurs in semi-

crystalline poly(ester amide)s the thermal properties of the polymers before and after hydrolytic degradation were examined. Before degradation, compression-moulded samples of PEA2,5-25 exhibit two melting temperatures, at 73 and 103 °C with a melt enthalpy of 18 and 8 J.g⁻¹, respectively. Exposure of PEA2,5-25 to PBS (pH 7.4) at 37 °C for 1 month caused the two melt endotherms to merge at a temperature of 90 °C with a melt enthalpy of ~ 25 J.g⁻¹. The melting temperature of PEA2,5-25 remained at 90 °C after 6 months of degradation but the melt enthalpy increased to ~40 J.g⁻¹. Thus additional crystallization appears to have occurred. At day 0, PEA2,5-50 has a melt endotherm at 78 and 144 °C with melt enthalpies of 15 and 28 J.g⁻¹, respectively. When PEA2,5-50 was exposed to PBS (pH 7.4) at 37 °C for 1 month the two melt endotherms merged to a bimodal endotherm, with peak maxima at 100 and 138 °C, and a melt enthalpy of 41 J.g⁻¹. After 6 months of degradation the peak positions of PEA2,5-50 remained unchanged but the melt enthalpy increased to ~ 50 J.g⁻¹. Thus additional crystallization was also observed for PEA2,5-50.

Cytotoxicity

The cytotoxicity of the poly(ester amide)s was assessed by studying the effects of extracts of the different polymers on the metabolic activity of fibroblasts *in vitro*. This convenient assay is based on the ability of pyridine nucleotides, generated in viable cells by numerous dehydrogenases, to reduce the tetrazolium salts such as WST-1 to the intensely coloured formazan, which can be measured spectrophotometrically¹⁹⁻²¹. It is assumed that only viable cells produce pyridine nucleotides and thus convert the tetrazolium salt into formazan. According to EN 30993 a cell activity above 70% with respect to the control DMEM (100% ± 22.5) indicates that the polymer does not release any cytotoxic compound. All poly(ester amide) extracts allowed a metabolic activity above 70%, except for the undiluted extracts of PEA2,5-50 (table 7.3). In that respect it can be concluded that the polymer extracts are non-cytotoxic.

Table 7.3: Cytotoxicity tests on PEA4,5 and PEA2,5 polymer extracts.

polymer code	metabolic activity (%)	
	Undiluted	Diluted 1:2 in DMEM
PEA4,5-25	104.6 ± 15.5	104.9 ± 15.1
PEA4,5-85	95.8 ± 22.3	102.8 ± 13.1
PEA2,5-25	81.2 ± 26.6	103.1 ± 25.3
PEA2,5-50	63.4 ± 7.0	83.3 ± 9.5

Cell adherence and proliferation

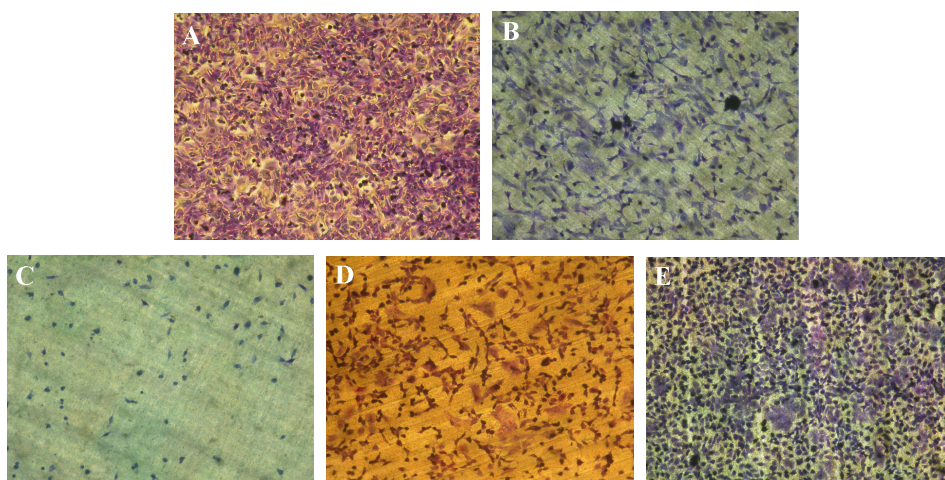


Figure 7.8: Micrographs of mouse fibroblasts grown for 3 days on TCPS (A), PEA4,5-25 (B), PEA4,5-85 (C), PEA2,5-25 (D) and PEA2,5-50 (E) films (100x magnification).

As shown in figure 7.8, cell densities on polymer films after 3 days of culture appear as follows: TCPS \approx PEA2,5-50 > PEA4,5-25 \approx PEA2,5-25 > PEA4,5-85. The morphology of the cells on PEA2,5-50 films was similar to that of the cells on the control surface TCPS, e.g. both films showed elongated as well as round cells. PEA4,5-25 and PEA2,5-25 films appear to have the same number of cells. However, cells grown on PEA4,5-25 films have a higher cell volume. Only some cells are present on PEA4,5-85 films indicating that hardly any cells adhere to this polymer film.

From the pictures in figure 7.8 it was shown that PEA2,5-25 and PEA2,5-50 films have the highest number of cells present after 72 h of cell culture. However, it is possible that

some cells are not viable and thus a quantitative analysis was also performed for the PEA2,5 polymers. The viability in terms of metabolic activity in cells was determined with a WST-1 kit, assuming that only cells with functional mitochondria show metabolic activity. The absorbance, measured by the reduction of the tetrazolium salt into the intensely coloured formazan, shows a linear relation with the cell density²¹⁻²³. At relatively high cell densities the absorbance is lower and the relation is not linear anymore. Providing that the cell density on the PEA films after 3 days of culture are within the linear part of the curve, the amount of formazan produced is directly proportional to the number of living cells (proliferation). The proliferation of fibroblasts grown on PEA2,5-50 films is $78.2 \pm 9.6\%$ with respect to $100 \pm 19.1\%$ for fibroblasts grown on TCPS. PEA2,5-25 films showed a cell proliferation of $61.9 \pm 16.8\%$, which is much lower compared to that of TCPS and which is probably caused by the higher hydrophobicity of the PEA2,5-25 film.

***In vivo* experiments**

To investigate the *in vivo* degradation and the tissue response of aliphatic poly(ester amide)s PEA4,5-50 and PEA2,5-50 discs were implanted subcutaneously in the back of rats. Explants at 5, 10 days and 6 wks were investigated for their degradation by changes in macroscopic appearance, mass, intrinsic viscosity, molecular weight and hard segment content while histology was performed to follow tissue reactions.

Degradation

At any day of explantation, all polymer samples were encapsulated with connective tissue. After removal of the capsule the PEA4,5-50 and PEA2,5-50 discs showed no changes in macroscopical appearance or dimensions at day 5 and 10 (fig. 7.9). The edges of the disks at day 42 appeared to be eroded.



Figure 7.9: Polymer PEA4,5-50 and PEA2,5-50 discs after subcutaneous implantation in rats and subsequent explantation at d0, d5, d10 and d42.

It must be noted that a different batch of PEA2,5-50 was used for this study as compared to the hydrolytic degradation study described previously. The initial intrinsic viscosity after compression moulding was $\sim 0.65 \text{ g.dl}^{-1}$ for both polymer batches.

The polymers PEA4,5-50 and PEA2,5-50 showed a small decrease in intrinsic viscosity after 6 wks of implantation (table 7.4). The hard segment content hardly changed and an initial mass loss was already detected at day 5. However, with increasing implantation time no further mass loss was detected. After 6 weeks of implantation the cumulative mass loss of PEA4,5-50 is $\sim 3 \%$ while PEA2,5-50 showed a cumulative mass loss of $\sim 5 \%$. The lower mass loss observed at longer implantation time is due to ingrowth of tissue, which is difficult to fully remove from the explants.

The *in vitro* degradation of PEA2,5-50 in PBS at 37°C for 6 wks was comparable to the *in vivo* degradation after 6 wks of implantation as measured by the intrinsic viscosities of both polymers (table 7.4). Therefore enzymatic degradation *in vivo* can be excluded.

Table 7.4: Composition, molecular weight, intrinsic viscosity and mass loss of PEA4,5-50 and PEA2,5-50 after 0, 5, 10 and 42 days of implantation and after 42 days of degradation in PBS.

day	x ^b (mol %)	[η] ^c (g.dl ⁻¹)	mass loss (%)
PEA4,5-50			
0	56.8	0.52	0
5	56.8	0.54	3.6 ± 0.3
10	56.8	0.47	3.5 ± 0.1
42	56.8	0.45	2.5 ± 0.2
42 ^a	56.5	0.42	1.2
PEA2,5-50			
0	52.0	0.65	0
5	52.5	0.64	5.7 ± 0.4
10	52.5	0.65	5.8 ± 0.1
42	52.5	0.6	4.3 ± 0.5
42 ^a	52.5	0.6	1.8

^a after hydrolytic degradation in PBS buffer (pH 7.4) at 37 °C, same polymer batch as *in vivo* study ^b according to ¹H-NMR, ^c CHCl₃/MeOH (1:1 vol/vol) at 25 °C

As observed from SEM pictures, the surface of the two polymer films became rougher after 42 days of implantation (fig. 7.10). Similarly, roughening was also observed for polymer films exposed to PBS (pH 7.4) at 37 °C for 42 days, indicating that the roughening of the surface is probably caused by hydrolytic degradation.

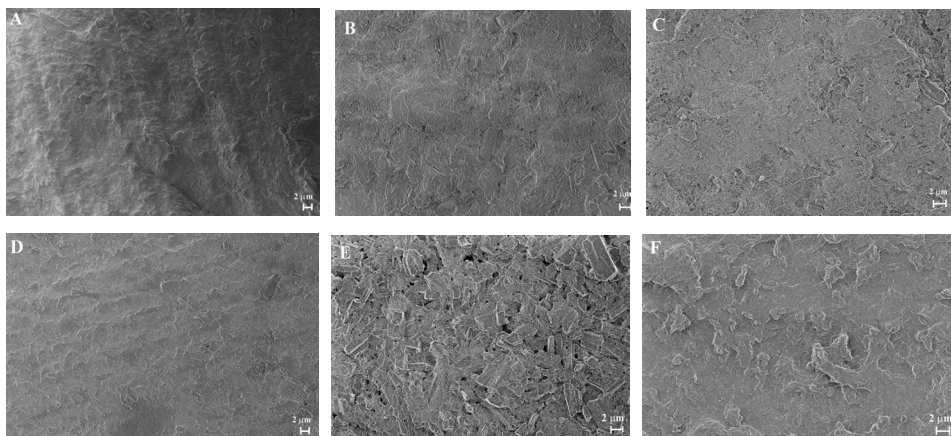


Figure 7.10: SEM pictures of the PEA4,5-50 surface after compression moulding (A), 42 days of degradation in PBS (B) 42 days of implantation (C) and of the PEA2,5-50 surface after compression moulding (D) 42 days of degradation in PBS (E) and 42 days of implantation (F) .

Both polymers show a melt endotherm at 70-80 °C and at ~137 °C. Exposure of these polymers to PBS (pH 7.4) at 37 °C for 6 wks caused the low melt endotherm to merge with the high melt endotherm at a temperature of 137 °C which is probably due to crystal reorganization. The melt enthalpy of this higher melting transition increased to 50-60 J.g⁻¹ (table 7.5). After implantation of PEA4,5-50 and PEA2,5-50 for 5, 10 and 42 days similar results were obtained.

Table 7.5: Thermal properties of PEA4,5-50 and PEA2,5-50 after implantation.

time (days)	PEA4,5-50				PEA2,5-50			
	T _{m,1} (°C)	ΔH _{m,1} (J.g ⁻¹)	T _{m,2} (°C)	ΔH _{m,2} (J.g ⁻¹)	T _{m,1} (°C)	ΔH _{m,1} (J.g ⁻¹)	T _{m,2} (°C)	ΔH _{m,2} (J.g ⁻¹)
0	84	23	137	29	73	19	136	29
5	-	-	139	61	-	-	133	59
10	-	-	139	67	-	-	134	62
42	-	-	138	61	-	-	142	57
42 ^a	-	-	138	53	-	-	136	60

^a after hydrolytic degradation in PBS buffer at 37 °C, same polymer batch as in vivo study.

Histology

Table 7.6 gives an overview of the nature and extent of the observed tissue reactions during subcutaneous implantation of PEA4,5-50 and PEA2,5-50. Both polymers showed good tissue tolerance after subcutaneous implantation. In accordance with the cytotoxicity tests and the cell growth experiments, the polymers did not cause any toxic, i.e. no granulocytes, hardly lymphocytes, or adverse reactions. The tissue response upon implantation was a mild foreign body reaction characterized by the presence of macrophages and foreign body giant cells and granulation tissue, which consisted of fibroblasts and newly formed blood vessels. Granulocytes (PMN), which may play a role in the early stages of the acute inflammatory response, were not detected at any time point. Lymphocytes were only sporadically detected. As a result of the foreign body response, encapsulation of the implants was observed. Both polymers showed no phagocytosed polymer particles at the interface or surrounding tissue.

Table 7.6: Tissue response to PEA4,5-50 and PEA2,5-50

polymer	Interface				Surroundings		
	fibrin	MØ	GC	fibro	MØ	lymp	vasc
PEA4,5-50							
d5	±	+	+ ±	+	±	sp	+
d10	±	+	sp	+ ±	+ ±	sp	+ ±
d42	-	sp	-	++ ±	sp	-	+
PEA2,5-50							
d5	++ ±	+	sp	+	++	sp	+ ±
d10	+ ±	++	+	+	+	±	++
d42	-	sp	±	++	±	sp	+ ±

MØ = macrophages, GC = giant cells, fibro = fibroblasts, lymp = lymphocytes, vasc = vascularization, scoring system: - = no infiltration, sp to +++ = sporadic to relatively high infiltration.

PEA4,5-50

At day 5 (fig. 7.11A) the tissue reaction of PEA4,5-50 at the biomaterial interface was mainly dominated by the presence of macrophages and giant cells. Fibrin and fibroblasts were present at the interface but not excessively. In the surrounding tissue of the biomaterial some vascularization was observed. A small amount of macrophages was present in between blood vessels but lymphocytes were only sporadically observed.

Ten days after implantation (fig. 7.11C) the amount of fibrin and macrophages present at the polymer interface was similar to that observed after 5 days but the number of giant cells had diminished. In the surroundings the number of macrophages had clearly increased and vascularization had proceeded. Also more fibroblasts were present but lymphocytes were again only occasionally observed.

At day 42 (fig. 7.11E) a fibrous capsule (15 cell layers) was present around the polymer. Fibrin and giant cells were no longer present at the polymer interface while macrophages were sporadically detected. In the surrounding tissue, macrophages were also observed sporadically and the number of blood vessels clearly diminished.

PEA2,5-50

At day 5 (fig. 7.11B) the tissue reaction of PEA2,5-50 at the polymer interface was also characterized by the presence of fibrin and macrophages. Compared to PEA4,5-50 the amount of fibrin was significantly higher. Giant cells were only detected occasionally. In the surroundings macrophages and vascularization were clearly present and both much more pronounced as compared to PEA4,5-50. Lymphocytes were only detected sporadically.

At day 10 (fig. 7.11D), higher numbers of macrophages and giant cells were present at the polymer interface. Compared to PEA4,5-50 both numbers were higher. In the surroundings no or hardly any macrophages were present. The number of macrophages were higher compared to PEA4,5-50. Vascularization had increased and in between these vessels more lymphocytes were observed. Compared to PEA4,5-50, vascularization was more pronounced and the vessels were located further from the interface.

At day 42 (fig. 7.11F) a fibrous capsule of 15 cell layers, comparable to PEA4,5-50, was present around the polymer. Fibrin was no longer observed and macrophages or giant cells were detected only sporadically. In the surrounding tissue macrophages and

lymphocytes were observed occasionally and the presence of blood vessels had diminished. Compared to PEA4,5-50 vascularization remains higher at any time point. At all time points PEA2,5-50 showed the highest activity in terms of fibrin, macrophages, giant cell, lymphocytes and vascularization as compared to PEA4,5-50.

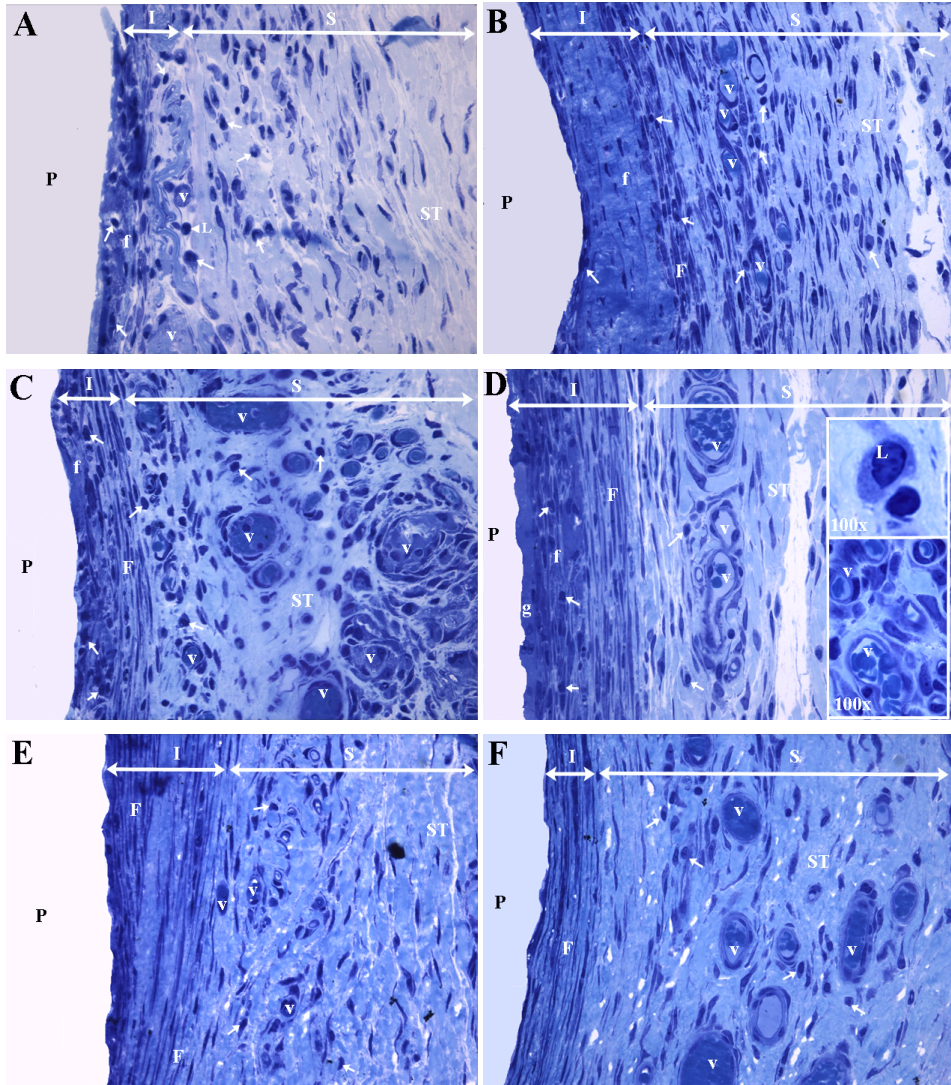


Figure 7.11: Light micrographs (400x) of PEA4,5-50 (A) after 5 days, (C) 10 days and (E) 6 wks of implantation and of PEA25-50 (B) after 5 days, (D) 10 days and (F) 6 wks of implantation. (I) interface, (S) surrounding, (P) polymer, (ST) surrounding tissue, (f) fibrine, (F) fibroblasts, (→) macrophages, (v) blood vessels and (L) lymphocytes.

It can be concluded that the poly(ester amide)s with 50 mol% of amide content appear non-cytotoxic and sustain cell growth of fibroblasts onto polymer films. In future studies, the cell behaviour of different types of cells on poly(ester amide) films should be studied at different time intervals. Upon implantation, these polymers did not cause any toxic or adverse reactions. As the *in vitro* as well as *in vivo* degradation of the aliphatic poly(ester amide)s is very slow, these polymers are applicable as long-term biodegradable implants. However, an *in vivo* study for at least 2 years should then be performed to study the long-term degradation and tissue response of these polymers during degradation.

Conclusions

Aliphatic poly(ester amide)s were evaluated with respect to their mechanical properties, cytotoxicity, adhesion and growth of fibroblasts, *in vitro* and *in vivo* degradation and tissue response to study their applicability in the biomedical field. The thermal and mechanical properties of these segmented poly(ester amide)s, comprising a crystallizable amide phase and a flexible amorphous ester phase, can readily be tuned by changing the amide content. The degradation of the aliphatic poly(ester amide)s in PBS (pH 7.4) at 37 °C is very slow and takes place preferentially through ester bond cleavage. The polymers with 25 and 50 mol% of amide content are non-cytotoxic and sustain growth of fibroblasts onto polymer films. The *in vivo* degradation and the tissue response of aliphatic poly(ester amide)s with 50 mol% of amide content were studied by subcutaneous implantation in rats. Upon implantation the polymers show a mild foreign body reaction in the first week characterized by the presence of macrophages and sporadically a lymphocyte. The *in vivo* degradation of these polymers, followed over a time period of 6 wks, is slow which make them suitable as long-term biodegradable implants. A long-term *in vivo* degradation study is recommended.

Acknowledgement

The authors would like to thank Mark Smithers (University of Twente) for the scanning electron microscopy. This study was financially supported by the European Commission, project: QLK5-1999-01298.

References

1. Y.H. An, S.K. Woolf, J. Friedman, *Biomaterials*, **2000**, 21, 2635.
2. J.E. Bergsma, W.C. de Bruijn, F.R. Rozema, R.R.M. Bos, G. Boering, *Biomaterials*, **1995**, 16, 25.
3. F.R. Rozema, W.C. de Bruijn, R.R.M. Bos, G. Boering, A.J. Nijenhuis, A.J. Pennings, Late tissue response to bone-plates and screws of poly(L-lactide) used for fracture fixation of the zygomatic bone., in *Biomaterials-tissue interfaces*, P.J. Doherty, *et al.*, Editors. **1991**, Elsevier. p. 349.
4. K.A. Hooper, N.D. Macon, J. Kohn, *J. Biomed. Mater. Res*, **1998**, 41, 443.
5. P.A.M. Lips, chapter 4, in *this thesis*. **2004**.
6. P.A.M. Lips, chapter 5, in *this thesis*. **2004**.
7. H.R. Stapert, **1998**, University of Twente, The Netherlands: p. 259.
8. T.H. Barrows, **1986**, *The design and synthesis of bioabsorbable poly(ester-amides)*, Plenum, New York.
9. V.L. Horton, P.E. Blegen, T.H. Barrows, R.L. McQuin, **1988**, *Progress Biomed. Polym.*, Los Angeles.
10. S. Bera, Z. Jedlinski, *Polymer*, **1993**, 34, (16), 3545.
11. A.A. Deschamps, A.A. van Apeldoorn, J.D. de Bruijn, D.W. Grijpma, J. Feijen, *Biomaterials*, **2003**, 24, (15), 2643.
12. J.M. Schakenraad, H.J. Busscher, C.R.H. Wildevuur, J. Arends, *J. Biomed. Mater. Res.*, **1986**, 20, 773.
13. Y. Ito, M. Kajihara, Y. Imanishi, *J. Biomed. Mater. Res.*, **1991**, 25, 1325.
14. P.B. van Wachem, T. Beugeling, J. Feijen, A. Bantjes, J.P. Detmers, W.G. van Aken, *Biomaterials*, **1986**, 6, 403.
15. J.H. Lee, G. Khang, J.W. Lee, H.B. Lee, *J. Coll. Interf. Sci.*, **1998**, 205, 323.
16. P.J.A. in 't Veld, **1992**, University of Twente, The Netherlands: p. chapter 7.
17. A.P. Pego, A.A. Poot, D.W. Grijpma, J. Feijen, *Macromol. Biosci.*, **2002**, 2, (9), 411.
18. A.A. Deschamps, A.A. van Apeldoorn, H. Hayen, J.D. de Bruijn, U. Karst, D.W. Grijpma, J. Feijen, *Biomaterials*, **2002**, 25, (2), 247.
19. M. Ishiyama, Y. Miyazono, K. Sasamoto, Y. Ohkura, K. Ueno, *Talanta*, **1997**, 44, 1299.

20. Y. Mackewa, Y. Kyouko, A. Nonomura, R. Kuraoku, E. Nishiura, E. Uchibori, K. Takeuchi, *Thrombosis. Res.*, **2003**, 109, 307.
21. M. Ishiyama, H. Tominaga, M. Shiga, K. Sasamoto, Y. Ohkura, K. Ueno, M. Watanebe, *In vitro toxicology*, **1995**, 8, (2), 187.
22. M. Ishiyama, H. Tominaga, M. Shiga, K. Sasamoto, Y. Ohkura, K. Ueno, *Biol. Pharm. Bull.*, **1996**, 19, (11), 1518.
23. A.M. Sieuwerts, J.G.M. Klijn, H.A. Peters, J.A. Foekens, *Eur. J. Clin. Chem. Clin. Biochem.*, **1995**, 33, 813.

Chapter 8

Gas foaming of segmented poly(ester amide) films

P.A.M. Lips¹, I.W. Velthoen¹, P.J. Dijkstra¹, M. Wessling², J. Feijen¹

¹ *Institute for Biomedical Technology (BMTI) and Department of Polymer Chemistry and Biomaterials, Faculty of Science and Technology, University of Twente, P.O. Box 217, 7500 AE Enschede, The Netherlands.*

² *Membrane Technology Group, Faculty of Science and Technology, University of Twente, P.O. Box 217, 7500 AE Enschede, The Netherlands.*

Abstract

Biodegradable segmented poly(ester amide)s, based on dimethyl adipate, 1,4-butanediol and N,N'-1,2-ethanediyl-bis[6-hydroxy-hexanamide], with two distinct melting transitions were gas foamed using carbon dioxide (CO₂). Polymer films were saturated with CO₂ at 50 bar for 6 h after which the pressure was released. The samples were immersed in octane at the desired temperature after which foaming started immediately. Just above the lower melt transition the polymers retain adequate mechanical properties and dimensional stability, while the chain mobility increased sufficiently to nucleate and expand gas cells during the foaming process. In this way semi-crystalline poly(ester amide)s can be gas foamed below the flow temperature.

Two poly(ester amide)s with 25 mol% (PEA2,5-25) and 50 mol% (PEA2,5-50) of bisamide segment content were foamed at 70 and 105 °C, respectively. The storage modulus (G') of both pure polymers at the onset foaming temperature is 50–60 MPa. Closed-cell foams were obtained with a maximum porosity of ~90%. The average pore size of PEA2,5-25 ranges from 77-99 µm. In contrast, the average pore size of PEA2,5-50 is in between 2-4 µm and can be increased to 100 µm by lowering the CO₂ saturation

pressure to 20 bar. The porosity of PEA2,5-50 foams using this saturation pressure decreased to 70%.

Introduction

Polyurethane (PU), polystyrene (PS) and polyvinyl chloride (PVC) are materials traditionally applied for the manufacturing of polymer foams. PU foams are prepared by in-situ generation of carbon dioxide (CO₂) while PS and PVC foams are prepared using physical blowing agents like nitrogen (N₂) and CO₂. The concept of foaming using physical blowing agents is very promising because of the lack of contaminating solvents. The use of CO₂ has a number of advantages including chemical inertness, non-combustibility, natural occurrence, low cost, ready availability, environmental acceptability (no ozone depletion) and low human toxicity. Foaming of polymers with a physical blowing agent usually results in closed-cell foams, which are generally rigid and are most suitable for thermal insulation and buoyancy.

All polymer foaming techniques using physical blowing agents rely on the same principle: (1) saturation of the polymer with a gaseous penetrant (blowing agent) at high pressure, (2) quenching of the polymer/gas mixture into a super-saturated stage either by reduced pressure or increased temperature, and (3) nucleation and growth of gas cells dispersed throughout the polymer matrix. Upon quenching of the polymer/gas mixture the solubility of the gas in the polymer decreases, which results in clustering of gas molecules in the form of nuclei. As the gas diffuses into the forming cells, the free energy of the system is lowered. The cell nucleation process is very important as it governs the cell morphology of the material and to a large extent, the properties of the material. This process can occur homogeneously throughout the material or heterogeneously at high-energy regions such as phase boundaries. In such regions the free energy necessary to nucleate a stable void is less compared to homogeneous nucleation, resulting in preferential nucleation of voids at the interface. In semi-crystalline polymers the crystalline domains may serve as heterogeneous nucleation points to generate gas bubbles ¹⁻⁷. In general, cell growth is controlled by the time allowed for the gas to diffuse into the cells before quenching, the temperature of the system, the degree of supersaturation, the rate of gas diffusion into the cells, the hydrostatic pressure or stress applied to the polymer matrix, the interfacial energy and

the visco-elastic properties of the polymer/gas mixture ³⁻⁵. The stiffness of the polymer is typically controlled by the foaming temperature and a reduction in average cell size is observed at increasing stiffness ³. The work necessary to expand the gas cell must overcome the additional stress resulting from the increased stiffness. By increasing the saturation pressure the free energy barrier for the formation of stable nuclei is decreased and additional nucleation sites are formed due to matrix swelling, free volume changes, and/or the formation of crystalline interfaces. This results in an increased cell density and consequently a decreased average cell diameter ^{3, 4, 6, 8}.

It is generally accepted that the sorption of gases by semi-crystalline polymers occurs exclusively in the amorphous regions ⁹. The crystalline regions act as impermeable barriers due to the tight packing of the polymer chains. Many polymers do show a substantial sorption (solubility) of gas, which leads to a dramatic decrease in glass transition temperature (T_g) of these materials (plasticization), even at modest pressures ¹⁰. Sorption of CO₂ can induce crystallization in polymers and occurs when the rate of polymer chain-segment motions makes crystallization kinetically feasible through the realignment of the chains ^{3, 11, 12}. This process may even lead to an increase in melting enthalpy and temperature of polymers upon saturation with CO₂. This phenomenon has been observed for polyethylene terephthalate (PET) where the crystallinity increases when saturated with CO₂ at high pressures ³. In addition, the crystallization of the polymer results in a lower solubility of CO₂, an increased matrix stiffness and a lower diffusivity.

In recent years, micro-cellular foams using CO₂ have been prepared from amorphous as well as semi-crystalline polymers ^{1-6, 8, 13-17}. A micro-cellular foam has closed-cells with an average cell sizes smaller than 10 microns and can be applied in food packaging, construction and as insulation materials ¹⁸. Micro cellular processing follows the same foam formation mechanism as conventional prepared foams using a physical blowing agent. Semi-crystalline polymers like polypropylene (PP) ^{2, 19, 20}, PET ²⁻⁵, high-density polyethylene (HDPE) ² and polybutylene (PB) ² have been processed into micro-cellular foams below their melting temperature. Semi-crystalline polymers exhibited considerably higher cell densities than amorphous polymers, which is attributed to a significant contribution of heterogeneous nucleation at the amorphous/crystalline interfacial regions. Since the gas does not dissolve in crystallites, the nucleation is non-

homogeneous which makes it difficult to control the cellular structure of semi-crystalline foams. Polymers with a low crystallinity afforded foams with an almost uniform structure. When the crystallinity was increased, non-uniform foams with irregular cell sizes were obtained. No foaming was observed for highly crystalline polymers²⁻⁵. Micro-cellular foaming of high T_g semi-crystalline polymers like polysulfone (PSU), poly(ether sulfone) (PES), and cyclic olefin copolymer (COC) films has been studied by Krause^{6, 15}. Closed-cell foams were prepared with a maximum porosity of 60% and an average pore size of 1-5 μm . The polymer was saturated with CO_2 at a temperature below the T_g of the pure polymer and the foaming process was initiated by rapidly increasing the temperature above the T_g of the mixture. Foaming does not occur by release of the pressure at a temperature below the T_g , because nucleation and growth of gas cells is inhibited by the rigidity of the glassy structure. However, during the time required for heating the sample, gas will desorb from the surface of the polymer sample, which leads to a reduced gas concentration near the polymer surfaces. Therefore, the foams always show dense (unfoamed) surface layers and foamed cores^{6, 13, 21}.

Foaming using physical blowing agents is thus a versatile technique to prepare closed-cell polymer foams. Amorphous as well as semi-crystalline polymers can be processed at a range of temperatures close to T_g up to temperatures just below the melting of the material.

Previous research showed that the incorporation of symmetrical bisamide-diol monomers into the backbone of biodegradable polyesters enhanced the thermal and mechanical properties of these materials²²⁻³². These poly(ester amide)s have a micro-phase separated structure with an amide-rich hard phase and an ester-rich flexible soft phase. Depending on the amount of hard segment incorporated these aliphatic poly(ester amide)s have, besides a T_g below room temperature, a lower melt transition in between 50 and 80 $^{\circ}\text{C}$ and a higher melt transition which increased with increasing hard segment content up to 140 $^{\circ}\text{C}$. These materials are biodegradable, have thermal, physical and mechanical properties that can be tuned and have potential in foam applications. In this paper the preparation of closed-cell poly(ester amide) foams well below the highest melting temperature is described⁶. The porosity and pore size of the foams were determined as a function of foaming temperature and CO_2 saturation pressure. The

relation between the thermal and mechanical properties and the foam morphology of these materials will be discussed.

Experimental

Materials

n-Octane was obtained from Merck (Darmstadt, Germany). All other solvents were obtained from Biosolve, the Netherlands. Carbon dioxide was obtained from Hoekloos (Schiedam, the Netherlands).

Polymer synthesis

A two-step polycondensation of dimethyl adipate, 1,4-butanediol and N,N'-1,2-ethanediyl-bis[6-hydroxy-hexanamide] was performed in the presence of tetrabutyl(orthotitanate) as a catalyst, as described previously³³. The molar ratio of hard (x) and soft (y) segments of the poly(ester amide) (fig. 8.1) can be varied by changing the ratio of N,N'-1,2-ethanediyl-bis[6-hydroxy-hexanamide] and 1,4-butanediol. The polymers PEA2,5-25 and PEA2,5-50 with a hard segment content x of 25 and 50 mol%, respectively, were used to prepare foams.

Methods

The intrinsic viscosity of polymer samples was determined by a single point measurement with a capillary Ubbelohde type 0C at 25 °C, using a polymer solution with a concentration of 0.1 g.dl⁻¹ in chloroform-methanol (1:1 vol/vol).

Polymer films were prepared by compression moulding using a hot press (THB 008, Fontijne Holland BV, the Netherlands). Polymers were heated for 6-8 min at 20 °C above their melting temperature, pressed for 3 min at 300 kN, and cooled in approximately 5 min under pressure to room temperature.

Thermal analysis of the polymers was carried out using a Perkin-Elmer DSC-7 Differential Scanning Calorimeter equipped with a PE7700 computer and TAS-7 software. Calibration was performed with pure indium. Measurements were performed on samples of dried polymer films after compression moulding, after CO₂ sorption (and subsequent desorption) and after gas foaming. The samples (5-10 mg) were heated from -20 °C to 180 °C at a rate of 20 °C.min⁻¹, annealed for 5 min, cooled to -80 °C at a rate

of $20\text{ }^{\circ}\text{C}\cdot\text{min}^{-1}$, and subsequently heated from $-80\text{ }^{\circ}\text{C}$ to $180\text{ }^{\circ}\text{C}$ at a rate of $20\text{ }^{\circ}\text{C}\cdot\text{min}^{-1}$. Melting (T_m) and crystallization (T_c) temperatures were obtained from the peak maxima, melt (ΔH_m) and crystallization enthalpy (ΔH_c) were obtained from the area under the curve and the glass transition temperature (T_g) was taken at the inflection point. The data presented are from the second heating step, unless stated otherwise.

Differential mechanical analysis was performed with a Myrenne ATM3 torsion pendulum at a frequency of approximately 1 Hz. The storage modulus (G') and the loss modulus (G'') were measured as a function of temperature. Samples ($75\times 4\times 2\text{ mm}$) were first cooled to $-100\text{ }^{\circ}\text{C}$ and then heated at a rate of $1\text{ }^{\circ}\text{C}\cdot\text{min}^{-1}$. The temperature at which the loss modulus reached a maximum was taken as the T_g . The flow temperature (T_{flow}) was defined as the temperature at which the storage modulus reached 1 MPa.

The solubility of CO_2 in polymer films ($10\times 4\times 0.4\text{ mm}$), at $25\text{ }^{\circ}\text{C}$, as a function of CO_2 pressure (5-50 bar) was determined using a Rubotherm magnetic suspension balance operated by MessPro software. This balance has an accuracy of $1\text{ }\mu\text{g}$. The samples were first exposed to a pressure lower than 1.10^{-4} bar, before subjecting the sample to CO_2 at the elevated pressure. The measurement was completed after a sorption plateau (constant value of the sample mass) was reached (6-8 h). The data obtained were corrected for buoyancy effects, because of the increased gas density at higher pressures.

Preparation of porous structures by gas foaming

Compression moulded films ($20\times 20\times 0.5\text{ mm}$) of PEA2,5-25 or PEA2,5-50 were placed in a pressure vessel connected to a CO_2 cylinder. The samples were saturated for 6 h with CO_2 at room temperature and 50 bar. Subsequently, the pressure was quickly released and the polymer films were immersed into an octane bath, maintained at a desired temperature ($40\text{--}120\text{ }^{\circ}\text{C}$). When visually no more gas escaped, the samples were removed from the octane bath and dried. Typical exposure times were $\sim 1\text{ min}$.

PEA2,5-50 foams were also prepared using different CO_2 saturation pressures (20 to 50 bar) applying the same procedure as mentioned above. Samples were subsequently immersed in an octane bath at a temperature of $105\text{ }^{\circ}\text{C}$.

Experiments were carried out in duplo.

Methods

The porosity of the gas foamed samples was determined by the flotation weight loss method, based on the Archimedes principle (ASTM D-792). The mass of a sample in air and in hexane was determined. With the known density of hexane (0.6637 g.ml⁻¹) at 20 °C, the density of the sample (polymer film or foam) can be calculated according to the following equation:

$$\rho_{sample} = \frac{m}{\left(\frac{m - m_{hexane}}{\rho_{hexane}} \right)} \quad (\text{eq. 8.1})$$

in which m is the mass of the dry sample in air, m_{hexane} the mass of the sample immersed in hexane and ρ_{hexane} the density of hexane. The porosity p was calculated from equation 8.2:

$$p = \left(1 - \frac{\rho_{foam}}{\rho_{unfoamed}} \right) \quad (\text{eq. 8.2})$$

Scanning Electron Microscopy (SEM) was carried out with a LEO Gemini 1550 field emission microscope at a voltage of 2 kV. Freeze fractured samples of the porous structures were sputter-coated with gold before analysis. The average pore size and the pore size distribution were obtained by measuring the size of at least 100 pores at the cross section of the fractured foam sample.

Microcomputed tomography (μ -CT) analysis was carried out using a desktop Micro-CT 40, (Scanco Medical, Bassersdorf, Switzerland) at a resolution of 6 μ m in all three spatial dimensions to provide three-dimensional reconstructions of the foam. For PEA2,5-25 foams (0.8x10x10 mm), 180 slices were scanned with 1024x1024 pixels per slice. For evaluation, volumes of interest slightly smaller than the diameter of the sample were chosen to exclude crushed boundaries. The resulting gray-scale images were improved by using a low-pass filter to remove noise, and segmented with a fixed threshold to extract the polymer phase. For the 3D evaluation of the structure of the samples, ‘direct’ three-dimensional techniques without model-assumptions for the appearance of the structure were used. Pore voxels can be defined as voxels corresponding to the void space and polymer voxels as voxels corresponding to the polymer phase. The porosity can be calculated from the number of polymer voxels and

the total number of voxels. To determine the pore sizes, pores are completely filled with modelled spheres of different diameters. The pore diameter assigned to a pore voxel is then the diameter of the largest sphere (still containing that pore voxel) that fits inside the pore ³⁴. In the case of non-spherical cubic pores, this method underestimates the pore size assigned to pore voxels present in the corners of these pores. Therefore the algorithm was modified to assign the diameter of the largest sphere fitting in the pore to all pore voxels within that pore ³⁵. The average pore size was calculated by averaging the product of pore voxels with their assigned pore diameters over the total amount of pore voxels, according to equation 8.3:

$$\text{average pore size} = \frac{\sum_i (\text{pore voxel}_i \times \text{pore size}_i)}{\sum_i \text{pore voxel}_i} \quad (\text{eq. 8.3})$$

Results and Discussion

The synthesis and properties of segmented poly(ester amide)s (fig. 8.1) with a hard segment content x of 25 mol% (PEA2,5-25) and 50% (PEA2,5-50), used for the preparation of foams have previously been described ³³. These aliphatic copolymers show structural organisation through hydrogen bonding by incorporation of symmetrical rigid amide segments. The induced phase separation between the different chemical blocks leads to polymers with a glass transition temperature (T_g) below room temperature and a melting temperature (T_m) dependent on the hard segment content. The thermal and dynamic mechanical properties of these block copolymers are summarized in table 8.1.

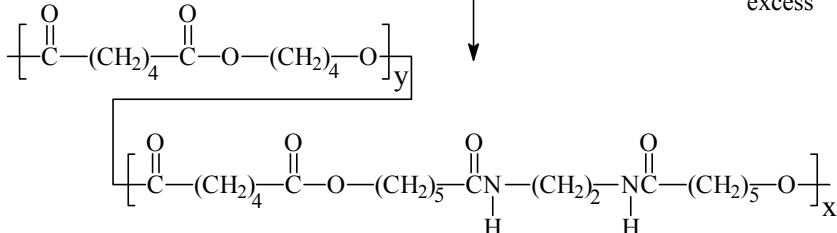


Figure 8.1: Synthesis of segmented poly(ester amide)s (PEA2,5) with different hard segment content x .

*Table 8.1: Thermal and physical properties of PEA2,5-25 and PEA2,5-50*³³.

polymer code	$[\eta]^a$ (dl.g ⁻¹)	T _g ^b (°C)	T _{m,1} ^c (°C)	$\Delta H_{m,1}^c$ (J.g ⁻¹)	T _{m,2} ^c (°C)	$\Delta H_{m,2}^c$ (J.g ⁻¹)	T _n ^b (°C)	w _c ^d (%)
PEA2,5-25	0.73	-45	48-73 ^e	16	77-115 ^e	14	87	12.5 ± 2.5
PEA2,5-50	0.63	-25	52-80 ^e	7	136	26	130	27.5 ± 2.5

^a CHCl₃/MeOH (1:1 vol/vol) at 25 °C ^b from DMA ^c from DSC, 2nd heating scan^d crystallinity according to amide I band in FT-IR spectra ^e melting range

Sorption of CO₂ in poly(ester amide) films was measured at different CO₂ pressures (fig. 8.2). At all pressures PEA2,5-50 has a lower CO₂ sorption compared to PEA2,5-25, which is in line with the higher crystallinity of PEA2,5-50 (table 8.1). For PEA2,5-25 and PEA2,5-50 a linear relationship between the applied CO₂ pressure and CO₂ sorption is found. CO₂ sorption may induce crystallization in the poly(ester amide)s due to enhanced mobility of the polymer chains and reorganization into a more favourable state¹¹. DSC measurements revealed no change in melting temperature and enthalpy after CO₂ sorption and subsequent desorption of CO₂.

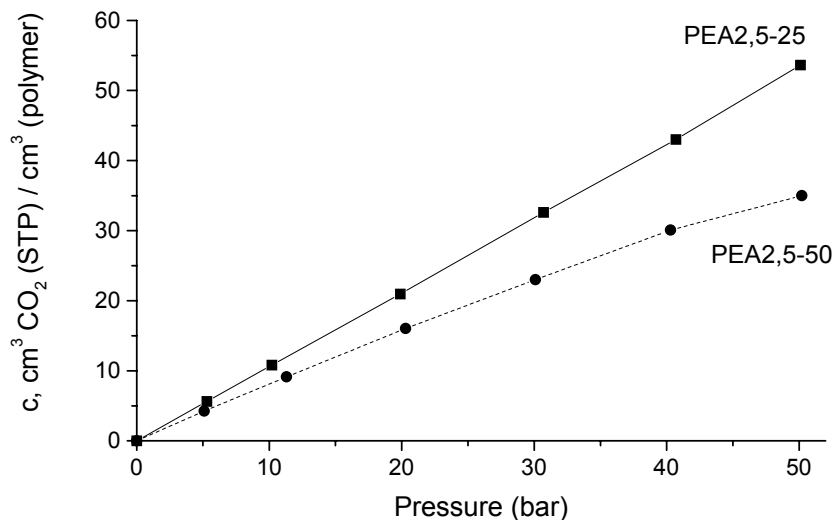


Figure 8.2: CO_2 sorption isotherm of PEA2,5-25 and PEA2,5-50 at 25 °C.

Foaming at different temperatures

Polymer films of PEA2,5-25 and PEA2,5-50 were saturated for 6 h with CO_2 at room temperature and 50 bar. This pressure was applied in the foaming experiments to give a maximal CO_2 sorption. When the pressure was released and the samples were immersed in an octane bath, kept at the appropriate temperature, foaming started immediately. The porosity (fig. 8.3) and average pore size of the foams (table 8.2) were determined as a function of foaming temperature (T_{foam}).

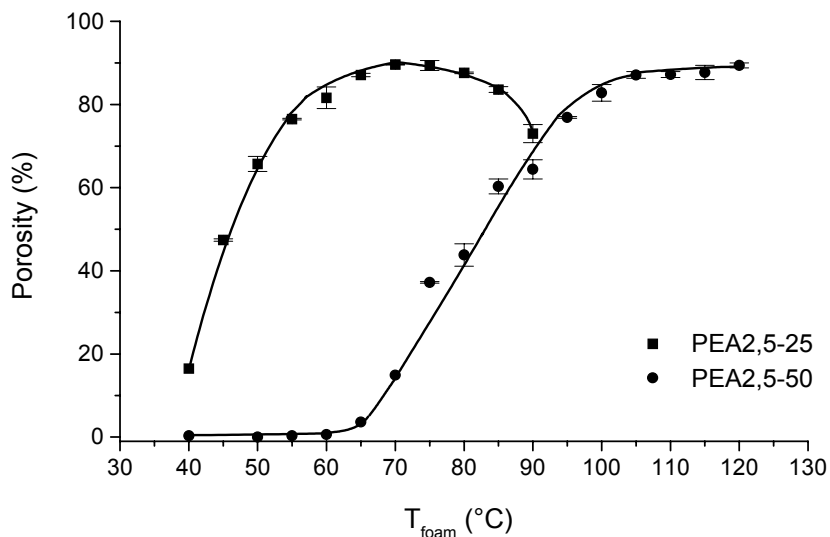


Figure 8.3: Porosity as a function of foaming temperature for PEA2,5-25 and PEA2,5-50. Polymer films (20x20x0.5 mm) were subjected to a pressure of 50 bar for 6 h at room temperature and subsequently immersed in an octane bath at different temperatures (T_{foam}).

Table 8.2: Porosity and average pore size of PEA2,5-25 and PEA2,5-50 foamed at different temperatures (T_{foam}).

polymer code	T_{foam} ($^{\circ}\text{C}$)	porosity (%)	average pore size (μm)
PEA2,5-25	60	81.6 ± 2.6	99 ± 42
	70	89.6 ± 0.1	77 ± 38
	75	89.4 ± 1.2	87 ± 44
PEA2,5-50	105	87.1 ± 0.8	2.4 ± 1.6
	110	87.2 ± 0.7	3.8 ± 2.5
	120	89.4 ± 0.6	4.3 ± 3.0

The porosity increases with increasing foaming temperature (fig. 8.3). A maximum porosity of ~90% is obtained for both PEA2,5-25 and PEA2,5-50, although at a different T_{foam} . The average pore size (table 8.2) and pore size distribution (fig. 8.4) of PEA2,5-25 and PEA2,5-50 foams were determined. Foams with a maximum porosity of ~90% and the smallest pore size distribution are obtained at 70 °C for PEA2,5-25 and at 105 °C for PEA2,5-50, respectively. The foams have closed cells and a thin dense skin.

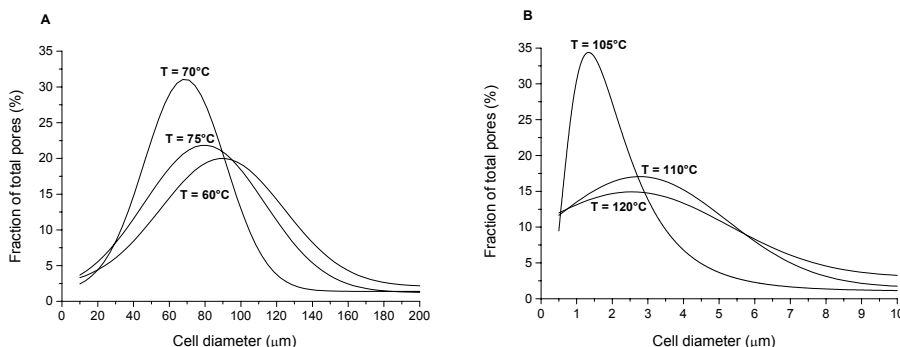


Figure 8.4: Pore size distribution of foamed PEA2,5-25 (A) and PEA2,5-50 (B) plotted with a gaussian fit ($T = 105^{\circ}\text{C}$ was plotted with a log normal fit). The foaming process was performed after saturation of the polymer film with CO_2 at 50 bar and subsequent immersion in an octane bath at various temperatures.

With micro computed tomography ($\mu\text{-CT}$) 3D images of PEA2,5-25 foamed at 70 °C were generated. Porosity and average pore size were calculated with an algorithm for cubic like pores although the pores are “honeycomb” shaped. The porosity and average pore size obtained are 87.1% and 89 μm , respectively. The porosity is comparable to that measured by the flotation weight loss method (89.6%) whereas the average pore size is higher compared to that measured with SEM ($77 \pm 38 \mu\text{m}$). Because the thickness of the cell walls is smaller than the resolution of the $\mu\text{-CT}$ scanner (6 μm), higher pore sizes are generally determined. The pore size distribution was also determined by $\mu\text{-CT}$ and corresponds with that obtained from SEM pictures (fig. 8.5). As the pores of the PEA2,5-50 foams were smaller than the resolution of the $\mu\text{-CT}$ scanner (6 μm), no data could be obtained.

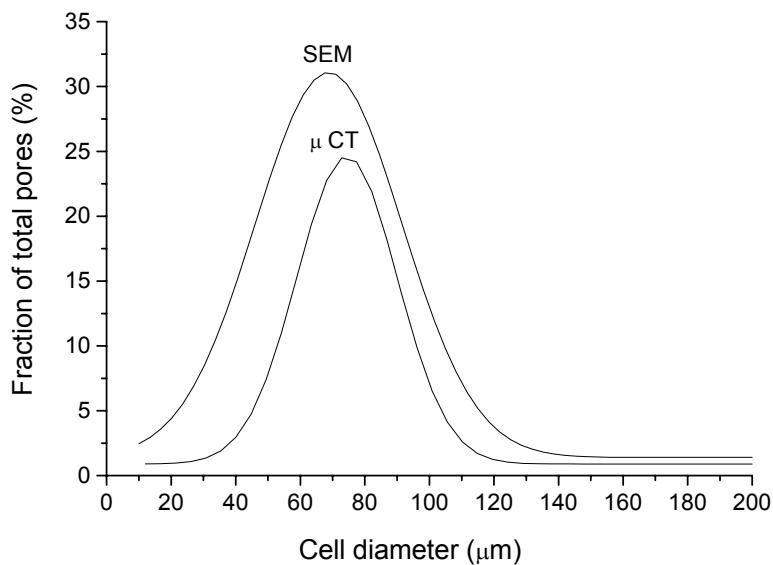


Figure 8.5: Pore size distribution of foamed PEA2,5-25 derived from μ -CT and SEM, plotted with a gaussian fit. The foaming process was performed after saturation of polymer films with CO_2 at 50 bar and subsequent immersion in an octane bath at 70 °C.

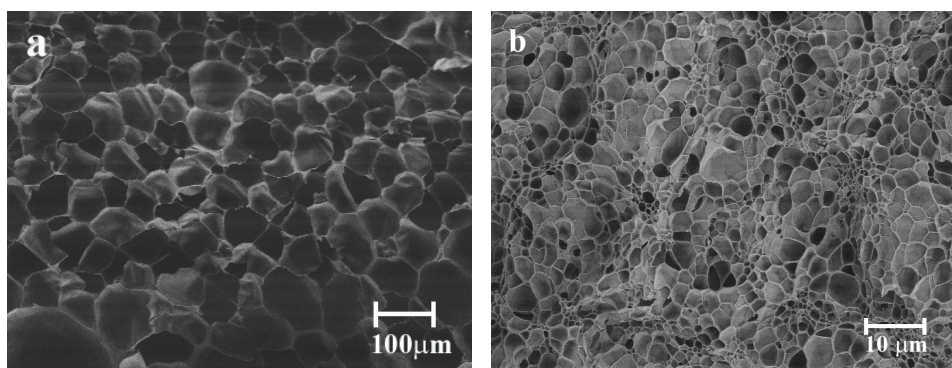


Figure 8.6: SEM images of PEA2,5-25, $T_{\text{foam}} = 70$ °C (a) and PEA2,5-50, $T_{\text{foam}} = 105$ °C (b).

The average pore size of PEA2,5-25 is significantly larger than that of PEA2,5-50 foams at a porosity of $\sim 90\%$ (table 8.2 and fig. 8.6). The crystalline domains in the CO_2 saturated polymers serve as heterogeneous nucleation agents to generate gas cells. These

crystalline domains are in direct contact with the amorphous polymer matrix saturated with CO₂, providing a large interfacial area for cell nucleation. Combined with a high nucleation rate this leads ultimately to a higher cell density¹⁻⁷. When a similar amount of gas is available, more cells will nucleate in the polymer matrix with the highest crystallinity (PEA2,5-50), leading to a reduction in average pore size. Furthermore, PEA2,5-50 has a higher modulus compared to PEA2,5-25 and thus will be more difficult to expand (during cell growth) which also reduces the average pore size³. Thus even though the CO₂ sorption for PEA2,5-50 is lower than for PEA2,5-25 at the same CO₂ pressure, the higher crystalline PEA2,5-50 affords foams with smaller pore sizes. The pore size of the foam can thus be tuned by the hard to soft segment ratio of the polymer using similar foaming conditions.

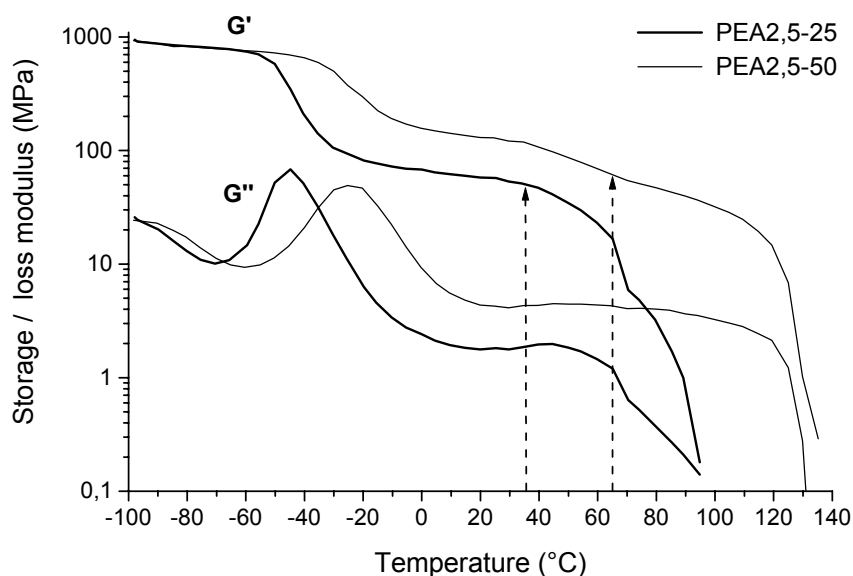


Figure 8.7: DMA plot with storage (G') and loss (G'') modulus as a function of temperature for PEA2,5-25 and PEA2,5-50. Dashed lines represent the onset temperature of foaming.

Foaming of the poly(ester amide), which is saturated with CO₂ above its T_g , did not start before the temperature reached a critical value of 35 °C for PEA2,5-25 and 65 °C for

PEA2,5-50 (fig 8.3). The driving force, which is the gas pressure gradient, below these temperatures is not high enough to overcome the attractive forces and entanglements of the polymer chains. The poly(ester amide)s show a lower melt transition ($T_{m,1}$) and a higher melt transition ($T_{m,2}$) (table 8.1) ³³. It is believed that at the lower transition crystals comprising single ester amide (EA) sequences melt while at the higher transition crystals composed of 2 or more EA sequences melt. Above the lower melt transition but below the $T_{m,2}$ the polymers will retain adequate mechanical properties and dimensional stability, while the chain mobility has increased sufficiently to nucleate and expand gas cells during the foaming process. These results show that foaming of poly(ester amide)s comprising two distinct melting temperatures can be carried out well below the flow temperature. Uncontrollable cell growth, which is caused by a dramatic decrease in viscosity upon melting of the polymer is hereby prevented ¹⁹.

DMA measurements (fig. 8.7) revealed a storage modulus (G') at room temperature for PEA2,5-50 of 129 MPa, which is twice as high as that for PEA2,5-25 (57 MPa). The DMA curves also reveal a transition in the rubber plateau of both poly(ester amide)s in a temperature range of 50-80 °C, similar to the $T_{m,1}$ determined with DSC (table 8.1). The onset temperatures for foaming of PEA2,5-25 (35 °C) and PEA2,5-50 (65 °C) are close to these transitions. In this temperature range the storage modulus is 50–60 MPa for both pure polymers and only when the G' is lower than this value foaming can take place. Note that the plasticizing nature of CO₂ results in a shift of the storage modulus curve of the pure polymer along the temperature axis representing a depression in T_g .

No foams were obtained when the gas-saturated PEA2,5-25 and PEA2,5-50 were immersed in the heating bath with a temperature of 90 and 120 °C, respectively. As this upper foaming temperature (T_{upper}) is reached, deformation of the polymer foams is observed which was confirmed with SEM. Most likely, cells can not grow to large sizes because CO₂ diffuses to the exterior under the strong plasticizing conditions caused by the onset of melting. The exact value of T_{upper} will depend on the melt viscosity and molecular weight of the polymer ⁶.

DSC measurements were performed on polymer films before and after foaming (fig. 8.8). The melt enthalpy of the lower melt transition ($T_{m,1}$) of PEA2,5-50 has decreased after foaming whereas the melt enthalpy of the higher melt transition ($T_{m,2}$) has

increased. However, the total melt enthalpy has not changed, indicating a reorganisation to a more stable crystal structure for PEA2,5-50. The $T_{m,1}$ of PEA2,5-25 has broadened after foaming but the total melt enthalpy has not changed which is similar to that observed for the PEA2,5-50.

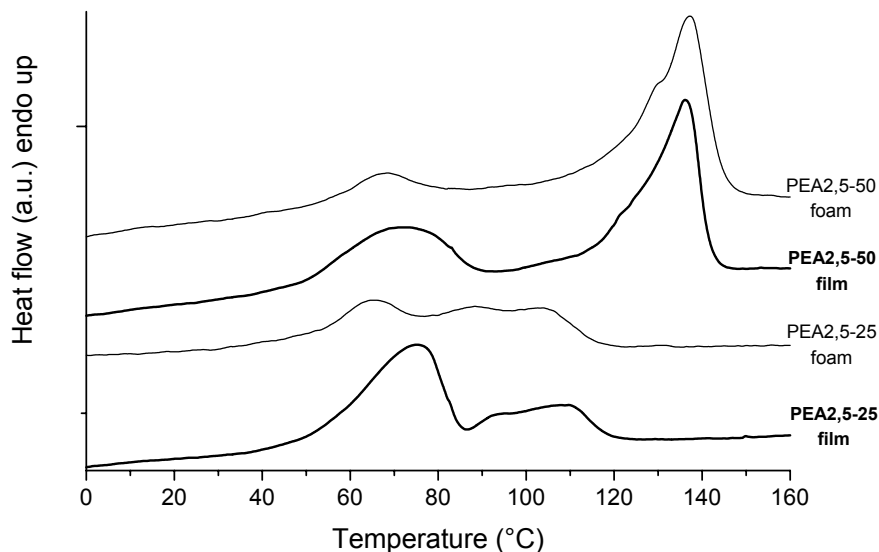


Figure 8.8: DSC curves (1st heating scan) of polymer films before and after foaming of PEA2,5-25 at T_{foam} is 70 °C and PEA2,5-50 at T_{foam} is 105 °C.

Foaming at different saturation pressures

One way to decrease the cell density and increase the average cell diameter of the foams is to decrease the CO₂ sorption by decreasing the saturation pressure^{3, 4, 6, 8}. Polymer samples of PEA2,5-50 were subjected to different CO₂ saturation pressures and subsequently foamed at 105 °C. With increasing CO₂ concentration in the polymer the concentration of nucleation points is increased. A higher amount of gas cells will be initiated which results in smaller pores (fig. 8.9). Foams with an average pore size of ~100 µm were obtained when the saturation pressure was 20 bar and an average pore size of 6 µm was obtained when the pressure was elevated to 50 bar (table 8.3). Also the porosity decreased slightly with decreasing saturation pressure as at lower saturation

pressures less CO_2 dissolves in the polymer. Changing the saturation pressure thus allows tuning of the average pore size of these foams.

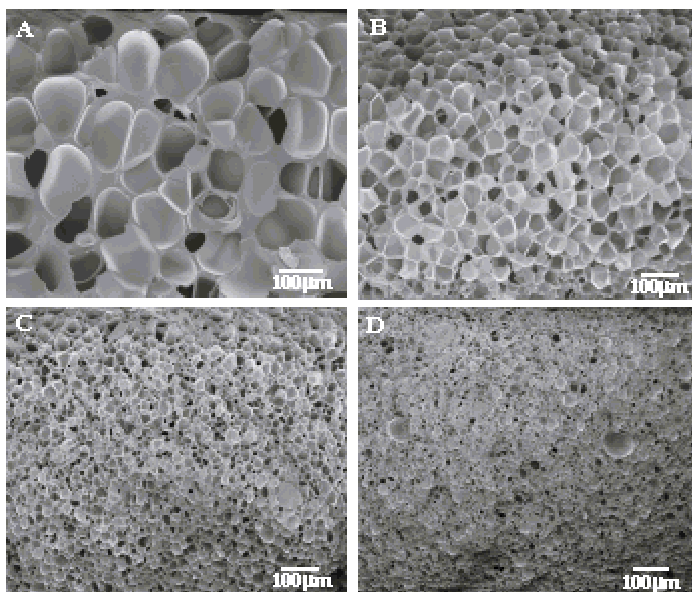


Figure 8.9: SEM images of gas foamed PEA2,5-50 at $T_{\text{foam}} = 105\text{ }^{\circ}\text{C}$, saturated at different CO_2 saturation pressures: (A) 20 bar, (B) 30 bar, (C) 40 bar and (D) 50 bar.

Table 8.3: Porosity and average pore size as a function of CO_2 saturation pressure of gas foamed PEA2,5-50 at $T_{\text{foam}} = 105\text{ }^{\circ}\text{C}$.

saturation pressure (bar)	porosity (%)	average pore size (μm)
20	70.3 ± 1.6	103 ± 29
30	83.0 ± 0.7	46 ± 23
40	87.0 ± 0.6	21 ± 9
50	86.6 ± 1.6	6 ± 5

Conclusions

Segmented poly(ester amide)s, comprising two melt transitions, have been gas foamed by saturation with CO₂ at elevated pressures and subsequent immersion in octane at temperatures just above the lower melt transition. At these temperatures the polymers have adequate mechanical properties and dimensional stability, while the chain mobility has increased sufficiently to nucleate and expand gas cells. The storage modulus of both pure polymers at the onset foaming temperature is 50–60 MPa. With increasing saturation pressure, the CO₂ sorption in the polymer is increasing leading to a higher concentration of nucleation points, which results in smaller pores. This study reveals that closed cell foams with a maximum porosity of ~ 90% and various pore sizes (2.5-100 µm) can be prepared. The pore size can be tuned by changing the saturation pressure or the bisamide to ester ratio of the poly(ester amide).

Acknowledgements

Hylke Sijbesma and Siebrand Metz (University of Twente) are acknowledged for their help with the pressure cell set up and the sorption measurements. The authors would like to thank Mark Smithers (University of Twente) for the scanning electron microscopy. Andres Laib and Markus Burkhart (Scanco Medical AG, Bassersdorf, Switzerland) are acknowledged for the micro-CT measurements. This study was financially supported by the European Commission, project: QLK5-1999-01298.

References

1. C.B. Park, D.F. Baldwin, N.P. Suh, *Polym. Eng. Sci.*, **1995**, 35, (5), 432.
2. S. Doroudiani, C.B. Park, M.T. Korschot, *Polym. Eng. Sci.*, **1996**, 36, (21), 2645.
3. D.F. Baldwin, C.B. Park, N.P. Suh, *Polym. Eng. Sci.*, **1996**, 36, (11), 1446.
4. D.F. Baldwin, C.B. Park, N.P. Suh, *Polym. Eng. Sci.*, **1996**, 36, (11), 1437.
5. D.F. Baldwin, M. Shimbo, N.P. Suh, *J. Eng. Mater. Tech.*, **1995**, 117, (62-74), .
6. B. Krause, M. Wessling, *Macromolecules*, **2001**, 34, (4), 874.
7. D.J. Mooney, D.F. Baldwin, N.P. Suh, L.P. Vacanti, R. Langer, *Biomaterials*, **1996**, 17, (14), 1417.
8. K.L. Parks, E.J. Beckman, *Polym. Eng. Sci.*, **1996**, 36, (19), 2417.

9. D. Chen, G. Hsue, *Polymer*, **1993**, 35, (13), 2808.
10. A.I. Cooper, *J. Mater. Chem.*, **2000**, 10, 207.
11. S.G. Kazarian, *Macromol. Symp.*, **2002**, 184, 215.
12. Y. Shieh, *J. Appl. Polym. Sci.*, **1996**, 59, 695.
13. M. Wessling, Z. Borneman, T. van den Boomgaard, C.A. Smolders, *J. Appl. Polym. Sci.*, **1994**, 53, 1497.
14. K.A. Arora, A.J. Lesser, T.J. Mc Carthy, *Macromolecules*, **1998**, 31, (14), 4614.
15. B. Krause, N.F.A. van der Vegt, M. Wessling, *Macromolecules*, **2001**, 34, (25), 8792.
16. S. Doroudiani, C.B. Park, M.T. Kortschot, *Polym. Eng. Sci.*, **1998**, 38, (7), 1205.
17. C.M. Stafford, T.P. Russel, T.J. McCarthy, *Macromolecules*, **1999**, 32, (22), 7610.
18. D. Klempner, K.C. Frisch, **1991**, *Handbook of polymeric foams and foam technology*, Hanser, New York.
19. J.S. Colton, *Mater. Manuf. Proces.*, **1989**, 4, (2), 253.
20. J.S. Colton, N.P. Suh, *Polym. Eng. Sci.*, **1987**, 27, (7), 485.
21. L.D. Harris, B.S. Kim, D.J. Mooney, *J. Biomed. Mater. Res.*, **1998**, 42, (3), 396.
22. S. Bera, Z. Jedlinski, *Polymer*, **1992**, 33, (20), 4331.
23. S. Bera, Z. Jedlinski, *J. Polym. Sci. Part A: Polym. Chem.*, **1993**, 31, (3), 731.
24. S. Bera, Z. Jedlinski, *Polymer*, **1993**, 34, (16), 3545.
25. T.H. Barrows, The design and synthesis of bioabsorbable poly(ester-amides), in *Polymers in medicine II*. **1986**, Plenum: New York. p. 85.
26. V.L. Horton, P.E. Blegen, T.H. Barrows, R.L. McQuin, **1988**, *Progress Biomed. Polym.*, Los Angeles.
27. J.D. Sudha, C.K.S. Pillai, S. Bera, *J. Polym. Mat.*, **1996**, 13, (4), 317.
28. J.D. Sudha, *J. Polym. Sci. Part A: Polym. Chem.*, **2000**, 38, 2469.
29. H.R. Stapert, A.M. Bouwens, P.J. Dijkstra, J. Feijen, *Macromol. Chem Phys.*, **1999**, 200, (8), 1921.
30. H.R. Stapert, P.J. Dijkstra, J. Feijen, *Macromol. Symp*, **1998**, 130, 91.
31. S. Katayama, T. Murakami, *J. Appl. Polym. Sci.*, **1976**, 20, 975.
32. S. Katayama, H. Horikawa, *J. Appl. Polym. Sci.*, **1971**, 15, 775.

- 33. P.A.M. Lips, chapter 5, in *this thesis*. **2004**.
- 34. T. Hildebrand, P. Ruegsegger, *J. Microscopy*, **1997**, 185, 67.
- 35. M.B. Claase, *J. Biomed. Mat. Res.*, **2004**, submitted.

Appendix A

Preparation of open-cell porous structures of segmented poly(ester amide)s

P.A.M. Lips, I.W. Velthoen, P.J. Dijkstra, J. Feijen

Institute for Biomedical Technology (BMTI) and Department of Polymer Chemistry and Biomaterials, Faculty of Science and Technology, University of Twente, P.O. Box 217, 7500 AE Enschede, The Netherlands.

Abstract

Aliphatic segmented poly(ester amide)s, prepared by melt polycondensation of dimethyl adipate, 1,4-butanediol and a preformed bisamide-diol based on 1,2-diaminoethane and ϵ -caprolactone were investigated as potential scaffold materials for biomedical applications. The polymers comprising crystallizable amide blocks and flexible amorphous ester blocks, have thermal and mechanical properties that can readily be tuned by changing the amide content. These polymers are biocompatible and degrade very slowly in PBS (pH 7.4) at 37 °C and upon subcutaneous implantation in rats. Poly(ester amide)s can easily be processed into highly porous scaffolds (up to 95% porosity) having interconnected pores by both salt leaching and 3D deposition techniques. All polymer scaffolds prepared by salt leaching with pore sizes ranging from 220 to 325 μm have a compressive modulus, varying from 30 kPa at high porosity (95%) and 25 mol% of amide content and 5500 kPa at low porosity (70%) and 50 mol% amide content. Scaffolds with a porosity of 70% and adjustable fiber deposition geometries were successfully constructed with the 3D deposition technique

Introduction

Poly(ethylene oxide terephthalate)/poly(butylene terephthalate (PEOT/PBT) segmented block copolymers (fig. A.1), also known as Polyactive, have recently been investigated in our group as potential scaffold materials for tissue engineering applications ¹⁻⁵. Variations in the PEOT/PBT block copolymer composition and the molecular weight of the PEO (300 or 1000) allowed the synthesis of a family of copolymers with widely differing thermal and mechanical properties ^{2, 4}. By increasing the hard block content of the copolymers (PEO molecular weight of 1000) from 30 to 70 wt%, the melting temperature (T_m) increased from 149 to 204 °C and the glass transition temperature (T_g) increased from -50 to -38 °C. Correspondingly, the elastic modulus and maximum stress increased from 40 to 300 MPa and from 13 to 19 MPa, respectively, while the elongation at break decreased from 1280 to 670%. The *in vivo* degradation and tissue response of PEOT/PBT films was followed over a period up to 24 wks ³. Upon implantation, all materials gave a mild foreign body reaction. Polymers with soft blocks based on PEO with a molecular weight of 300 and a hard block content of 35 and 50 wt% slowly degraded as indicated by a low mass loss (2-3%) and reduction in intrinsic viscosity of ~25% upon 24 wks of implantation. Polymers based on PEO with a molecular weight of 1000 and a hard segment content of ~30 wt% showed a weight loss of 50% and the intrinsic viscosity decreased to 25% of its initial value after 24 wks of implantation. Claase *et al.* prepared well-interconnected porous structures of the latter by a salt leaching technique with porosities ranging from 60 to 90% and pore sizes of 250 to 1000 μm ⁵. Porous scaffolds with a porosity of maximally 90% appeared stable during the leaching process. The compressive modulus of the PEOT/PBT scaffolds decreased from 900 to 50 kPa when the porosity was increased from 60 to 90%. Woodfield *et al.* recently reported the fabrication of PEOT/PBT scaffolds using a custom designed 3D deposition technique ⁶. By controlling fiber deposition geometries, scaffolds with a 100% interconnected pore network have been produced. To study the influence of pore architecture on the formation of cartilage, PEOT/PBT scaffolds (n=300, y=55 wt%) with a porosity of 75 to 80% were prepared both by 3D deposition and by salt leaching techniques ¹. The 3D deposited polymer scaffolds have a less tortuous and more accessible pore volume compared to the salt leached polymer scaffolds and create an environment *in vivo* that enhances cartilaginous matrix deposition.

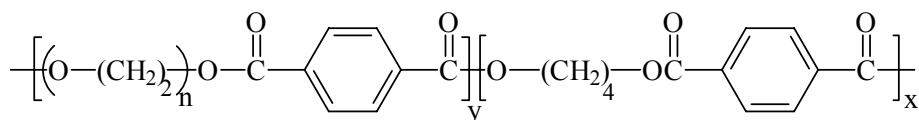


Figure A.1: A segmented poly(ether ester) (PEOT/PBT) with a soft block (y) based on dimethyl terephthalate and poly(ethylene oxide) and a hard block (x) based on dimethyl terephthalate and 1,4-butanediol.

Poly(ϵ -caprolactone), a biocompatible semi-crystalline polymer, has been extensively studied for a wide range of biomedical applications. Poly(ϵ -caprolactone) scaffolds were investigated for the reconstruction of craniofacial and orbital defects ⁷. Fully interconnected 3D scaffolds were constructed by fused deposition modeling and bone ingrowth was induced. Depending on the matrix architecture compressive moduli of poly(ϵ -caprolactone) scaffolds with a porosity of ~60% were found in the range of 20 to 42 MPa ⁸. Hou *et al.* also prepared scaffolds from poly(ϵ -caprolactone) by a technique involving coagulation, compressive moulding and salt leaching ⁹. By increasing the porosity from 70 to 90% the compressive modulus of poly(ϵ -caprolactone) scaffolds decreased from 5 to 0.5 MPa.

In Chapter 7 a study on the potential use of aliphatic poly(ester amide)s as temporary biomedical implant materials was presented ¹⁰. These segmented poly(ester amide)s (fig. A.2), consisting of well-defined crystalline amide and amorphous polyester blocks, have thermal, physical and mechanical properties that can be readily tuned by variation of the x/y ratio ^{11, 12}. The melting temperatures of these poly(ester amide)s increase from 80 to 140 °C and the glass transition temperatures increase from -45 to -8 °C by increasing the amide content from 10 to 85 mol%. Correspondingly, the modulus (70-550 MPa) and stress at break (8-25 MPa) increase, while the strain at break (850-400%) decreases. The degradation of these materials was followed by subcutaneous implantation in rats ¹⁰. The *in vivo* degradation is rather slow and appeared comparable to degradation in PBS (pH 7.4) at 37 °C. As an example the *in vivo* degradation and tissue response of aliphatic poly(ester amide)s with 50 mol% of hard block (x) was followed over a period of 6 wks. The mass loss of the polymers was ~5% while the reduction in intrinsic viscosity

reduction was 10-20% after 6 wks of implantation. A mild foreign body reaction, characterized by the presence of macrophages and sporadically a lymphocyte was observed in the first week of implantation. After 6 wks the implant site is characterized by fibrous encapsulation with no signs of inflammation. Poly(ester amide)s with a 25 or 50 mol% hard block content are non-cytotoxic and sustain adherence and growth of fibroblasts, *in vitro*. It is concluded that high molecular weight aliphatic poly(ester amide)s as presented in fig. A.2 are biocompatible.

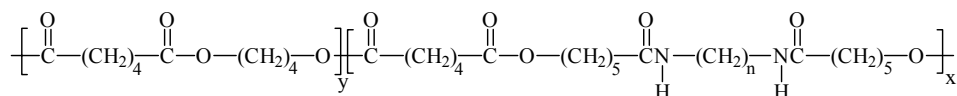


Figure A.2: A segmented poly(ester amide) with a soft block (y) based on 1,4-butanediol and dimethyl adipate and a hard block (x) based on ϵ -caprolactone, 1,2-diaminoethane ($n=2$) or 1,4-diaminobutane ($n=4$) and dimethyl adipate.

Based on their mechanical properties and biocompatibility aliphatic segmented poly(ester amide)s (fig. A.2) have potential as scaffold materials for tissue engineering. A potential major advantage of poly(ester amide)s compared to PEOT/PBT and poly(ϵ -caprolactone) would be the prevention of formation of highly crystalline remnants upon degradation, because the formed monomers and oligomers are water-soluble. To ensure a high specific surface area for cell attachment and tissue in-growth and to promote nutrient and waste exchange highly porous scaffolds with interconnected pores should be prepared. In this respect, poly(ester amide) scaffolds were prepared by two techniques, salt leaching and a 3D deposition, and the preliminary results are described in this appendix. To evaluate these materials for potential tissue engineering applications, the mechanical properties of the scaffolds were also determined.

Experimental

Polymers

The poly(ester amide)s (fig. A.2), PEA2,5-25 and PEA2,5-50 comprising 26 and 51 mol% of N,N'-1,2-ethanediyl-bis[6-hydroxy-hexanamide], respectively, were prepared as previously described ¹².

Salt leaching

The polymers were dissolved in chloroform at a concentration of 10% (w/v) at 45 °C. Amounts of salt particles (sieved, particle size 250–425 µm) ranging from 70 to 97 v% relative to the polymer were added to rapidly stirred polymer solutions. The desired volume fractions were calculated using a salt density of 2.2 g.cm⁻³, and a polymer density of 1.16 g.cm⁻³. The rapid stirring ensured a homogeneous dispersion, which was then precipitated into a 10-fold excess of rapidly stirred diethyl ether. The solid polymer–salt composites were filtrated and dried at room temperature. The composites were compression moulded into discs (14 mm diameter, 8 mm height) with a hot press (THB 008, Fontijne Holland BV, the Netherlands). The composites were heated for 6-8 min at 20 °C above the melting temperature of the polymer as measured by DSC, pressed for 3 min at 300 kN, and cooled in approximately 5 min under pressure to room temperature. The compression moulded polymer–salt composite discs were placed in milliQ water for a period of 48 h to leach out the salt. The water was changed 3 to 4 times a day. The resulting polymer scaffolds were subsequently dried in vacuum at room temperature.

3D deposition

3D scaffolds were constructed at Isotis (Bilthoven, The Netherlands) using a Bioplotter (Envisiontec GmbH, Germany) with an XYZ plotter construction as previously described by Landers *et al.* ¹³. The cartridge and the syringe are mounted on the X-arm. Extruded PEA2,5-50 granules were placed in a stainless steel syringe and heated to 190 °C through a heated cartridge unit. Subsequently, a 5 bar nitrogen pressure was applied to the syringe through a pressurized cap. The nozzle used to extrude polymer fibres of 260 µm in diameter was a stainless steel needle with an internal diameter of 400 µm and a length of 16.2 mm. The Bioplotter CAM software required input of the fiber diameter,

the spacing between deposited fibers, the layer thickness, the overall scaffold dimensions and the speed at which the X-arm is translated. While the X-arm is going up layer by layer in the z-direction, successive layers of rapidly solidifying polymer fibres were laminated to previous layers in a 0–90° pattern creating a constant pore size and a 100% interconnecting pore volume. Fibre layers could be continuously deposited resulting in scaffolds with dimensions of 20x20x4 mm.

The porosity depends on the nozzle diameter, the spacing between deposited layers in horizontal and vertical direction according to the following equation ¹³:

$$p = \left(1 - \frac{\pi}{4} \cdot \frac{1}{\frac{d_2}{d_1}} \cdot \frac{1}{\frac{d_3}{d_1}} \right) \cdot 100 \% \quad (\text{eq. A.1})$$

where p is the porosity, d₁ the nozzle diameter, d₂ the repeat length in the layer and d₃ is the repeat length in the vertical direction.

Methods

Porosity: The porosity of the scaffolds obtained by salt leaching was determined by measuring mass and dimensions (volume) before and after salt leaching.

SEM: Scanning Electron Microscopy was carried out with a LEO Gemini 1550 field emission microscope at a voltage of 2 kV. Freeze fractured samples of the porous structures were sputter-coated with gold before analysis. The average pore size and the pore size distribution were obtained by measuring the size of at least 100 pores at the cross section of the fractured sample.

μ-CT: Microcomputed tomography analysis was carried out using a desktop Micro-CT 40, (Scanco Medical, Bassersdorf, Switzerland) at a resolution of 8 μm in all three spatial dimensions to provide three-dimensional reconstructions of the scaffold. For scaffolds with a diameter of 14 mm and a height of 4 mm, 500 slices were scanned. The method is described in chapter 8 ¹⁴⁻¹⁶.

The average pore size was calculated by taking the average of the product of pore voxels with their assigned pore diameters over the total amount of pore voxels, according to equation A.2:

$$\text{average pore size} = \frac{\sum_i (\text{pore voxel}_i \times \text{pore size}_i)}{\sum_i \text{pore voxel}_i} \quad (\text{eq. A.2})$$

The accessible pore volume was determined by employing an algorithm mimicking mercury intrusion porosimetry by use of a simulated sphere with diameter d . Using a threshold operation, all the pores not accessible for the sphere with diameter d are suppressed. All pores of this thresholded structure not (inter)connected to the outside of the scaffold are discarded with a component labelling operation. The volume of the resulting pore structure is calculated and plotted versus sphere diameter d , resulting in a graph of accessible pore volume (as a function of the total volume) versus sphere diameter d . The surface area of the accessible pore volume as a function of sphere diameter d was calculated using a triangularization algorithm¹⁷. The calculated surface consists of triangular surfaces contacting the scaffolds, and triangular surfaces not contacting the scaffold. Triangular surfaces not contacting the scaffold are suppressed, resulting in a surface area of the pore volume of the scaffold that is accessible for the simulated sphere.

Compressive modulus: Compressive moduli of porous scaffolds (14 mm diameter, 8 mm height) were determined at room temperature using the Zwick Z020 universal tensile machine. Moduli were measured at 10% compressive strain and a strain rate of 2 mm.min⁻¹ with a 500 N load cell and a 0.1 N pre-load.

Compression set: Porous scaffolds (14 mm diameter, 8 mm height) were placed between two metal plates at 25 °C and 70 °C (ASTM 395 B standard) and compressed to 50% of their original thickness for 24 h. The sample thickness was determined half an hour after the load was released. The compression set (CS) is calculated according to:

$$CS = \frac{d_0 - d_2}{d_0 - d_1} \times 100\% \quad (\text{eq. A.3})$$

where d_0 , d_1 , and d_2 are the sample thickness before, during, and after compression respectively.

Results and Discussion

The poly(ester amide)s PEA2,5-25 and PEA2,5-50 were used to prepare porous scaffolds by a technique involving coagulation, compression moulding and particulate leaching ⁹. This technique combines the benefits of thermal processing and particulate leaching. In this method a polymer solution containing dispersed salt particles is precipitated in a non-solvent, followed by thermal processing of the composite into devices of any shape or size. During precipitation the salt remains entrapped within the coagulating polymer matrix, which ensures a homogeneous distribution of the water-extractable salt component. Furthermore the polymer scaffold obtained after leaching of the salt has interconnected pores and the porosities could be varied between 70 and 95% by adjusting the polymer to salt weight ratio.

For both polymers the obtained porosities are in good accordance with the theoretical porosities (table A.1). The average pore size, as determined by SEM, was similar to the salt particle size (250-425 μm) used. Only the PEA2,5-25 scaffold with a porosity of 95% has an average pore size smaller than the average salt particle size, which is probably due to the dimensional instability of this highly porous scaffold.

Table A.1: Porosity and average pore size of the scaffolds prepared from PEA2,5-25 and PEA2,5-50 as obtained by salt leaching.

porosity ^a (%)	porosity ^b (%)		average pore size (μm)	
	PEA2,5-25	PEA2,5-50	PEA2,5-25	PEA2,5-50
70	74.8 ± 1.4	73.3 ± 1.5	260 ± 45	297 ± 55
80	83.0 ± 1.4	84.8 ± 0.9	253 ± 39	279 ± 51
90	91.1 ± 0.4	92.4 ± 0.8	325 ± 43	257 ± 70
95	95.7 ± 0.2	94.9 ± 0.6	218 ± 28	244 ± 36

^a theoretical porosity ^b obtained porosity

SEM analysis of the scaffolds revealed that the interconnectivity of the pores increased at higher porosities (fig. A.3). Scaffolds prepared from PEA2,5-25 afforded similar results (data not shown).

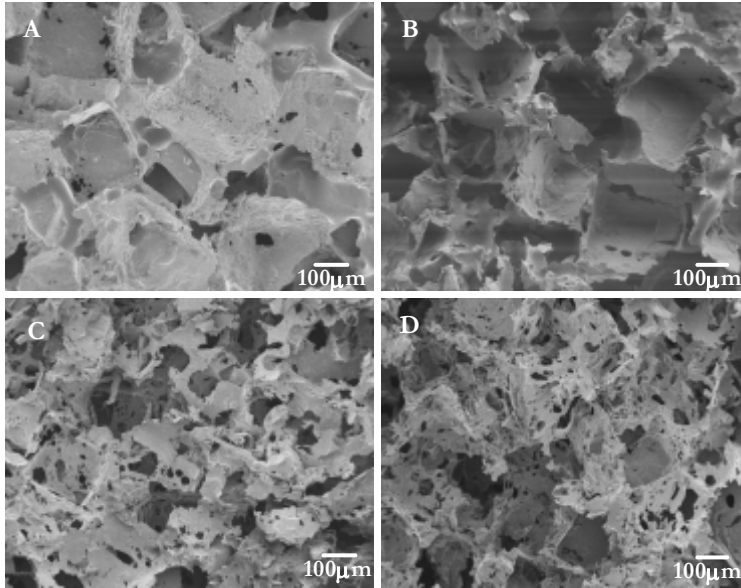


Figure A.3: SEM images of porous scaffolds prepared from PEA2,5-50 with different porosities: (A) 70%, (B) 80%, (C) 90%, and (D) 95%.

Regarding the intended biomedical application, these scaffolds should maintain their structure until seeded cells can organize and develop into a desired tissue. The mechanical properties, especially the compression modulus, of porous materials are mainly governed by porosity. An empirical relationship relates properties like tensile strength, compressive and flexural modulus to the relative density or porosity:

$$\alpha_{foam} = \alpha_0 \left(\frac{\rho_{foam}}{\rho_0} \right)^x \quad (\text{eq. A.4})$$

where α is a mechanical property of the scaffold, α_0 is the same mechanical property of the material and in which the exponent x has a value in between 2 and 3. Experimentally, the exponent can easily be obtained from log-log plots of the relative compression modulus versus relative density. The compressive modulus of PEA2,5-25 and PEA2,5-50 scaffolds decreased with increasing porosity (table A.2), which is in accordance with theory¹⁸. At similar porosities, PEA2,5-50 scaffolds have a higher compressive modulus compared to PEA2,5-25 scaffolds, which is expected as the polymer PEA2,5-50 has a

higher stiffness. PEA2,5-50 scaffolds have compressive moduli similar to poly(ϵ -caprolactone) scaffolds with similar porosities (70 to 90%).

Table A.2: Compressive modulus (E_c) and compression set (CS) at 25 and 70 °C for PEA2,5-25 and PEA2,5-50 scaffolds.

Porosity (%)	E_c (kPa)		CS at 25 °C (%)		CS at 70 °C (%)	
	PEA2,5-25	PEA2,5-50	PEA2,5-25	PEA2,5-50	PEA2,5-25	PEA2,5-50
70	2400 \pm 590	5500 \pm 1670	-	-	-	-
80	670 ^a	1110 ^a	-	-	-	-
90	130 \pm 30	150 \pm 50	62 \pm 1	58 \pm 2	91 \pm 2	84 \pm 2
95	30 \pm 1	70 \pm 10	29 \pm 5	24 \pm 4	-	38 \pm 3

^a single point measurement

In figure A.4 the log value of the compression modulus is presented as a function of the log value of (1-p) of the PEA2,5-25 and PEA2,5-50 scaffolds. For the different polymers, the compressive moduli could be related to the porosities of the scaffolds according to the following power-law relationships:

$$\text{PEA2,5-25: } E_c = k_1 (1 - p)^{2.41} \quad (\text{eq. A.5})$$

$$\text{PEA2,5-50: } E_c = k_2 (1 - p)^{2.43} \quad (\text{eq. A.6})$$

in which parameters k_1 and k_2 are the compressive moduli of the non-porous polymers. The experimental values determined are in good accordance with theory as for an isotropic porous structure with cubic pores, the exponent is expected to be 2 ¹⁸. The obtained relation allows us to accurately predict the compression modulus of a scaffold of any porosity and thus enables us to tune the mechanical properties to a specific need.

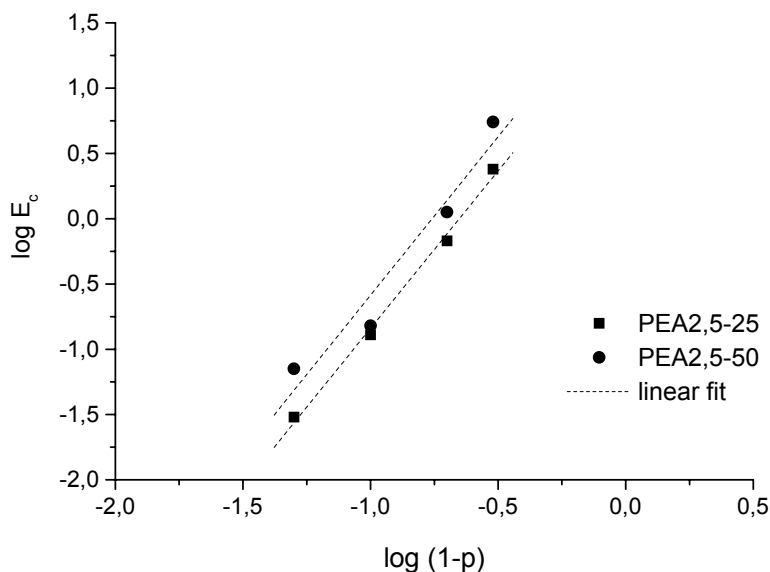


Figure A.4: Relationship between the compressive modulus (E_c) in MPa and $(1-p)$ for PEA2,5-25 and PEA2,5-50 scaffolds.

Pore interconnectivity is a critical factor in scaffold design. The dimensions of the interconnections between pores should be large enough to allow cell proliferation and to maximize the diffusion and exchange of nutrients throughout the entire scaffold. Micro computed tomography (μ -CT), which utilizes 3D imaging to generate computer models of porous materials, has recently been developed for analyzing scaffold architecture¹⁹. Scaffolds, prepared from PEA2,5-25 and PEA2,5-50 with a porosity of 90%, were analyzed by μ -CT (fig. A.5) and their porosities, average pore sizes and pore size distributions were calculated. The porosity of PEA2,5-50 obtained by μ -CT matches the value determined by density measurements quite well (table A.3). The porosity and average pore size of PEA2,5-25 as determined by μ -CT is considerably lower than those measured by the density method and SEM, respectively. This difference may be caused by a slight compression of the sample upon fixation in the sample holder of the μ -CT scanner. As the poly(ester amide) PEA2,5-50 is stiffer than PEA2,5-25 the scaffold is less easily compressed, which is reflected in an almost similar porosity.

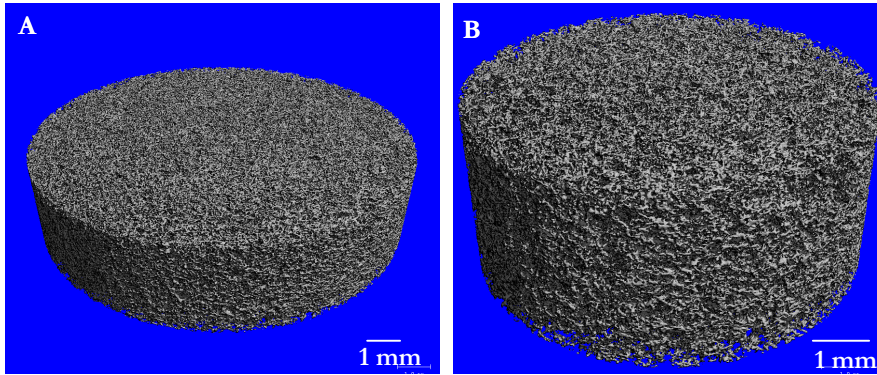


Figure A.5: 3D generated computer images constructed from μ -CT scans of salt leached scaffolds with a porosity of 90% PEA2,5-25 (A) and PEA2,5-50 (B)

Table A.3: Porosity and average pore size of PEA2,5-25 and PEA2,5-50 scaffolds as determined by different methods.

polymer code	porosity (%)		average pore size (μm)	
	density	μ -CT	SEM	μ -CT
PEA2,5-25	91.1 ± 0.4	83.9	325 ± 43	152
PEA2,5-50	92.4 ± 0.8	88.0	257 ± 70	219

Not only the average pore size but also the pore size distribution of the PEA2,5-25 and PEA2,5-50 scaffolds differs considerably (fig. A.6). Even though the pore size of the PEA2,5-50 scaffold is higher, the pore size distribution is much broader compared to the PEA2,5-25 scaffold.

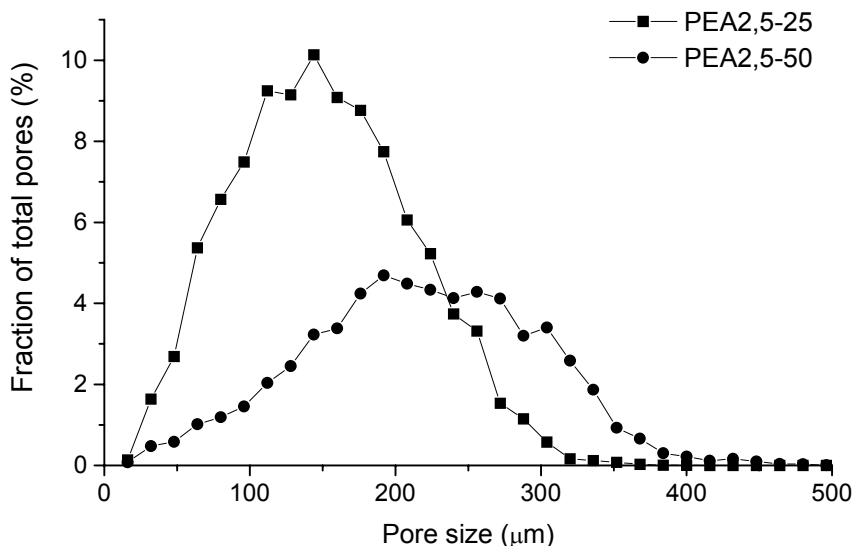


Figure A.6: Pore size distribution of PEA2,5-25 (A) and PEA2,5-50 (B) scaffolds with a porosity of 90% as determined by μ -CT.

As a measure of pore interconnectivity, the accessible pore volume or permeability, of the scaffolds was determined. The accessible pore volume is defined as the total volume of pores, which can be infiltrated by a simulated permeating sphere with increasing diameter from all peripheral borders to the interior of the scaffold. The accessible pore volumes (given as a fraction of the total volume) as a function of the sphere diameter d , as determined with μ -CT are shown in figure A.7. For all sphere diameters the accessible pore volume of the PEA2,5-50 scaffold is higher than that of the PEA2,5-25 scaffold. An accessible pore volume of over 50% (of the total volume) was found for spheres with diameters up to 87 μ m and 137 μ m for PEA2,5-25 and PEA2,5-50, respectively.

At sphere diameters smaller than 100 μ m the PEA2,5-25 scaffold has a higher accessible surface area compared to that of the PEA2,5-50 scaffold (fig. A.8). Above a sphere diameter of 100 μ m the accessible surface area decreases very fast for the PEA2,5-25 scaffolds.

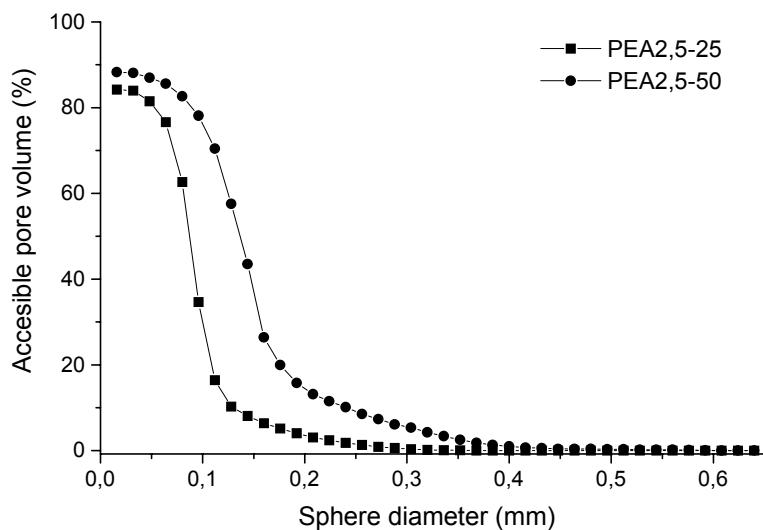


Figure A.7: Accessible pore volume (as fraction of the total volume) versus sphere diameter of PEA2,5-25 and PEA2,5-50 scaffolds with a porosity of 90%.

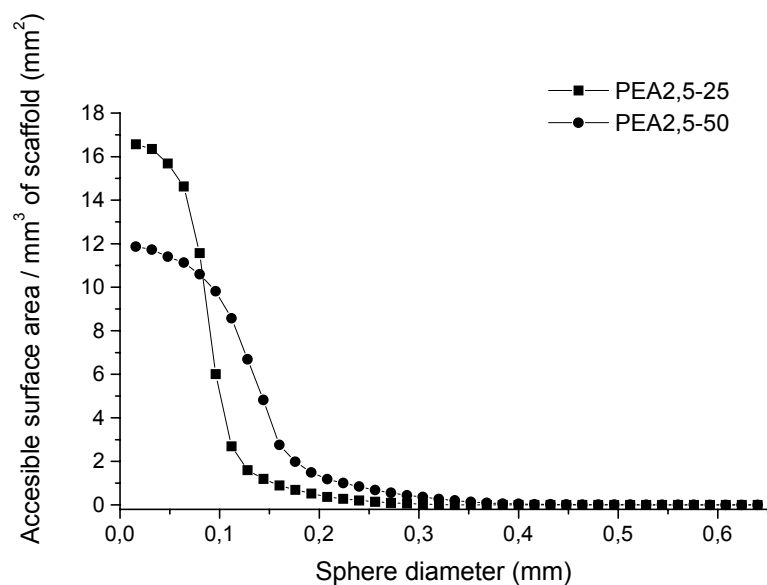


Figure A.8: Accessible pore surface area per mm³ of scaffold versus sphere diameter of PEA2,5-25 and PEA2,5-50 scaffolds with a porosity of 90%.

To construct porous scaffolds with a completely interconnected porous network and a highly regular and reproducible scaffold morphology rapid prototyping has been developed^{6, 13, 20, 21}. Rapid prototyping is a mechanical processing technique in which scaffolds are fabricated one layer at a time via computer-aided design models and computer-controlled tooling processes. Poly(ester amide) scaffolds were prepared with a Bioplotter in which the polymer is heated in a syringe and extruded through a nozzle to form a continuous strand that is deposited in 3D onto a stage. In our first experiments a low molecular weight PEA2,5-50 was used to optimize fabrication parameters like temperature of the melt chamber and pressure in the nozzle. Regular scaffolds with a fiber diameter (d_1) of 260 μm , a layer thickness (d_3) of 225 μm and a fiber spacing (d_2) of 0.8 and 1 mm corresponding with a porosity of 71 and 76 %, respectively, were constructed. A temperature of 190 $^{\circ}\text{C}$ in the melt chamber and a pressure of 5 bar led to regular shapes and reproducible scaffold preparation. SEM analysis showed that the 3D deposited scaffolds were composed of relatively smooth fibers and had interconnecting pores (fig. A.9).

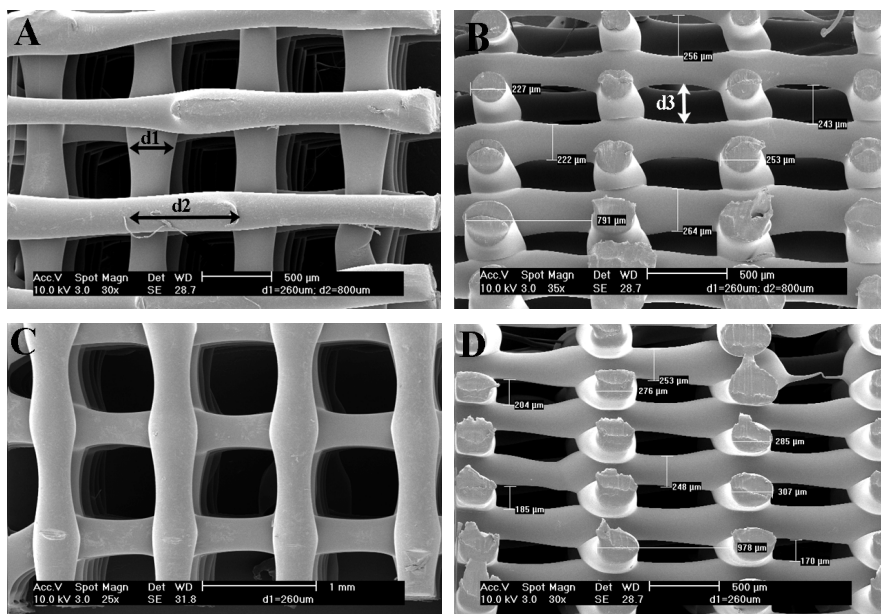


Figure A.9: SEM pictures of 3D deposited PEA2,5-50 scaffolds with a porosity of 71 %: top view (A) and cross section (B) or with a porosity of 76%: top view (C) and cross section (D).

High molecular weight PEA_{2,5-50} was also used to construct 3D deposited scaffolds. Scaffolds with a fiber diameter of 260 μm , a fiber spacing of 1000 μm and a layer thickness of 175 μm corresponding with a porosity of 70% were fabricated (fig A.10a). Compared to the scaffolds shown in figure A.9, these scaffolds have a smaller layer thickness due to compression of the fibers.

The fiber deposition geometry can be tuned by changing the deposition angle or by translating the fiber spacing in the XY plane in successive layers. The scaffolds described above had a deposition angle of 0-90° and a homogeneous fiber spacing. By keeping the deposition angle constant but translating the fiber spacing in each successive layer by 400 μm , scaffolds with a staggered fiber spacing were obtained (fig. A.10b). The scaffolds had a fiber diameter of 260 μm , a fiber spacing of 800 μm and a layer thickness of 225 μm corresponding with a porosity of 71%. These scaffolds have a higher surface area compared to scaffolds prepared with a homogeneous fiber spacing. These preliminary results show that 3D deposition is a suitable technique to prepare scaffolds with fully interconnected pores and with adjustable fiber deposition geometries.

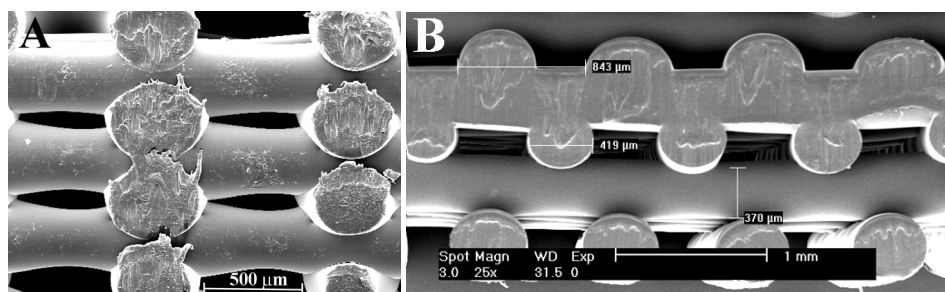


Figure A.10: SEM pictures of 3D deposited PEA_{2,5-50} scaffolds with a porosity of 62% and a homogeneous 1 mm fiber spacing (A) or a porosity of 71% and a staggered 0.8 mm fiber spacing (B).

Conclusions

Aliphatic segmented poly(ester amide)s, comprising a crystallizable amide phase and a flexible amorphous ester phase, were investigated as potential scaffold materials for biomedical applications. By varying the amide content and the type of crystallizable amide segments the polymers thermal and mechanical properties can readily be tuned. These aliphatic segmented poly(ester amide)s can be easily processed into highly porous scaffolds (up to 95%) with interconnected pores by salt leaching and 3D plotting techniques. The compressive modulus of the salt leached poly(ester amide) scaffolds, depending on the porosity and polymer composition, is in the range of 30 to 5500 kPa. At a fixed porosity, the poly(ester amide) scaffolds have a similar compressive modulus as poly(ϵ -caprolactone) scaffolds. These poly(ester amide)s are thus considered a good alternative scaffold materials in tissue engineering applications. However, an *in vivo* study up to 2 years is recommended to investigate the long-term degradation and tissue response of these polymers during degradation.

Acknowledgement

Andres Laib and Markus Burkhart (Scanco Medical AG, Bassersdorf, Switzerland) are acknowledged for the micro-CT measurements. The authors would like to thank Mark Smithers (University of Twente) for the scanning electron microscopy. Lorenzo Moroni (Isotis, Bilthoven) is greatly acknowledged for the preparation of the scaffolds with the 3D deposition technique. This study was financially supported by the European Commission, project: QLK5-1999-01298.

References

1. J. Malda, T.B.F. Woodfield, F. van der Vloodt, C. Wilson, D.E. Martens, J. Tramper, C.A. van Blitterswijk, J. Riesle, *Biomaterials*, **2005**, 26, 63.
2. A.A. Deschamps, M.B. Claase, W.J. Sleijster, J.D. de Bruijn, D.W. Grijpma, J. Fijen, *J. Ctrl. Release*, **2002**, 78, (175-186), .
3. A.A. Deschamps, A.A. van Apeldoorn, H. Hayen, J.D. de Bruijn, U. Karst, D.W. Grijpma, J. Feijen, *Biomaterials*, **2002**, 25, (2), 247.
4. A.A. Deschamps, D.W. Grijpma, J. Feijen, *Polymer*, **2001**, 42, 9335.

5. M.B. Claase, D.W. Grijpma, S.C. Mendes, J. de Bruijn, *J. Biomed. Mater. Res. Part A*, **2003**, 64A, (2), 291.
6. T.B.F. Woodfield, J. Malda, J. de Wijn, F. Peters, J. Riesle, C.A. van Blitterwijk, *Biomaterials*, **2004**, 25, 4149.
7. D. Rohner, D.W. Hutmacher, T.K. Cheng, M. Oberholzer, B. Hammer, *J. Biomed. Mater. Res. Part B: Appl. Biomater.*, **2003**, 66B, 574.
8. D.W. Hutmacher, T. Schantz, I. Zein, K.W. Ng, S.H. Teoh, K.C. Tan, *J. Biomed. Mater. Res.*, **2001**, 55, 203.
9. Q. Hou, D.W. Grijpma, J. Feijen, *Biomaterials*, **2003**, 24, (11), 1937.
10. P.A.M. Lips, chapter 7, in *this thesis*. **2004**.
11. P.A.M. Lips, chapter 4, in *this thesis*. **2004**.
12. P.A.M. Lips, chapter 5, in *this thesis*. **2004**.
13. R. Landers, A. Pfister, U. Hubner, H. John, R. Schmelzeisen, R. Mulhaupt, *J. of Mater. Sci*, **2002**, 37, 3107.
14. P.A.M. Lips, chapter 8, in *this thesis*. **2004**.
15. T. Hildebrand, P. Ruegsegger, *J. Microscopy*, **1997**, 185, 67.
16. M.B. Claase, *J. Biomed. Mat. Res.*, **2004**, submitted.
17. W.E. Lorensen, H.E. Cline, *Comp. Graphics*, **1987**, 21, 163.
18. L.J. Gibson, M.F. Ashby, **1988**, *Cellular Solids, Structure and Properties*, Pergamon Press, Oxford.
19. A. Laib, P. Ruegsegger, *Bone*, **1999**, 24, (1), 35.
20. A. Pfister, R. Landers, A. Laib, U. Hubner, R.M. Schmelzeissen, *J. Polym. Sci. Part A: Polym. Chem.*, **2004**, 42, 624.
21. D.W. Hutmacher, *J. Biomater. Sci: Polymer Edn.*, **2001**, 12, (1), 107.

Summary

A major issue nowadays is the increasing material and energy consumption, which leads to a rapid increase in the world's waste volume and to exhaustion of natural energy resources, such as gas and oil. The development of degradable plastics from renewable resources e.g. non-fossil organic sources such as plants and animals, can bring a solution to this problem. However, features like the polymer performance requirements, the size of the potential value of the market and the cost-performance of the polymer as compared to existing petroleum-based polymers are essential for a commercial success. In the last 4 years a European consortium of companies, research institutes and universities has cooperated to meet all these demands. This project, called Biofoam, aims at developing foams from renewable resources that have comparable or better properties than commercially available foams. To achieve this goal new biodegradable polymers at a cost of less than 1 Euro per kg need to be developed to compete with polyurethane, polystyrene and polyvinyl chloride that currently dominate the foam market.

A well-known class of synthetic biodegradable polymers are the aliphatic polyesters. Most of these polyesters have a low melting transition and insufficient mechanical properties. One way to enhance these performance properties is to incorporate chain segments that are symmetrical and have the ability to organize by H-bonding.

In this thesis the synthesis and characterization of aliphatic segmented poly(ester amide)s are described. To understand the structure-property relations of these polymers, thermal, physical and mechanical properties have been determined and linked to features like phase separation, crystallization behaviour and morphology.

The combination of the favourable properties of polyesters and polyamides has been the fundament for the design and synthesis of poly(ester amide)s. Two different strategies can be followed; placing the amide groups randomly in the polymer chain or incorporate well-defined bisamide containing blocks or segments. These polymers are conveniently synthesized by polycondensation techniques as applied in the synthesis of polyesters and polyamides. In **chapter 2**, aliphatic poly(ester amide)s are reviewed for their structural

characteristics, physical and mechanical properties and biodegradability. The placement of amide and ester groups along the polymer chain can be regulated and alternating, segmented (block) or random polymers can be prepared depending on the starting compounds and procedures applied. In general, the degradation of these aliphatic poly(ester amide)s in buffer solution takes place by hydrolysis of ester linkages and degradation rates are increased at elevated temperatures and at low or high pH values. Also enzymes like proteases, esterases and lipases were found to increase the degradation of these materials. An important outcome was that alternating and block poly(ester amide)s are more stable than random poly(ester amide)s to hydrolytic as well as enzymatic degradation.

Segmented poly(ester-amide)s belong to the family of thermoplastic elastomers and have a micro-phase separated structure with an amide-rich hard phase and an ester-rich flexible soft phase. The amide-rich phase usually contains crystalline lamellae and acts as a thermo-reversible physical crosslinker for the amorphous phase. The soft phase has a sub-ambient glass transition temperature (T_g) and gives the polymer its flexibility and extensibility at room temperature. The properties depend on the type of hard and soft segment, their ratio and on the degree of phase separation between these segments. An effective way to improve phase separation is using short, symmetrical and uniform amide blocks. **Chapter 3** describes the synthesis and characterization of symmetrical preformed monomers, named bisamide-diols, which are essential building blocks to be incorporated in the aliphatic polyester matrix of poly(butylene adipate). These bisamide-diols are synthesized through ring-opening of ϵ -caprolactone or γ -butyrolactone with 1,4-diaminobutane or 1,2-diaminoethane and were studied as model compounds to elucidate the crystallization behaviour of the corresponding poly(ester amide)s. The monomer prepared from 1,4-diaminobutane crystallizes predominantly in an α -type phase while bisamide-diols prepared from 1,2-diaminoethane afforded a mixture of α - and γ -type crystals. Upon heating, multiple endothermic transitions were detected which are related to crystal-to-crystal transformations.

High molecular weight segmented poly(ester amide)s were prepared by melt polycondensation of the preformed bisamide-diols, 1,4-butanediol and dimethyl adipate. By varying the ratio of the 1,4-diaminobutane based bisamide-diol and 1,4-butanediol a series of polymers (PEA4,5) was obtained with a hard segment content between 10 and

85 mol%. The effect of the polymer composition on the thermal, physical and mechanical properties of these poly(ester amide)s is discussed in **chapter 4**. FT-IR and WAXD analysis revealed that the poly(ester amide)s crystallize in an α -type phase similar to even-even nylons. The polymers have a low ($T_{m,1}$) and a high ($T_{m,2}$) melt transition, corresponding with the melting of crystals comprising single ester amide sequences or 2 or more ester amide sequences, respectively. The low melt transition (50–70 °C) is independent of the polymer composition. By increasing the hard segment content from 10 to 85 mol% the high melt transition increased from 80 and 140 °C while the T_g increased from –52 to –8 °C. Correspondingly, the elastic modulus and stress at break increased from 70 to 550 MPa and from 8 to 28 MPa, respectively, while the strain at break decreased from 850 to 350%. Thus by varying the polymer composition the thermal and mechanical properties of the segmented poly(ester amide)s can easily be tuned for specific applications.

The effect of structural variation of the bisamide-diol on the above-mentioned properties is described in **chapter 5**. Polymers based on bisamide-diols containing either 1,4-diaminobutane (PEA4,5) or 1,2-diaminoethane (PEA2,5) were prepared with 25 and 50 mol% of hard segment. The PEA4,5 polymers have an α -type crystalline phase while the PEA2,5 polymers have a mixture of α - and γ -type crystalline phases. The γ -type crystalline structure is similar to γ -crystals present in odd-even nylons. Both PEA2,5 and PEA4,5 have a T_g below room temperature and melt transitions are present at 60 to 70 °C ($T_{m,1}$) and at 110 to 130 °C ($T_{m,2}$) with the latter being highest at higher hard segment content. By increasing the hard segment content from 25 to 50 mol% the elastic modulus and stress at yield increased from ~170 to ~300 MPa and from 8 to 15 MPa, respectively, while the strain at break ranges from 600 to 800%. The thermal and mechanical properties are not influenced by the different crystalline structures of the polymers, only by the amount of crystallizable hard segment present.

Chapter 6 presents the crystallization behaviour and morphological aspects as a function of polymer composition as studied with DSC, AFM, temperature dependent FT-IR, WAXD and SAXS. Upon heating to the first melt transition, IR-bands characteristic of ordered H-bonded amide groups decrease which indicates that at $T_{m,1}$ some crystals melt and form disordered H-bonded N-H groups as well as unassociated groups. This decrease is much more pronounced for PEA4,5 with 25 mol% of hard segment content

as compared to polymers with 50 mol% of hard segment content. This confirms that the transition at $T_{m,1}$ is associated with the melting of a crystalline structure comprising ordered hard segments. By increasing the temperature above $T_{m,2}$ the remaining crystals melt but H-bonds between amide groups remain present. A similar behaviour was observed for PEA2,5 with 50 mol% of hard segment. WAXD measurements at room temperature of PEA4,5 polymers showed diffraction peaks at 3.7 and 4.4 Å which are characteristic for the α -crystalline phase of even-even nylons. These diffraction peaks shift significantly upon heating for the polymers PEA4,5 with 50 and 75 mol% of hard segment content but do not actually meet. Thus before the actual Brill transition is reached the polymers have melted. With increasing hard segment content the average length of the hard segments increases, i.e. the crystal lamellar size increases which is in agreement with the increasing melting temperature. By increasing the hard segment content from 25 to 75 mol%, the average lamellar thickness of the PEA4,5 polymers, as measured by SAXD, increased from 19 to 57 Å, which is in line with the increasing ester amide sequence length. The average lamellar thickness of PEA2,5 with 50 mol% of hard segment is substantially lower compared to the corresponding PEA4,5 polymer.

In **chapter 7**, poly(ester amide)s were evaluated with respect to their mechanical properties in the hydrated state, cytotoxicity, cell adhesion and growth, *in vitro* and *in vivo* degradation and tissue response to study their applicability in the biomedical field. PEA4,5 and PEA2,5 with 25 and 50 mol% of amide content are non-cytotoxic and sustain growth of fibroblasts onto polymer films. The *in vitro* degradation of these polymers (PBS, pH 7.4, 37 °C) and *in vivo* degradation by subcutaneous implantation in rats was followed in time. The *in vitro* degradation followed up to 7 months showed a gradual decrease in molecular weight and almost no mass loss, characteristic of a bulk degradation process. Upon 6 weeks of implantation no additional degradation was observed compared to the *in vitro* degraded samples. The presence of macrophages and sporadically a lymphocyte showed that a mild foreign body reaction is taken place during the first week. After 6 weeks the implant is surrounded by a fibrous capsule with no signs of inflammation. The poly(ester amide)s tested are biocompatible but their *in vitro* as well as *in vivo* degradation is very slow.

Based on their mechanical properties and biocompatibility aliphatic segmented poly(ester amide)s might be applicable as scaffold materials for tissue engineering.

However, an *in vivo* study for at least 2 years should be performed to study the long-term degradation and tissue response during degradation. To ensure a high specific surface area for cell attachment and tissue in-growth and to promote nutrient and waste exchange, highly porous scaffolds with interconnected pores are required. As specific cells also require different pore sizes or even geometries for optimal attachment and growth, good control over pore sizes and morphology is needed. In this respect, poly(ester amide) scaffolds were prepared by two techniques, salt leaching and a 3D deposition, and the preliminary results are described in **appendix A**. It was shown that aliphatic segmented poly(ester amide)s can be easily processed into highly porous scaffolds (up to 95%) with interconnected pores by a salt leaching and 3D deposition technique. Depending on the porosity and polymer composition the compressive modulus of the poly(ester amide) scaffolds, prepared by salt leaching, ranges from 30 to 5500 kPa.

The strategic goal of the Biofoam project was to prepare aliphatic segmented poly(ester amide)s for flexible foam applications. A method to prepare closed-cell poly(ester amide) foams using the physical blowing agent carbon dioxide (CO₂) was investigated and the results are described in **chapter 8**. In this approach PEA2,5 films with 25 and 50 mol% of hard segment content were saturated with CO₂ at 50 bar for 6 h after which the pressure was released. The samples were immersed in octane at the desired temperature after which foaming started immediately. Just above the lower melt transition the polymers retained adequate mechanical properties and dimensional stability, while the chain mobility increased sufficiently to nucleate and expand gas cells during the foaming process. In this way semi crystalline poly(ester amide)s can be gas foamed below the flow temperature and uncontrollable cell growth was suppressed. The storage modulus (G') of both pure polymers at the onset foaming temperature is 50–60 MPa. PEA2,5 with 25 or 50 mol% of hard segment content were foamed at 70 and 105 °C, respectively. Closed-cell foams were obtained with a maximum porosity of ~90%. The average pore size of PEA2,5 with 25 mol% of hard segment content ranges from 77-99 µm. In contrast, the average pore size of PEA2,5 with 50 mol% of hard segment content was in between 2-4 µm and can be increased to 100 µm by lowering the CO₂ saturation pressure to 20 bar. The porosity of PEA2,5-50 foams using this saturation pressure decreased from 90 to 70%.

Samenvatting

Het toenemende materiaal- en energieverbruik leidt tot een steeds verdere toename van de hoeveelheid afval en tot uitputting van natuurlijke energiebronnen zoals gas en olie. De ontwikkeling van afbreekbare plastics gemaakt uit hernieuwbare grondstoffen, bijv. planten en dieren, kunnen een mogelijke bijdrage leveren aan een oplossing van dit probleem. Echter, voor een commercieel succes, zijn facetten als polymeer eigenschappen en productiekosten in relatie tot de eigenschappen van cruciaal belang. Gedurende de laatste 4 jaren heeft een consortium van bedrijven, onderzoeksinstituten en universiteiten in een EEG-project samengewerkt op dit gebied onder de projectnaam “Biofoam”. De onderzoekers hebben zich ten doel gesteld schuimen te ontwikkelen op basis van hernieuwbare grondstoffen met gelijke of betere eigenschappen dan schuimen die momenteel op de markt zijn. Om dit doel te bereiken en om te kunnen concurreren met polyurethaan-, polystyreen- en polyvinylalcohol-schuimen die de huidige markt domineren, is het noodzakelijk nieuwe (afbreekbare) polymeren te ontwikkelen waarvan de kostprijs minder dan 1 euro per kg bedraagt.

Een bekende groep afbreekbare polymeren zijn de alifatische polyesters. De meeste van deze polyesters hebben een laag smeltpunt en onvoldoende mechanische eigenschappen voor schuimapplicaties. Een manier om deze eigenschappen te verbeteren is door symmetrische amide groep bevattende segmenten in de polyesterketens in te bouwen die zich kunnen organiseren door waterstofbruggen.

De synthese en karakterisering van alifatische gesegmenteerde poly(ester amide)s is beschreven in dit proefschrift. Thermische, fysische en mechanische eigenschappen zijn bepaald om structuur-eigenschap relaties te onderzoeken en deze te koppelen aan kenmerken zoals fasescheiding, kristallisatiegedrag en morfologie.

De bijzondere en specifieke eigenschappen van zowel polyesters als polyamides hebben geleid tot onderzoek naar poly(ester amide)s. Twee verschillende strategieën zijn gehanteerd: het willekeurig plaatsen van amide groepen in de polymeerketen, of het inbouwen van goed gedefinieerde blokken of segmenten opgebouwd uit bisamides. Deze polymeren zijn te synthetiseren door middel van polycondensatiereacties zoals toegepast

in de synthese van polyesters en polyamides. In **hoofdstuk 2** is een overzicht gegeven van reeds bekende poly(ester amide)s en de fysische en mechanische eigenschappen en biodegradeerbaarheid van deze materialen. De plaatsing van amide- en estergroepen kan verschillend zijn en is afhankelijk van de monomere uitgangsstoffen. Alternierende, gesegmenteerde (blok) of random polymeren kunnen worden gemaakt, afhankelijk van de beginstoffen en toegepaste procedure. Over het algemeen vindt de degradatie van deze alifatische poly(ester amide)s plaats door hydrolyse van ester bindingen. De degradatiesnelheden nemen toe bij verhoogde temperatuur en lage of hoge pH, maar ook door toevoeging van enzymen zoals proteases, esterases en lipases. Alternierende en blok poly(ester amide)s blijken meer resistent tegen hydrolytische en enzymatische degradatie dan random poly(ester amide)s.

Gesegmenteerde poly(ester amide)s zijn thermoplastische elastomeren en hebben een fase gescheiden structuur met een amide-rijke harde fase en een ester-rijke zachte fase. De amide-rijke fase bestaat meestal uit kristallijne lamellen en gedraagt zich als een fysische crosslinker voor de amorfe fase. De zachte amorfe fase heeft een glasovergangstemperatuur (T_g) beneden kamertemperatuur wat het polymeer zijn flexibiliteit en uittrekbaarheid geeft bij kamertemperatuur. De eigenschappen van het polymeer hangen af van het type hard en zacht segment, hun ratio en de mate van fasescheiding tussen deze segmenten. Een effectieve manier om de fasescheiding te verbeteren is door gebruik te maken van korte, symmetrische en uniforme amide blokken.

In **hoofdstuk 3** is de synthese en karakterisering van symmetrische bisamide-diol monomeren, voor inbouw in de alifatische poly(butyleen adipaat) matrix, beschreven. Het kristallisatiegedrag van de bisamide-diolen, welke gesynthetiseerd zijn door middel van een ring-openingsreactie van ϵ -caprolacton of γ -butyrolacton met 1,4-diaminobutaan of 1,2-diaminoethaan, is bestudeerd teneinde inzicht te krijgen in het kristallisatiegedrag van de poly(ester amide)s.

De monomeren uitgaande van 1,4-diaminobutaan kristalliseren voornamelijk in een α -type fase, terwijl de bisamide-diolen op basis van 1,2-diaminoethaan een mengsel of α - en γ -type kristallen geven in analogie met het kristallisatiegedrag van verschillende typen nylons. Tijdens het opwarmen van deze monomeren worden er meerdere

endothermische transitie waargenomen welke gerelateerd zijn aan overgangen van genoemde kristalvormen.

Hoogmoleculair gesegmenteerde poly(ester amide)s zijn vervolgens gemaakt uit de bisamide-diolen, op basis van 1,4-diaminobutaan, door ze te condenseren met 1,4-butaandiol en dimethyladipaat in de smelt. Door de ratio bisamide-diol / 1,4-butanediol te variëren werd er een serie polymeren (PEA4,5) gemaakt met een hard segment percentage tussen de 10 en de 85 mol%. Het effect van de polymeersamenstelling op de thermische, fysische en mechanische eigenschappen van deze poly(ester amide)s is beschreven in **hoofdstuk 4**. Met behulp van FT-IR en WAXD metingen is vastgesteld dat deze poly(ester amide)s kristalliseren in een α -type fase analoog aan even-even nylons. De polymeren hebben een lage ($T_{m,1}$) en een hoge ($T_{m,2}$) smeltovergang corresponderend met het smelten van de kristallijne fasen die hoofdzakelijk opgebouwd zijn uit respectievelijk enkele ester amide sequenties of 2 of meer ester amide sequenties. De lage smeltovergang (50-70 °C) is onafhankelijk van de polymeersamenstelling. De hoge smeltovergang neemt toe (80 tot 140 °C) en de T_g neemt toe (-52 tot -8 °C) bij een toenemend hard segment percentage van 10 naar 85 mol%. Evenzo nemen de elasticiteitsmodulus (70 tot 550 MPa) en breukspanning (8 tot 28 MPa) toe, terwijl de rek bij breuk afneemt van 850 naar 350%. Kortom, door het variëren van de polymeersamenstelling is het mogelijk de thermische en mechanische eigenschappen af te stemmen op een specifieke applicatie.

Het effect van de structuur van het ester-amide segment op de bovengenoemde eigenschappen is vervolgens onderzocht en beschreven in **hoofdstuk 5**. Hiertoe zijn de polymeren PEA4,5 en PEA2,5 gesynthetiseerd uitgaande van de bisamide-diolen gebaseerd op respectievelijk 1,4-diaminobutaan en 1,2-diaminoethaan. De gemaakte polymeren bevatten 25 of 50 mol% hard segment. De PEA4,5 polymeren hebben een α -type kristallijne fase en de PEA2,5 polymeren hebben een mengsel van α - en γ -type kristallijne fasen. De γ -type kristallijne structuur is vergelijkbaar met de γ -kristallen aanwezig in oneven-even nylons. Zowel PEA4,5 als PEA2,5 hebben een T_g onder kamertemperatuur en smeltovergangen bij 60-70 °C ($T_{m,1}$) en bij 110-130 °C ($T_{m,2}$). De thermische en mechanische eigenschappen nemen toe bij toenemend percentage hard segment, maar worden niet beïnvloed door de verschillende structuur van de kristallijne fase.

Het bijzondere kristallisatiegedrag van de poly(ester amide)s is vervolgens in detail bestudeerd met DSC, AFM, temperatuur afhankelijke FT-IR, WAXD en SAXS en beschreven in **hoofdstuk 6**. IR banden, karakteristiek voor geordende waterstofbrug gebonden N-H groepen, nemen af door voorbij de eerste smelttransitie te gaan terwijl IR banden, karakteristiek voor ongeordende waterstofbrug gebonden N-H groepen of niet geassocieerde groepen, toenemen. Deze afname is meer uitgesproken voor de PEA4,5 polymeren met 25 mol% hard segment in vergelijking met dezelfde polymeren met 50 mol% hard segment. Dit laat zien dat de transitie bij $T_{m,1}$ geassocieerd kan worden met het smelten van een kristallijne structuur die bestaat uit geordende harde segmenten. De resterende kristallen smelten door de temperatuur te verhogen tot boven de $T_{m,2}$. Echter, de spectra laten zien dat waterstofbruggen tussen amide groepen blijven bestaan. Eenzelfde gedrag is waargenomen voor de PEA2,5 polymeren met 50 mol% hard segment. WAXD metingen bij kamertemperatuur aan de PEA4,5 polymeren geven diffractiepieken bij 4.4 en 3.7 Å welke karakteristiek zijn voor een α -kristallijne fase als aanwezig in even-even nylons. De diffractiepieken van de PEA4,5 polymeren met 50 en 75 mol% hard segment schuiven naar elkaar toe bij hogere temperaturen maar komen nooit samen. Dit wijst op een zogenaamde Brill overgang, maar deze wordt niet volledig bereikt voordat de polymeren smelten. Uit SAXS metingen blijkt dat door het verhogen van het percentage hard segment van 25 tot 75 mol%, de gemiddelde lameldikte van de PEA4,5 polymeren toeneemt van 19 tot 57 Å, corresponderend met de toenemende ester amide sequentiellengte. De gemiddelde lameldikte van PEA2,5 met 50 mol% hard segment is significant lager dan het overeenkomstige PEA4,5 polymeer.

Om te onderzoeken of gesegmenteerde poly(ester amide)s toe te passen zijn als afbreekbaar biomateriaal zijn de PEA4,5 en PEA2,5 polymeren met 25 en 50 mol% amide gehalte getest op cytotoxiciteit, celadhesie en -groei, *in vitro* en *in vivo* degradatie en weefselreacties. De resultaten staan beschreven in **hoofdstuk 7**. De polymeren blijken niet cytotoxisch en groei van fibroblasten op polymere films is aangetoond. De *in vitro* degradatie in PBS (pH 7.4, 37 °C) en *in vivo* degradatie na subcutane implantatie van de polymeren is gevolgd als functie van de tijd. De polymeren die blootgesteld zijn aan PBS lieten over een periode van 7 maanden een geleidelijke afname zien in molgewicht, maar vertoonden geen massaverlies, wat karakteristiek is voor bulkdegradatie. Na 6 weken implantatie laat PEA2,5 met 50 mol% hard segment concentratie geen

toenemende degradatie zien ten opzichte van hetzelfde polymeer maar dan na *in vitro* degradatie (ook na 6 weken). De aanwezigheid van macrofagen en enkele lymphocyten duidt op een lichte vreemd-lichaamsreactie tijdens de eerste week van implantatie. Na 6 weken was het implantaat volledig ingekapseld en waren er geen tekenen van ontsteking. Er is geconcludeerd dat de geteste poly(ester amide)s biocompatibel zijn, hoewel hun *in vitro* en *in vivo* degradatie erg langzaam is. Deze alifatische poly(ester amide)s zouden gebruikt kunnen worden als poreuze dragers in de weefseltechnologie, hoewel een *in vivo* studie van minimaal 2 jaar nodig is om de lange-termijn degradatie en de weefselreactie tijdens degradatie te bestuderen. Om verzekerd te zijn van een hoog specifiek oppervlak voor celhechting en ingroei van weefsel en om de uitwisseling van voedingsstoffen en afvalstoffen te stimuleren zijn hoog poreuze dragers nodig met doorverbonden poriën. Omdat ieder celtype een bepaalde poriegrootte en geometrie nodig heeft voor optimale hechting en groei is een goede controle over poriegrootte en morfologie nodig. Om aan al deze eisen te voldoen zijn er met behulp van twee technieken, uitwassen van zout uit een polymeer-zout composiet en 3D depositie, poreuze structuren van de poly(ester amide)s gemaakt. De resultaten staan beschreven in **appendix A**. Hoog poreuze poly(ester amide) dragers (tot 95%) met doorverbonden poriën zijn vrij eenvoudig te construeren met behulp van de twee bovengenoemde technieken. De compressiemodulus (30 tot 5500 kPa) van poly(ester amide) matrices, gemaakt door uitwassen van zout, is sterk afhankelijk van de porositeit en de polymeer samenstelling.

In **hoofdstuk 8** is de bereiding van poly(ester amide) schuimen, gemaakt met behulp van het fysisch blaasmiddel koolstofdioxide (CO₂), beschreven. Door PEA_{2,5} films met 25 en 50 mol% hard segment concentratie te verzadigen met CO₂ bij 50 bar gedurende 6 uur, vervolgens de druk eraf te halen en de films onder te dompelen in octaan bij hogere temperatuur start het schuimproces. Boven de eerste smeltovergang behouden de polymeren adequate mechanische eigenschappen en dimensionale stabiliteit terwijl de mobiliteit van de ketens voldoende toeneemt om gasbellen te initiëren en te laten groeien. Op deze manier is het mogelijk semi-kristallijne polymeren te schuimen onder hun vloeitemperatuur waardoor ongecontroleerde celgroei onderdrukt kan worden. Op het moment dat de polymeren beginnen te schuimen is de opslagmodulus (G') van de polymeren 50-60 MPa. Schuimen met een gesloten celstructuur en een maximum

porositeit van 90% zijn gemaakt van PEA2,5 met 25 of 50 mol% hard segment bij respectievelijk een temperatuur van 70 en 105 °C. De gemiddelde poriegrootte van PEA2,5 schuimen met 25 mol% hard segment varieert van 77 tot 99 µm. De gemiddelde poriegrootte van PEA2,5 schuimen met 50 mol% hard segment concentratie is 2 tot 4 µm en kan verhoogd worden naar 100 µm door de CO₂ verzadigingsdruk te verlagen tot 20 bar. De porositeit van het PEA2,5 schuim wordt hierdoor verlaagd van 90 naar 70%.

Curriculum vitae

Priscilla Lips werd geboren op 19 september 1974 te Didam. In 1990 behaalde ze haar MAVO diploma aan de Albertus Magnus Mavo te Geldrop. In de 4 jaar daarna werden ook nog het HAVO en VWO diploma behaald aan het Strabrecht College te Geldrop. In 1994 begon ze aan de opleiding Hoger Laboratoriumonderwijs (HLO) aan de Fontys Hogescholen te Eindhoven met Chemie als hoofdrichting. Tijdens het vierde jaar heeft ze stage gelopen bij Philips Research in de groep Polymeren en Organische Chemie onder begeleiding van Dr. Herman Schoo. De stageopdracht was getiteld: 'Synthesis and characterization of electroluminescent, conducting polymers for display applications'. Na deze stage begon ze met afstuderen bij DSM Research te Geleen waar ze zich 6 maanden bezig hield met het opzetten van een chemisch modelonderzoek ten behoeve van reversie en recycling van EPDM-rubber. De afstudeeropdracht werd uitgevoerd binnen de afdeling Engineering Plastics (Elastomers) onder leiding van Dr. Martin van Duin. Direct na het behalen van haar HLO diploma in 1998 ging ze werken bij Philips Research in dezelfde groep als waar ze stage gelopen had. Ze heeft zich hier voornamelijk bezig gehouden met de ontwikkeling van nieuwe materialen voor 'polymere light-emitting diodes'. Tijdens haar baan heeft ze de volledige post doctorale TOP opleiding polymeren van de Stichting Polymeer Technologie Nederland (PTN) met goed gevolg afgelegd. Na 2 jaar vertrok ze naar Enschede om te gaan werken als assistent in opleiding aan de Universiteit Twente binnen de vakgroep Polymeren en Biomaterialen en onder begeleiding van Prof. Dr. J. Feijen en Dr. P.J. Dijkstra. Het promotieonderzoek is uitgevoerd in het kader van een EEG-project getiteld: 'Biofoam: Bio-source based recyclable poly(ester-co-amide)s and poly(ester-co-urethane)s for industrial foam applications (QLK5-1999-01298). De resultaten van dit onderzoek staan beschreven in het boekje voor u.